

**Brought to light:  
The Bcl-2 transmembrane domain interactome  
elucidated by a bimolecular split luciferase assay and  
its impact on apoptosis signalling**

Von der Fakultät Energie-, Verfahrens- und Biotechnik der Universität Stuttgart  
zur Erlangung der Würde eines  
Doktors der Naturwissenschaften (Dr. rer. nat.) genehmigte Abhandlung

Vorgelegt von

**Tobias Benjamin Beigl**

aus Backnang

Hauptberichter:	Prof. Dr. Markus Morrison
Mitberichter:	Prof. Dr. Stephan Nussberger
Mitberichter:	PD Dr. Frank Essmann
Tag der mündlichen Prüfung:	25.07.2024

**Robert Bosch Center für Tumorerkrankungen des Bosch Health Campus  
und  
Institut für Zellbiologie und Immunologie der Universität Stuttgart  
2024**



*“Tobi or not Tobi – that is the question.”*

*- Tobias Beigl (adapted from William Shakespeare’s Hamlet, Act III, scene I)*



# Table of contents

Abbreviations.....	VIII
List of figures .....	XII
List of tables .....	XIII
Abstract .....	XIV
Zusammenfassung .....	XV
1 Introduction .....	1
1.1 Apoptosis – a programmed cell death.....	1
1.1.1 Extrinsic apoptosis signalling .....	3
1.1.2 Intrinsic apoptosis signalling.....	6
1.1.3 Apoptosis in disease.....	8
1.2 The Bcl-2 protein family .....	12
1.2.1 Pro-apoptotic effector proteins .....	14
1.2.2 Anti-apoptotic Bcl-2-like proteins.....	18
1.2.3 BH3-only proteins.....	22
1.2.4 Bcl-2 protein interactions and anti-cancer therapy.....	24
1.3 Transmembrane domains (TMDs) .....	26
1.3.1 Transmembrane domains in the Bcl-2 protein family.....	28
1.3.2 Functions of Bcl-2 transmembrane domains.....	29
1.4 Aims of the thesis.....	36
2 Materials and Methods.....	37
2.1 Materials .....	37
2.1.1 Antibodies.....	37
2.1.2 Cell culture media and reagents.....	38
2.1.3 Cell lines and bacteria .....	39
2.1.4 Chemicals, buffers and solutions .....	39
2.1.5 Consumables.....	41
2.1.6 Enzymes.....	41
2.1.7 Instruments.....	42
2.1.8 Kits.....	42
2.1.9 Plasmids.....	42
2.1.10 Oligonucleotides.....	46
2.1.11 Software .....	49

2.2	Methods.....	50
2.2.1	DNA sequences.....	50
2.2.2	Cloning .....	50
2.2.3	NEBuilder HiFi DNA assembly (Gibson assembly).....	54
2.2.4	Site-directed mutagenesis.....	55
2.2.5	Cell culture.....	56
2.2.6	Seeding cells on coverslips .....	56
2.2.7	Transient transfection .....	56
2.2.8	NanoBiT split luciferase assay (NanoBiT assay) .....	57
2.2.9	Flow cytometry .....	58
2.2.10	Cell fixation and immunofluorescence staining .....	59
2.2.11	Confocal laser scanning microscopy (cLSM) .....	60
2.2.12	SDS-PAGE and Western Blot .....	61
2.2.13	siRNA-mediated knockdown .....	63
2.2.14	Caspase-Glo 3/7 assay .....	63
2.2.15	Application of cell death-inducing compounds .....	64
2.2.16	Incucyte time-lapse imaging (cell death assay) .....	64
2.2.17	<i>In silico</i> protein sequence analyses.....	65
2.2.18	Molecular dynamics simulations.....	65
2.2.19	Statistical analysis .....	66
3	Results.....	67
3.1	Development of a split luciferase assay for detection of TMD interaction ....	67
3.1.1	Investigation of NanoBiT assay parameters and fluorescence normalisation .....	68
3.1.2	Validation of the NanoBiT assay with TMD interaction controls .....	74
3.2	Systematic analysis of the Bcl-2 TMD interactome .....	77
3.2.1	Effector TMDs interact preferentially in a homotypic manner .....	77
3.2.2	BAX and BAK TMDs interact both with anti-apoptotic BCL-XL and BCL-W TMDs ....	80
3.2.3	NanoBiT assay reveals a unique TMD interaction of BOK and BCL-2 .....	83
3.2.4	BAX- and BAK-TMD localise to Mitochondria, while BOK-TMD is ER-localised .....	85
3.2.5	TMDs of anti-apoptotic Bcl-2 proteins show distinct subcellular localisation .....	88
3.2.6	BOK-TMD and BCL-2-TMD colocalise at ER membranes.....	91
3.3	Impact of TMD interactions on apoptosis signalling .....	93
3.3.1	The TMD of BAX is crucial for BAX auto-inhibition .....	93
3.3.2	BAX-TMD mutation crucially interferes with BAX function .....	99
3.3.3	Inhibition of BAK by BCL-2 is TMD-independent .....	108
3.3.4	The TMD, not BH3 region, influences BOK and BCL-2 colocalisation .....	112
3.3.5	BOK-induced cell death is inhibited by BCL-2 which is influenced by their TMDs ...	114
3.3.6	BOK-TMD and BCL-2-TMD interact in molecular dynamics simulations.....	121
3.3.7	BCL-2 TMD mutation impairs its ability to counteract cell death induction .....	125
3.3.8	BOK-dependent ER stress response is modulated by the presence of BCL-2 .....	133

4	Discussion .....	137
4.1	Harnessing NanoBiT for the detection of TMD interactions .....	139
4.1.1	NanoBiT assay parameters and fluorescence normalisation.....	139
4.1.2	NanoBiT assay validation.....	141
4.2	Identification of novel and known TMD interactions .....	143
4.2.1	Homotypic interaction of effector TMDs .....	145
4.2.2	BCL-XL and BCL-W – universal TMD-scavengers of effector proteins? .....	146
4.2.3	A newly identified Interaction of BOK and BCL-2 via their TMDs .....	147
4.2.4	Subcellular localisation of TMD interactions .....	148
4.3	Investigating the functional relevance of TMD interactions .....	151
4.3.1	The TMD has a crucial role for regulation of BAX activity.....	152
4.3.2	BAK-TMD has limited influence on BAK activity and regulation .....	154
4.3.3	Cancer-related TMD mutations shift the Bcl-2 network homeostasis .....	155
4.3.4	Functional characterisation of the newly identified BOK-/BCL-2-TMD interaction....	161
4.3.5	TMD interaction of Bcl-2 proteins – a new drug target?.....	173
5	Conclusion .....	175
6	References .....	176
7	Appendix.....	206
	Acknowledgements .....	220
	Declaration of authorship.....	222
	Publications and conference contributions .....	223
	Curriculum vitae.....	224

## Abbreviations

$\Delta\Psi_m$	Mitochondrial transmembrane potential
A1	Bcl-2-related protein A1
AA	Amino acid
BH	Bcl-2 homology
BAD	Bcl-2-associated agonist of cell death
BAX	Bcl-2-associated X protein
BAK	Bcl-2 homologous antagonist killer (gene name: <i>BAK1</i> )
Bcl-2	B-cell lymphoma 2 (protein family)
BCL-2	B-cell lymphoma 2 protein
BCL-G	BCL-Gonad
BCL-W	Bcl-2-like protein 2
BCL-XL	B-cell lymphoma-extra large
BET	Bromodomain and extra-terminal
BFK	Bcl-2 family kin protein
BFL-1	Bcl-2-related gene expressed in fetal liver
BID	BH3-interacting domain death agonist
BiFC	Bimolecular fluorescence complementation
BIK	Bcl-2-interacting killer
BIM	Bcl-2-interacting mediator of cell death
BMF	Bcl-2-modifying factor
BOK	Bcl-2-related ovarian killer
BPR	Bcl-2-related proline rich protein
BSA	Bovine serum albumin
CARD	Caspase recruitment domain
cb5	Cytochrome b5
cFLIP	Cellular FLIP
CG	Coarse-grained
cGAS	cyclic GMP–AMP synthase
CHOP	C/EBP homologous protein
cIAP	Cellular IAP
CL	Cardiolipin
cLSM	Confocal laser scanning microscopy
CMV	Cytomegalovirus immediate-early



---

COSMIC	Catalogue of somatic mutations in cancer
(c)PARP	(Cleaved) poly (ADP-ribose) polymerase
Ct	C-terminal
Ctrl	Control
CytC	Cytochrome C
DAPI	4',6-Diamidin-2-phenylindol
DISC	Death-inducing signalling complex
dNTPs	Deoxynucleosidtriphosphates
ECL	Electro-generated chemiluminescence
EGFP	Enhanced green fluorescent protein
em.	Emission
ER	Endoplasmic reticulum
ERAD	ER-associated protein degradation
EYFP	Enhanced yellow fluorescent protein
ex.	Excitation
FACS	Fluorescence-activated cell sorting
FasL	Fas antigen ligand
FBS	Fetal bovine serum
FLIM	Fluorescence lifetime imaging microscopy
FLIP	FADD-like interleukin-1 $\beta$ -converting enzyme inhibitory protein
FRET	Förster resonance energy transfer
GMP	Guanosine monophosphate
HRK	Activator of apoptosis hara-kiri
HSV TK	Herpes simplex virus thymidine kinase
IAP	Inhibitor of apoptosis protein
IF	Immunofluorescence
IP3R	Inositol 1,4,5-trisphosphate receptor
IQR	Interquartile range
JNK	c-Jun N-terminal kinase
K <sub>D</sub>	Dissociation constant
KD	Knockdown
KO	Knockout
LB	Lysogeny broth
LUV	Large unilamellar vesicle

mC	mCherry
mCitr	mCitrine
MCL-1	Induced myeloid leukaemia cell differentiation protein Mcl-1
MD	molecular dynamics
MOM	Mitochondrial outer membrane
MOMP	Mitochondrial outer membrane permeabilization
MOPC	1-myristoyl-2-oleoyl-sn-glycero-3-phosphocholine
MOPE	1-myristoyl-2-oleoyl-sn-glycero-3-phosphoethanolamine
mTurq2	mTurquoise2
NCCD	Nomenclature comitee on cell death
NF- $\kappa$ B	Nuclear factor 'kappa-light-chain-enhancer' of activated B-cells
Nt	N-terminal
o/n	Overnight
PCD	Programmed cell death
PCR	Polymerase chain reaction
PDB	Protein data bank
PDI	Protein-disulfide isomerase
PI	Propidium Iodide
PMAIP1	Phorbol-12-myristate-13-acetate-induced protein 1 (NOXA)
PODG	$\alpha$ -palmitoyl-2-oleoyl-sn-glycerol
POPI	1-palmitoyl-2-oleoyl-sn-glycero-3-phosphoinositol
PS	Phosphatidyl serine
PTP	Permeability transition pore
PUMA	p53 up-regulated modulator of apoptosis
RCD	Regulated cell death
RLU	Relative light units
RMSD	Root mean square deviation
ROI	Region of interest
rpm	Rounds per minute
RT	Room temperature
SASA	Solvent accessible surface area
SDS-PAGE	Sodium dodecyl sulfate polyacrylamide gel electrophoresis
SMALP	Styrene malic acid lipid particles
SOB	Super optimal broth

T <sub>m</sub>	Melting temperature
TEMED	Tetramethylethylenediamine
TM	Tunicamycin
TMD	Transmembrane domain
TMRM	Tetramethylrhodamine methyl ester
TNF $\alpha$	Tumor necrosis factor $\alpha$
TNFR	Tumor necrosis factor receptor
TOM5	Translocase of the outer membrane 5
TRAIL	TNF-related apoptosis inducing ligand
TRAILR	TRAIL receptor
TRC40	Transmembrane Recognition Complex of 40 kDa
UPR	Unfolded protein response
VDAC2	Voltage-dependent anion-selective channel protein 2
WB	Western Blot
WT	wild-type
XIAP	X-linked inhibitor of apoptosis protein

## List of figures

Figure 1: Schematic of intrinsic and extrinsic apoptosis signalling. ....	5
Figure 2: Schematic structure of Bcl-2 proteins. ....	14
Figure 3: Structure and activation of Bcl-2 effector protein BAX. ....	17
Figure 4: Structure of Bcl-2 transmembrane domains. ....	27
Figure 5: Functions of Bcl-2 transmembrane domains (TMDs). ....	35
Figure 6: NEBuilder HiFi DNA assembly (Gibson assembly) reaction overview. ....	55
Figure 7: Principle and workflow of the NanoBiT assay to detect TMD interaction. ....	58
Figure 8: Coelenterazine-h is a suitable substrate for the NanoBiT split luciferase assay. ....	70
Figure 9: Fluorophore expression of co-transfected NanoBiT plasmids is comparable. ....	73
Figure 10: BAX-TMD homotypic interaction is a reliable positive control for the NanoBiT assay. ....	76
Figure 11: TMDs of BAX, BAK and BOK show a homotypic interaction pattern. ....	79
Figure 12: BAX-TMD interacts moderately with BCL-XL- and BCL-W-TMDs. ....	80
Figure 13: BAK-TMD interacts with both BCL-XL- and BCL-W-TMD. ....	82
Figure 14: BOK-TMD interacts with BCL-2-, BCL-XL- and BCL-W-TMDs. ....	84
Figure 15: BAX and BAK TMDs predominantly localise to mitochondria, TMDs of BOK to the ER. ....	87
Figure 16: Anti-apoptotic Bcl-2 TMDs have distinct subcellular localisation patterns. ....	90
Figure 17: TMDs of BOK and BCL-2 colocalise at the ER, not mitochondria. ....	92
Figure 18: Exchange of TMD in BAX to BAK- or BOK-TMD enhances BAX pro-apoptotic activity. ....	95
Figure 19: BAX inhibition by BCL-2 is abolished for BAX with BAK-TMD. ....	98
Figure 20: BAX TMD mutation modulates interaction capacity with wild-type BAX-TMD. ....	100
Figure 21: BAX TMD mutation drastically influences subcellular localisation of TMD peptides. ....	102
Figure 22: BAX TMD mutation modulates localisation but not clustering of BAX. ....	103
Figure 23: BAX S184D mutation abolishes colocalisation with BCL-2. ....	105
Figure 24: BAX TMD mutation modulates apoptosis and inhibition by anti-apoptotic proteins. ....	107
Figure 25: TMD exchange in BAK to BAX- or BOK-TMD has no influence on inhibition by BCL-2. ....	109
Figure 26: Colocalisation of BAK and BCL-2 is not affected by changes in TMD sequence. ....	111
Figure 27: Colocalisation of BOK and BCL-2 is dictated by their TMD sequences. ....	113
Figure 28: BOK-induced cell death is pronounced in absence of BCL-2. ....	114
Figure 29: BOK-induced Cytochrome C release is dampened by BCL-2 co-expression. ....	115
Figure 30: TMD exchange in BOK to BAX-TMD or BAK-TMD shifts localisation to Mitochondria. ....	117
Figure 31: BOK-induced apoptosis is inhibited by BCL-2 in a TMD-dependent manner. ....	120
Figure 32: BOK-TMD and BCL-2-TMD form stable heterotetramers in an ER membrane mimic. ....	123
Figure 33: Patient-derived BCL-2 TMD mutations abolish interaction with BOK-TMD. ....	126
Figure 34: BCL-2 TMD mutation A224D affects TMD peptide localisation. ....	128
Figure 35: BCL-2 TMD mutation A224D leads to diffuse localisation of full-length BCL-2. ....	130
Figure 36: BCL-2 TMD mutation A224D interferes with BCL-2 anti-apoptotic function. ....	132
Figure 37: BCL-2 reduces ER stress-induced cell death mediated by BOK. ....	135
Figure 38: Summary of hypothesized BOK mode of action and inhibition by BCL-2 via the TMD. ....	172

## List of tables

Table 1: Subcellular localisation of Bcl-2 proteins.....	31
Table 2: List of primary antibodies. ....	37
Table 3: List of secondary antibodies.....	38
Table 4: List of cell culture media and reagents.....	38
Table 5: List of human cell lines and bacteria. ....	39
Table 6: List of chemicals, buffers and solutions. ....	39
Table 7: List of selected consumables. ....	41
Table 8: List of enzymes used for cloning. ....	41
Table 9: List of instruments. ....	42
Table 10: List of kits.....	42
Table 11: DNA template and expression plasmids. ....	42
Table 12: Plasmids generated during the course of the present thesis.....	44
Table 13: List of oligonucleotides used as primers. ....	46
Table 14: List of software applications and online tools.....	49
Table 15: Overview of protein sequence references at UniProt protein data base (uniprot.org).....	50
Table 16: Overview of transmembrane domain amino acid sequences in generated plasmids.....	51
Table 17: PCR reaction mix.....	52
Table 18: PCR program.....	52
Table 19: Restriction digestion reaction mix.....	53
Table 20: Overview restriction digestion reactions and pursued applications. ....	53
Table 21: T4 DNA ligase reaction. ....	54
Table 22: Components of self-cast gradient polyacrylamide gels.....	62
Table 23: List of smart-pool siRNAs (Horizon Discovery).....	63
Table 24: BOK and BCL-2 TMD sequences used for molecular dynamics simulations. ....	65
Table 25: Comparison of NanoBiT substrates. ....	69
Table 26: Summary of TMD interactions identified via the NanoBiT luciferase assay.....	143
Table 27: Summary of TMD subcellular localisation found for mTurq2-conjugated TMD peptides....	149

## Abstract

Apoptosis is a form of programmed cell death which is frequently dysregulated in various diseases such as cancer. A key event of apoptosis is mitochondrial outer membrane permeabilization (MOMP) which is governed by the B-cell lymphoma 2 (Bcl-2) family of proteins. Bcl-2 proteins form a complex interaction network in which pro- and anti-apoptotic members mutually inhibit each other to promote cell death or survival. The network is defined by binding of the Bcl-2 homology 3 (BH3) motif and the hydrophobic groove. A new class of small-molecule drugs, so-called BH3 mimetics, that occupy the hydrophobic groove of anti-apoptotic Bcl-2 proteins is effective in cancer therapy. However, a growing body of evidence suggests that the far less studied C-terminal transmembrane domain (TMD) of Bcl-2 proteins, which traditionally functions as a membrane anchor, can act as an additional interaction interface.

To further elucidate interactions of the Bcl-2 protein family via the TMD, a cell-based assay was developed and validated which combines the bimolecular luciferase system NanoBiT fused to TMD sequences with simultaneous expression of fluorescent proteins for signal normalisation. Systematic analysis of TMD interactions between pro-apoptotic effector Bcl-2 proteins (BAX, BAK and BOK) and anti-apoptotic Bcl-2-like proteins (BCL-2, BCL-XL, BCL-W, MCL-1 and A1) revealed homotypic interaction among effector TMDs and interaction of effector TMDs with BCL-XL-TMD and BCL-W-TMD. Intriguingly, a yet undescribed interaction of BOK-TMD and BCL-2-TMD was identified. Subcellular localisation of fluorophore-conjugated TMD peptides provided evidence that some TMDs preferentially reside at mitochondria (BAX, BAK, BCL-XL, BCL-W), while others (BOK, BCL-2, MCL-1) predominantly colocalised with the endoplasmic reticulum (ER). TMD exchange and mutation in BAX confirmed a vital role of the BAX-TMD in BAX inhibition, while TMD exchange in BAK had negligible influence on BAK regulation by BCL-2. Furthermore, both colocalisation of BOK and BCL-2 as well as inhibition of BOK overexpression-induced cell death by BCL-2 depended on their TMD sequences. Accordingly, BCL-2 TMD mutation modulated interaction with BOK-TMD, subcellular localisation and BCL-2's anti-apoptotic capacity. Lastly, absence of BCL-2 promoted BOK-dependent ER-stress-induced cell death indicating a physiological context for the functional relevance of their TMD interaction. Thus, this work emphasizes that elucidation of the Bcl-2 TMD interactome is important for our understanding of apoptosis regulation and paves the way for future investigations of the TMD as a target for clinical intervention.

## Zusammenfassung

Apoptose ist eine Form des programmierten Zelltods, die häufig bei verschiedenen Krankheiten wie Krebs gestört ist. Ein Schlüsselereignis der Apoptose ist die Permeabilisierung der äußeren Mitochondrienmembran (MOMP), die von der B-Zell-Lymphom 2 (Bcl-2) Proteinfamilie gesteuert wird. Bcl-2-Proteine bilden ein komplexes Interaktionsnetzwerk, in dem sich pro- und anti-apoptotische Mitglieder gegenseitig zugunsten von Zelltod oder -Überleben hemmen. Das Netzwerk wird durch die Interaktion zwischen dem Bcl-2 Homologie 3 Motiv (BH3) und der hydrophoben Furche definiert. Eine neue Art von niedermolekularen Wirkstoffen, sogenannte BH3-Mimeticka, welche die hydrophobe Furche anti-apoptotischer Bcl-2 Proteine besetzen, ist wirksam in der Krebstherapie. Es verdichten sich jedoch Hinweise darauf, dass die weit weniger untersuchte C-terminale Transmembrandomäne (TMD) von Bcl-2 Proteinen, die traditionell als Membrananker fungiert, ebenfalls als Interaktionsfläche dienen kann.

Zur weiteren Aufklärung der Interaktionen in der Bcl-2-Proteinfamilie über die TMD wurde ein zellbasierter Assay entwickelt und validiert, bei dem das mit TMD-Sequenzen fusionierte bimolekulare Luziferase-System NanoBiT mit gleichzeitiger Expression von Fluorophoren zur Signalnormalisierung kombiniert wird. Eine systematische Analyse der TMD-Interaktionen zwischen pro-apoptotischen Effektor-Bcl-2-Proteinen (BAX, BAK und BOK) und anti-apoptotischen Bcl-2-ähnlichen Proteinen (BCL-2, BCL-XL, BCL-W, MCL-1 und A1) offenbarte homotypische Interaktionen zwischen Effektor-TMDs und Interaktionen von Effektor-TMDs mit BCL-XL-TMD und BCL-W-TMD. Interessanterweise wurde eine bisher unbekannte Interaktion von BOK-TMD und BCL-2-TMD identifiziert. Die subzelluläre Lokalisierung Fluorophor-konjugierter TMD-Peptide verdeutlichte, dass einige TMDs präferentiell in Mitochondrien (BAX, BAK, BCL-XL, BCL-W) lokalisiert sind, während andere (BOK, BCL-2, MCL-1) vorwiegend mit dem endoplasmatischen Retikulum (ER) kolokalisiert sind. TMD-Austausch und Mutation in BAX bestätigten eine wichtige Rolle der BAX-TMD bei der BAX-Inhibition, während der TMD-Austausch in BAK einen vernachlässigbaren Einfluss auf die BAK-Regulierung durch BCL-2 hatte. Darüber hinaus hingen sowohl die Kolokalisierung von BOK und BCL-2 als auch die Hemmung des durch BOK-Überexpression induzierten Zelltods durch BCL-2 von den TMD Sequenzen ab.

Dementsprechend modulierte TMD-Mutation von BCL-2 die Interaktion mit BOK-TMD, die subzelluläre Lokalisierung und die anti-apoptotische Kapazität von BCL-2. Letztlich steigerte die Abwesenheit von BCL-2 den BOK-abhängigen ER-Stress-induzierten Zelltod, was auf einen physiologischen Kontext für die funktionelle Bedeutung ihrer TMD-Interaktion hinweist. Somit hebt diese Arbeit hervor, dass die Aufklärung des Bcl-2-TMD-Interaktoms für unser Verständnis der Apoptose-Regulation wichtig ist und ebnet den Weg für zukünftige Untersuchungen der TMD als Ziel für klinische Interventionen.



# 1 Introduction

## 1.1 Apoptosis – a programmed cell death

In multicellular organisms there is a constant need for clearance of excess, damaged or aberrant cells (reviewed in (1)). Even under physiologically normal conditions, for example, during embryonal development or for the replacement of cells in adult organisms, a tight balance between cell proliferation and demise has to be maintained. For balancing the delicate homeostasis between cell renewal and removal, genetically encoded programs for cell death initiation developed throughout evolution termed as programmed cell death (PCD).

One form of PCD, apoptosis (denoted from Greek ‘falling of sth.’), and its phenotypic characteristics were first described in 1972 (2). Although molecular mechanistic details were yet to be revealed, Kerr *et al.* observed that cells which undergo apoptosis display distinct morphological features like condensation of chromatin, cell shrinkage and eventually membrane blebbing and breakdown into so-called apoptotic bodies - membrane-enclosed vesicles which can be phagocytosed by Macrophages and nearby cells (reviewed in (3)). Hence, apoptosis is resolved without spilling of cell contents and subsequent inflammatory responses of the surrounding tissue in contrast to accidental cell death, generally named as necrosis, which causes uncontrolled cell rupture because of harsh physical, chemical or pathological insults (reviewed in (4)).

However, stress irreversibly disrupting cellular homeostasis can also trigger other genetically regulated cell death signalling pathways which together with PCD are referred to as regulated cell death (RCD). The major modalities of RCD described by the Nomenclature committee on cell death (NCCD, (5)) are necroptosis, pyroptosis, ferroptosis, parthanatos, mitochondrial permeability transition (MPT)-driven necrosis, autophagy-dependent cell death, lysosome-dependent cell death, immunogenic cell death, entotic cell death, NETotic cell death and, more recently defined, alkaliptosis (6), cuproptosis (7) and PANoptosis (8). To complicate things further, many forms of RCD share common features, are activated simultaneously and display a high degree of interconnectivity (reviewed in (5)). In general, apoptosis is distinguished from other forms of RCD by occurring also (but not only) under physiologically healthy conditions and the dependency on a family of cysteine-aspartic proteases, the caspases.

These proteases are present in the cell as inactive pro-caspases (zymogens) which, once activated, cleave a variety of cellular substrates to promote apoptosis such as anti-apoptotic proteins, critical components of the cytoskeleton or other vital cellular machinery including cyclins and kinases. Of note, caspases are also found in pathways other than apoptosis such as pyroptosis (reviewed in (9)). According to their cellular function and substrate specificities, caspases of the apoptosis signalling pathway are subdivided into two groups, initiator caspases (caspase-8, -9 and -10) and executioner caspases (caspase-3, -6 and -7). As the names suggest, initiator caspases are integrated in apoptosis signalling upstream of the executioner caspases which, once activated, cleave a broad spectrum of cellular substrates ultimately resulting in the apoptotic phenotype (reviewed in (10)). Important examples for molecular features caused by caspase activity are the exposure of phosphatidyl serine (PS) on the extracellular leaflet of the plasma membrane (11), shredding of DNA by activation of caspase-activated DNase (12) and cleavage of poly(ADP-ribose) polymerase (PARP) (13). Some of these features are commonly used for detection of apoptosis, for example, flow cytometric detection of exposed PS using Annexin V conjugates (14), agarose gel-based detection of DNA fragmentation ("DNA laddering") or antibody-based detection of cleaved PARP (cPARP, (15)). However, it is worth mentioning that, in mammals, with exception of caspase-8, caspases rather accelerate than regulate cell death execution. In fact, only recently, the NCCD endorsed the notion that with activation of executioner caspases the point-of-no-return for cell death commitment in mammalian organisms has already been passed (16). Consequently, cell death cannot be fully prevented by pharmacological or genetic inhibition of caspases alone.

Apoptosis is highly conserved throughout the animal kingdom (17) and represents a major evolutionary leap in eukaryotes as it was already found in some of the most basal organisms including sponges and cnidarians (18). In mammals, the apoptosis signalling network can be split into two major arms depending on the origin of the apoptosis-inducing stimulus (Figure 1): i) The extrinsic apoptosis pathway is initiated by perturbations of the extracellular microenvironment detected by extracellular receptors such as the binding to death ligands (reviewed in (19, 20)). ii) The intrinsic apoptosis pathway is triggered by various intracellular sensors as consequence of intracellular stresses including the absence of growth factors or oxygen, DNA damage or damage by reactive oxygen species (ROS), endoplasmic reticulum (ER) stress as well as microtubular or mitotic defects (reviewed in (21–24)).

### 1.1.1 Extrinsic apoptosis signalling

As mentioned previously, the extrinsic apoptosis signalling pathway is initiated by receptors on the cell surface in consequence of, generally spoken, perturbations in the extracellular microenvironment (reviewed in (5)). There are two major types of extrinsic apoptosis signalling: cell death is either induced by death ligands, which initiate apoptosis by binding their cognate death receptors (DRs) on the cell surface or via autonomous cell death signalling of dependence receptors which are activated upon ligand deprivation (reviewed in (19, 20)).

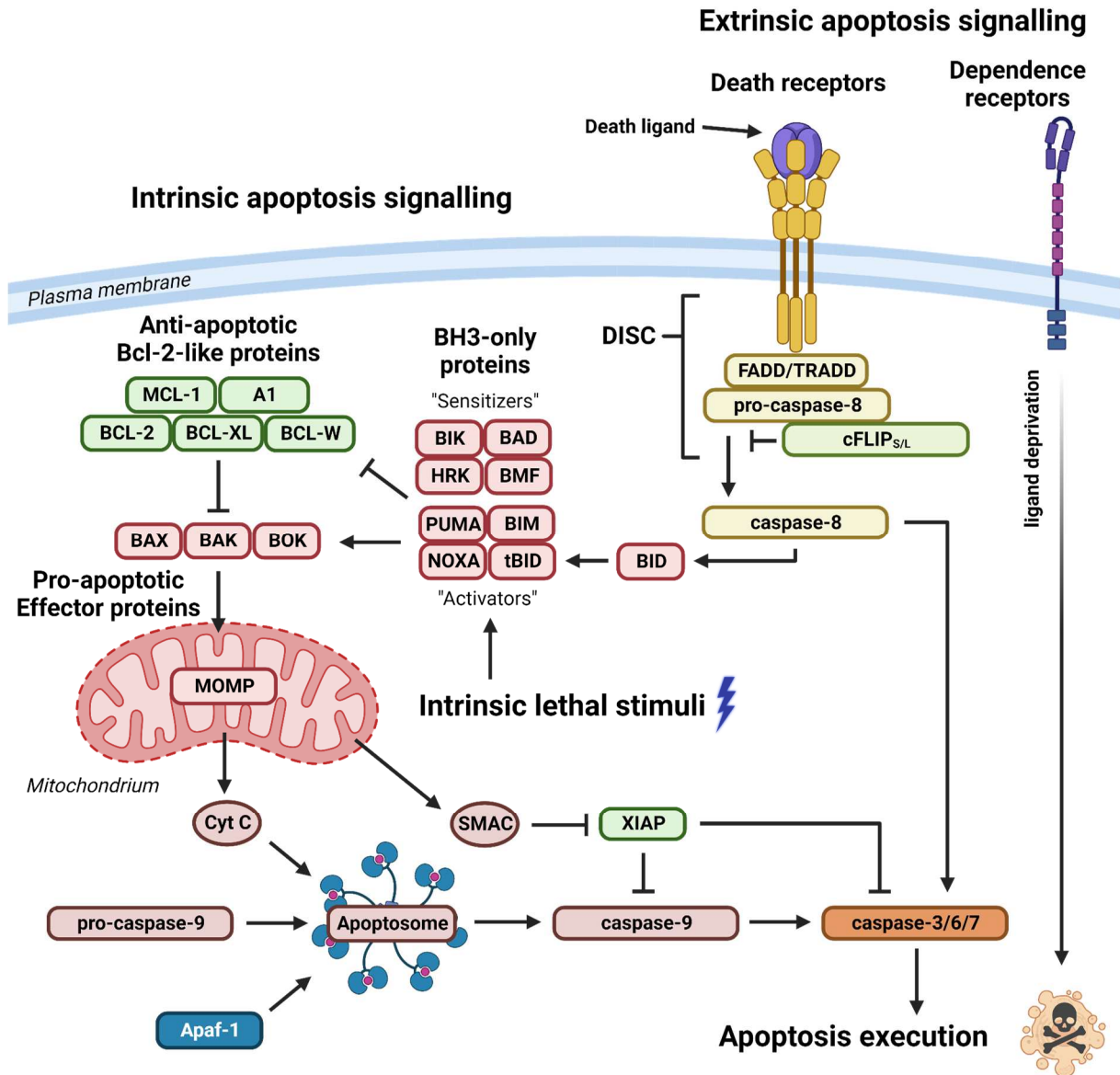
Death ligands such as FasL (also known as CD95L), tumor necrosis factor  $\alpha$  (TNF $\alpha$ ) or TNF-related apoptosis inducing ligand (TRAIL) are usually displayed on the membrane of immune cells but can also be cleaved off to enter solution. The respective DRs belong to the TNF receptor super-family (TNFRSF) in which Fas/CD95, TRAIL receptor 1 (TRAILR1, also known as DR4) and TRAIL receptor 2 (TRAILR2, also known as DR5) belong to the first subclass recruiting the adapter protein Fas-associated death domain protein (FADD) upon ligand binding, while TNF $\alpha$  receptors (TNFR1 and TNFR2) belong to the second subclass binding adapter protein TNFRSF1A associated via death domain protein (TRADD) (reviewed in (19, 20)).

In the case of FasL and TRAIL, upon binding on the extracellular cysteine-rich domains of their respective DRs, receptor oligomerisation is stabilised enabling recruitment of FADD by interaction of death domains (DDs) present in both FADD and the intracellular side of the DRs. FADD in turn functions as the basis of the death-inducing signalling complex (DISC) which forms by recruitment of pro-caspase-8/-10 and cellular FADD-like interleukin-1 $\beta$ -converting enzyme inhibitory proteins (cFLIP) via homotypical interactions of their death effector domains (DEDs). Pro-caspase-8/-10 and cFLIP participate in formation of long linear filaments which facilitates, in the case of pro-caspase-8/-10, homodimerization and proteolytic activation (25). Caspase activation, however, is kept in check mainly by association of short cFLIP isoforms (cFLIP<sub>s</sub> and cFLIP<sub>R</sub>), while the long cFLIP isoform (cFLIP<sub>L</sub>) still enables caspase-8/-10 activation to a limited extent (26, 27). Hence, competitive binding of cFLIP and pro-caspases is an important regulatory step of extrinsic apoptosis signalling underscored by the fact that transcription of the cFLIP-encoding gene (*CFLAR*) is directly controlled by pro-survival nuclear factor 'kappa-light-chain-enhancer' of activated B-cells (NF- $\kappa$ B) signalling (28).

For TNF $\alpha$ , activation of TNFR1 leads to the formation of diverse intracellular multiprotein complexes. In general, these complexes base on the association of TRADD with TNF receptor associated factor 2 (TRAF2), TRAF5 and receptor-interacting serine/threonine-protein kinase 1 (RIPK1) followed by recruitment of cellular inhibitor of apoptosis 1 (cIAP-1) and cIAP-2. Depending on the ubiquitination status of RIPK1 either so-called complex I or complexes IIa-c are formed (reviewed in (29, 30)). While complex I promotes proliferation and cell survival by activation of various cell survival pathways including NF- $\kappa$ B, c-Jun N-Terminal kinase (JNK) and p38 signalling, complexes IIa-c initiate cell death via caspase-8 activation and apoptosis (complexes IIa and IIb) or necroptosis (complex IIc). The diverse signalling of TNFR1, thus, exemplifies the complexity of cell death decisions and high degree of interconnectivity between signalling pathways. However, pleiotropic signalling is not unique for TNFR1 as pro-survival signalling is also mediated by some other DRs. Also TRAIL and FasL can trigger necroptosis, inflammation or pro-invasive signalling (reviewed in (31, 32)).

Besides DR signalling, extrinsic apoptosis comprises activation of dependence receptors of which approx. 20 different members are known to date (reviewed in (33)). Dependence receptors promote cell differentiation, proliferation and survival as long as their ligands are present, while apoptosis is actively initiated once the level of ligand falls below a specific threshold. The mechanisms of apoptosis induction are still not fully understood. Most frequently, dependence receptors undergo proteolytic cleavage by caspases, but also other cellular proteases, releasing or exposing a dependence domain responsible for recruitment and activation of additional caspases and other pro-apoptotic factors (34).

Pro-caspase-8/-10 activation facilitates apoptosis via two different pathways (reviewed in (10)). Caspase-8/-10 directly cleaves and activates executioner caspases. However, this is only sufficient for cell death commitment in so-called type I cells (e.g. mature lymphocytes). In type II cells (e.g. many cancer cells), executioner caspase activation is profoundly inhibited by members of the inhibitor of apoptosis (IAP) family such as X-linked inhibitor of apoptosis protein (XIAP), cIAP-1 and cIAP-2. Hence, cell death commitment in type II cells requires the caspase-8-catalysed proteolytic maturation of BH3-interacting domain death agonist (BID) to truncated BID (tBID). tBID translocates to mitochondria and promotes intrinsic apoptosis signalling which will be described in the following, thereby, representing one major interface between the extrinsic and intrinsic apoptosis pathway (35).



**Figure 1: Schematic of intrinsic and extrinsic apoptosis signalling.**

Colour coding: yellow = pro-apoptotic components / light green = anti-apoptotic components of the extrinsic apoptosis pathway. Red = Pro-apoptotic components / dark green = anti-apoptotic components of the intrinsic apoptosis pathway. Orange = pro-apoptotic components of apoptosis execution. Purple = pro-apoptotic stimuli. MOMP = Mitochondrial outer membrane permeabilization, Cyt C = Cytochrome C. DISC = death-inducing signalling complex. Adapted from Vitale *et al.* (2023) (16). Created with biorender.com.

### 1.1.2 Intrinsic apoptosis signalling

Intrinsic apoptosis signalling, as mentioned earlier, manifests after prolonged and irreversible intrinsic stress such as DNA damage or ER stress. However, intrinsic apoptosis signalling also occurs as a consequence of cell detachment and loss of integrin-dependent contacts, so-called anoikis (reviewed in (36)). Depending on the stressor and cellular sensor, various target proteins or genes are activated to promote apoptosis. In general, lethal intrinsic stress is characterised by fatal upregulation and/or activation of pro-apoptotic proteins and/or inhibition of anti-apoptotic proteins.

One prominent example for a cellular component involved in intrinsic apoptosis signalling is the tumour suppressor p53 (gene name: *TP53*), which functions as a central hub for DNA damage responses (but also other stress like hypoxia) regulating hundreds of target genes. When DNA damage is irreparable and persistent, p53 induces expression or release of the intrinsic apoptosis machinery including members of the B-cell lymphoma 2 (Bcl-2) family of proteins (reviewed in (37)). For persistent ER stress, on the other hand, intrinsic apoptosis can be mediated via the unfolded protein response (UPR). Although UPR induces clearance of unfolded proteins, for example, via the ER-associated degradation (ERAD) pathway, also apoptosis-inducing genes are targets of the UPR signalling cascade. For example, UPR-induced transcription factor C/EBP homologous protein (CHOP) upregulates expression of pro-apoptotic proteins such as TRAIL2, while suppressing expression and activity of anti-apoptotic Bcl-2 proteins such as B-cell lymphoma 2 (BCL-2) (38, 39). These two examples already illustrate the complexity and versatility how intrinsic stress signals are integrated in cell death signalling. However, all mechanisms culminate in the most critical event of intrinsic apoptosis signalling: mitochondria outer membrane permeabilization (MOMP). MOMP is regulated by an intimate interplay of pro- and anti-apoptotic members of the Bcl-2 family of proteins (reviewed in (40)). The Bcl-2 protein family consists of three major subgroups: i) pro-apoptotic effector proteins, ii) anti-apoptotic Bcl-2-like proteins and iii) pro-apoptotic BH3-only proteins. The anti-apoptotic family members such as BCL-2 itself, B-cell lymphoma-extra large (BCL-XL) or induced myeloid leukaemia cell differentiation protein (MCL-1) bind and sequester pro-apoptotic members. BH3-only proteins either inhibit anti-apoptotic members or, in addition, bind to and directly activate effector proteins. Once activated, the effectors Bcl-2-associated X protein (BAX) and Bcl-2 homologous antagonist killer (BAK) form pores in the mitochondrial outer membrane (MOM) which initiates MOMP.

Also Bcl-2-related ovarian killer (BOK) disputedly counts to the pore-forming effectors. However, BOK's role in apoptosis, as further discussed in section 1.2.1.3, is far less understood than that of the other effector proteins. Pore formation releases pro-apoptotic factors from the mitochondrial intermembrane space into the cytosol like cytochrome C (CytC) and second mitochondria-derived activator of caspases (SMAC, also known as DIABLO) (reviewed in (41)). The major contribution of CytC to apoptosis is the formation of the so-called apoptosome together with pro-caspase-9 and apoptotic protease activating factor-1 (Apaf-1). In a deoxyadenosine triphosphate (dATP)-dependent manner, Apaf-1 and CytC form a heptameric complex which exposes caspase recruitment domains (CARDs) of Apaf-1 molecules. Binding homotypically via their own CARD domains, pro-caspase-9 molecules associate to the complex. Caspase-9 activation is catalysed by formation of pro-caspase-9 homodimers and pro-caspase-9:Apaf-1 heterodimers/multimers (42–44). Active caspase-9 then cleaves and activates executioner caspases, particularly pro-caspase-3/-7, to mediate apoptosis. Caspase-9 as well as executioner caspase activation is counteracted by IAP proteins of which XIAP is the only IAP protein directly binding and inhibiting caspase-3, -7 and -9 activity (45). In contrast, proteins cIAP-1 and cIAP-2 bind to caspases as well but block apoptosis mainly by upregulation of other anti-apoptotic proteins such as cFLIP, caspase inactivation via ubiquitination followed by degradation and RIPK1 ubiquitination which promotes pro-survival NF- $\kappa$ B signalling (46, 47). However, upon MOMP IAPs are sequestered by released SMAC via its latent IAP-binding domain. Consequently, SMAC relieves IAP-mediated inhibition of caspase-3, -7 and -9 and accelerates apoptosis execution (48, 49).

Another characteristic consequence of widespread MOMP is the loss of the mitochondrial transmembrane potential ( $\Delta\Psi_m$ ).  $\Delta\Psi_m$  is mainly disrupted due to the release of electron transport chain-sustaining CytC and the subsequent impairment of ATPase function. Hence, cells suffer a breakdown of  $\Delta\Psi_m$ -dependent functions such as ATP synthesis which inevitably disrupts cellular bioenergetics (reviewed in (50)). Along these lines, the general view is that MOMP commits cells to death independent of executioner caspase activation which, as mentioned, merely accelerates cell death execution (16). But, caspases exert additional important functions, for example, cleavage of cyclic guanosine monophosphate – adenosine monophosphate synthase (cGAS) or Interferon regulatory factor 3 (IRF3) implemented in cytokine release and inflammatory signalling (51, 52).

### 1.1.3 Apoptosis in disease

As the preceding chapters underlined, the essential functions of apoptosis such as tissue homeostasis, embryonal development and removal of infected or abnormal cells require a tightly regulated network with a myriad of cellular components. Dysregulation of apoptosis, thus, can occur at various levels and has far-reaching consequences not only on cellular but also on a systemic level (reviewed in (16)). Therefore, apoptosis is naturally linked to many pathophysiological conditions and diseases. Of note, most of the following connections between apoptosis and disease were revealed by using mouse models comprising knockdown (KD) or knockout (KO) of genes and/or transgenic expression of proteins.

In neurodegenerative disorders, such as Alzheimer's and Parkinson's, apoptosis was found as a underlying mechanism for excessive neuronal cell death driven by various components of the apoptotic machinery including BH3-only proteins as well as effector proteins BAX and BAK (53–56). Along similar lines, apoptotic signalling has functional implications in a great number of neurological diseases including neuromuscular disorders such as amyotrophic lateral sclerosis (ALS), traumatic brain injuries, neurotoxicities, pre-/post ischemic injuries and retinal disorders (57–60). Studies generally agree that loss or inhibition of pro-apoptotic proteins as well as overexpression of anti-apoptotic proteins ameliorates disease. In the same way, impact of severe cardiovascular conditions was linked to apoptosis signalling, for example, in mouse models of myocardial infarction, cardiomyopathy, atherosclerosis and other myocardial dysfunctions (61–67). Adding to this, apoptotic proteins were found to be involved in development and progression of hepatic diseases including acute (ischemic) liver injury, viral hepatitis, cirrhosis as well as alcohol-related and alcohol-unrelated chronic liver diseases (68–72). Likewise, components of apoptosis signalling are implicated in kidney-specific pathologies such as acute (ischemic) kidney injury, renal fibrosis and other chronic kidney disorders (73–77). The other way round, the non-inflammatory character of apoptosis can limit the impact of autoimmune and inflammatory diseases. Here, blocked or impaired apoptosis mostly exacerbated disease progression, for example, in mouse models with autoimmune encephalomyelitis (recapitulating human multiple sclerosis) or chronic inflammatory diseases such as colitis (78–80). However, blockage of apoptosis can also limit auto-immune-dependent cell death, for example, in models of type 1 or type 2 diabetes emphasising the need for individual consideration (81, 82).



Such opposing effects might be explained by differences in the mainly affected cell populations like immune cells or their target cells. Of note, the role of DR signalling is rather complex in such diseases because of its pleiotropic character including apoptosis-unrelated pro-inflammatory signalling (reviewed in (30)). In contrast, a large body of evidence suggests a clear anti-infectious role of extrinsic and intrinsic apoptosis signalling (reviewed in (83)). In fact, also beyond apoptosis, RCD constitutes important protective measures against infections. Infected cells which undergo RCD do not facilitate pathogen reproduction and thereby limit harm to the host organism while propagating the host immune response. Thus, viruses and bacteria have developed various means to shut down RCD and apoptosis signalling. Examples are numerous reaching from viral homologs of anti-apoptotic Bcl-2 proteins and transcriptional activation of survival pathways to *M.tuberculosis*-mediated secretion of TNFR2 to neutralise the death-inducing effect of TNF on the cell surface (84–86).

However, it has to be mentioned that the high degree of interconnectivity between different RCD modalities and multifunctionality of pleiotropic signalling platforms such as pro-inflammatory and pro-survival signalling by certain DRs (reviewed in (30)) generally complicate the drawing of conclusions about the direct contribution of apoptosis to disease. That said, most disease scenarios do not allow for an isolated view on the apoptosis signalling pathway which is underlined by studies describing also major contributions of other RCD modalities in several of the above-mentioned diseases. For example, in certain settings also necroptosis and ferroptosis were described to be mainly responsible for neuron loss during Alzheimer's disease (87, 88), while other results suggest high interconnection of necroptosis and pyroptosis together with apoptosis in the host response to Influenza A virus (89, 90).

Finally, one of the most well studied roles of apoptosis signalling in disease is preventing the development and progression of neoplastic diseases (reviewed in (10)). 'Resisting cell death' is defined as one of the hallmarks of cancer which were first described by Hanahan and Weinberg (91). Hence, oncogenesis has been linked to apoptosis dysregulation in multiple ways including animal models of haematological malignancies as well as solid tumours. Especially many forms of leukaemia and lymphomas demonstrably rely on anti-apoptotic Bcl-2-like proteins BCL-2, BCL-XL and MCL-1 through deregulation of the Myc proto-oncogene protein (92–94).

Another major strategy of cancers to dodge apoptosis is the loss or inactivation of various pro-apoptotic Bcl-2 proteins counteracting, for example, the tumour-suppressive role of BAX in multiple cancer types (95–97). Apoptosis-regulating tumour suppressor genes such as p53 are deregulated or rendered inactive in many cancers (reviewed in (37)). Moreover, also anoikis is considered a part of onco-suppressive apoptosis signalling since some degree of cell detachment is required for cancer cells to attach on improper matrices and form metastases (98). Thus, cancer cells avoid anoikis generally by upregulation of cell death suppressive pro-survival pathways such as MAPK/ERK signalling (99).

Taken together, apoptosis harbours functional implications in numerous diseases and, in consequence, a great potential for therapy by pharmacological targeting. For blockage of apoptosis, caspase inhibition with compounds such as Z-VAD-FMK or Q-VD-OPh was tested in many preclinical settings (100–102). Absence or inhibition of caspases can redirect cell death to other RCD modalities, for example, necroptosis which substantially modulates the release of danger-associated molecular patterns (DAMPs) and the subsequent inflammatory and immunogenic response (reviewed in (103)). Therefore, caspase inhibition proved to be a vital tool in many disease models of neurodegenerative, metabolic and inflammatory diseases. In addition, other apoptosis inhibitors were developed for blocking DR signalling, neutralizing death ligands or mimicking functions of anti-apoptotic proteins such as XIAP-derived peptides. These strategies showed disease-ameliorating effects for multiple apoptosis-related diseases (104–106). However, none of these compounds are yet in clinical use. Especially in anti-cancer therapy many therapeutic strategies were developed aiming to induce or sensitize cells for apoptosis. Conventional chemotherapy as well as radiotherapy often induces apoptosis which is, however, not specifically targeted at cancer cells nor the apoptosis pathway (reviewed in (107)). The usage of death ligands or pro-apoptotic receptor agonists (PARAs) to kill cancer cells was long hoped to find application in the clinic because of compelling pre-clinical results (reviewed in (108)).

Of note, DR signalling generally has miscellaneous roles in cancer because of its implications in pro-survival and inflammation signalling which promotes rather than prevents tumour growth in some cases (109, 110). However, especially the potential of TRAIL as an anti-cancer agent was heralded for its outstanding ability to kill cancer cells while sparing healthy cells - an advantage that, in view of the low effect in the clinic, lost its significance (reviewed in (111, 112)). Hence, clinical usability of TRAIL and PARAs is still under investigation in combination with sensitizers, such as cyclin-dependent kinase 9 (CDK9) inhibitors which was effective in a wide range of cancers (113). On the other hand, to target IAP-dependent tumours SMAC-mimicking drugs (SMAC mimetics) were developed and by now entered several clinical trials (reviewed in (114)). The most successful advance in apoptosis-targeting drugs was achieved by development of so-called BH3-mimetics, small-molecule compounds which recapitulate the action of pro-apoptotic BH3-only proteins. These molecules demonstrated effective anti-cancer action in countless preclinical studies but also for use in other diseases such as autoimmune and pro-inflammatory disease (80, 115). One of these, the BCL-2-specific inhibitor ABT-199/Venetoclax, is to date the only FDA-approved anti-cancer drug targeting the apoptosis signalling pathway. Besides Venetoclax, many other BH3-mimetics are in clinical evaluation as further discussed in 1.2.4 (reviewed in (116)).

Despite of the striking importance of apoptosis across a broad panel of diseases including neurological, cardiovascular, renal, hepatic, autoimmune and inflammatory disorders, infections as well as cancer and the consequent extra-ordinary potential as a target for therapy, most apoptosis-targeting drugs exert limited efficacy. This poor record illustrates that further studies enlightening the molecular details of apoptosis signalling are urgently needed. Only one anti-cancer agent, namely Venetoclax, was approved for clinical application. The cellular role of the Bcl-2 protein family which is targeted by drugs like Venetoclax and the here outlined importance for anti-cancer therapy will be discussed in the next chapter.

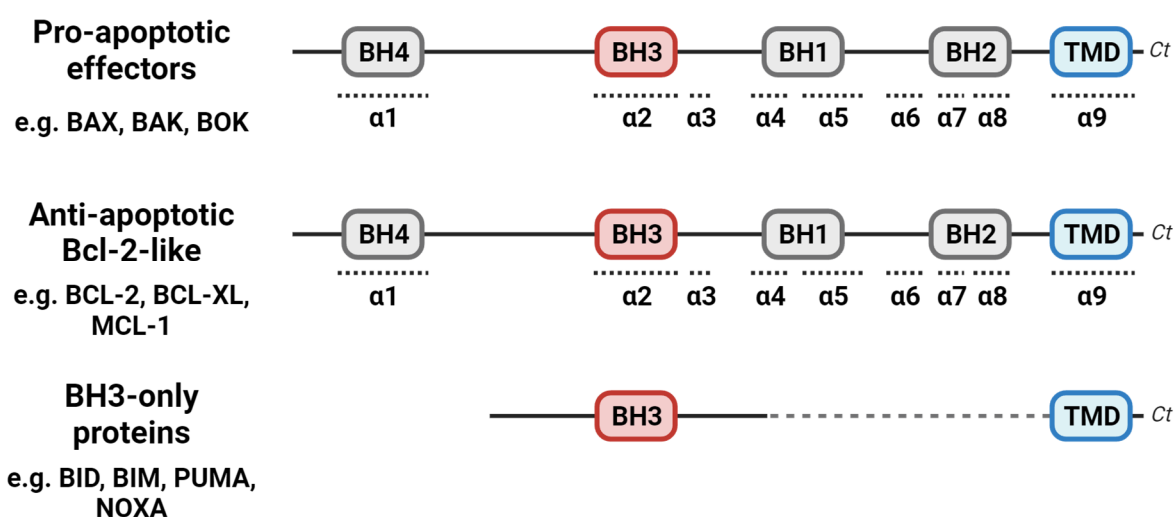
## 1.2 The Bcl-2 protein family

The critical step of intrinsic apoptosis, MOMP, is controlled by the Bcl-2 family of proteins. The first member and namesake of the family, the anti-apoptotic protein BCL-2, was discovered in the 1980s by cloning the breakpoint of the chromosomal translocation t(14;18) in human follicular B-cell lymphomas (117). Additional members of the Bcl-2 protein family were identified in the following decades of which all share the possession of at least one of the four different Bcl-2 homology (BH) motifs (also known as BH domains). According to their structure similarity and function in apoptosis signalling, the Bcl-2 protein family is divided into three major subgroups (reviewed in (118), Figure 2): Pro-apoptotic effector proteins responsible for pore formation (BAX, BAK and BOK) harbour all four BH motifs. Anti-apoptotic Bcl-2-like proteins (BCL-2, BCL-XL, Bcl-2-like protein 2 (BCL-W), MCL-1 and Bcl-2-related protein A1 (A1, also known as Bcl-2-related gene expressed in fetal liver (BFL-1)) also possess BH motifs 1-4. Both subgroups contain also a deep elongated hydrophobic cleft (hydrophobic groove, here in short: groove) which generally constitutes the binding site for BH3 motifs of other family members. The third subgroup comprises the more distantly related pro-apoptotic BH3-only proteins characterised by (as their name indicates) containing solely the BH3 motif. There are two modes of action proposed for BH3-only proteins: 'sensitizer' BH3-only proteins (e.g. Bcl-2-associated agonist of cell death (BAD), Bcl-2-modifying factor (BMF), Bcl-2-interacting killer (BIK), activator of apoptosis hara-kiri (HRK)) bind and sequester anti-apoptotic family members rendering them inactive and thereby indirectly promote pore-formation by effector proteins. 'Activator' BH3-only proteins (e.g. p53-upregulated modulator of apoptosis (PUMA), Bcl-2-interacting mediator of cell death (BIM), tBID, Phorbol-12-myristate-13-acetate-induced protein 1 (PMAIP1, also known as NOXA)) additionally bind to and directly activate effector proteins.

Both effectors and anti-apoptotic Bcl-2-like proteins (summarized as multi-domain proteins) fold into a generally globular protein structure consisting of nine  $\alpha$ -helices ( $\alpha$ 1- $\alpha$ 9). While the BH3 motif is situated in helix  $\alpha$ 2, the groove is formed by parts of helices  $\alpha$ 2- $\alpha$ 5. The other BH motifs are located either at helix  $\alpha$ 1 (BH4) or in vicinity of helix  $\alpha$ 5 (BH1) and helices  $\alpha$ 7- $\alpha$ 8 (BH2). Of note, BH3-only proteins, with exception of BID, generally remain unstructured in solution (119).

The decision over life and death in intrinsic apoptosis results from the balance of Bcl-2 protein interactions between pro- and anti-apoptotic forces. This equilibrium is influenced by multiple factors including protein abundance, subcellular localisation, stability, post-translational modifications and binding affinities between different family members (reviewed in (40)). Thereby, binding affinities are classically defined by the BH3:groove interaction. The individual amino acid sequences cause varying binding affinities among different family members and, thus, lay the basis for a complex interaction network. Some Bcl-2 proteins can bind a broad panel of BH3 motifs while others are less promiscuous in their binding specificities (120). Hence, the calculation of the net interactions is rather complex and was approximated with different frameworks for Bcl-2 interactions which were postulated throughout the last 30 years.

The original 'rheostat' model by Korsmeyer and colleagues merely determined the ratio of pro- and anti-apoptotic protein as the deciding factor for cell fate (121), which the authors redefined in the 'direct activation' model implementing the concept of activator and sensitizer BH3-only proteins (122). The 'embedded together' model highlights the role of the membrane as an interaction platform for Bcl-2 proteins as part of the interaction equilibria (123, 124). Furthermore, Llambi *et al.* presented the 'unified' model for Bcl-2 interactions comprising two modes of MOMP prevention by anti-apoptotic proteins – either by sequestration of activator BH3-only proteins (Mode 1) or effector proteins (Mode 2) (125). Lastly, using cells with multiple KO of Bcl-2 proteins Chen and coworkers introduced the 'hierarchical' model of Bcl-2 interaction which extends the previous models by autoactivations of effector proteins in absence of anti-apoptotic Bcl-2 proteins (126). More recently, the spontaneous activation of effector proteins was validated in cells lacking either all BH3-only proteins (OctaKO cells) or all Bcl-2 proteins (Bcl-2allKO cells) underlining that the membrane environment is sufficient to directly activate effector proteins (127) – a concept which was taken up for creation of the 'membrane-mediated spontaneous' model (128).



**Figure 2: Schematic structure of Bcl-2 proteins.**

Positions of BH (= Bcl-2 homology) motifs and C-terminal (Ct) transmembrane domain (TMD) are shown as boxes. Position of  $\alpha$ -helices ( $\alpha 1 - \alpha 9$ ) in effector and Bcl-2-like proteins are indicated as dashed lines. Grey dashed line in BH3-only protein structure indicates gap. Adapted from Uren *et al.* (2017) (148). Created with Biorender.com.

## 1.2.1 Pro-apoptotic effector proteins

### 1.2.1.1 BAX

The first-discovered member of the effector subgroup is BAX which was found to predominantly localise to the cytosol in healthy cells and translocate to mitochondria upon cell death stimuli (129). This snapshot description, however, is based on a dynamic equilibrium of BAX molecules constantly shuttling between cytosol and MOM – a process termed as retrotranslocation (130). BAX retrotranslocation is mediated by anti-apoptotic Bcl-2 proteins, foremost BCL-XL. Consequently, blocked or impaired retrotranslocation leads to BAX accumulation at the MOM, spontaneous BAX activation and MOMP. In the cytosol, BAX resides in an inactive, predominantly monomeric form (131, 132). Inactive BAX monomers (Figure 3A) possess a unique structure among effector proteins with the C-terminal (Ct)  $\alpha 9$  helix folded back onto the protein core, more precisely, occupying the groove (131, 133). Upon BAX activation, for example, by tBID the  $\alpha 9$  helix is removed from the protein core which facilitates BAX insertion into the MOM via the  $\alpha 9$  helix - also referred to as the transmembrane domain (TMD) (134). Multiple studies validated that BAX undergoes specific conformational changes when inserted into the MOM.

The current view is that the N-terminal (Nt)  $\alpha 1$  helix and the so-called latch domain (helices  $\alpha 6 - \alpha 8$ ) dislodge from the core regions (helices  $\alpha 2 - \alpha 5$ ), while parts of the BH3 motif become exposed (125, 135–137). According to the ‘hit-and-run’ model, activator:effector interactions are of transient nature and, once activated, BAX dissociates from tBID to engage and activate additional BAX monomers (135). In the active conformation, BAX forms homodimers in the MOM via the now enabled BH3:groove interaction (Figure 3B, C) (135–138). However, through the same interaction interface, active BAX can be intercepted by anti-apoptotic proteins such as BCL-XL and BCL-2 (139). BAX homodimerization represents the key event for BAX oligomerisation since the globular monomers switch to an amphipathic platform-like shape responsible for increasing protein-lipid interactions (135, 136). Recent structural analyses support two models of BAX oligomerisation (140): The ‘clamp’ model by Bleicken and colleagues comprises MOM-spanning dimers with  $\alpha 6$  helices “clamping” the membrane and anti-parallel TMDs (138), while the model proposed by Mandal *et al.* involves a parallel TMD composition of dimers concentrated to the upper edge of the pore (141). Both models support the notion of dimer-dimer interactions via helices  $\alpha 6 - \alpha 9$ . Macroscopically, BAX oligomers were visualised as aggregates, lines, arcs and ring structures which can pierce the lipid bilayer (142). In cellular membranes as well as artificial liposomes, BAX pores with diameter of  $\sim 50$  nm were observed (134) which allow the release of molecules such as Cyt C and SMAC. BAX pores, however, can reach an extremely large size to form so-called “macropores” sufficient to release mitochondrial DNA to the cytosol which reportedly leads to type I interferon secretion in absence of active caspases (143).

#### 1.2.1.2 BAK

BAX’s unlike twin is the closest-related protein BAK (144). In contrast to BAX, BAK is constitutively localised to mitochondria with the Ct TMD permanently inserted into the MOM (145). BAK mitochondrial localisation mainly depends on interaction with a large mitochondrial complex including voltage-dependent anion-selective channel protein 2 (VDAC2) (146) – a voltage-sensitive ion channel which is also reportedly involved in recruiting BAX to mitochondria (147). The mode of BAK activation is similar to that of BAX (reviewed in (148)) and even formation of BAX/BAK heterodimers was described - however, present to a much lesser extent than homodimerization (137). Functional interplay is further supported by a recent study revealing distinct dynamics of BAX and BAK pore formation conditioning mutual recruitment and pore co-assembly (149).

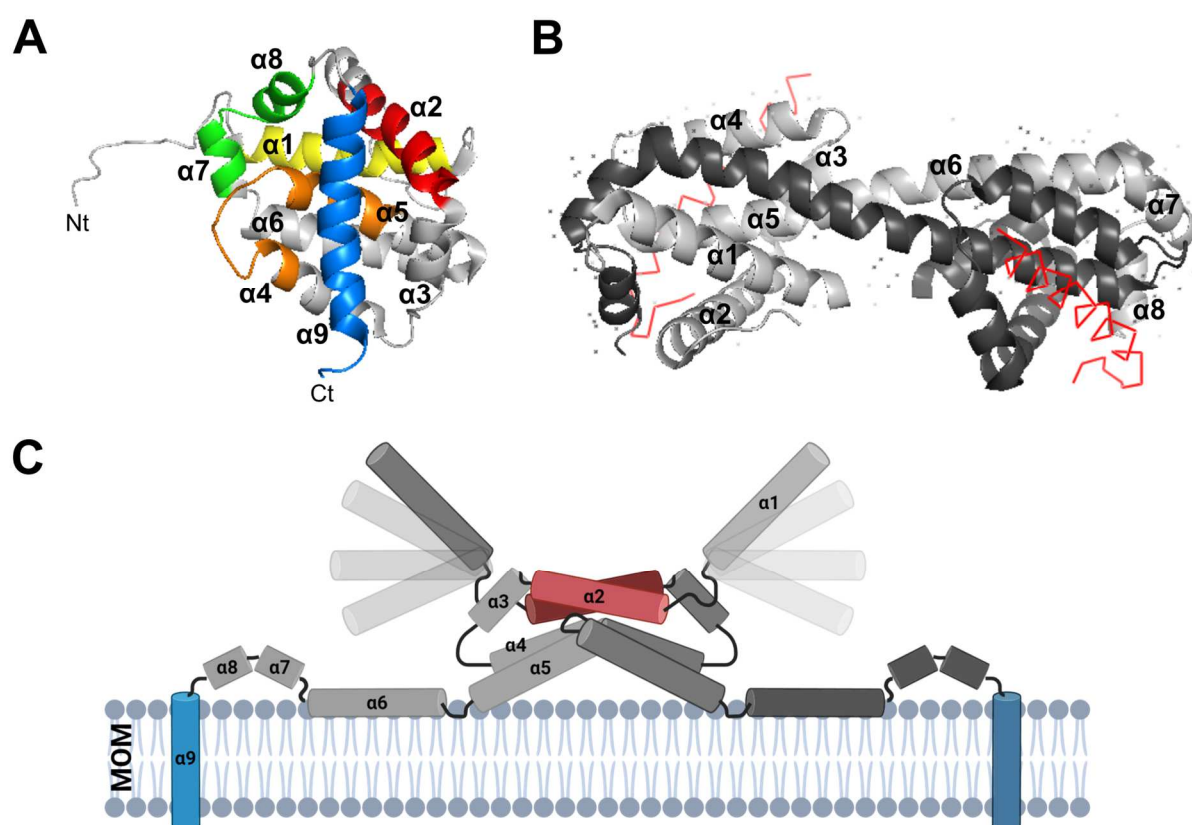
Some redundancy of BAX and BAK (gene name: *BAK1*) function was also found in KO mice which reach adulthood without major complications after single ablation of either *BAX* or *BAK1*, while *BAX<sup>-/-</sup>BAK1<sup>-/-</sup>* double KO (DKO) proved to be prenatally lethal in over 90% of cases (150). Despite of apparent functional redundancy of BAX and BAK, differences in stimuli-dependent engagement as well as binding preferences, for example, preferential binding of BCL-2 to BAX over BAK was reported emphasising the importance of the respective cellular context such as the expression pattern of other Bcl-2 proteins (151, 152).

### 1.2.1.3 BOK

The final and most controversial effector protein, BOK, was initially grouped together with BAX and BAK because of their sequence similarity when BOK was identified in a yeast two-hybrid assay which suggested interaction with anti-apoptotic MCL-1 and A1 (153). Pro-apoptotic activity of BOK was repeatedly confirmed after overexpression or in response to pro-apoptotic stimuli (154, 155). Since BOK was found frequently deleted in cancers, BOK was attributed a tumour suppressor role (156). In contrast to BAX and BAK, BOK is predominantly localised to membranes of the ER and Golgi apparatus by its TMD (157). Despite of ER localisation, several studies support the notion of BOK as a bona fide pore-forming effector protein: Einsele-Scholz and colleagues observed BOK oligomerisation at mitochondria after BOK overexpression and apoptosis promotion in absence of BAX and BAK (158). In addition, Ct truncated BOK permeabilizes liposomes as reported by Fernández-Marrero *et al.* (159). Just recently, visualization of BOK pores in liposomes and mitochondria using super-resolution microscopy revealed a mode of pore formation similar to pores of BAX and BAK. Here, pore formation was not affected by anti-apoptotic Bcl-2 proteins but limited by BOK's subcellular localisation (160). In line, regulation of BOK activity was postulated not to rely on interaction with anti-apoptotic Bcl-2 proteins, but on proteasomal degradation via the ERAD pathway (161). Accordingly, BOK is a constitutively active effector protein inducing cell death once stabilized. However, the mode and physiological role of BOK-induced apoptosis remains elusive and is still a matter of debate. Although BOK was found to be widely expressed in tissues, BOK KO, *BAX<sup>-/-</sup>BOK<sup>-/-</sup>* as well as *BAK1<sup>-/-</sup>BOK<sup>-/-</sup>* mice developed and reproduced without major morphological aberrations suggesting a completely redundant or more specialised role for BOK (162). Indeed, there is evidence that BOK deficiency confers protection specifically against ER stress-induced apoptosis (163).



Also, it was reported that BOK-induced apoptosis depends on pore-forming activity of BAX and BAK (157). BOK's function as an ER-stress sensor is further backed by findings of Schulman *et al.* showing that virtually all cellular BOK is bound to inositol 1,4,5-trisphosphate receptors (IP3Rs) which function as calcium ( $\text{Ca}^{2+}$ ) channels in ER membranes (164, 165). This added another layer of BOK regulation since IP3R-binding protects BOK from degradation via the ERAD pathway, while, at the same time, blocking BOK pro-apoptotic activity. Recently, BOK's function at the ER was further underscored by a role of BOK in controlling ER proteostasis (166) and mediating  $\text{Ca}^{2+}$  influx into mitochondria via IP3Rs at mitochondria-associated membranes (MAMs) which promotes apoptosis (167). Independent of apoptosis, BOK was also assigned a metabolic role to promote mitochondrial fusion and, hence, influence mitochondrial bioenergetics, for example, mitochondrial spare respiratory capacity and  $\Delta\Psi_m$  (168).



**Figure 3: Structure and activation of Bcl-2 effector protein BAX.**

**A** – Ribbon diagram of monomeric, inactive BAX adapted from Suzuki *et al.* (2000) (133) (protein data bank (PDB): 1F16).  $\alpha$ -helices ( $\alpha 1$ - $\alpha 9$ ) and N-/C-terminus (Nt/Ct) are labelled. Colours indicate motifs BH1 (orange), BH2 (green), BH3 (red) and BH4 (yellow) as well as transmembrane domain (TMD, blue). **B** – Ribbon diagram of C-terminally truncated BAX $\Delta$ C21 homodimer from Czabotar *et al.* (2013) (135) (PDB: 4BD6). Helices  $\alpha 1$ - $\alpha 8$  are labelled in the light grey BAX molecule (symmetrical equivalent in dark grey molecule). Bound BID BH3 peptides are shown as red wires. **C** – Schematic of membrane-inserted BAX dimer adapted from Bleicken *et al.* (2018) (140).  $\alpha$ -helices ( $\alpha 1$ - $\alpha 9$ ) are labelled in the light grey BAX molecule (symmetrical equivalent in dark grey molecule). Colours indicate BH3 motifs (red) and TMDs (blue). MOM = mitochondrial outer membrane (top layer faces the cytosol).

## 1.2.2 Anti-apoptotic Bcl-2-like proteins

### 1.2.2.1 BCL-2

The founding-member of the family, anti-apoptotic BCL-2, is probably the most intensively studied anti-apoptotic Bcl-2 protein and best characterised by its “guardian” function to counteract BAX- and BAK-induced apoptosis via the BH3:groove interaction (169, 170). However, there are possible additional interaction interfaces vital for apoptosis inhibition involving the BH4 motif and Ct TMD of BCL-2 (169, 171). Importantly, also additional functions of BCL-2 were described concentrated at the ER to which BCL-2 is predominantly localised via its TMD in healthy cells (172). Recently, Lalier *et al.* identified the translocase of the outer membrane (TOM) subunit TOM20 as a key mediator for shuttling BCL-2 between ER, MAMs and the MOM where BCL-2 mainly exerts its “guardian” function (173). At the ER, BCL-2 is involved in calcium signalling by binding to IP3Rs via the BH4 motif (174). Reportedly, BCL-2 binding to IP3Rs promotes Ca<sup>2+</sup> oscillation, periodical flux of small Ca<sup>2+</sup> amounts from the ER to cytosol and mitochondria which balances Ca<sup>2+</sup> homeostasis and promotes cell survival (175). On the other hand, BCL-2 was proposed to lower the Ca<sup>2+</sup> levels in the ER which limits the pro-apoptotic potential of Ca<sup>2+</sup> efflux from the ER (176). Also direct BCL-2-dependent inhibition of major Ca<sup>2+</sup> efflux from IP3Rs confers protection against apoptosis underlining the versatility of BCL-2’s anti-apoptotic role (177). The means by which BCL-2 regulates IP3R function are likewise manifold, for example, by direct binding, maintaining IP3R phosphorylation status or serving as an adapter protein for other regulatory proteins (reviewed in (178)). Furthermore, BCL-2 regulates Ca<sup>2+</sup> signalling by additional mechanisms such as binding to sarco/endoplasmic reticulum ATPases (SERCA) or inhibition of ryanodine receptors and Na<sup>+</sup>/Ca<sup>2+</sup> exchangers (179–181). Last, but not least, because of BCL-2’s multifaceted anti-apoptotic function, it is involved in survival strategies of many, foremost haematological, malignancies and was early recognised as an important cellular oncogene (182).

### 1.2.2.2 BCL-XL

BCL-XL shares high sequence similarity (45%) with BCL-2. However, both proteins have functional differences in several critical points. For example, a lysine in the BH4 motif of BCL-2 which is exchanged to aspartic acid in BCL-XL renders BCL-XL unable to overtake BH4 motif-mediated functions of BCL-2 at the ER, while the Ct TMD of BCL-XL localise it to the MOM (172, 177).

Nevertheless, also BCL-XL seems to be implicated in pro-survival Ca<sup>2+</sup> signalling – also by binding to IP3Rs (183). Another previously mentioned key function of BCL-XL is the retrotranslocation of active BAX from the MOM to the cytosol. Of note, BCL-XL-mediated retrotranslocation was also shown for BAK to a minor extent despite of BAK's constitutive localisation to mitochondria (130). In steady state, BAX/BCL-XL heterodimers constantly shuttle to the cytosol where BAX is released. Thus, BCL-XL functions as a competitor for BAX oligomerisation, a facet well-studied in conjunction with counteraction by tBID (184). Upon identification of the *BCL-X* gene, also a short isoform, BCL-XS, was found which lacks the BH1 and BH2 motifs due to alternative splicing. Hence, BCL-XS as well as caspase-cleaved BCL-XL exert pro-apoptotic activity similar to that of BH3-only proteins by binding BCL-XL and BCL-2 (185, 186). Splicing ratio of BCL-XL to BCL-XS depends on multiple factors including presence and activity of certain serine/arginine-rich proteins, heterogeneous nuclear ribonucleoproteins and RNA binding proteins which either promote or inhibit splice site selection in the critical Exon 2 for *BCL-X* alternative splicing. Consequently, these proteins dictate *BCL-X* gene-associated apoptosis sensitivity or resistance (reviewed in (187)). Consistently, *BCL-X* splicing is often dysregulated during oncogenesis and can serve as a prognostic marker in some malignancies (188–190).

### 1.2.2.3 *BCL-W*

Most similar to BCL-XL is BCL-W with a sequence similarity of 51%. Although BCL-W is known to function similar to BCL-XL and BCL-2 by sequestering pro-apoptotic proteins such as BAX and BAK, much less is known about binding affinities or the physiological role. Similar to BCL-XL, the Ct TMD localises BCL-W to the MOM. However, BCL-W is mainly localised to the cytosol in healthy cells (191). Interestingly, similar to cytosolic BAX, the TMD of cytosolic BCL-W seems to be bound in the groove. However, the hereof resulting increased conformational flexibility seems to decrease binding affinity of BCL-W to pro-apoptotic siblings compared to BCL-XL (192, 193). Upon apoptosis, cytosolic BCL-W localisation shifts towards the MOM. Thus, BCL-W recruitment to the MOM was hypothesized to represent an early buffering system to neutralize pro-apoptotic proteins (194, 195). In addition to its canonical anti-apoptotic function, for example, vital for spermatogenesis (196), BCL-W is involved in senescence, migration and invasion processes and thus is relevant for development of malignant phenotypes in different cancers (197–199).

#### 1.2.2.4 MCL-1

The *MCL1* gene was first isolated from ML-1 human myeloid leukaemia cells by Kozopas *et al.* who already postulated its pro-survival activity (200). Indeed, MCL-1's function as a canonical anti-apoptotic protein blocking BAX- and, more potently, BAK-induced apoptosis was thoroughly investigated and confirmed (reviewed in (201)). MCL-1 structure and regulation, however, shows some interesting peculiarities mainly based on a prolonged Nt segment. As one of few Bcl-2 proteins, MCL-1 can be localised to the mitochondrial matrix through a Nt targeting sequence which is cleaved off upon matrix insertion. Here, MCL-1 evidently impacts on mitochondrial bioenergetics in various ways, for example, by facilitating mitochondrial fusion, ATP production and respiration (202). In addition, MCL-1 was found to localise to the MOM, MAMs and ER where it is also involved in Ca<sup>2+</sup> signalling (203, 204). Another important feature of MCL-1's Nt region are four, so-called PEST regions which serve as a degradation signal and phosphorylation site (200). Consistently, MCL-1 molecules were shown to have a relatively short half-life compared to other Bcl-2 proteins so that MCL-1 function is sensitively regulated through proteasomal degradation (205). In addition, the preferential binding partner of MCL-1 is the BH3-only protein NOXA which facilitates phosphorylation and degradation of MCL-1 (206). Moreover, MCL-1 levels substantially change throughout cell cycle phases and degradation is initiated upon persisting problems during cell cycle progression which led to the hypothesis of MCL-1 working as a "mitotic clock" (207). Similar to BCL-XL, also for MCL-1 alternative splicing variants and caspase-cleavage products with pro-apoptotic activity were found pointing out additional means of MCL-1 regulation (208, 209). The various ways of how MCL-1 is regulated (post-)transcriptionally and post-translationally, make it a delicate target for dysregulation as found in many cancers (reviewed in (201, 210)).

### 1.2.2.5 A1/BFL-1 and others

The anti-apoptotic protein A1/BFL-1 (here in short: A1) is the smallest anti-apoptotic Bcl-2 protein and less studied than most of its anti-apoptotic siblings. While A1 localisation was vaguely associated to the ER, nuclear envelope and mitochondria dependent on alternative splicing/truncation of the C-terminus (211–213), A1 potentially intercepts BH3-only proteins and effector proteins to inhibit apoptosis (170, 214). Conversely, A1 proteolytic cleavage was reported to switch A1 to a pro-apoptotic state. Cleavage of A1 by  $\mu$ -calpain is dependent on proteasomal turnover of A1 and inducible by TNF $\alpha$  and cycloheximide (215). Similar to MCL-1, A1 turnover is rather quick (<1 h) compared to other anti-apoptotic Bcl-2 proteins. Uniquely, A1 contains an amphipathic  $\alpha$ 9 helix instead of a bona fide Ct TMD which's presence was shown to mediate A1 degradation by facilitating A1 polyubiquitination next to anchoring A1 to membranes (213, 216). Adding to this, an exposed cysteine-residue (C55) in A1 was found to be involved in BH3 motif binding (217).

In addition to the above described anti-apoptotic Bcl-2-like proteins which are relevant for the work in this thesis, there are also other anti-apoptotic Bcl-2 homologs that have either been little studied or found in other taxa. Worth mentioning is the last identified and probably most obscure member present in humans, BCL-B (also known as BCL2L10). BCL-B contains all four BH motifs as well as a predicted Ct TMD (218). BCL-B also binds pro-apoptotic family member BAX (but not BAK) to counteract apoptosis. Besides a potential role in autophagy (219), little is known about BCL-B *in vivo* function. However, it was reportedly upregulated in many cancers (220). Of note, two prominent examples for anti-apoptotic Bcl-2 homologs in other taxa are the *C.elegans* BCL-2 homolog CED-9 or *Drosophila*-derived BUFFY (221, 222).

### 1.2.3 BH3-only proteins

#### 1.2.3.1 Canonical pro-apoptotic BH3-only proteins

As mentioned, BH3-only proteins are either classified as sensitizers (including BAD, BIK, HRK, BMF) or activators (including PUMA, NOXA, BIM, tBID) depending on their ability to either efficiently interact with and inhibit anti-apoptotic Bcl-2-like proteins or, in addition, interact with and activate effector proteins. Conventionally, the pro-apoptotic function of BH3-only proteins depends on the binding of their BH3 motif into the groove of their binding partners (reviewed in (223)).

Binding affinities of BH3-only proteins to other Bcl-2 proteins can vary substantially based on the residues in their specific binding regions. Thus, some BH3-only proteins possess a broad binding spectrum, while others are rather specific. Particularly, activator BH3-only proteins tBID, PUMA and BIM efficiently bind to all anti-apoptotic siblings and pro-apoptotic BAX and BAK, the sensitizer BAD binds to BCL-2, BCL-XL and BCL-W, while NOXA is the lead-example for a specific MCL-1 antagonist (224–226). Although for sensitizers there is generally no empirical evidence for interaction with and activation of effector proteins (122), there is no consent on an affinity threshold which differentiates sensitizers from activators which causes some discord about the grouping of BH3-only proteins. In the case of NOXA, it bound and activated BAX *in vitro* – the reason why it is classified as an activator (227). However, the binding affinity is so low ( $K_D \sim 25 \mu\text{M}$ ) that it barely has any physiological relevance at nanomolar concentrations of most Bcl-2 proteins in the cell (reviewed in (40)). Thus, NOXA is occasionally grouped as a sensitizer rather than activator (40, 228).

To further complicate the subgroup composition, *in silico* analyses suggest another distinct group related to the BH3-only protein BID including less known Bcl-2-related proline rich protein (BPR), BCL-rambo, BCL-Gonad (BCL-G) and Bcl-2 family kin protein (BFK) which with regard to their sequence are BCL-2 homologs (reviewed in (229)). However, the apoptotic function of these proteins is divergent and remains poorly investigated (with exception of BID).

### 1.2.3.2 *Non-canonical BH3-only proteins*

In addition to the canonical BH3-only proteins, the subgroup of BH3-only proteins also comprises a large number of 'non-canonical' BH3-only proteins which are Bcl-2-unrelated proteins containing a BH3 motif. For instance, BCL-XL was found in complex with Beclin-1, a protein which also possesses a BH3 motif and is involved in autophagy regulation (230). Also previously mentioned IP3Rs possess two putative BH3 motifs involved in binding of BCL-XL (231). Other examples are the E3 ubiquitin ligase Mule which binds to the groove of MCL-1 via a BH3 motif catalysing MCL-1 ubiquitination and degradation (232) and the recently identified activation of BAK by peroxisomal testis-specific 1 (Pxt1) (233). However, the function of BH3 motifs in many such proteins and their role in apoptosis is yet to be defined and not necessarily linked to interaction with canonical Bcl-2 proteins, for example, in the case of BCL2/adenovirus E1B 19kd-interacting proteins (BNIPs) (224). Especially application of bioinformatic tools produces vast lists of yet-uncharacterised BH3-only candidates which is, however, dependent on the chosen consensus sequence. In fact, the structural as well as functional definition of the BH3 motif is one of the ongoing major debates in the field (reviewed in (234)).

It is also worth mentioning that most of the binding affinities of BH3-only proteins, but also other Bcl-2 proteins, were assessed with BH3 motif-containing peptides. Hence, data of physiological affinities between full-length Bcl-2 proteins are insufficient to deliver a precise map of Bcl-2 protein interactions. Nevertheless, peptides of BH3-only proteins constituted a valuable basis for the development of the previously mentioned specific small-molecule inhibitors of anti-apoptotic Bcl-2-like proteins, the BH3 mimetics. One of the first developed and effective BH3 mimetics, ABT-737, was based on the BH3 motif of BAD and likewise showed specific affinity to BCL-2, BCL-XL and BCL-W (235). The hereof arising importance of BH3 mimetics in cancer therapy will be further discussed in the following chapter of this thesis.

#### 1.2.4 Bcl-2 protein interactions and anti-cancer therapy

As discussed in 1.1.3, Bcl-2 proteins play a central role for oncogenesis and resistance of cancers towards apoptosis. Various mechanisms either lead to downregulation or inactivation of pro-apoptotic members or upregulation/activation of anti-apoptotic members. Cancer cells generally seem to depend more on apoptosis blockage than normal cells since oncogenesis is often linked to accumulation of cellular stress, for example, replication stress or metabolic stress (reviewed in (236, 237)). This stress results in generally higher expression levels of pro-apoptotic proteins engaging effector proteins to induce MOMP (238). Also many therapies aim to increase cellular stress like microtubule-disturbing drugs, DNA-damaging agents or other cytotoxic molecules used for chemotherapy (239, 240). However, many cancer cells are able to efficiently block apoptosis and, hence, survive therapeutic treatment. Cells harbouring an otherwise lethal pro-apoptotic load of Bcl-2 proteins which is efficiently blocked by pro-survival proteins are referred to as cells 'primed' for apoptosis. Especially haematopoietic malignancies such as chronic lymphoid leukaemia (CLL), acute myeloid leukaemia (AML) or multiple myeloma (MM) frequently depend on expression of BCL-2, BCL-XL and MCL-1 (241–244).

Consequently, development of anti-apoptotic Bcl-2 protein-targeting therapies was pursued with great effort over the last decades. First pre-clinical evidence for the success of such therapies was achieved in murine models of leukaemia and lymphoma with inducible downregulation of BCL-2 and later MCL-1 (245, 246). Antisense technology, however, was not successful in clinical application (247). Subsequent screenings for small-molecule inhibitors culminated in the development of BH3 mimetics which resemble function and structure of BH3-only proteins. Based on the first specific BH3 mimetic ABT-737, Abbott Laboratories (Abbvie) developed Navitoclax (ABT-263) which is orally bioavailable and likewise specifically inhibits BCL-2, BCL-XL and BCL-W (248). When used *in vivo*, both ABT-737 and ABT-263 caused thrombocytopenia due to inhibition of BCL-XL which is vital for platelet survival thus complicating their use in the clinic (249). However, several studies confirmed their specific mode of action and response to treatment (250–252). Hence, circumventing the drawback of thrombocytopenia upon BCL-XL inhibition the succeeding BH3 mimetic Venetoclax (ABT-199) was engineered to specifically bind BCL-2 with 100x higher affinity than ABT-263 (244).



The success of ABT-199 in clinical trials facilitated its approval by the FDA in 2016 for single use in CLL patients which since then was extended to the use in combination with azacitidine, decitabine and low dose cytarabine in AML (253, 254). In the meantime, a multitude of ongoing clinical trials evaluate an even broader usage of BH3 mimetics as anti-cancer drugs in haematopoietic as well as solid cancers. This includes a growing number of new BH3 mimetics, for example, specific inhibitors for BCL-XL and MCL-1 which show promising pre-clinical results (reviewed in (255)). Since BH3 mimetics efficiently kill cancer cells primed for apoptosis, many combinatorial approaches with ‘apoptosis-priming’ drugs proved auspicious, as demonstrated by studies with DNA-damaging agents, bromodomain and extra-terminal (BET) protein inhibitors or kinase inhibitors (256–258).

Although the BH3:groove interaction targeted by BH3 mimetics clearly bundles most scientific and clinical interest for Bcl-2 proteins in anti-cancer therapy at the time, it is not the only interaction interface of Bcl-2 proteins which can be exploited for anti-cancer therapy. For instance, the vital role of the BH4 motif in mediation of BCL-2’s anti-apoptotic function is underpinned by possible usage of BH4 peptides as high-affinity BAX antagonists (259). Hence, effective BCL-2 inhibition via BH4 motif-binding compounds might be another promising strategy to break cancer’s anti-apoptotic defence (260).

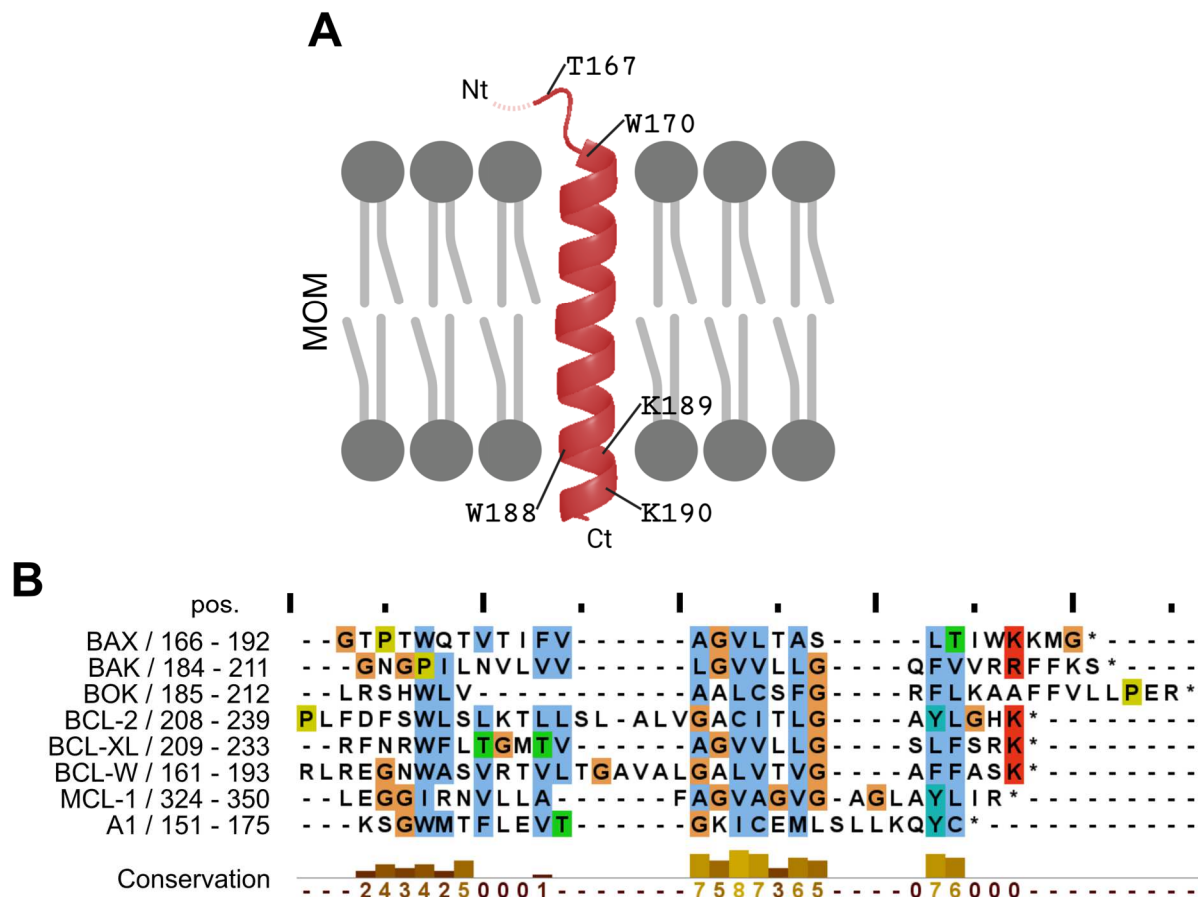
Another possible, previously neglected, target for clinical intervention is the Ct TMD of Bcl-2 proteins. Recent advances studying this domain as a regulatory interaction interface underline that further investigations of the impact of TMD interaction on apoptosis signalling might represent an important factor for even more precise targeting of Bcl-2-inhibiting drugs (reviewed in (261)). Since this thesis will focus on TMD interaction of Bcl-2 proteins, TMD structure and functions will be dissected more thoroughly in the following sections.

### 1.3 Transmembrane domains (TMDs)

Roughly a quarter of all proteins encoded by the human genome are membrane proteins (262, 263). Besides the  $\beta$ -barrel structure, their membrane-spanning moieties usually consist of one or more  $\alpha$ -helical TMDs. Transmembrane helices generally comprise roughly 20 foremost hydrophobic residues crossing the lipid bilayer (264). Situated at important cellular interfaces connecting cytosolic with luminal or extra-cellular compartments TMDs vitally contribute to the essential functions of transmembrane proteins including signal transduction, protein targeting, membrane trafficking and intracellular transport processes (reviewed in (265)).

As an essential function focused on in this thesis, TMDs frequently mediate protein-protein interactions within membranes and, hence, inevitably with other TMDs. For TMD-TMD interaction, various interaction motifs have been identified. The most common of these motifs is the GxxxG (GG<sub>4</sub>) motif first found for glycophorin A TMD dimerization which is a surface protein of erythrocytes (266, 267). An extension of the GG<sub>4</sub> motif is the glycine zipper motif GxxxGxxxG, for example, present in the TMD of myelin protein zero (268). Bioinformatic analysis further revealed overrepresentation of the general small-xxx-small motif (with G, A and S as small amino acids (AAs)) in TMD sequences (269). Other common motifs are II<sub>4</sub>, GA<sub>4</sub>, IG<sub>1</sub>, leucine zipper motifs, polar-xx-polar (with polar AAs including S, T, E, Q, D and N), aromatic-xx-aromatic and Ser/Thr rich sequences (reviewed in (270, 271)). For example, Ser/Thr rich sequences were found in Hepatitis C virus non-structural protein 4B (272). In general, next to interhelical Van der Waals contacts which are best described by the 'knobs-into-holes' packing model (273), hydrogen bonds via polar residues frequently facilitate TMD-TMD interaction (274). Although positively charged residues can stabilise TMD dimerization by hydrogen bonds in certain cases, it is most likely that their presence at the TMD interaction surface introduces repulsion (reviewed in (271)). In addition, also the membrane itself is a crucial contributor to TMD-TMD interactions as membrane characteristics such as membrane fluidity and lipid solvation evidently impact on TMD-TMD interaction, for example, through lipid-protein interactions (275–277).

Proteins harbouring one or more TMD can be categorized in different subgroups according to number and arrangement of their TMDs, for example, single-pass or multi-pass transmembrane proteins. While TMDs generally can be located at different positions within the protein sequence, one subset of TMD-bearing proteins, the tail-anchored proteins, possess a single TMD near the C-terminus. More precisely, these proteins are characterized by a single  $\alpha$ -helical TMD with less than 30 subsequent AAs on the luminal side (reviewed in (278)). The group of tail-anchored proteins includes not only enzymatic proteins such as cytochrome b5 (Cyt b5) (279), components of intracellular transport processes such as TOM5 and TOM6 (280) or the N-ethylmaleimide–sensitive factor attachment protein receptors (SNAREs) (reviewed in (281)), but also members of the Bcl-2 protein family.



**Figure 4: Structure of Bcl-2 transmembrane domains.**

**A** – Schematic structure of the BAX-TMD (comprising helix  $\alpha$ 9 from PDB: 1F16) inserted into the mitochondrial outer membrane (MOM, top layer faces the cytosol). Ct = C-terminus. Nt = towards N-terminus (not shown). Adapted from Ausili *et al.* 2009 (325). Created with biorender.com. **B** – Multiple sequence alignment of Bcl-2 protein C-terminal segments performed using ClustalOmega and visualised using Jalview.

### 1.3.1 Transmembrane domains in the Bcl-2 protein family

TMDs are abundant in most members of the Bcl-2 protein family and, as typical for tail-anchored proteins, usually comprise ~20 AA in form of a single-pass  $\alpha$ -helix at the C-terminus – also referred to as helix  $\alpha_9$  in all effectors or Bcl-2-like proteins (schematically shown in Figure 4A). An exception is given by A1 which was postulated to possess a merely membrane-inserted, not membrane-spanning, Ct sequence (213). Moreover, also the majority of BH3-only proteins are known to be membrane-bound by their Ct sequences such as BIM, BIK, HRK, tBID, and PUMA. In contrast, data are controversial for NOXA and BMF, while no empirical nor bioinformatic data indicate TMD-dependent membrane targeting of BAD (282–284). In fact, for many Bcl-2 proteins TMD orientation within the membrane remains unclear. Most structural data originate from C-terminally truncated Bcl-2 proteins to increase their solubility (136, 285, 286) attributed to the technical difficulties in obtaining membrane-bound protein structures in their natural composition (reviewed in (287)).

Intriguingly, alignment of Bcl-2 protein TMDs does not reveal a high degree of similarity or conserved motifs across different family members (Figure 4B). Most frequently, the  $\alpha$ -helical sequences consist of foremost hydrophobic AAs which are flanked by one or more charged residues on either side (reviewed in (288)). Along these lines, the Ct TMDs developed a quite individual set of functionalities for the different Bcl-2 proteins: Often, but not always, the presence of the TMD is crucial for the pro- and anti-apoptotic functions of Bcl-2 proteins (216, 289–291). Additionally, TMDs can be subject of posttranslational modification which crucially alters TMD and thus protein functionality such as phosphorylation of S184 in BAX by Akt which crucially impacts on BAX pro-apoptotic activity (292, 293). Ubiquitination and degradation is another possible mechanism mediated by the TMD in the case of A1 and NOXA although lysines in the TMD are not the target of ubiquitination (216, 294). Hence, studying the molecular determinants of TMD function is a prerequisite for the understanding of apoptosis regulation by the Bcl-2 protein family.

Three of the Bcl-2 TMD main functions, namely targeting of Bcl-2 proteins to their subcellular localisation, proper membrane-integration and mediating interaction will be portrayed in the following (Figure 5).

### 1.3.2 Functions of Bcl-2 transmembrane domains

#### 1.3.2.1 Subcellular localisation

An early recognised function of the TMDs in Bcl-2 proteins is the specific targeting of Bcl-2 proteins to subcellular membranes similar to other tail-anchored proteins (295). Experiments with TMD-tagged chimeric proteins showed that TMDs of Bcl-2 proteins are sufficient to relocate fluorophores like GFP and other unrelated proteins to the Bcl-2 protein-specific respective subcellular localisation, for example, the ER membrane in the case of BCL-2-TMD (172, 283, 296, 297). This suggests that information encrypted either in and/or directly up- or downstream of the TMD is sufficient to target Bcl-2 proteins to their subcellular localisation. Interestingly, for initial insertion of tail-anchored proteins into the target membrane there is only a discrimination between ER or MOM-targeted TMDs. Tail-anchored proteins destined for other subcellular membranes such as Golgi or the plasma membrane are inserted into the ER membrane and further distributed to their target membrane (298–300). Later studies, however, demonstrated that TMD characteristics such as length and AA composition actually contain information about organelle-specificity suggesting at least some degree of computational predictability (301).


















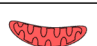

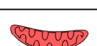



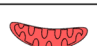

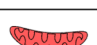

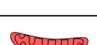





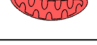
Several TMDs of BCL-2 proteins (including BAX, BAK, BCL-XL, BCL-W, MCL-1) were reported to preferentially bind to the MOM, while others (including BCL-2, BIK, BOK) are dominantly ER-targeted in healthy cells (157, 172, 191, 205, 282, 302). TMD localisation is often, but not always, consistent with the subcellular localisation of the respective Bcl-2 protein (Table 1). Besides MOM and ER, Bcl-2 proteins were also found in additional subcellular compartments such as the Golgi network or nuclear envelope (157, 303). As mentioned, there is no common targeting sequence which regulates, for example, MOM-targeting of BAX-TMD and BAK-TMD. Instead, general variations in hydrophobicity and number as well as position of flanking charged residues determine specific targeting (reviewed in (278, 288)). MOM-targeting TMDs are generally shorter (<20 AAs), more hydrophobic and carry more flanking positively charged residues towards the C-terminus than ER-targeting TMDs, such as  $\geq$  two positive charges at the luminal side of the bilayer in the case of MOM-inserted BAX-, BAK- and BCL-XL-TMD (Figure 4B).

The other way round, TMDs missing the MOM-targeting features are generically re-routed to the ER. However, also dual targeting (to MOM and ER) was reported indicating not a strictly binary decision process (300, 304, 305).

Although the Ct domain of Bcl-2 proteins is a necessary factor to establish subcellular localisation, it is not a sufficient one in all cases. Also, the molecular basis of apoptosis-dependent changes in Bcl-2 protein subcellular localisation is still incompletely understood causing, for example, shuttling of BCL-2 and BIK from the ER to MOM under apoptotic conditions (173, 306). Such phenomena are, at least partially, explained by the involvement of cytosolic features of Bcl-2 proteins which influence and fine-tune their subcellular localisation: BH3:groove interaction can directly or indirectly lead to significant shifts in Bcl-2 protein subcellular localisation, for example, shown for BCL-XL-dependent retrotranslocation of BAX (130) or recruitment of BCL-W and MCL-1 by BH3-only proteins (191, 307). As another exception of TMD-dependent targeting, BH3-only proteins BMF and BIM are bound by components of the cytoskeleton via distinct residues and released upon apoptosis-promoting phosphorylation (308, 309). In the case of BAX and MCL-1, also the N-terminus is reportedly implied in Bcl-2 protein subcellular targeting, while BCL-2's and BCL-XL's localisation at mitochondria is influenced by interaction with mitochondrial FK506-binding protein 38 (310–312). However, to which degree additional interactions and targeting motifs delegate protein localisation despite of the TMD must be considered individually for each Bcl-2 protein and, in some cases, remains largely unexplored.

**Table 1: Subcellular localisation of Bcl-2 proteins.**

List of reported predominant Bcl-2 protein subcellular localisations at mitochondria (Mito), ER or other compartments. Subcellular localisation is further distinct between normal conditions (grey symbols, healthy cells) and apoptotic conditions (red symbols). 'TMD-targeting' indicates presence and protein subcellular targeting of C-terminal TMD sequence. ✓ = present/targeting. (✓) = present/targeting with restrictions. ✗ = not present/targeting. Based on Kale *et al.* 2018 (40).

Sub-type	Protein	Predominant localisation Normal conditions			Predominant localisation Apoptotic conditions			TMD- targeting
		 Mito	 ER	 Others	 Mito	 ER	 Others	
Effector	BAX			Cytosol				✓
	BAK							✓
	BOK							✓
Anti-apoptotic Bcl-2-like	BCL-2							✓
	BCL-XL			Cytosol				✓
	BCL-W			Cytosol				✓
	MCL-1							✓
	A1							(✓)
BH3-only protein	(t)BID			Cytosol				(✓)
	BIM			Cytoskeleton				(✓)
	NOXA							✓
	PUMA							✓
	BMF			Cytoskeleton				(✓)
	BIK							✓
	HRK	Not expressed						✓
	BAD			Cytosol				✗

### 1.3.2.2 Membrane integration

The means by which tail-anchored proteins such as Bcl-2 proteins transition from a nascent protein chain at ribosomes to be anchored in their respective target membranes remains incompletely understood. It is sufficiently proven, however, that the eventual localisation is encoded by the TMD, in contrast to signal recognition particle (SRP)-mediated localisation of proteins with an N-terminal signal peptide (reviewed in (313)). Initially, speculations included the involvement of conventional transport and integration machinery such as cytosolic chaperones, the ER-specific Sec61 or mitochondria-specific TOM complex. Subsequent studies showed that Sec61 is dispensable for anchoring tail-anchored proteins to the ER (314, 315). Some studies revealed a key role of the cytosolic chaperone Transmembrane Recognition Complex of 40 kDa (TRC40) in ER-targeting of tail-anchored proteins (316, 317), while others proved the possibility of unassisted insertion (305, 318). Intriguingly, a growing body of evidence suggests cytosolic factor and TOM-independent membrane insertion of Bcl-2 proteins (296, 319). This is underpinned by *in vitro* studies in which TMD peptides were able to associate with artificial membranes and effectively cause membrane disturbance as well as release of encapsuled large molecules (320). Furthermore, Andreu-Fernández and coworkers found that TMD peptides of Bcl-2 proteins preferentially bind to artificial membranes reconstituting the MOM indicating specific targeting and suggested to use TMDs as mitochondrial priming tools (321). However, contradictory studies, for example, the dependency of BAX mitochondrial targeting on the porin VDAC2 suggest individual fine-tuning of membrane integration (322, 323). Adding to this, also modification of BAX outside the TMD, for example, S-palmitoylation at C126 can control integration of BAX into the MOM (324).

Once synthesized, many Bcl-2 proteins reside at membranes with their TMD constitutively inserted in the lipid bilayer (reviewed in (288)). However, some Bcl-2 proteins also reside in the cytosol. As mentioned, the BAX TMD is folded back into the groove of cytosolic BAX effectively shielding the hydrophobic residues from solvent molecules (133). Once activated, for example, by BH3-only activator tBID, the Ct TMD is displaced from the groove and inserts perpendicular to the lipid bilayer into the MOM (131, 325). Impairing membrane insertion of BAX, therefore, is a vital regulatory step for BAX-induced apoptosis which depends on the BAX TMD. In an early study by Nechushtan *et al.* phosphomimetic mutation of the BAX TMD at S184 rendered BAX unable to integrate into membranes and reduced its apoptotic activity (302).



This posttranslational regulation model was confirmed by Kale and collaborators for phosphorylation of BAX S184 by Akt (293). However, Ct-truncated BAX is still able to induce MOMP in certain settings challenging the view of a TMD-dependent BAX activation (289). Interestingly, what first seemed to be a special case for BAX, emerges as a common pattern among Bcl-2 proteins: also in cytosolic BCL-XL and BCL-W the TMD sequence is sequestered by the protein core. Hinds *et al.* speculated that the TMD folded back onto the protein core not only increases solubility of the Bcl-2 proteins, but also regulates binding of BH3-only proteins to the groove of BCL-W and BCL-XL (194). While BCL-XL constantly shuttles between the MOM and the cytosol where it resides in form of soluble homodimers, cytosolic BCL-W is vastly recruited to the MOM upon apoptosis induction (194, 326). For both proteins, however, TMD insertion into the MOM is a vital component of their anti-apoptotic activity and, thus, clearly shows that the TMD sequence is a central feature for the localisation-switching functionality of these proteins.

### 1.3.2.3 Protein-protein interaction

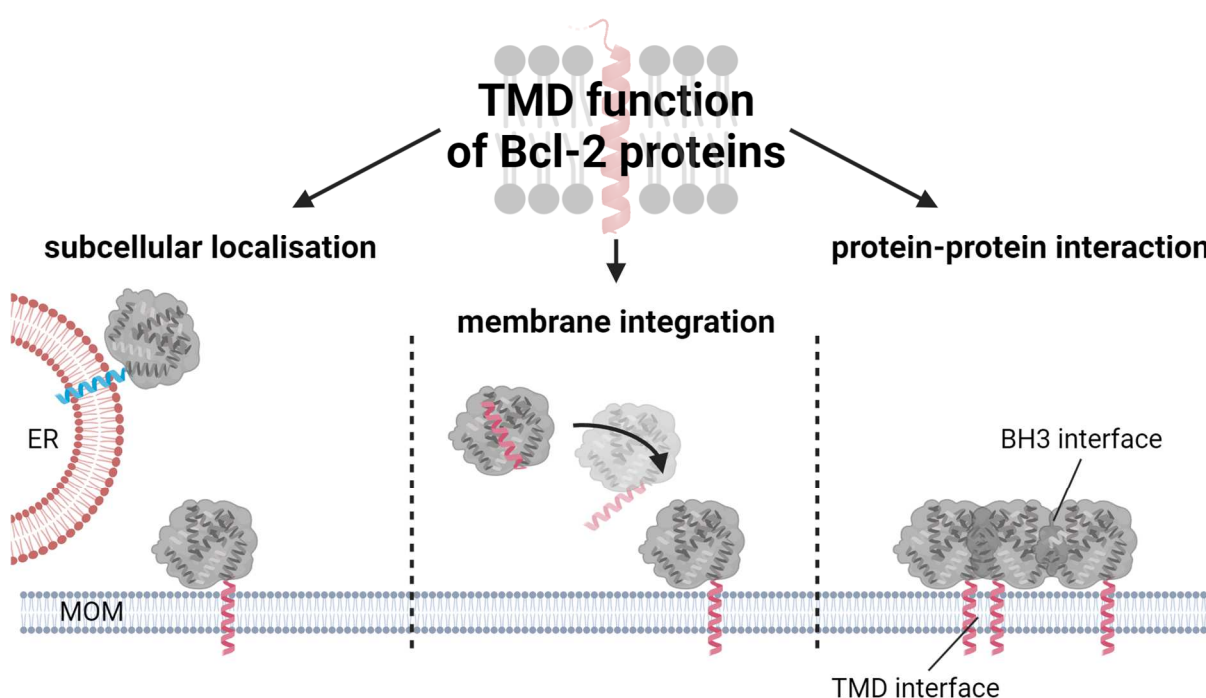
Classically, Bcl-2 protein interaction is determined by the binding affinity of BH3 motif and groove of the respective binding partners. Binding affinities were often acquired from BH3 motif-derived peptides (170, 224, 327). However, neither do BH3 motif-derived peptides bind to membranes as full-length proteins would nor could these experiments take into account the presence of putative secondary interaction sites. Hence, it was not surprising that in this way acquired affinity data often failed to reflect the physiological situation (328). Consequently, not all protein-protein interactions among Bcl-2 proteins fully depend on BH3:groove interaction alone. One early observation by Jeong *et al.* in 2004 was the TMD-dependent formation of BCL-XL homodimers in the cytosol (326). In the following two decades, other studies repeatedly obtained results that indicate a crucial involvement of Bcl-2 protein TMDs in protein-protein interaction and, thus, questioned the archetypical view of TMDs as mere membrane anchors. In 2013, a group around Todt *et al.* found that the TMD of BCL-XL is not only involved in homodimerization of BCL-XL but also in retrotranslocation of BAX/BCL-XL heterodimers from the MOM to the cytosol (329). Also in the intensively studied process of BAX activation, a photo crosslinking study in artificial micelles indicated the presence of an additional interaction interface for BAX oligomerisation apart from the BH3 region (330).

A few years later, this interface was pinpointed to the  $\alpha 9$  helices by disulfide-crosslinking in a BAX mutant constitutively bound to the MOM as well as in BAK which undergoes a similar oligomerisation process (331). Zhang and collaborators subsequently confirmed the dependency of BAX pore enlargement on the  $\alpha 9$  interface rendering the TMD a critical interaction-mediating domain for BAX-dependent MOMP and apoptosis (332). The current view on BAX oligomerisation, thus, includes the BH3:groove interaction as a necessity for BAX homodimerization, while the BAX-TMD homotypic interaction forms dimer-dimer interactions and hence promotes oligomerisation. Moreover, using the ToxRed interaction assay Andreu-Fernández *et al.* demonstrated homo- and heterotypical interactions of BAX-TMD, BCL-2-TMD and BCL-XL-TMD in *E.coli* membranes (171). In the same study, the authors applied bimolecular fluorescence complementation (BiFC) to confirm the TMD interactions in the MOM and postulated modulation of apoptosis by interaction of TMD peptides with full-length Bcl-2 proteins. Interestingly, while pro-apoptotic BAX-TMD interacted both homotypically and with BCL-XL-TMD and BCL-2-TMD, the latter two TMDs of anti-apoptotic Bcl-2 proteins did not interact with each other indicating a more complex network of interactions than previously anticipated. More recent findings by Stehle and coworkers highlight participation of the BOK-TMD in regulation of BOK-induced cell death, while Förster resonance energy transfer (FRET) data indicated interaction of BOK-TMD with MCL-1-TMD (291). In agreement, a regulatory role of BOK-TMD and MCL-1-TMD interaction in apoptosis was confirmed soon after by Lucendo *et al.* using BiFC assays and molecular dynamics (MD) simulations of TMD interaction in model membranes (333).

However, the TMD interaction network is not limited to effector and anti-apoptotic Bcl-2-like proteins: the TMD-bearing BH3-only protein BIM binds to BCL-2 and BCL-XL not only with the BH3 motif but also via the TMD thereby effectively multiplying the necessary effort to displace BIM from its binding partners as shown for BH3 mimetic anti-cancer drugs (334). Using the same automated FRET fluorescence lifetime imaging microscopy (FLIM) approach as in the latter study, Chi *et al.* revealed that BIM evidently binds BAX with both BH3 motif and TMD which enables BAX activation (335). Just recently, the same group described the same mechanism for PUMA which also binds its anti-apoptotic counterparts with both BH3 motif and TMD (336). This, by the authors referred to as 'double-bolt locking', mechanism seems to lay the basis for the high affinity binding of BIM and PUMA to anti-apoptotic Bcl-2 proteins.

Thus, TMD-mediated interactions were discovered across all three subgroups of Bcl-2 proteins – but it does not stop there: an increasing number of publications describes also TMD-mediated interactions between Bcl-2 proteins and other, unrelated, proteins. One previously mentioned example is the interaction of BCL-2 with IP3R channels: Ivanova and colleagues revealed that BCL-2 is targeted to IP3Rs not only via the BH4 motif but, more importantly, by its TMD (337). In fact, the interaction via the BH4 motif is of too low affinity ( $K_D \sim 1 \mu\text{M}$ , (177)) to explain potent inhibition of IP3Rs. Thus, Ivanova *et al.* propose a model in which the TMD interaction facilitates binding of the BH4 motif on IP3Rs. Moreover, sequestration and inhibition of BAK in a 400 kDa complex including VDAC2 is dependent on the BAK-TMD (338). Intriguingly, also viral Bcl-2 protein homologs such as ORF16 from herpes virus may exploit TMD-TMD interactions to hijack the apoptosis machinery since they were shown to interact with pro- and anti-apoptotic family members via their Ct sequences (339).

Taken together, the Ct sequences, alias TMDs, of Bcl-2 proteins are not only fundamental features for subcellular localisation and membrane integration, but also crucial mediators of protein-protein interactions which fine-tune apoptosis signalling.



**Figure 5: Functions of Bcl-2 transmembrane domains (TMDs).**

Schematic of Bcl-2 TMD main functions including subcellular localisation (left), membrane integration (middle) and protein-protein interactions (right). MOM = mitochondrial outer membrane. Created with biorender.com.

## 1.4 Aims of the thesis

The preceding chapters illustrate the importance of the Bcl-2 interaction network for regulation of apoptosis and, hence, in diseases associated with apoptosis dysregulation such as cancer. Conventionally, the Bcl-2 interaction network is defined by BH3:groove interactions (reviewed in (40)). However, this dogmatic view is challenged by the emerging functional importance of the Ct TMD segment of Bcl-2 proteins in mediating interaction (171, 291, 333). Despite the amassing of publications on TMD interactions of Bcl-2 proteins regulating apoptosis signalling, surprisingly little is known about the specificity, molecular basis and functional effects of the TMD interaction network – here referred to as the TMD interactome of Bcl-2 proteins. Inspired by previous work from the research group (291), this thesis was devoted to the further enlightenment of the dark spots within the TMD interaction network.

To achieve this, firstly, it was aimed to develop and establish an innovative assay platform to characterise Bcl-2 TMD interactions in living cells. In order to obtain an unambiguous readout which allows for (relative) quantification of TMD interaction data, the work includes selection and optimisation of assay parameters as well as development and validation of the assay workflow comprising appropriate controls and normalisation tools.

Secondly, this assay platform was sought to be utilized for a systematic analysis of Bcl-2 TMD interactions enlightening interactions between effector TMDs (BAX, BAK, BOK) and furthermore effector TMDs with TMDs of anti-apoptotic Bcl-2-like proteins (BCL-2, BCL-XL, BCL-W, MCL-1, A1). To be able to trace obtained interactions back to their subcellular membranes, efforts were next focused towards identifying the subcellular localisation of fluorophore-conjugated TMDs.

Thirdly and lastly, the functional relevance of uncovered TMD interactions was to be investigated with focus on the effector proteins BAX, BAK and BOK. This was mainly pursued by studying the effect of TMD sequence alteration on subcellular localisation, pro-apoptotic activity and inhibition by anti-apoptotic Bcl-2 proteins. In addition, the impact of (cancer-associated) mutation within the TMDs of BAX and BCL-2 on identified TMD interactions, subcellular localisation and cell death regulation was to be analysed.

## 2 Materials and Methods

### 2.1 Materials

#### 2.1.1 Antibodies

**Table 2: List of primary antibodies.**

WB = Western Blot, IF = Immunofluorescence staining.

Target	dilution	application	cat. no.	supplier
$\beta$ -actin	1:5000	WB	A5316	Merck KGaA, Darmstadt, Germany
Ac-Histone 3	1:500	IF	06-599	Merck
BAK	1:1000	WB	3814	Cell signalling technology Inc., Danvers, MA, USA
BAX	1:1000	WB	2772	Cell signalling technology
BCL-2	1:500	WB	15071	Cell signalling technology
BCL-XL	1:1000	WB	2762	Cell signalling technology
BOK	1:500	WB	ab186745	Abcam plc, Cambridge, UK
Cleaved Caspase-3	1:1000	WB	9661	Cell signalling technology
CHOP	1:1000	WB	2895	Cell signalling technology
Cytochrome C	1:500	IF	556432	Becton Dickinson corp., Franklin Lakes, NJ, USA
GAPDH	1:1000	WB	2118	Cell signalling technology
GFP	1:1000	WB	sc-9996	Santa Cruz Biotechnology Inc., Dallas, TX, USA
GM130	1:500	IF	610822	Becton Dickinson
LgBiT	1:1000	WB	N7100	Promega corp., Madison, WI, USA
mCherry	1:1000	WB	26765-1- AP	Proteintech group Inc., Rosemont, IL, USA
MCL-1	1:1000	WB	5453	Cell signalling technology
PARP	1:1000	WB	9542	Cell signalling technology
p-JNK	1:1000	WB	4671	Cell signalling technology
Tubulin	1:5000	WB	ab56676	Abcam
Vinculin	1:1000	WB	66305-1- IG	Proteintech group

**Table 3: List of secondary antibodies.**

WB = Western Blot, IF = Immunofluorescence staining.

Name	dilution	application	cat. no.	supplier
Anti-mouse HRP-linked	1:2000	WB	7076	Cell signalling technology Inc., Danvers, MA, USA
Anti-rabbit HRP-linked	1:2000	WB	7074	Cell signalling technology
AlexaFluor 488 goat $\alpha$ -rabbit	1:500	IF	A-11008	Thermo Fisher Scientific Inc., Waltham, MA, USA
AlexaFluor 594 goat $\alpha$ -mouse	1:500	IF	A-11032	Thermo Fisher Scientific
AlexaFluor 633 goat $\alpha$ -mouse	1:500	IF	A-21126	Thermo Fisher Scientific

## 2.1.2 Cell culture media and reagents

**Table 4: List of cell culture media and reagents.**

Name	supplier/formulation
Agarose for LB Agar (Bacto Agar)	Becton Dickinson corp., Franklin Lakes, NJ, USA
Ampicillin, sodium salt	Carl Roth GmbH + Co. KG, Karlsruhe, Germany
Fetal bovine serume (FBS Superior)	Sigma-Aldrich, Merck kGaA, Darmstadt, Germany
Gibco Dulbecco's Modified Eagle Medium (DMEM)	Thermo Fisher Scientific Inc., Waltham, MA, USA
Gibco Dulbecco's Modified Eagle Medium (DMEM) without phenol red	Thermo Fisher Scientific
Gibco Opti-MEM Reduced-serum medium	Thermo Fisher Scientific
Gibco Penicillin-Streptomycin 10 000 U/ml	Thermo Fisher Scientific
Gibco Roswell Park Memorial Institute (RPMI) 1640 Medium	Thermo Fisher Scientific
Gibco Trypsin-EDTA (0.05%), phenol red	Thermo Fisher Scientific
Kanamycin sulfate	Carl Roth
LB Agar	LB medium + 1.5% (w/v) Agarose
Lysogeny broth (LB) medium	1% (w/v) Peptone, 0.5% (w/v) yeast extract, 1% (w/v) NaCl in dH <sub>2</sub> O, pH – 7.0 – 7.5
Peptone	Carl Roth
SOB (super optimal broth) medium	2% (w/v) Peptone, 0.5% (w/v) yeast extract, 0.05% (w/v) NaCl, 2.5 mM KaCl, 10 mM MgCl <sub>2</sub> in dH <sub>2</sub> O pH – 7.0 – 7.5
SOC outgrowth medium	SOB medium + 2% 1 M Glucose (sterile filtered)
Yeast extract	Carl Roth

### 2.1.3 Cell lines and bacteria

**Table 5: List of human cell lines and bacteria.**

Name	supplier
DU145	Kindly provided by B. Gillisen, Charité Berlin, Germany, STR verified
HEK293(FT)	Thermo Fisher Scientific Inc., Waltham, MA, USA #R70007, STR verified
Hela (empty vector)	Kindly provided by M. Morrison, University of Stuttgart, Germany, STR verified
Hela Bax <sup>-/-</sup> /Bak <sup>-/-</sup> (DKO)	Kindly provided by M. Morrison, University of Stuttgart, Germany, STR verified
MCF-7 EYFP-ER	Generated by F.Essmann from MCF-7 wild-type, carrying pEYFP-ER from Clontech (Takara), Kusatsu, Japan
MCF-7 EYFP-Mito	Generated by F.Essmann from MCF-7 wild-type, carrying pEYFP-Mito from Clontech (Takara), Kusatsu, Japan
MCF-7 wild-type	Kindly provided by R. Jänicke, University of Düsseldorf, Germany, STR verified
NEB 5-alpha Competent <i>E.coli</i> (High efficiency)	New England Biolabs Inc., Ipswich, MA, USA

### 2.1.4 Chemicals, buffers and solutions

**Table 6: List of chemicals, buffers and solutions.**

Name	supplier/formulation
2-Mercaptoethanol	Thermo Fisher Scientific Inc., Waltham, MA, USA
ABT-199	Sellekchem Chemicals LLC, Houston, TX, USA
Acrylamide (30%) [37.5:1]	Bio-Rad Laboratories Inc., Hercules, CA, USA
Acrylamide (40%) [29:1]	Bio-Rad Laboratories
Agarose Ultrapure for gels	Thermo Fisher Scientific
Ammonium persulfate (APS)	Merck kGaA, Darmstadt, Germany
Annexin V APC-conjugated	Immunotools GmbH, Friesoythe, Germany
Bovine Serum Albumin (BSA)	Carl Roth GmbH, Karlsruhe, Germany
Bortezomib	Sellekchem
Calcium chloride (CaCl <sub>2</sub> )	Merck
Coelenterazine-h	stock: 500 µM in methanol, Promega corp., Madison, WI, USA
COmplete EDTA-free protease inhibitor tablets (PIC)	Roche Holding AG, Basel, Switzerland
CutSmart buffer	New England Biolabs Inc., Ipswich, MA, USA
Dako fluorescence mounting medium	Dako, Agilent Technologies Inc., Santa Clara, CA, USA
DarmaFECT 1 transfection reagent	Horizon Discovery Ltd., Waterbeach, UK

Digitonin	Merck
dNTPs	Equimolar mix of dATP, dCTP, dGTP and dTTP, New England Biolabs
Ethidium bromide solution (0.025%)	Carl Roth GmbH, Karlsruhe, Germany
Ethylenediaminetetraacetic acid (EDTA)	Merck
FuGene 6 transfection reagent	Promega
Gel loading dye, Purple (6x)	New England Biolabs
Glycine	Merck
HEPES	Carl Roth
Lipofectamine 2000	Thermo Fisher Scientific
Mitotracker Red CMXRos	Thermo Fisher Scientific
NEBuilder HiFi DNA Assembly Master Mix	New England Biolabs
Optifect transfection reagent	Thermo Fisher Scientific
Phosphate buffered saline (PBS) powder	Merck
Polyethylenimine Hydrochloride (PEI MAX 40K)	Polysciences Inc., Warrington, PA, USA
PhosSTOP phosphatase inhibitor tablets (PS)	Roche
Potassium chloride (KCl)	Carl Roth
Q-VD-Oph	Sellekchem
Ponceau S solution	Merck
ProLong Diamond Antifade Mountant with DAPI	Thermo Fisher Scientific
Propidiumiodide (PI)	Thermo Fisher Scientific
Restore PLUS Western Blot Stripping-Buffer	Thermo Fisher Scientific
ROTI Histofix, 4% formaldehyde, phosphate-buffered solution, pH 7	Carl Roth
Sodium chloride (NaCl)	Carl Roth
Sodium azide (NaN <sub>3</sub> )	Thermo Fisher Scientific
Sodium dodecyl sulfate (SDS)	Carl Roth
Tetramethylethylenediamine (TEMED)	Merck
Tetramethylrhodamine metyl ester (TMRM)	Thermo Fisher Scientific
Tris Base	Merck
Tris HCl	Merck
Triton X-100	Merck
Tunicamycin	Enzo Biochem Inc., New York, NY, USA
Tween 20	Merck
Annexin binding buffer	100 mM HEPES, 1.4 M NaCl, 25 mM CaCl <sub>2</sub> in dH <sub>2</sub> O, pH - 7.4
Blocking solution (for IF)	1% (w/v) BSA, 2% (v/v) FBS in 1x PBS
Blocking solution (for WB)	5% (w/v) skim milk powder in 1x TBS-T
Electrophoresis buffer	25 mM Tris, 192 mM Glycine, 0.1% (w/v) SDS in dH <sub>2</sub> O
FACS PBS	1x PBS + 2% (v/v) FBS



Laemmli sample buffer (5x)	10% (w/v) SDS, 20% (v/v) Tris HCl buffer (1 M, pH - 6.8), 25% (v/v) 2-Mercaptoethanol, 50% (v/v) Glycerol, 0.05% (w/v) Bromophenol blue
Lysis buffer	50 mM Tris-HCl pH 7.6, 250 mM NaCl, 5 mM EDTA, 0.1% Triton X-100 in dH <sub>2</sub> O
PEI solution for transfections	1 mg/ml PEI MAX in dH <sub>2</sub> O
TAE buffer	40 mM Tris, 0.1% (v/v) glacial acetic acid, 1 mM EDTA (pH – 8.0)
TBS	13.69 mM NaCl, 2.7 mM KCl, 3 mM Tris-Base, 22 mM Tris-HCl in dH <sub>2</sub> O, pH – 7.4
TBS-T	1x TBS + 0.1% (v/v) Tween 20
Transfer buffer (semi-dry)	48 mM Tris, 39 mM Glycine, 0.04% (w/v) SDS, 20% (v/v) Ethanol in dH <sub>2</sub> O

## 2.1.5 Consumables

**Table 7: List of selected consumables.**

Name	supplier
12 mm coverslips, #1.5H	Paul Marienfeld GmbH + Co. KG, Lauda-Königshofen, Germany
Microscopy slides, frost edge	VWR International LLC, Radnor, PA, USA
Nitrocellulose membrane 0.1 µm (Amersham Protran)	GE HealthCare Technologies Inc., Chicago, IL, USA
White-bottom 96-well plate (Lumitrac, high-binding, F-bottom)	Greiner Bio-One GmbH, Frickenhausen, Germany

## 2.1.6 Enzymes

**Table 8: List of enzymes used for cloning.**

Name	supplier
Agel	
Dpnl	
EcoRI-HF	
EcoRV-HF	
HindIII-HF	New England Biolabs Inc., Ipswich, MA, USA
T4 DNA ligase	
<i>Taq</i> DNA polymerase	
XbaI	
XhoI	

## 2.1.7 Instruments

**Table 9: List of instruments.**

<b>Name</b>	<b>supplier</b>
Applied Biosystems Veriti thermal cycler, 96-well	Thermo Fisher Scientific Inc., Waltham, MA, USA
Biometra Fastblot, Blotting chamber	Analytik Jena GmbH + Co.KG, Jena, Germany
Bioruptor sonification system	Diagenode SA, Seraing, Belgium
Ebox CX5 TS (UV-transilluminator)	Vilber Lourmat GmbH, Eberhardzell, Germany
EnSpire multimode plate reader	PerkinElmer Inc., Waltham, MA, USA
EVE Automated Cell Counter	NanoEntek, Seoul, Korea
Incucyte S3 imaging system	Sartorius AG, Göttingen, Germany
Mini-PROTEAN Tetra cell system	Bio-Rad Laboratories Inc., Hercules, CA, USA
Nanodrop 2000c spectrophotometer	Thermo Fisher Scientific
Stella Modular High Performance Imaging System	Raytest Isotopengeräte GmbH, Straubenhardt, Germany
TCS SP8 confocal microscope	Leica Microsystems GmbH, Wetzlar, Germany
Victor Nivo, multimode plate reader	PerkinElmer

## 2.1.8 Kits

**Table 10: List of kits.**

<b>Name</b>	<b>supplier</b>
NucleoBond Xtra Midi Plus kit	Macherey-Nagel GmbH + Co. KG, Düren, Germany
Phusion site-directed mutagenesis kit	Thermo Fisher Scientific Inc., Waltham, MA, USA
Pierce BCA Protein Assay Kit	Thermo Fisher Scientific
QIAprep Spin Miniprep kit	Qiagen N.V., Venlo, Netherlands
QIAquick Gel Extraction Kit	Qiagen
SuperSignal West Dura Extended Duration Substrate (ECL substrate)	Thermo Fisher Scientific

## 2.1.9 Plasmids

**Table 11: DNA template and expression plasmids.**

<b>Name</b>	<b>internal ID</b>	<b>insert</b>	<b>provider</b>
pBiT_1.1-C[TK/LgBiT]	#E087	LgBiT subunit (NanoBiT luciferase)	Promega, O. Burk
pBiT_2.1-C[TK/SmBiT]	#E088	SmBiT subunit (NanoBiT luciferase)	Promega, O. Burk
pEGFP_mCitrine-N1	#E076	mCitrine	F. Essmann

mKOkappa-2A-mTurquoise2	#E075	mKOk-T2A-mTurquoise2	F. Essmann
pENTR/D-Topo-(ATG)-hBax	#089	BAX	F. Essmann
pENTR/D-Topo-(ATG)-hBak	#088	BAK	F. Essmann
pENTR/D-Topo-(ATG)-hBok	#090	BOK	F. Essmann
cDNA4/mycHis/HA-Bcl-2	#377	HA-BCL-2	F. Essmann
cDNA4/mycHis/HA-Bcl-W	#378	HA-BCL-W	F. Essmann
cDNA4/mycHis/HA-Bcl-XI	#379	HA-BCL-XL	F. Essmann
pCDNA4/mycHis/HA-Mcl-1	#380	HA-MCL-1	F. Essmann
pCDNA4/mycHis/HA-A1	#381	HA-A1	F. Essmann
NanoBiT Negative Control Vector	#660	HaloTag-SmBiT	Promega, O. Burk
NanoBiT pos. Ctrl LgBiT-PRKAR2A	#661	LgBiT-PRKAR2A	Promega, O. Burk
NanoBiT pos. Ctrl SmBiT-PRKACA	#662	SmBiT-PRKACA	Promega, O. Burk
p-lenti2-CRISPR- hBcl2-E1.1 (Exon1)	#566	Cas9, gRNA BCL-2	F. Essmann
pEGFP-C1/Bax	#268	EGFP-BAX	F. Essmann
pEGFP-C1/Bak	#269	EGFP-BAK	F. Essmann
pEGFP-C1/Bok	#266	EGFP-BOK	F. Essmann
pEGFP-C1/Bcl-2	#270	EGFP-BCL-2	F. Essmann
pCDNA4/mycHis/mCherry/RfA/	#E013	mCherry	F. Essmann
pCDNA4/mycHis/mCherry/RfA/Bcl-2	#277	mCherry-BCL-2	F. Essmann
pcDNA3-ER-mCarmine	#676	ER-mCarmine	O. Griesbeck
pEGFP-C1/BOK-BAK-TMD	#475	EGFP-BOK-BAK-TMD	F. Essmann
pEGFP-C1/BOK-BAX-TMD	#476	EGFP-BOK-BAX-TMD	F. Essmann
pEGFP-C1/BAK-BOK-TMD	#477	EGFP-BAK-BOK-TMD	F. Essmann
pEGFP-C1/BAX-BOK-TMD	#478	EGFP-BAX-BOK-TMD	F. Essmann
pEGFP-C1	#E023	EGFP	Clontech (Takara) F. Essmann
pcDNA4/mycHis/EGFP-hBok/L70E	#510	EGFP-BOK L70E	F. Essmann
pCDNA4/mycHis/mCherry-hBok- $\Delta$ TM	#597	mCherry-BOK- $\Delta$ TM	F. Essmann

**Table 12: Plasmids generated during the course of the present thesis.**

“Based on” indicates original backbone plasmid and means of generation in brackets.

<b>Name</b>	<b>internal ID</b>	<b>insert</b>	<b>based on</b>
pBiT_mCitrine-T2A-LgBiT-BAX-TMD	#647	mCitrine-T2A-LgBiT-BAX-TMD	#E087 (NEBuilder)
pBiT_mCitrine-T2A-LgBiT-BAK-TMD	#648	mCitrine-T2A-LgBiT-BAK-TMD	#E087 (NEBuilder)
pBiT_mCitrine-T2A-LgBiT-BOK-TMD	#649	mCitrine-T2A-LgBiT-BOK-TMD	#E087 (NEBuilder)
pBiT_mTurquoise2-T2A-SmBiT-BAX-TMD	#650	mTurquoise2-T2A-SmBiT-BAX-TMD	#E087 (NEBuilder)
pBiT_mTurquoise2-T2A-SmBiT-BAK-TMD	#651	mTurquoise2-T2A-SmBiT-BAK-TMD	#E087 (NEBuilder)
pBiT_mTurquoise2-T2A-SmBiT-BOK-TMD	#652	mTurquoise2-T2A-SmBiT-BOK-TMD	#E087 (NEBuilder)
pBiT_mTurquoise2-T2A-SmBiT-BCL-2-TMD	#653	mTurquoise2-T2A-SmBiT-BCL-2-TMD	#E087 (NEBuilder)
pBiT_mTurquoise2-T2A-SmBiT-BCL-XL-TMD	#654	mTurquoise2-T2A-SmBiT-BCL-XL-TMD	#E087 (NEBuilder)
pBiT_mTurquoise2-T2A-SmBiT-BCL-W-TMD	#655	mTurquoise2-T2A-SmBiT-BCL-W-TMD	#E087 (NEBuilder)
pBiT_mTurquoise2-T2A-SmBiT-MCL-1-TMD	#656	mTurquoise2-T2A-SmBiT-MCL-1-TMD	#E087 (NEBuilder)
pBiT_mTurquoise2-T2A-SmBiT-A1-TMD	#657	mTurquoise2-T2A-SmBiT-A1-TMD	#E087 (NEBuilder)
pBiT_mTurquoise2-T2A-SmBiT-TOM5-TMD	#659	mTurquoise2-T2A-SmBiT-TOM5-TMD	#E087 (NEBuilder)
pEGFP-C1/BAX-BAK-TMD	#604	EGFP- BAX-BAK-TMD	#E023 (NEBuilder)
pEGFP-C1/BAK-BAX-TMD	#686	EGFP- BAK-BAX-TMD	#E023 (NEBuilder)
pBiT_mCitrine-BAX-TMD	#687	mCitrine-BAX-TMD	#647 (NEBuilder)
pBiT_mCitrine-BAK-TMD	#688	mCitrine-BAK-TMD	#647 (NEBuilder)
pBiT_mCitrine-BOK-TMD	#689	mCitrine-BOK-TMD	#647 (NEBuilder)
pBiT_mTurquoise2-BAX-TMD	#690	mTurquoise2-BAX-TMD	#650 (NEBuilder)
pBiT_mTurquoise2-BAK-TMD	#691	mTurquoise2-BAK-TMD	#650 (NEBuilder)
pBiT_mTurquoise2-BOK-TMD	#692	mTurquoise2-BOK-TMD	#650 (NEBuilder)
pBiT_mTurquoise2-BCL-2-TMD	#693	mTurquoise2-BCL-2-TMD	#690 (Res./Lig.)
pBiT_mTurquoise2-TOM5-TMD	#694	mTurquoise2-TOM5-TMD	#690 (Res./Lig.)
pEGFP_mCitrine-BAX-TMD	#695	mCitrine-BAX-TMD	#E023 (NEBuilder)
pEGFP_mCitrine-BAK-TMD	#696	mCitrine-BAK-TMD	#695 (Res./Lig.)
pEGFP_mCitrine-BOK-TMD	#697	mCitrine-BOK-TMD	#695 (Res./Lig.)
pEGFP_mTurquoise2-BAX-TMD	#698	mTurquoise2-BAX-TMD	#E023 (NEBuilder)

pEGFP_mTurquoise2-BAK-TMD	#699	mTurquoise2-BAK-TMD	#698 (Res./Lig.)
pEGFP_mTurquoise2-BOK-TMD	#700	mTurquoise2-BOK-TMD	#698 (Res./Lig.)
pEGFP_mTurquoise2-BCL-2-TMD	#701	mTurquoise2-BCL-2-TMD	#698 (Res./Lig.)
pEGFP_mTurquoise2-BCL-XL-TMD	#702	mTurquoise2-BCL-XL-TMD	#698 (Res./Lig.)
pEGFP_mTurquoise2-BCL-W-TMD	#703	mTurquoise2-BCL-W-TMD	#698 (Res./Lig.)
pEGFP_mTurquoise2-MCL-1-TMD	#704	mTurquoise2-MCL-1-TMD	#698 (Res./Lig.)
pEGFP_mTurquoise2-A1-TMD	#705	mTurquoise2-A1-TMD	#698 (Res./Lig.)
pEGFP_mTurquoise2-TOM5-TMD	#706	mTurquoise2-TOM5-TMD	#698 (Res./Lig.)
pEGFP_mCitrine-BCL-2-TMD	#708	mCitrine-BCL-2-TMD	#695 (Res./Lig.)
pEGFP_mTurquoise2-cb5-TMD	#714	mTurquoise2-cb5-TMD	#695 (NEBuilder)
pEGFP_BOK-cb5-TMD	#719	EGFP-BOK-cb5-TMD	#266 (NEBuilder)
pcDNA4_mCherry-BCL-2-BOK-TMD	#720	mCherry-BCL-2-BOK-TMD	#277 (NEBuilder)
pcDNA4_mCherry-BCL-2-cb5-TMD	#721	mCherry-BCL-2-cb5-TMD	#277 (NEBuilder)
pcDNA4_mCherry-BCL-2-TOM5-TMD	#722	mCherry-BCL-2-TOM5-TMD	#277 (NEBuilder)
pBiT_mTurq2-SmBiT-BCL-2-TMD A234D	#723	mTurq2-T2A-SmBiT-BCL-2-TMD A234D	#653 (Mutagenesis)
pEGFP_mTurq2-BCL-2-TMD A234D	#724	mTurquoise2-BCL-2-TMD A234D	#701 (Mutagenesis)
pcDNA4_mCherry-BCL-2 A234D	#725	mCherry-BCL-2 A234D	#277 (Mutagenesis)
pBiT_mTurq2-SmBiT-BCL-2-TMD A224D	#726	mTurq2-T2A-SmBiT-BCL-2-TMD A224D	#653 (Mutagenesis)
pEGFP_mTurq2-BCL-2-TMD A224D	#727	mTurquoise2-BCL-2-TMD A224D	#701 (Mutagenesis)
pcDNA4_mCherry-BCL-2 A224D	#728	mCherry-BCL-2 A224D	#277 (Mutagenesis)
pBiT_mTurq2-SmBiT-BCL-2-TMD W214C	#729	mTurq2-T2A-SmBiT-BCL-2-TMD W214C	#653 (Mutagenesis)
pEGFP_mTurq2-BCL-2-TMD W214C	#730	mTurquoise2-BCL-2-TMD W214C	#701 (Mutagenesis)
pcDNA4_mCherry-BCL-2 W214C	#731	mCherry-BCL-2 W214C	#277 (Mutagenesis)
pBiT_mTurq2-SmBiT-BAX-TMD S184A	#732	mTurq2-T2A-SmBiT-BAX-TMD S184A	#650 (Mutagenesis)
pEGFP_mTurq2-BAX-TMD S184A	#733	mTurquoise2-BAX-TMD S184A	#698 (Mutagenesis)
pEGFP_BAX S184A	#734	EGFP-BAX S184A	#268 (Mutagenesis)
pBiT_mTurq2-SmBiT-BAX-TMD S184D	#735	mTurq2-T2A-SmBiT-BAX-TMD S184D	#650 (Mutagenesis)

pEGFP_mTurq2-BAX-TMD S184D	#736	mTurquoise2-BAX-TMD S184D	#698 (Mutagenesis)
pEGFP_BAX S184D	#737	EGFP-BAX S184D	#268 (Mutagenesis)
pBiT_mTurq2-SmBiT-BAX-TMD V180G	#738	mTurq2-T2A-SmBiT-BAX-TMD V180G	#650 (Mutagenesis)
pEGFP_mTurq2-BAX-TMD V180G	#739	mTurquoise2-BAX-TMD V180G	#698 (Mutagenesis)
pEGFP_BAX V180G	#740	EGFP-BAX V180G	#268 (Mutagenesis)
pEGFP_mCitrine-BOK-TMD K202A	#746	mCitrine-BOK-TMD K202A	#697 (Mutagenesis)
pEGFP_mTurquoise2-BOK-TMD K202A	#747	mTurquoise2-BOK-TMD K202A	#700 (Mutagenesis)
pEGFP-C1_BOK_K202A	#748	EGFP-BOK K202A	#266 (Mutagenesis)

### 2.1.10 Oligonucleotides

**Table 13: List of oligonucleotides used as primers.**

All primers were ordered at metabion GmbH, Planegg, Germany.

Name	internal ID	sequence	application
Insert1_mCitrine_fw	#37	cctgcagcgaccccgcttaaagatatcatggtgagcaagggcgag	NEBuilder
Insert1_mCitrine_rv	#38	agccgaattccttgtacagctcgtccatgc	NEBuilder
Insert1_GSGT2A_fw	#39	gctgtacaaggaattcggctccggcgagggcagaggaagtc	NEBuilder
Insert1_GSGT2A_rv	#40	tgaagaccattgcgcaagggccgggattctctcc	NEBuilder
Insert1_LgBiT_fw	#41	cccttgcgcaatggtcttcacactcgaag	NEBuilder
Insert1_LgBiT_rv	#42	aagcttgctgccgcccgcgctgccgcccggccactggtgatggttactcg	NEBuilder
Insert1_BaxTMD_fw	#43	ggcggcgggcggcagcggcgggcgggcagcagcaagcttgggacgcccacgtggcag	NEBuilder
Insert1_BaxTMD_rv	#44	agcggccggcccgcgactctcgagtcagccatcttctccagatggtg	NEBuilder
Insert4_SmBiT_Bax_rv	#45	agcggccggcccgcgactctcgagtcagccatcttctcc	NEBuilder
I4_BaxTMDsmBiT_fw	#50	cagcggcgggcgggcagcaagcttgggacgcccacgtggcag	NEBuilder
I4_BaxTMDsmBiT_rv	#51	gcgccggcccgcgactctcgagtcagccatcttctccagatggtg	NEBuilder
I5_BakTMDsmBiT_fw	#52	cagcggcgggcgggcagcaagcttggcaacggccccatcctg	NEBuilder
I5_BakTMD_opt_rv	#90	gcgccggcccgcgactctcgagtcagccatcttctccagatggtg	NEBuilder
I6_BokTMDsmBiT_fw	#54	cagcggcgggcgggcagcaagcttctgaggagccactggctg	NEBuilder

I6_BokTMDSmBiT_rv	#55	gcggccggccgccccgactctcgagtcacct ctcgggcagcag	NEBuilder
I7_Bcl2TMD_opt_fw	#86	cagcggcgggcgggcagcaagcttcctctg tttgatttctcc	NEBuilder
I7_Bcl2TMD_opt_rv	#87	gcggccggccgccccgactctcgagtcactt gtggcccagatag	NEBuilder
I14_TOM5TMDLgBiT_fw	#58	cagcggcgggcgggcagcaagcttgacgtg atcagcagcatc	NEBuilder
I14_TOM5TMDLgBiT_rv	#59	gcggccggccgccccgactctcgagtcagat gctgtccagcttc	NEBuilder
HSV_TK_end_fw	#60	tattaaggtgacgcgtgtgg	Sequencing
SV40_PolyA_rv	#61	gtggtttgtccaaactcatc	Sequencing
I8_BclXITMD_opt_fw	#109	cagcggcgggcgggcagcaagcttcgcttc aaccgctggttc	NEBuilder
I8_BclXITMD_opt_rv	#110	gcggccggccgccccgactctcgagtcattt ccgactgaagagtgag	NEBuilder
I2_BakTMDLgBiT_fw	#68	ctcaggaggtggaggctcaaagcttggcaac ggccccatcctg	NEBuilder
I3_BokTMDLgBiT_fw	#69	ctcaggaggtggaggctcaaagcttctgagg agccactggctg	NEBuilder
I9_BclWTMDSmBiT_fw	#91	cagcggcgggcgggcagcaagcttcgtctg cgggaggggaac	NEBuilder
I9_BclWTMDSmBiT_rv	#92	gcggccggccgccccgactctcgagtcactt gctagcaaaaaaggccc	NEBuilder
I10_Mcl1TMDSmBiT_fw	#93	cagcggcgggcgggcagcaagcttctagaa ggtggcatcagg	NEBuilder
I10_Mcl1TMDSmBiT_rv	#94	gcggccggccgccccgactctcgagtcactt tattagatatgccaacc	NEBuilder
I11_A1TMDSmBiT_fw	#95	cagcggcgggcgggcagcaagcttaaatct ggctggatgacttttc	NEBuilder
I11_A1TMDSmBiT_rv	#96	gcggccggccgccccgactctcgagtcaaca gtattgcttcagg	NEBuilder
FC_linker_fw	#145	catggacgagctgtacaaggaattcggagggt ggaggctcaggag	NEBuilder
pEGFPC1fw	#150	gatcactctcggcatggac	Sequencing
pEGFPC1rv	#151	cattttatgtttcagggttcagggt	Sequencing
BaxBakTMD_fix_fw	#158	ggactcagatctcgagctcataagcttatgg acgggtccggggag	NEBuilder
BaxBakTMD_fix_rv	#159	ccgtcgactgcagaattcgatctagatcatg atttgaagaatcttcgtaccacaaactg	NEBuilder
BakBaxTMDfix_fw	#160	ggactcagatctcgagctcataagcttatgg cttcggggcaaggc	NEBuilder
BakBaxTMDfix_rv	#161	ccgtcgactgcagaattcgatctagatcagc ccatcttcttcagatgg	NEBuilder
FTc1_fw	#162	cgtcagatccgctagecgtageccaccatggt gagcaagggcgag	NEBuilder
FTc1_rv	#163	gcagaattcgaagcttgagcctcgagtcagc ccatcttc	NEBuilder

Tobias Beigl		Dissertation	Materials and Methods
FTc_Hind_Eco_havoc_fw	#165	gaggctcaagctacgtattctgcagtc	Mutagenesis
FTc_Hind_Eco_havoc_rv	#166	gactgcagaatacgtagcttgagcctc	Mutagenesis
FTc12_cb5 TMD_fw	#169	ctcaggaggtggaggctcaaagcttgacact actattgattctagtt	NEBuilder
FTc12_cb5_TMD_rv	#170	cagaatacgtagcttgagcctcgagtcaatc ttcagccatgtac	NEBuilder
T7 For Sdt Primer	#143	taatacgactcactataggg	Sequencing
BGH Rev Sdt Primer	#144	tagaaggcacagtcgagg	Sequencing
pEGFP_EGFP_fw	#181	cgtcagatccgctagcgcctaccggctcgccac catgggtgagcaagg	NEBuilder
BOK-Core_cb5TMD_rv	#182	tagtagtgctcgtgggagcggaggccagg	NEBuilder
BOK-Core_cb5TMD_fw	#183	ccgctcccacgacactactattgattctagt tc	NEBuilder
cb5TMD_pEGFP_rv	#184	cgcggtaccgtcgactgcaggaattctcaat cttcagccatgtac	NEBuilder
pcDNA4_mCherry_fw	#185	agacccaagctggctagttaaagcttatggg gagcaagggcgagg	NEBuilder
Bcl-2-Core_BOKTMD_rv	#186	ggctcctcagccgcctgctggggccgt	NEBuilder
Bcl-2-Core_BOKTMD_fw	#187	cagcatgcccgtgaggagccactggctg	NEBuilder
BOKTMD_pcDNA4_rv	#188	cggccgccactgtgctggatgaattctcacc tctcgggcagcag	NEBuilder
Bcl- 2_Core_TOM5TMD_rv	#189	tgatcacgtcccgcctgctggggccgta	NEBuilder
Bcl-2- Core_TOM5TMD_fw	#190	cagcatgcccggacgtgatcagcagcatc	NEBuilder
TOM5TMD_pcDNA4_rv	#191	cggccgccactgtgctggatgaattctcaga tgctgtccagcttc	NEBuilder
Bcl-2-Core_cb5TMD_rv	#192	tagtagtgctcccgcctgctggggccgta	NEBuilder
Bcl-2-Core_cb5TMD_fw	#193	cagcatgcccggacactactattgattctagt tc	NEBuilder
cb5TMD_pcDNA4_rv	#194	cggccgccactgtgctggatgaattctcaat cttcagccatgtac	NEBuilder
BAX TMD S184A fw_2	#216	gctcaccgcccgcctcaccatct	Mutagenesis
BAX TMD S184A rv_2	#217	agatggtgagcgcggcggtgagc	Mutagenesis
BAX TMD S184D fw_2	#218	gctcaccgcccgcctcaccatctg	Mutagenesis
BAX TMD S184D rv_2	#219	cagatggtgaggcggcggtgagc	Mutagenesis
BAX TMD V180G fw_2	#220	tgtggcgggagggtcaccgcct	Mutagenesis
BAX TMD V180G rv_2	#221	aggcggtgagccctcccgcacaca	Mutagenesis
Bcl-2 TMD A234D fw_3	#222	caccctgggtgactatctgggcc	Mutagenesis
Bcl-2 TMD A234D rv_3	#223	ggcccagatagtcaccaggggtg	Mutagenesis
Bcl-2 TMD A224D fw_3	#224	gctcagtttgacctgggtgggag	Mutagenesis
Bcl-2 TMD A224D rv_3	#225	ctcccaccaggtccaaactgagc	Mutagenesis



Tobias Beigl	Dissertation	Materials and Methods
Bcl-2 TMD W214Cfw_3 #226	tgatttctcctgtctgtctctgaagac	Mutagenesis
Bcl-2 TMD W214C rv_3 #227	gtcttcagagacagacaggagaaatca	Mutagenesis
BOK-TMD K202A_fw #247	ccgcttcctggcggtgccttcttc	Mutagenesis
BOK-TMD K202A_rv #248	gaagaaggcagccgccaggaagcgg	Mutagenesis

### 2.1.11 Software

**Table 14: List of software applications and online tools.**

Name	supplier
Alphafold Colab	Colab.research.google.com; Jumper <i>et al.</i> 2021 (340)
BioRender	Science Suite Inc., Toronto, Canada
Clustal Omega	ebi.ac.uk, EMBL-EBI, Cambridge, UK
Fiji ImageJ	Schindelin <i>et al.</i> 2012 (341)
Graphpad Prism 9	GraphPad Software Inc., San Diego, CA USA
Leica Application Suite X (LAS X)	Leica Microsystems GmbH, Wetzlar, Germany
MS Office 365	Microsoft Corporation Inc., Redmond, WA, USA
NEBuilder Assembly tool, V2.7.1	nebuilder.neb.com, New England Biolabs Inc., Ipswich, MA, USA
ProtScale	web.expasy.org/protscale/, Swiss Institute of Bioinformatics, Lausanne, Switzerland
PyMOL	Schrödinger <i>et al.</i> 2023 (342)
Jalview 2.11.2.7	Barton Group, University of Dundee, Scotland, UK; Waterhouse <i>et al.</i> 2009 (343)

## 2.2 Methods

### 2.2.1 DNA sequences

Plasmids used as template for cloning in section 2.2.2 are listed in Table 11. Reference cDNA sequences of plasmid-encoded proteins are listed in Table 15. TMD segment used for TMD fusion proteins are listed in Table 16.

**Table 15: Overview of protein sequence references at UniProt protein data base (uniprot.org).**

Name	function	UniProt entry
<b>BAX</b>	Pro-apoptotic Bcl-2	Q07812-1
<b>BAK</b>	Pro-apoptotic Bcl-2	Q16611-1
<b>BOK</b>	Pro-apoptotic Bcl-2	Q9UMX3-1
<b>BCL-2</b>	Anti-apoptotic Bcl-2	P10415-1
<b>BCL-XL</b>	Anti-apoptotic Bcl-2	Q07817-1
<b>BCL-W</b>	Anti-apoptotic Bcl-2	Q92843-1
<b>MCL-1</b>	Anti-apoptotic Bcl-2	Q07820-1
<b>A1</b>	Anti-apoptotic Bcl-2	Q16548-1
<b>TOM5</b>	Mitochondrial import (Mito control)	Q8N4H5-1
<b>cb5</b>	Heme reductase (ER control)	P00167-1
<b>EGFP</b>	Fluorophore	Derived from P42212 by mutation (M1_S2insV/F64L/S65T/H231L)
<b>mCherry</b>	Fluorophore	X5DSL3
<b>mCitrine</b>	Fluorophore	Derived from P42212 by mutation (M1_S2insV/S65G/V68L/Q69M/S72A/T203Y/A 206K/H231L)
<b>mTurquoise2</b>	Fluorophore	Derived from P42212 by mutation (M1_S2insV/F64L/Y66W/S72A/N146F/H148D/ M153T/V163A/S175G/A206K/H231L)

### 2.2.2 Cloning

#### 2.2.2.1 Plasmid amplification and preparation

Plasmid DNA was gently mixed with freshly thawed NEB 5-alpha competent *E.coli* on ice (1 – 20 ng/μl cells) and cells were incubated on ice for 30 min. Heat shock transformation was performed at 42°C for 45 s with subsequent cool down on ice for 3 min. After addition of pre-warmed SOC medium (50 μl per 10 μl cells), samples were incubated in a horizontal shaker for 1 h (37°C, 300 rpm).

**Table 16: Overview of transmembrane domain amino acid sequences in generated plasmids.**

<b>Name</b>	<b>positions</b>	<b>amino acid sequence</b>
<b>BAX</b>	166 - 192	GTPTW QVTIIFVAGV LTASLTIWKK MG
<b>BAK</b>	184 - 211	GNGPILN VLVVLGVVLL GQFVVRREFK S
<b>BOK</b>	185 - 212	LRSHWL VAALCSFGRF LKAAFFVLLP ER
<b>BCL-2</b>	208 - 239	PLF DFSWLSLKTL LSLALVGACI TLGAYLGHK
<b>BCL-XL</b>	209 - 233	RF NRWFLTGMTV AGVVLLGSLF SRK
<b>BCL-W</b>	161 - 193	RLREGNWASV RTVLTGAVAL GALVTVGAFK ASK
<b>MCL-1</b>	328 - 350	LEGGIRN VLLAFAGVAG VGAGLAYLIR
<b>A1</b>	151 - 175	KSGWMTFLEV TGKICEMLSL LKQYC
<b>TOM5</b>	23 - 51	DVISSIRN FLIYVALLRV TPFILKKLDS I
<b>cb5</b>	100 - 134	D TTIDSSSSWW TNWVIPAISA VAVALMYRLY MAED

Cell suspensions were plated on LB Agar plates with antibiotics and incubated o/n at 37°C. Then, single colonies were transferred to 3 ml LB medium with antibiotics and incubated (spinning wheel, 37°C) i) o/n for analytical scale (Mini-preparation) or ii) 6-8 h for production scale (Midi-preparation). i) For Mini-preparation, DNA was isolated from 2 ml of cell suspension using the QIAprep Spin Miniprep Kit according to the manufacturer's protocol. ii) For Midi preparation, 100 ml LB medium with antibiotics was inoculated with 2 ml of pre-culture and incubated o/n (37°C, 180 rpm). DNA was isolated from 100 ml main culture using the Nucleobond Xtra Midi Plus kit according to the manufacturer's protocol. After isolation, DNA content was determined via absorbance at 260 nm using the Nanodrop 2000c spectrophotometer.

#### *2.2.2.2 DNA amplification via PCR and colony PCR*

For generation and amplification of linear DNA fragments by PCR template DNA, dNTPs and primers were prepared in Standard *Taq* Reaction buffer on ice as shown in Table 17. *Taq* DNA polymerase was added to the reaction and PCR was performed as shown in Table 18 using a thermal cycler. For colony PCR, the PCR reaction mix (Table 17) was prepared without addition of template DNA. Then, during colony transfer (2.2.2.1), both PCR reaction mix and pre-culture for Mini/Midi preparation were inoculated with bacteria from the same colony. Subsequently, PCR was performed as described above and products analysed via agarose gel electrophoresis.

**Table 17: PCR reaction mix.**

Component	final concentration
10x Standard <i>Taq</i> reaction buffer	1x
dNTPs	200 $\mu$ M
Forward primer	0.2 $\mu$ M
Reverse primer	0.2 $\mu$ M
Template DNA	< 1 $\mu$ g
<i>Taq</i> DNA polymerase	1.25 U/50 $\mu$ l PCR mix

**Table 18: PCR program.**

Annealing temperature was optimised to  $T_m$  of used primers.

Phase	no. of cycles	temperature [ $^{\circ}$ C]	duration [min]
Initial denaturation	1	95	2
Denaturation	30-40	95	0.5
Annealing		55 – 68	0.5
Elongation		68	1
Final Elongation	1	68	5
End		4	$\infty$

### 2.2.2.3 Agarose gel electrophoresis and gel extraction

Agarose gels were cast from pre-mixed Ultrapure Agarose (1 – 2%) in 1xTAE buffer stained with approx. 150  $\mu$ l – 300  $\mu$ l (3 - 6 drops) of 0.025% EtBr solution. DNA samples were mixed 1:6 with 6x purple gel loading dye and electrophoresis was performed at 100 V for 30 – 90 min. Gels were imaged using the E-Box UV-transilluminator system. DNA isolation and purification from gels was performed using the QIAquick gel extraction kit according to the manufacturer's protocol. DNA concentration of purified DNA was assessed via absorbance at 260 nm using the Nanodrop 2000c spectrophotometer.

### 2.2.2.4 Restriction enzyme digestion and *T4* ligase reaction

Linearisation of vectors was achieved by incubation with two desired restriction endonucleases in recommended buffer according to the manufacturer's protocol.

In general, restriction enzyme mix was prepared on ice (Table 19), digestion reaction was performed at 37°C for 0.5 – 1 h and fragments were subsequently separated by agarose gel electrophoresis and DNA purification via gel extraction. A list of performed digestions and pursued applications is given in Table 20.

**Table 19: Restriction digestion reaction mix.**

As a control, undigested DNA or single digestions with one enzyme only were analysed in parallel.

<b>Component</b>	<b>final concentration</b>
<b>10x CutSmart reaction buffer</b>	1x
<b>Template DNA</b>	0.02 – 0.1 µg/µl reaction mix
<b>Restriction enzyme 1</b>	0.04 U/µl reaction mix
<b>Restriction enzyme 2</b>	0.04 U/µl reaction mix

**Table 20: Overview restriction digestion reactions and pursued applications.**

Plasmid IDs are listed in 2.1.9.

<b>Plasmid ID</b>	<b>enzyme 1</b>	<b>enzyme 2</b>	<b>application</b>
<b>#E087</b>	HindIII-HF	XbaI	NEBuilder template
<b>#E023</b>	AgeI	XhoI	NEBuilder template
<b>#647 - 659</b>	EcoRV-HF	XhoI	NEBuilder control
<b>#647 - 659 #693, 694 #695, 698</b>	HindIII-HF	XhoI	TMD exchange (ligation)
<b>#647, 650</b>	EcoRI-HF	XhoI	NEBuilder template
<b>#277</b>	HindIII-HF	EcoRV-HF	NEBuilder template

Insert of DNA fragments into linearised vectors was achieved by ligation using the T4 DNA ligase following the manufacturer's protocol. Reaction overview is shown in Table 21. Ligated plasmids were subsequently amplified and sequence validated.

**Table 21: T4 DNA ligase reaction.**

<b>Component</b>	<b>final concentration</b>
<b>T4 DNA ligase buffer (10x)</b>	1x
<b>Vector DNA</b>	0.001 pmol/ $\mu$ l reaction mix
<b>Insert DNA</b>	0.003 – 0.005 pmol/ $\mu$ l reaction mix
<b>T4 DNA ligase</b>	2,000 U/ $\mu$ l reaction mix

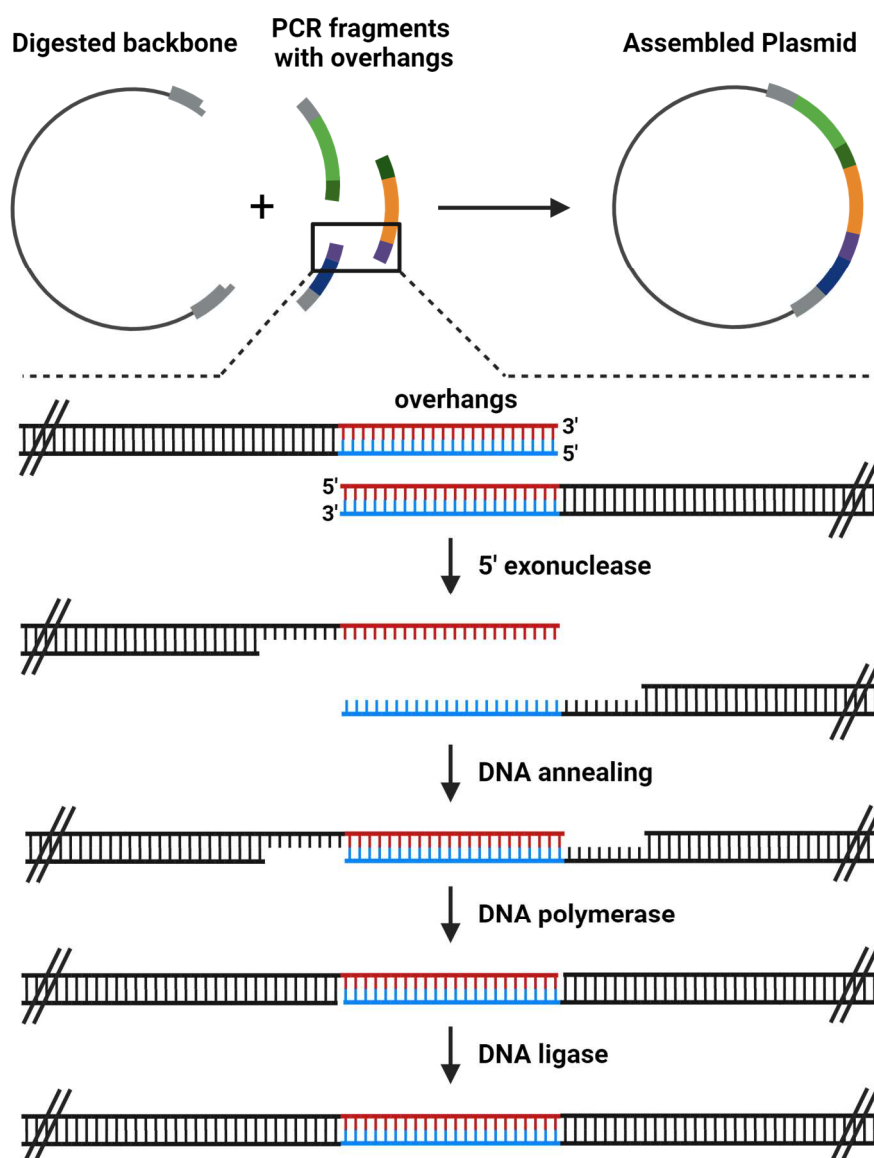
#### 2.2.2.5 Sequence validation

Initial validation of successful integration of inserts into plasmid backbone was achieved by colony PCR (2.2.2.2). Positive clones were subsequently analysed by Sanger sequencing. For Sanger sequencing, DNA was mixed with respective sequencing primers (oligonucleotides) according to the Easy Run protocol (Microsynth AG, Balgach, Switzerland) and sent to be sequenced by Microsynth Seqlab GmbH (Göttingen, Germany).

#### 2.2.3 NEBuilder HiFi DNA assembly (Gibson assembly)

Plasmid generation was done following the NEBuilder HiFi DNA assembly protocol (New England Biolabs). In short, new plasmids were constructed out of a linearised vector backbone (restriction digestion) and PCR-generated insert fragments with 15 - 25 nt at 3' and 5' end overlapping with neighbouring fragments or vector backbone (Figure 6). PCR primers with overhangs (Table 13) were designed by the online NEBuilder Assembly Tool ([nebuilder.neb.com](http://nebuilder.neb.com), V.2.7.1). Fragments and backbone were mixed with NEBuilder HiFi DNA assembly master mix and incubated at 50°C for 60 min. As shown in Figure 6, an exonuclease first creates single-stranded 3' overhangs which can anneal with the complement overlaps of neighbouring fragments followed by complementation of gaps by DNA polymerase and ligation of remaining nicks in assembled DNA. Generated plasmids were subsequently amplified and sequence-validated.

Plasmids based on the NEBuilder HiFi DNA assembly are listed in Table 12.



**Figure 6: NEBuilder HiFi DNA assembly (Gibson assembly) reaction overview.**

Plasmids are generated by combination of linearised vector backbone and insert fragments with overhangs (upper panel). Joining of overlapping regions in fragment overhangs is shown step -by-step (lower panel). Created with biorender.com.

#### 2.2.4 Site-directed mutagenesis

TMD mutagenesis was performed according to the Phusion site-directed mutagenesis kit (Thermo Fisher Scientific Inc., Waltham, MA, USA). In short, template DNA produced in Dam+ *E.coli* strain (NEB 5-alpha Competent *E.coli* (high efficiency), New England Biolabs Inc., Ipswich, MA, USA) was mixed in reaction buffer on ice with oligonucleotide primers carrying the desired mutation.

Then, Phusion High-Fidelity DNA polymerase was added to the reaction and PCR was performed according to the manufacturer's protocol. DpnI restriction endonuclease was added to the reaction to digest template DNA. Remaining plasmid was analysed with gel electrophoresis, amplified and sequence-validated as stated in 2.2.2.

Plasmids generated by site-directed mutagenesis and mutagenesis primers are listed in Table 12 and Table 13.

### 2.2.5 Cell culture

Human embryonic kidney cells HEK293(FT) and breast cancer cells MCF-7 were cultured in Roswell Park Memorial Institute (RPMI) 1640 medium supplemented with 10% fetal bovine serum and 1% penicillin-streptomycin (10 000 U/ml). DU145 prostate carcinoma and Hela cervix carcinoma cells were cultured in Dulbecco's modified eagle medium (DMEM) supplemented with 10% fetal bovine serum (FBS) and 1% penicillin-streptomycin. Cells were maintained at 37°C and 5% CO<sub>2</sub> in a humidified cell culture incubator and passaged approx. every 2-3 days.

For seeding cells for experiments, medium was aspirated and cells were rinsed with 1x PBS. Then, cells were detached with 0.05% trypsin-EDTA and counted using the EVE Automatic Cell Counter according to the manufacturer's protocol.

### 2.2.6 Seeding cells on coverslips

12 mm glass coverslips were transferred to wells of a 24-well plate and sterilised by adding 70 % ethanol. After short incubation with gentle shaking, ethanol was aspirated, coverslips were washed once in sterile MiliQ H<sub>2</sub>O and left to dry. Cells were then seeded on coverslips at a density of 5·10<sup>4</sup> cells in 1 ml cell culture medium per well and cell attachment was facilitated by incubation at RT for 20 min. Then, cells were further incubated o/n (37°C).

### 2.2.7 Transient transfection

Cells were seeded 24 h prior to transfection either on coverslips or in tissue culture plates (1·10<sup>5</sup>/12-well, 2·5·10<sup>5</sup>/6-well). Plasmid DNA was mixed with pre-warmed Opti-MEM (37°C) in a sterile reaction tube (1 µg DNA in 50 µl Opti-MEM per 1 ml cell culture medium). In another reaction tube, PEI solution was mixed with pre-warmed Opti-MEM (3 µl in 50 µl Opti-MEM per 1 ml cell culture medium).



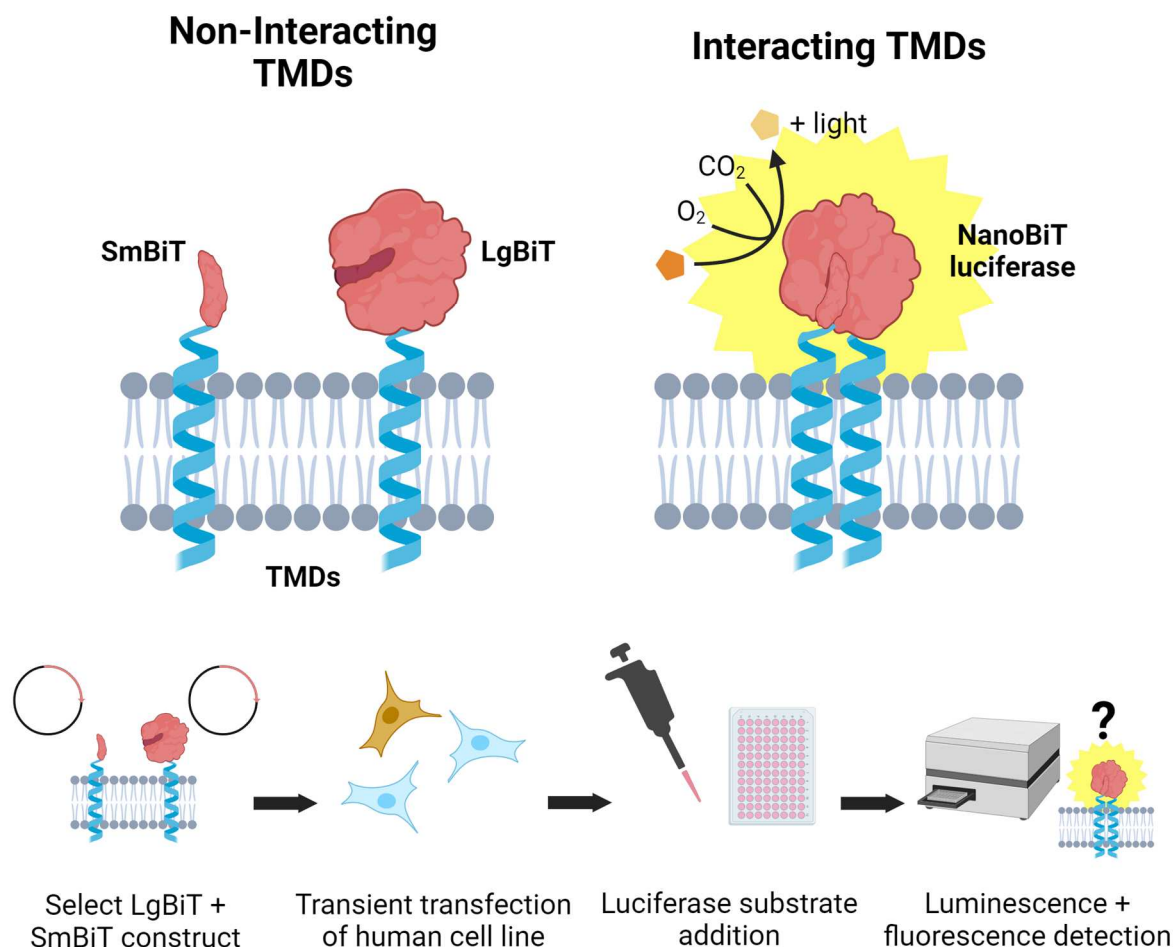
Then, PEI mix was added to DNA mix (DNA/PEI-ratio 1:3), the transfection mix was briefly vortexed and incubated (RT, 20 min). Afterwards, transfection mix was added dropwise to the cell culture and cells were incubated for another 18 h or 24 h respectively (37°C, 5%CO<sub>2</sub>).

Microscopy samples transfected with plasmids expressing full-length Bcl-2 effector proteins were additionally supplemented with 10 µM Q-VD-Oph after transfection.

### 2.2.8 NanoBiT split luciferase assay (NanoBiT assay)

The NanoBiT assay described here was developed to identify Bcl-2 TMD interactions *in vitro* and is based on the commercially-available NanoBiT luciferase developed by Dixon *et al.* (344). As illustrated in Figure 7, cells were seeded in 6-well plates and transiently transfected (2.2.7) with a combination of a LgBiT- and SmBiT-TMD-encoding plasmid (Table 12) in a 1:1 ratio (if not stated otherwise). After 24 h incubation, medium was aspirated and cells detached with trypsin-EDTA. Cells were collected in a 15 ml reaction tube and centrifuged (400xg, 5 min). Supernatant was discarded and cells resuspended in 2 ml of 1x PBS. Then, cell suspension was split as follows: 50% was used for preparation of Western Blot samples. For assay validation, the remaining 50% of cell suspension were split to i) 25% which was analysed by flow cytometry and ii) 25% of cell suspension for the NanoBiT assay. For interaction analysis, the remaining 50% were solely used for the NanoBiT assay.

The proportion of cells intended for the NanoBiT assay was centrifuged (400xg, 5 min), supernatant aspirated and cells resuspended in 150 µl pre-warmed Opti-MEM (37°C). Cell suspension was split into three wells of a white-bottom 96-well plate (50µl/well). If not stated otherwise, NanoBiT substrate Coelenterazine-h was diluted in pre-warmed Opti-MEM to a concentration of 10 µM and added 1:1 (final concentration 5 µM) to each well shortly before starting luminescence/fluorescence detection. Data was acquired using the EnSpire Multimode plate reader if not stated otherwise. Initially, mTurq2 and mCitr fluorescence was assessed with appropriate filter combinations (mTurq2: ex. 434 nm, em. 474 nm; mCitr: ex. 516 nm, em. 531 nm). Then, luminescence was detected every 5 min for 30 min with an exposure time of 1 sec/well. Data were exported and analysed using MS Excel and displayed with Graphpad Prism 9 software.



**Figure 7: Principle and workflow of the NanoBiT assay to detect TMD interaction.**

**A** - Schematic showing the working principle of using the NanoBiT split luciferase system for detection of TMD interaction (SmBiT = Small BiT, LgBiT = Large BiT). **B** – Schematic workflow for the developed NanoBiT split luciferase assay. Created with biorender.com.

If not stated otherwise, luminescence data at  $t = 30$  min after substrate addition was used for calculations. Luminescence data was normalised by dividing luminescence by mTurq2 fluorescence intensity for each well. Technical triplicates were then combined to a mean value for each sample which was set in relation to either positive (BAX-/BAX-TMD) or negative (BAX-/TOM5-TMD) control.

### 2.2.9 Flow cytometry

For cell death detection, cell culture supernatant of (un-)treated and/or transiently transfected (2.2.7) cells was collected in a 5 ml polystyrene tube. For all other flow cytometric analyses supernatant was discarded. Adherent cells were detached by incubation in 0.05 % trypsin-EDTA, resuspended in respective supernatant and wells were once washed in 1x PBS to collect remaining cells.

Afterwards, cells were centrifuged (600xg, 5 min), supernatant aspirated and cells further processed according to subsequent analysis.

#### *2.2.9.1 NanoBiT assay fluorescence analysis*

Cell suspensions which originated from NanoBiT assay samples (2.2.8) were again centrifuged (600xg, 5 min) and cells were resuspended in 0.5 ml FACS PBS. mTurq2 and mCitr fluorescence was detected using a BD FACS Lyric.

#### *2.2.9.2 TMRM staining*

Cells were resuspended in 0.2 ml FACS PBS containing 50 nM TMRM. After incubation (37°C, 20 min), cells were centrifuged (600xg, 5 min) and staining solution was aspirated. Then, cells were subsequently stained with Annexin V-APC.

#### *2.2.9.3 Annexin V-APC staining*

Samples were resuspended in 0.3 ml of Annexin binding buffer containing Annexin V-APC (1:200). Samples were then incubated on ice for 10 min and proportion of APC positive (APC+) cells was determined using a BD FACS Lyric. For cells previously transfected with EGFP (-conjugated fusion protein), gating was adjusted to allow cell death analysis of solely EGFP positive (EGFP+, transfected) cells.

### 2.2.10 Cell fixation and immunofluorescence staining

#### *2.2.10.1 Mitotracker staining*

Cell culture medium was aspirated and cells were incubated with 100 nM Mitotracker Red CMXRos in unsupplemented cell culture medium (RPMI/DMEM, 30 min, 37°C). Afterwards, staining solution was removed and cells were washed once in fresh medium followed by formaldehyde fixation.

#### *2.2.10.2 Formaldehyde fixation*

Cell culture medium of cells seeded on coverslips was aspirated and cells were fixed by incubation in 4% formaldehyde solution (20 min, 37°C). Fixation solution was removed and coverslips washed thrice in 1x PBS. Samples which did not undergo immunofluorescence (IF) staining were directly mounted hereafter. Otherwise, the IF staining protocol was continued.

### 2.2.10.3 *Immunofluorescence staining*

Fixed cells were permeabilized in 0.1% Triton X-100 (RT, 10 min) followed by washing thrice in 1x PBS. Then, blocking solution (1% BSA + 2% FBS in 1x PBS) was added for 1 h (RT, gentle shaking). Blocking solution was aspirated and primary antibodies were added to the wells (1:500 in blocking solution + 0.01% NaN<sub>3</sub>, 2 h, RT, gentle shaking). Again, cells were washed thrice in 1x PBS before applying fluorophore-conjugated secondary antibodies (1:500 in blocking solution + 0.01% NaN<sub>3</sub>, 1 h, RT, gentle shaking). Henceforth, samples were kept in a light-protected environment. Finally, cells were continuously washed in 1x PBS three times for at least 5 min and then mounted on microscopy slides.

### 2.2.10.4 *Coverslip mounting on microscopy slides*

Coverslips were carefully dipped in MiliQ water twice and shortly let to dry placed on folded tissue paper in an upright position. Microscopy slides were cleaned with ethanol and for each coverslip a drop of 5 µl mounting medium with or without DAPI was placed on the slide. Coverslips were carefully lowered with the cell-side down on the mounting medium and left to dry in the dark for at least 24 h at RT. Mounted samples were then stored at 4°C until further use.

### 2.2.11 Confocal laser scanning microscopy (cLSM)

Samples were imaged using a Leica TCS SP8 confocal laser scanning microscope equipped with a HC PL APO 63x/NA 1.40 OIL CS2 objective, lasers at 405 nm, 488 nm, 552 nm and 638 nm and appropriate filter combinations for the analysed fluorophores. Images were acquired as z-stacks with a resolution of 1024x1024 pixels at 600 Hz and 1x/3x zoom using Leica Application Suite X. Raw data images were exported as .TIFF and processed with Fiji software.

#### 2.2.11.1 *Colocalisation analysis*

The Pearson's correlation coefficient (Pearson's  $r$ ) of two images was calculated from isolated middle sections of z-stacks at 3x zoom. For that, sections were loaded into Fiji software, ROIs were drawn manually around cells of interest and analysed separately using the Coloc2 plugin of the Fiji software.

### 2.2.11.2 *BAX clustering quantification*

For quantification of BAX clustering in MCF-7 cells expressing EGFP-tagged BAX, images were taken by cLSM at randomly chosen fields of view (63x oil objective, 1x zoom). Number of cells containing bright and punctiform EGFP-BAX signals (clusters) and total number of EGFP-positive cells was determined and subsequently combined to a sum over all fields of view from one experiment including at least  $n = 100$  EGFP positive cells per sample.

### 2.2.11.3 *Quantification of cytochrome C release*

Transiently transfected (2.2.7) MCF-7 cells expressing EGFP(-BOK) alone or in combination with mCherry-BCL-2 were IF stained (2.2.10) for cytochrome C (CytC) and imaged by cLSM at randomly chosen fields of view (63x oil objective, 1x zoom). Number of EGFP-positive cells with diffuse, cytosolic signals for CytC (released CytC) in contrast to a spatially defined, mitochondria-like localisation and total number of EGFP-positive cells were determined. The sum over all fields of view was formed from one experiment including at least  $n = 50$  EGFP positive cells per sample.

## 2.2.12 SDS-PAGE and Western Blot

### 2.2.12.1 *Harvesting and cell lysis*

Dead cells were harvested by collecting the supernatant from wells into a sterile reaction tube on ice. After adding 1x PBS to the wells, adherent (viable) cells were scraped off and transferred to the same tube. Wells were subsequently washed once with 1x PBS to collect remaining cells. Cell suspension was centrifuged (600xg, 5 min, 4°C) and supernatant aspirated. Cell pellets were washed in 1x PBS and centrifuged again. Then, cell pellets were mixed with 50 – 100 µl of ice-cold lysis buffer complemented with protease and phosphatase inhibitor (PIC/PS). Cells were lysed using the Bioruptor sonification system for 4.5 min (cycle duration ~30 s at 4°C) and cell debris was subsequently removed by centrifugation (17.000xg, 15 min, 4°C).

### 2.2.12.2 *BCA assay*

For determining protein content, cell lysates were subjected to the Pierce BCA Protein Assay Kit according to the manufacturer's protocol. In short, 1 µl of cell lysate each was transferred to three wells (triplicates) of a flat-bottom 96-well plate.

As a standard, different amounts of BSA solution (0 – 10  $\mu$ l, c = 1 mg/ml) were transferred to wells of the same plate as duplicates. BCA reagent solution was added to each well (200  $\mu$ l/well) and the plate was incubated (30 min, 37°C). Afterwards, absorbance was detected at 562 nm using a multimode plate reader. Cell lysates were diluted to a final protein concentration of 2 mg/ml in 1x Laemmli buffer and stored at -20°C until further use.

### 2.2.12.3 SDS PAGE, Blotting and signal detection

SDS PAGE was performed with self-cast gradient polyacrylamide gels (12 – 20%, components listed in Table 22). Per lane, 20  $\mu$ g protein were separated at 200 V for 1 h. Afterwards, proteins were (semi-dry) blotted onto 0.1  $\mu$ m Nitrocellulose membrane (120 mA/gel, 1 h, RT). Blotting was verified with Ponceau staining followed by washing in 1x TBS-T for 5 min. If necessary, the membrane was cut in pieces allowing parallel detection of different proteins from the same blot. The membrane was then placed in a 50 ml tube and incubated in blocking solution on a roller shaker (1 h, RT). After blocking, primary antibodies (Table 2) diluted in 5% (w/v) BSA in 1x TBS-T were applied (o/n, 4°C, roller shaker). On the next day, the membrane was washed thrice in 1x TBS-T (3 x 10 min, roller shaker) and HRP-conjugated secondary antibodies (Table 3) were applied (1 h, RT, roller shaker) diluted in 5% (w/v) dry milk TBS-T.

**Table 22: Components of self-cast gradient polyacrylamide gels.**

Stock solutions were pre-mixed and kept at 4°C, while APS and TEMED were added to the respective amount of stock solution just before gel casting. Resolving gel was cast from 12% and 20% gel stock solution (1:1 ratio) which were gradient mixed in a serological pipette by air aspiration.

Resolving gel		Stacking gel stock solution
12% gel stock solution	20% gel stock solution	
30% (v/v) acrylamide 40 % [29:1]	50% (v/v) acrylamide 40 % [29:1]	13.5% (v/v) acrylamide 30% [37.5:1]
25% (v/v) 1.5 M Tris pH – 8.8	25% (v/v) 1.5 M Tris pH – 8.8	25% (v/v) 0.5 M Tris pH – 6.8
0.1% (w/v) SDS	0.1% (w/v) SDS	0.1% (w/v) SDS
in dH <sub>2</sub> O	in dH <sub>2</sub> O	in dH <sub>2</sub> O
For polymerisation (per 10 ml stock solution)		
100 $\mu$ l 10% (w/v) APS	100 $\mu$ l 10% (w/v) APS	100 $\mu$ l 10% (w/v) APS
5 $\mu$ l TEMED	4 $\mu$ l TEMED	10 $\mu$ l TEMED

The membrane was washed again thrice in 1x TBS-T (3 x 10 min, roller shaker). Then, the membrane was incubated with ECL substrate (SuperSignal West Dura, 5 min, RT) and chemiluminescence signals were detected with the Stella Modular High Performance Imaging System. Images were exported as 16-bit .TIFF raw files and edited in Fiji software. Densitometric analysis of band intensity was performed using Fiji software.

### 2.2.13 siRNA-mediated knockdown

siRNA-mediated knockdown was performed with cells seeded the day before following the “DharmaFECT Transfection Reagents – siRNA transfection protocol” (Horizon Discovery Ltd., Waterbeach, UK) with smart-pool siRNAs (listed in Table 23).

**Table 23: List of smart-pool siRNAs (Horizon Discovery).**

Stock concentration: 50  $\mu$ M.

name	abbreviation	Cat. no.
<b>siGENOME Non-Targeting siRNA #2</b>	siCtrl	D-001210-02-20
<b>siGENOME Human BOK (666) siRNA</b>	siBOK	M-004394-00-0005
<b>siGENOME Human BCL2 (596) siRNA</b>	siBCL-2	M-003307-06-0005

In short, siRNAs were diluted in pre-warmed OptiMEM (100  $\mu$ l per 1 ml cell culture medium) to a final concentration of 50 nM. In a separate tube, twice the volume of siRNA stock solution DharmaFECT #1 reagent was mixed with pre-warmed OptiMEM (100  $\mu$ l per 1 ml cell culture medium) followed by incubation (5 min, RT). siRNA solution was mixed into the DharmaFECT solution (siRNA-to-DharmaFECT volume ratio of 1:2) and the resulting transfection mix was incubated for 20 min at RT. Then, unsupplemented cell culture medium was added up to the final volume needed (1 ml total volume per 1  $\mu$ l siRNA stock). Medium was aspirated from cell culture vessels, transfection mix was added and cells were placed back in the incubator (37°C, 5% CO<sub>2</sub>). After 6 h, transfection mix was aspirated and supplemented cell culture medium added to the cells followed by another incubation o/n (37°C, 5% CO<sub>2</sub>).

### 2.2.14 Caspase-Glo 3/7 assay

Caspase activity was assessed by the Caspase-Glo 3/7 assay (Promega corp., Madison, WI, USA) according to the manufacturer’s protocol. In brief, Caspase-Glo 3/7 substrate and buffer were equilibrated to RT and mixed.

Cells were harvested 18 h post transfection (2.2.7) collecting the supernatant with floating (dead) cells as well as attached (viable) cells using 0.05% trypsin-EDTA. Wells were subsequently washed with 1x PBS to collect remaining cells. Cells were centrifuged (600xg, 5 min) and supernatant was aspirated followed by another washing step in 1x PBS and centrifugation (600xg, 5 min). Cell pellet was resuspended in 30  $\mu$ l of pre-warmed OptiMEM and cell suspension was split into three wells of a white-bottom 96-well plate (10  $\mu$ l per well, triplicates). To each well, 10  $\mu$ l of Caspase-Glo 3/7 substrate was added and the plate gently shaken for 30 s on a horizontal shaker followed by incubation for 30 min at RT. Luminescence was assessed using a multi mode plate reader (1 s/well) and data was analysed using MS Excel.

#### 2.2.15 Application of cell death-inducing compounds

The proteasome inhibitor Bortezomib (Velcade), the ER stress compound Tunicamycin and the BCL-2-specific inhibitor ABT-199 (Venetoclax) were applied to either cells seeded the day before or cells which underwent siRNA-mediated knockdown. For that, medium was aspirated from wells and exchanged with supplemented cell culture medium containing the indicated concentrations of compounds. Then, cells were incubated (37°C, 5%CO<sub>2</sub>) for the indicated time.

#### 2.2.16 Incucyte time-lapse imaging (cell death assay)

Cells were seeded in triplicates (96-well format), siRNA-mediated knockdown (2.2.13) was performed and the next day medium was aspirated and cells were incubated with 2  $\mu$ M Tunicamycin in phenol red-free medium containing 0.67  $\mu$ g/ml PI. Cells were then transferred to the Incucyte S3 imaging system (37°C, 5% CO<sub>2</sub>) and wells were imaged at 5 positions per well every hour using a 20x air Objective (brightfield + red fluorescence (ex. 567 – 607; em. 622 – 704 nm)). After 40 h, Digitonin was added to each well (final concentration 100  $\mu$ g/ml) to permeabilize all cells for PI and cells were imaged once more. Using the Incucyte software (Sartorius, Göttingen, Germany, v2022A), the ratio of PI positive area (red channel) to cell confluency area (from brightfield) was exported reflecting the ratio of dead cells to the total number of cells. Using MS Excel, the value for PI/Confluency after Digitonin addition was set to 100% PI positive cells and subsequently used to normalise PI/Confluency at all other time points. Data was plotted over time using Graphpad Prism 9 software.



## 2.2.17 *In silico* protein sequence analyses

### 2.2.17.1 *Hydropathy plots*

Hydropathy scores of TMD sequences were calculated using the ProtScale online tool ([web.expasy.org](http://web.expasy.org), (345)) according to Kyte and Doolittle (346). Scores were exported and displayed using Graphpad Prism 9.

### 2.2.17.2 *Protein folding prediction*

Protein folding of BAX and BCL-2 protein sequences (Table 15) was predicted by the Alphafold Colab online tool ([colab.research.google.com](http://colab.research.google.com), (340)) at default settings. Structures were visualised using PyMOL (342).

## 2.2.18 Molecular dynamics simulations

*In silico* modelling of BOK-TMD and BCL-2-TMD interaction was planned in collaboration with and performed by Thomas Fellmeth and Kristyna Pluhackova from the Stuttgart Research Center Systems Biology, University of Stuttgart, Germany.

Using high-throughput multiscaling molecular dynamics (MD) simulations BOK-TMD and BCL-2-TMD (sequences listed in Table 24) oligomerisation was studied by DAFT in combination with the Martini3 coarse-grained (CG) force-field (347, 348). After CG simulations over 50  $\mu$ s, structures were clustered and most frequent conformations were converted back to all-atom resolution via the backward method (349). With these representative structures all-atom simulations were performed for 1  $\mu$ s in the CHARMM36m force field (350–353) and TIP4p water model (354). Simulations were evaluated by GROMACS 2020 (355) followed by visualisation in PyMOL (342). Contact maps and secondary structure plots were obtained using Gnuplot (356). Simulations were performed in a mimic of the ER membrane consisting of a symmetrical lipid bilayer with 4.0%  $\alpha$ -palmitoyl-2-oleoyl-sn-glycerol (PODG), 7.0% cholesterol, 7.0% 1-myristoyl-2-oleoyl-sn-glycero-3-phosphoethanolamine (MOPE), 7.0% 1-palmitoyl-2-oleoyl-sn-glycero-3-phosphoinositol (POPI), and 75.0% 1-myristoyl-2-oleoyl-sn-glycero-3-phosphocholine (MOPC) (357) solvated with 0.1 mol/l NaCl solution.

**Table 24: BOK and BCL-2 TMD sequences used for molecular dynamics simulations.**

Name	positions	amino acid sequence
<b>BOK</b>	180 – 212	S YNPGLRSHWL VAALCSFGRF LKAAFFVLLP ER
<b>BCL-2</b>	208 - 239	PLF DFSWLSLKTL LSLALVGACI TLGAYLGHK

### 2.2.19 Statistical analysis

Statistical significance was determined using unpaired t-test with Welch's correction (two groups) or one-way ANOVA with a Tukey multiple comparison post-hoc test ( $\geq$  three groups) if not stated otherwise. Data from multiple independent experiments is either expressed as mean  $\pm$  standard deviation (sd) for  $n \geq 3$  or mean  $\pm$  range for  $n = 2$  experiments as stated in the figure legends. Statistical significance of differences between groups is denoted as follows: \* $p < 0.05$ , \*\* $p < 0.01$ , \*\*\* $p < 0.001$ , \*\*\*\* $p < 0.0001$ . Statistical tests were performed using the Graphpad Prism 9 software.

### 3 Results

#### 3.1 Development of a split luciferase assay for detection of TMD interaction

To be able to systemically analyse the TMD interaction network of Bcl-2 family proteins, the first aim of this thesis was to create a reliable tool for detecting TMD interactions. The assay platform should not only be suitable to characterise Bcl-2 TMD interactions in living cells, but also generate unambiguous, quantifiable data comprising appropriate controls and normalisation tools.

During the last decades, various methods were applied to study interactions of (Bcl-2 protein) TMDs. For example, Zhang *et al.* applied disulfide cross-linking to unravel TMD dimerization of BAX which, however, needs the use of cysteine-containing mutants for every new analysed combination (332). Hence, this method was not considered for the new interaction platform. Another possible alternative is the ToxRed system used by Andreu-Fernández and coworkers (171). In this assay, expression of red fluorescent protein as reporter gene depends on TMD-mediated oligomerisation of the virulence regulatory protein ToxR. However, the ToxRed system has the drawback to be used in *E.coli* membranes with fundamentally different composition than eukaryotic membranes – also a major drawback for the new interaction platform. Also bimolecular fluorescence complementation (BiFC) was used by the same authors for studying TMD interaction in living, human cells (171, 333). Here, TMD interaction is detected as a fluorescence signal which occurs when two fragments of a fluorescent protein are brought together by the fused TMDs of interest enabling fluorophore reconstitution. But, the BiFC assay has a potential risk of false positive signals because of the high affinity between fragments and irreversibility of fluorophore formation *in vitro* (358). Although more recently developed BiFC systems might circumvent the problem of false positive signals (359), BiFC was not selected as an interaction platform.

In 2016, Dixon *et al.* developed the NanoBiT luciferase system. NanoBiT, a bimolecular split luciferase derived from the NanoLuc luciferase for detection of protein-protein interaction, consists of a Large BiT (LgBiT) subunit of about 18 kDa and a Small BiT (SmBiT) subunit comprising an 11 amino acid (AA) sequence (344).

In contrast to the other mentioned interaction assays, NanoBiT has some outstanding advantages: firstly, the luciferase has a small size (~19 kDa) less likely to cause sterical hindrance and interfere with protein function. Secondly, LgBiT and SmBiT subunits have a low affinity towards each other outside the usual range of protein-protein interactions ( $K_D = 190 \mu\text{M}$ ). Thus, LgBiT and SmBiT only form functional NanoBiT luciferase when both subunits reside in close proximity through fused proteins of interest. In contrast to BiFC assays, the low affinity ensures the reversibility of reconstitution and thus minimalization of false positive signals. Thirdly and lastly, the system is applicable in living human cells enabling the detection of interactions in the natural subcellular environment (344, 360).

Taken together, the advantages in size, subunit affinity and applicability of NanoBiT in viable cells were decisive for the selection as the interaction platform to assess TMD interaction of Bcl-2 proteins. Also, additional reasons for selection of the NanoBiT system are the adaptability for various TMD combinations and that the produced luminescence signal can be combined with fluorescence as a normalisation tool. Therefore, the following chapters include the individual development steps of the NanoBiT split luciferase assay starting with the selection of luciferase substrate, definition of detection parameters and design of NanoBiT expression vectors. Simultaneously expressed fluorescence was examined as a possible normalisation tool and the final workflow was successfully validated with appropriate TMD interaction controls.

### 3.1.1 Investigation of NanoBiT assay parameters and fluorescence normalisation

NanoLuc and NanoBiT luciferase catalyse oxidation of the substrate furimazine to furimamide with light emission at 460 nm (361). For NanoBiT, so-called “extended live cell” substrates, Vivazine and Endurazine, are available, while also Coelenterazines, furimazine analogs, such as Coelenterazine-h, are possible substrates for NanoLuc or NanoBiT luciferase respectively.

To initially verify the NanoBiT assay workflow for the TMD interaction assay and select a suitable NanoBiT substrate, HEK293 cells were transfected to express either a positive or negative control for NanoBiT activity. The NanoBiT positive control is based on the interaction of PRKAR2A and PRKACA, two subunits of protein kinase A (reviewed in (362)), fused to LgBiT and SmBiT respectively. The NanoBiT negative control comprises Halo tag-SmBiT.

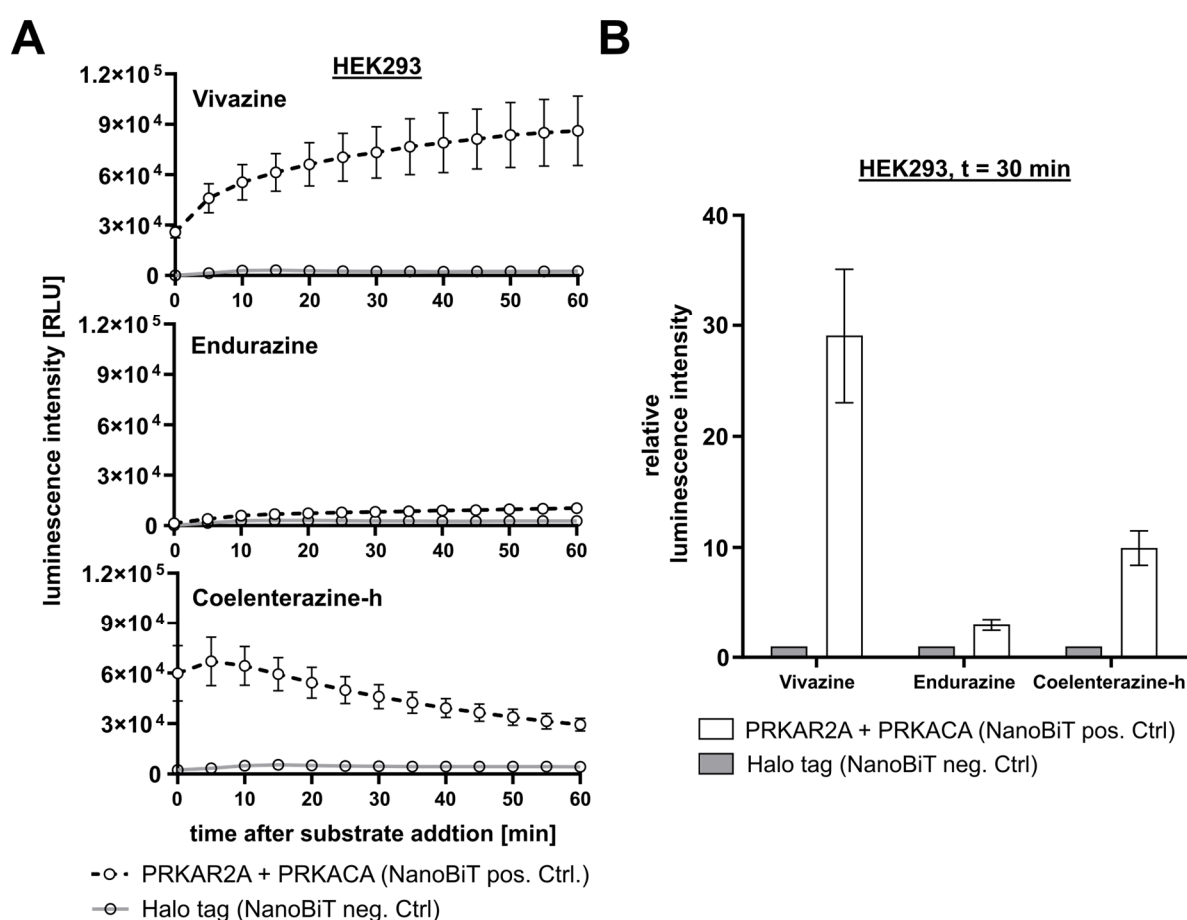
Initially, the three substrates Vivazine, Endurazine and Coelenterazine-h were added to the cells and luminescence was detected every 5 min using the ENspire multimode plate reader (Figure 8A). In the NanoBiT assay, Vivazine substrate led to an initial luminescence signal of  $2.6 \cdot 10^4$  RLU for the positive control which continuously increased over a 60 min detection window to  $8.6 \cdot 10^4$  RLU (Figure 8A). Luminescence of Endurazine also increased steadily starting, however, at  $1.5 \cdot 10^3$  RLU with a maximum luminescence of  $1.0 \cdot 10^4$  RLU at  $t = 60$  min. Coelenterazine-h showed the highest initial luminescence among substrates tested ( $6.0 \cdot 10^4$  RLU). But, Coelenterazine-h was also the only substrate for which luminescence started declining after peaking at  $t = 5$  min ( $6.7 \cdot 10^4$  RLU) to half the initial luminescence after 60 min ( $2.9 \cdot 10^4$  RLU). Expectedly, luminescence with all substrates in combination with cells expressing NanoBiT negative control remained substantially lower than the luminescence of the positive control. Highest absolute negative control luminescence was detected for Coelenterazine-h peaking at  $5.4 \cdot 10^3$  RLU. Background luminescence for control samples with untransfected cells or Coelenterazine-h substrate alone was, however, substantially lower than that ( $1.5 \cdot 10^3$  RLU, Supplementary Figure S2B). After  $t = 30$  min, relative luminescence compared to negative control was highest for Vivazine (29-fold), followed by Coelenterazine-h (10-fold) which was still 3.3-fold higher than for Endurazine (3-fold, Figure 8B). As summarized in Table 25, Endurazine though expected to have highest luminescence duration (363) showed least signal intensity, while Vivazine yielded highest signal intensity. Although generating the highest background signal and expected to have lowest luminescence duration, Coelenterazine-h performed well for signal intensity.

**Table 25: Comparison of NanoBiT substrates.**

Substrates were compared with respect to cost, luminescence duration, signal intensity and background luminescence. Prices originate from substrate amount needed per well when purchased at normal rate from Promega. Substrate characteristics are rated with score: + (least), ++ (middle), +++ (most) according to Figure 8 and manufacturer information.

Substrate	Cost/sample [€/well]	Luminescence duration	Signal intensity	Background luminescence
Vivazine	1.79	++	+++	++
Endurazine	1.79	+++	+	+
Coelenterazine-h	0.08	+	++	+++

Since Vivazine and Endurazine are considerably more expensive than Coelenterazine-h (22-fold price/well), Coelenterazine-h was selected as substrate for the NanoBiT assay. As fixed point of time for luminescence comparison after Coelenterazine-h addition,  $t = 30$  min was selected for all following experiments, since luminescence for NanoBiT positive control does not change as rapidly as in the first 20 min after substrate addition with calculated standard deviations from  $t = 20$  min to nearly  $t = 40$  min overlapping with the mean luminescence at  $t = 30$  min (Figure 8A). Of note, after comparison of different detection times per well, 1 s/well was selected for following experiments (Supplementary Figure S2A).



**Figure 8: Coelenterazine-h is a suitable substrate for the NanoBiT split luciferase assay.**

**A** – time kinetics showing luminescence after NanoBiT substrate addition assessed by a multimode plate reader. HEK293 cells were transfected with plasmids encoding LgBiT-PRKAR2A and SmBiT-PRKACA (NanoBiT pos. Ctrl) or the Halo tag-SmBiT (NanoBiT neg. Ctrl). After 24 h, cells were harvested and luciferase substrates Vivazine and Endurazine were applied in 1x concentration (manufacturer's manual), while Coelenterazine-h was used in a final concentration of 5  $\mu$ M. Mean  $\pm$  sd of technical triplicates from one representative experiment. **B** – luminescence data out of A for  $t = 30$  min after substrate addition. Luminescence for each substrate is shown relative to the respective negative control which is set to one. Values represent mean  $\pm$  sd of technical triplicates from one representative experiment.

With substrate and detection parameters set, a plasmid-based system should be developed to harness the potential of the NanoBiT system for detection of TMD interactions. Plasmids were prepared using the NEBuilder system (Gibson assembly cloning). The pBiT vector backbone (Promega) was combined with respective cDNA fragments to encode for mCitrine (mCitr, in LgBiT plasmids) or mTurquoise (mTurq2, in SmBiT-plasmids) followed by a T2A self-cleaving sequence (GDVEXNPGP) and a NanoBiT subunit (LgBiT or SmBiT respectively) which was C-terminally fused to a TMD sequence via a 14 AA hydrophilic linker (Figure 9A). Thereby, fluorophores mCitr or mTurq2 and NanoBiT-TMDs are expressed in equimolar amounts but not fused because of ribosomal skipping in the T2A sequence. Thus, simultaneously expressed fluorophores not only serve as a marker for transfected cells, but also constitute a normalisation tool for the detected NanoBiT luminescence. Moreover, expression is controlled by a herpes simplex virus thymidine kinase (HSV TK) promoter ensuring moderate gene expression (364) to avoid strong overexpression of NanoBiT-TMDs.

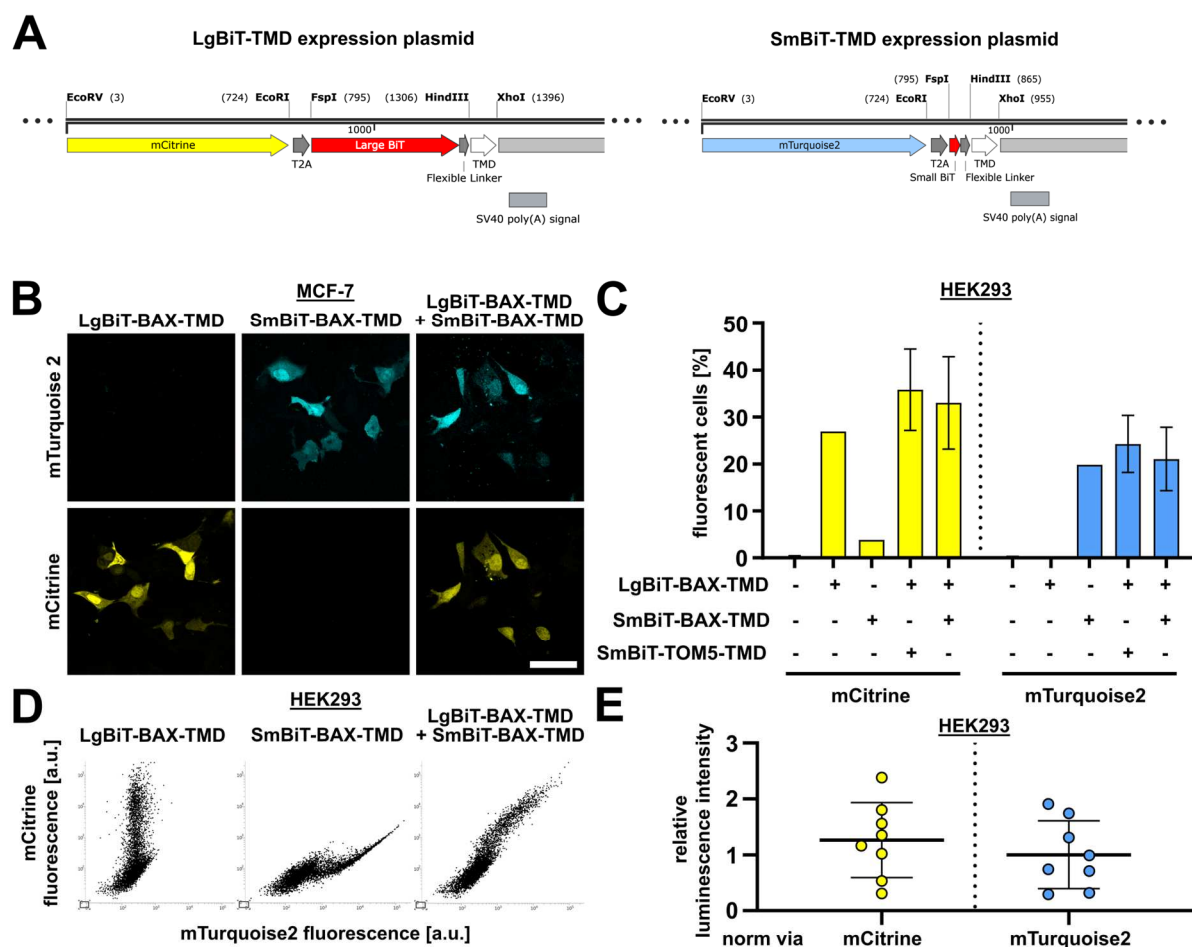
In a first step before transfection of NanoBiT-TMD-encoding plasmids, different liposome-based transfection reagents were compared by transfection with a GFP-encoding control plasmid in MCF-7 breast cancer cells and subsequent quantification of GFP positive (GFP+) cells. PEI transfection reagent was most efficient among reagents tested and selected for further experiments (Supplementary Figure S2C). To verify whether mCitr and mTurq2 were successfully expressed after PEI transfection of MCF-7 cells with NanoBiT-TMD-encoding plasmids, fixed cells were analysed using confocal laser scanning microscopy (cLSM, Figure 9B). Indeed, cells transfected to express LgBiT-BAX-TMD and SmBiT-BAX-TMD showed specific, cytosolic expression of mCitr and mTurq2 respectively. Moreover, co-transfection of both LgBiT- and SmBiT-BAX-TMD-encoding plasmid resulted in expression of mCitr and mTurq2 in the same cells. Since proportional expression of mCitr and mTurq2 was observed in cLSM images, relation of mCitr and mTurq2 expression in single HEK293 cells co-transfected to express different combinations of LgBiT- and SmBiT-TMDs was further analysed using flow cytometry. Here, percentage of mCitr positive (mCitr+) cells representing transfection efficiency 24 h post transfection for LgBiT-TMD-encoding plasmids ranged from 27% for LgBiT-BAX-TMD alone to 35% for the co-expression of LgBiT-BAX-TMD and SmBiT-BAX-TMD. On the other hand, percentage of mTurq2 positive (mTurq2+) cells was similar for expression of SmBiT-BAX-TMD alone (19%) and co-expression of LgBiT-BAX-TMD and SmBiT-BAX-TMD (24%).

Of note, expression of SmBiT-BAX-TMD alone resulted in detection of ~4% mCitr+ cells indicating slight crosstalk in the flow cytometry setting used, while virtually no mTurq2+ cells were detected for expression of LgBiT-BAX-TMD. Co-expression of LgBiT-BAX-TMD with another SmBiT-TMD (TOM5-TMD) did not change transfection efficiency (33% mCitr+ cells; 21% mTurq2+ cells). Also scatter plots in which mCitr fluorescence intensity is plotted over mTurq2 fluorescence intensity revealed a proportional fluorophore expression in single cells (Figure 9C), i.e. cells with high LgBiT/mCitr expression possess similar high levels of SmBiT/mTurq2. Therefore, normalisation of NanoBiT luminescence over mTurq2 or mCitr was assumed to yield similar results. However, scatter plot of cells transfected to express SmBiT-BAX-TMD alone also showed subtle increase in mCitr fluorescence intensity with increasing mTurq2 fluorescence intensity corroborating crosstalk for detection channels used.

In order to prove that normalisation over either fluorophore is sufficient, HEK293 cells were again co-transfected to express LgBiT-BAX-TMD and SmBiT-TOM5-TMD followed by luminescence and fluorescence detection. Normalised, relative luminescence was indeed comparable for normalisation via mCitr ( $1.26 \pm 0.67$ ) and mTurq2 (set to  $1.00 \pm 0.61$ , Figure 9E). Relative percentage of mCitr+/mTurq2+ cells detected by flow cytometry across a panel of different LgBiT-TMD and SmBiT-TMD combinations (co-expressed in HEK293 cells) was more similar to relative mTurq2 fluorescence than mCitr fluorescence detected in same samples using a multimode plate reader (Supplementary Figure S2D). Normalisation of luminescence data from NanoBiT assay, hence, was subsequently performed using mTurq2 fluorescence.

In sum, using NanoBiT negative and positive controls Coelenterazine-h was selected as substrate for subsequent NanoBiT experiments. As detection parameters, 1 s/well detection duration and time point of luminescence detection at  $t = 30$  min after substrate addition were determined. NanoBiT assay workflow was successfully optimised regarding transfection efficiency. Furthermore, simultaneously expressed fluorescence was shown to be expressed specifically and proportionally in single cells enabling normalisation of NanoBiT luminescence over mTurq2 fluorescence.





**Figure 9: Fluorophore expression of co-transfected NanoBiT plasmids is comparable.**

**A** –Horizontal sketch of plasmid structure for NanoBiT-TMD expression. **B** –cLSM images of MCF-7 cells transfected to express indicated NanoBiT-TMDs. 24 h post transfection cells were fixed and imaged. Upper row (mTurquoise2 (mTurq2)): ex. at 405 nm, lower row (mCitrine (mCitr)): ex. at 488 nm. Images are representative of two independent experiments. Scale bar = 50  $\mu$ m. **C** –Flow cytometric analysis of NanoBiT-TMD plasmid transfection efficiency in HEK293 cells via mCitr and mTurq2 fluorescence. Cells were transfected with indicated combinations of NanoBiT-TMD plasmids featuring simultaneous expression of mCitr or mTurq2 respectively and harvested for flow cytometry after 24 h. Graph shows percentage of mCitr and mTurq2 positive cells from one (single transfections) or three (untransfected, co-transfections; shown as mean  $\pm$  sd) independent experiments. **D** –Scatter plots showing mCitr fluorescence intensity plotted against mTurq2 fluorescence intensity of HEK293 cells transfected to express indicated NanoBiT-TMD plasmids, 24 h post transfection. One independent experiment. **E** –NanoBiT luminescence detection to compare normalisation via mCitr and mTurq2 fluorescence in HEK293 cells co-transfected with LgBiT-BAX-TMD and SmBiT-TOM5-TMD-encoding plasmids. Cells were harvested 24 h post transfection and subjected to NanoBiT assay detecting fluorescence as well as luminescence using a multimode plate reader. Single dots reflect mean luminescence (technical triplicates) out of  $n = 8$  independent experiments normalised via mCitr or mTurq2 fluorescence respectively. Values are plotted relative to mTurquoise2-normalised data which's mean was set to one. The mean  $\pm$  sd is indicated as a horizontal line.

### 3.1.2 Validation of the NanoBiT assay with TMD interaction controls

Previous experiments established the NanoBiT assay workflow regarding substrate, detection parameters, expression system and data normalisation via fluorescence. Thus, the final step prior to analysing TMD interactions of Bcl-2 family proteins was to validate the assay with robust positive as well as negative controls to ensure reliable detection of TMD interaction.

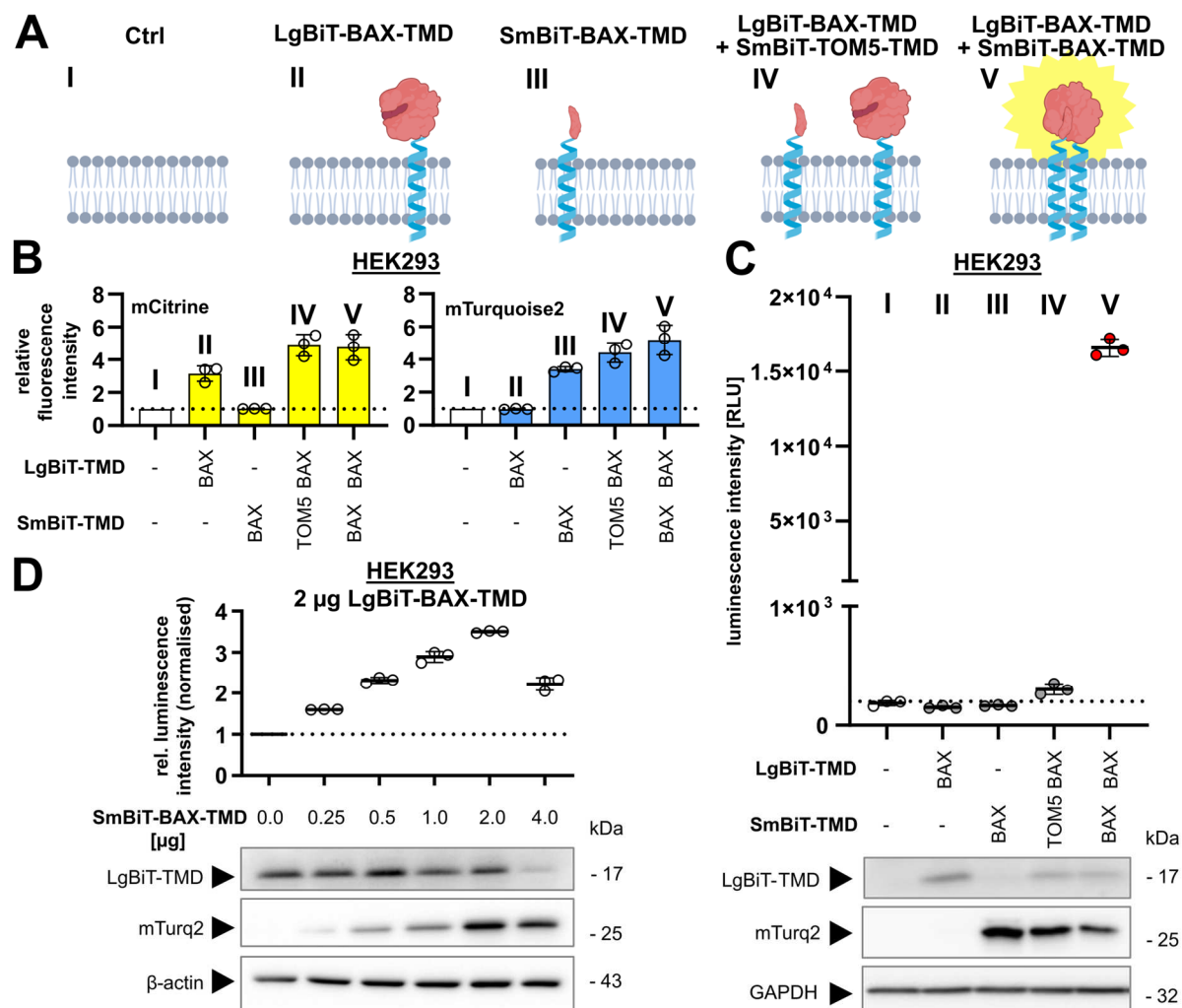
As illustrated in Figure 10A, to assess background luminescence, HEK293 cells were either left untransfected or transfected to express LgBiT-BAX-TMD alone or SmBiT-BAX-TMD alone. As a functional negative control for TMD interaction, HEK293 cells were co-transfected to express LgBiT-BAX-TMD and SmBiT-TOM5-TMD. The mitochondria-resident protein TOM5 harbours a Ct TMD with similar size and structure as TMDs of Bcl-2 proteins (365). Since TOM5 is not known to interact with any Bcl-2 protein such as BAX, combination of BAX-TMD and TOM5-TMD in the NanoBiT assay is expected to facilitate no NanoBiT complementation despite of their colocalisation. By contrast, dimerization of BAX is a well described TMD interaction (171) and essential for BAX pore enlargement during MOMP (331, 332). Hence, BAX-TMD homotypic interaction is expected to drive NanoBiT complementation reflected by an increased luminescence signal in the NanoBiT assay. Hence, co-expression of LgBiT-BAX-TMD and SmBiT-BAX-TMD was used as a functional positive control.

To validate the NanoBiT assay by the controls described above, HEK293 cells transfected to express the described combinations of LgBiT-TMDs and SmBiT-TMDs or left untransfected were subjected to the previously optimised NanoBiT assay workflow with simultaneous fluorescence and luminescence detection in a multimode plate reader. Expression of LgBiT-BAX-TMD alone resulted in relative fluorescence at 531 nm (for mCitr detection) of 3.2-fold compared to untransfected control (background fluorescence), while fluorescence at 474 nm (for mTurq2 detection) was comparable to background fluorescence (1.0-fold, Figure 10B). Expression of SmBiT-BAX-TMD alone led to a relative fluorescence at 474 nm of 3.4-fold, whereas fluorescence at 531 nm was similar to untransfected control. Combinations of LgBiT-BAX-TMD with SmBiT-TOM5-TMD or SmBiT-BAX-TMD resulted in significant increase of both fluorescence at 531 nm and 474 nm compared to untransfected cells (531 nm: 4.9-fold or 4.8-fold; 474 nm: 4.4-fold or 5.1-fold).

Luminescence for untransfected cells (185.9 RLU) was similar to cells transfected to express LgBiT-BAX-TMD alone (150.4 RLU) or SmBiT-BAX-TMD alone (164.2 RLU) indicating no increased background luminescence due to the presence of a single NanoBiT subunit (Figure 10C). Strikingly, expression of LgBiT-BAX-TMD in combination with SmBiT-TOM5-TMD (BAX-/TOM5-TMD) did barely increase luminescence (303.6 RLU), while expression of LgBiT-BAX-TMD and SmBiT-BAX-TMD (BAX-/BAX-TMD) yielded a drastically increased luminescence signal ( $1.7 \cdot 10^4$  RLU) compared to untransfected cells. In same samples, LgBiT-TMD and mTurq2 (as SmBiT surrogate marker) expression was validated using Western Blot (Figure 10C). Confirming system-independent functionality, BAX-/BAX-TMD yielded increased relative luminescence compared to the negative control BAX-/TOM5-TMD also in HeLa (1.7-fold) and MCF-7 cells (2.7-fold, Supplementary Figure S3A).

In addition to assay validation, the mode of BAX-TMD homotypic interaction was further investigated by detecting luminescence for HEK293 cells transfected with plasmid encoding LgBiT-BAX-TMD and varying amounts of plasmid encoding SmBiT-BAX-TMD as validated by Western Blot (Figure 10D, lower panel). Interestingly, relative luminescence increased with increasing amounts of SmBiT-BAX-TMD-encoding plasmid up to a LgBiT/SmBiT ratio of 1:1 with a maximum relative luminescence of 3.5-fold compared to control sample (0  $\mu$ g SmBiT-BAX-TMD). A LgBiT/SmBiT ratio of 1:2 led to relative luminescence of 2.2-fold compared to control sample. Thus, LgBiT/SmBiT TMD transfection ratio of 1:1 leading to a 1:1 expression ratio of both fusion proteins is presumed to result in most efficient NanoBiT complementation.

Taken together, fluorescence of mCitr and mTurq2 as well as expression of LgBiT and mTurq2 was found to be specific in respective control samples. Luminescence was substantially increased for the functional positive control (BAX-/BAX-TMD) in contrast to the near-background luminescence of the functional negative control (BAX-/TOM5-TMD) rendering the novel NanoBiT assay a reliable tool for identification and quantitative analysis of Bcl-2 TMD interaction.



**Figure 10: BAX-TMD homotypic interaction is a reliable positive control for the NanoBiT assay.**

**A** – Sketches of controls used to validate the NanoBiT split luciferase assay for detection of Bcl-2 TMD interactions. Generated with Biorender.com. **B** – Fluorescence intensity as assessed with a multimode plate reader during the NanoBiT split luciferase assay. HEK293 cells were transfected with indicated NanoBiT-TMD-encoding plasmids and harvested for NanoBiT assay 24 post transfection. mCitrine (531 nm) and mTurquoise2 (474 nm) fluorescence is shown relative to control (empty vector Ctrl, indicated by dashed line) as mean  $\pm$  sd of technical triplicates from one independent experiment. **C** – Luminescence data from NanoBiT assay. HEK293 cells were transfected as in B and subjected to NanoBiT assay (top) and Western Blot (bottom). Single dots represent technical triplicates from one independent experiment. Mean  $\pm$  sd is indicated as a horizontal line. Dashed line indicates level of untransfected control. Construct expression was verified via Western Blot (bottom) using antibodies against LgBiT, mTurquoise2 (mTurq2) to indirectly detect SmBiT-TMD and GAPDH as loading control. Representative Blot from two independent experiments. **D** – SmBiT-BAX-TMD titration in HEK293 cells. Cells were co-transfected with 2  $\mu$ g of LgBiT-BAX-TMD-encoding plasmid combined with indicated amounts of SmBiT-BAX-TMD-encoding plasmid. Total DNA amount per transfection was kept constant by the addition of empty vector. 24 h post transfection, cells were harvested and subjected to NanoBiT assay (top) and Western Blot (bottom). Fluorescence-normalised luminescence is shown relative to sample with 0  $\mu$ g SmBiT-BAX-TMD-encoding plasmid (indicated by dashed line) as mean  $\pm$  sd of technical triplicates from one independent experiment. Construct expression was verified via Western Blot (bottom) as shown in C with  $\beta$ -actin as loading control. Blot from one independent experiment.

### 3.2 Systematic analysis of the Bcl-2 TMD interactome

Although interactions of Bcl-2 family proteins are classically defined by BH3:groove interaction, increasing evidence suggests a role of the TMD in protein-protein interactions and apoptosis signalling (171, 291, 333). Most Bcl-2 family proteins possess a TMD as a membrane-anchoring Ct sequence. However, interactions of Bcl-2 proteins via their TMD as a whole have not yet been systematically investigated. Thus, this thesis next aims to shed more light on the entirety of all Bcl-2 TMD interactions – the Bcl-2 TMD interactome.

In the second chapter of the results part in this thesis, therefore, the newly developed NanoBiT assay described in chapter one (3.1) is utilized to systematically analyse the TMD interaction network of Bcl-2 multi-domain proteins. Firstly, interactions among TMDs of effector proteins BAX, BAK and BOK are investigated. Secondly, combinations of TMDs from anti-apoptotic BCL-2, BCL-XL, BCL-W, MCL-1 and A1 with effector protein TMDs are analysed. And thirdly, TMD subcellular localisation as a critical factor for the interpretation of interaction data is determined.

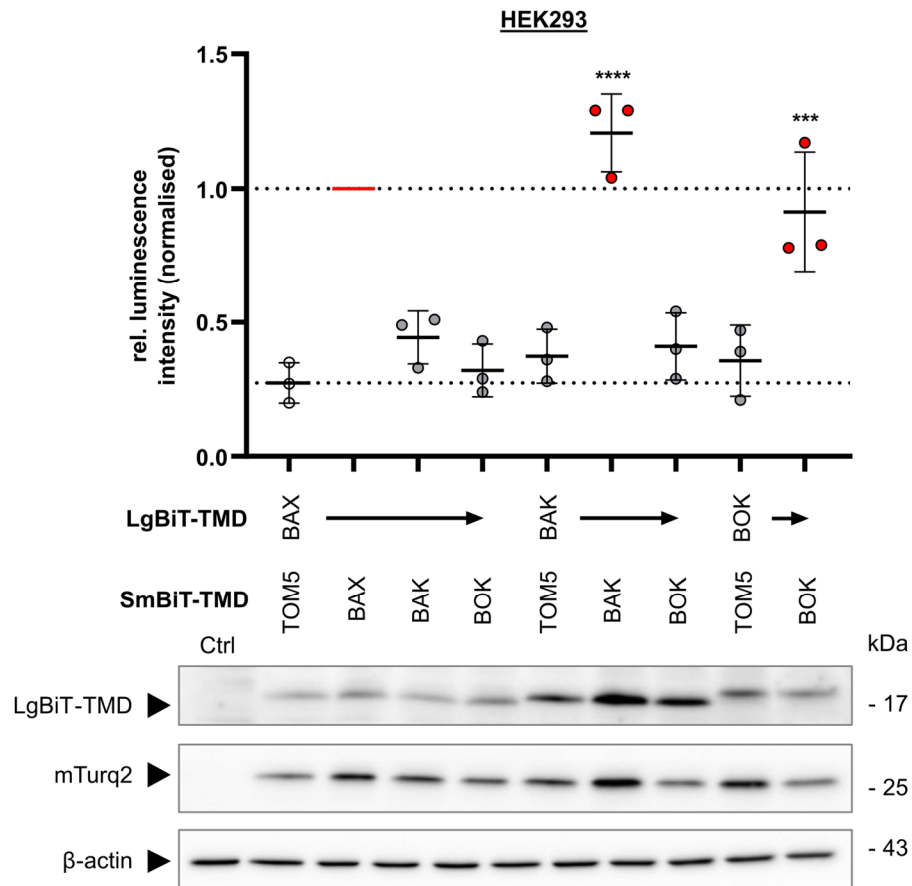
#### 3.2.1 Effector TMDs interact preferentially in a homotypic manner

TMD interaction of effector proteins can substantially influence pore formation in the MOM such as TMD dimerization in BAX pores (332). However, whether TMDs of effector proteins interact among each other and to what extent (TMD) functionality is redundant remains obscure.

To elucidate the interaction of the TMDs of BAX, BAK and BOK, HEK293 cells were co-transfected to express combinations of LgBiT-TMD and SmBiT-TMD covering all interactions among BAX-, BAK-, and BOK-TMD. Cells were then subjected to NanoBiT assay and expression of LgBiT-TMDs and mTurq2 were verified using Western Blot analysis. In detail, LgBiT-BAX-TMD was combined with SmBiT-BAX-, SmBiT-BAK- or SmBiT-BOK-TMD, LgBiT-BAK-TMD with SmBiT-BAK- or SmBiT-BOK-TMD and LgBiT-BOK-TMD with SmBiT-BOK-TMD. Also, all LgBiT-effector-TMDs were combined with SmBiT-TOM5-TMD as negative controls. As specified in 3.1.1, obtained luminescence was normalised to simultaneously detected mTurq2 fluorescence and set in relation to the BAX-/BAX-TMD positive control established in 3.1.2.

As seen for assay validation in Figure 10, relative luminescence for BAX-/BAX-TMD positive control (set to 1.00) was again substantially increased compared to BAX-/TOM5-TMD negative control (0.27, Figure 11, upper panel). Intriguingly, heterotypic combination of BAX-TMD with BAK-TMD or BOK-TMD resulted in relative luminescence which was insignificantly higher than for the negative control. However, a slight increase for BAX-/BAK-TMD could be observed (0.44) which was not seen for BAX-/BOK-TMD (0.32). Combination of BAK-/TOM5-TMD showed relative luminescence which was slightly increased but still comparable to negative control BAX-/TOM5-TMD (0.37) – likewise for heterotypic interaction BAK-/BOK-TMD (0.41). Homotypic combination of BAK-TMD, however, yielded the highest luminescence signal among combinations tested with 1.21-fold luminescence intensity compared to BAX-/BAX-TMD positive control. Interestingly, also homotypic interaction of BOK-TMD resulted in a significantly increased luminescence signal (0.91) compared to negative control BAX-/TOM5-TMD. Relative luminescence of combination BOK-/TOM5-TMD was slightly, but not significantly, increased (0.36) compared to negative control BAX-/TOM5-TMD. Detection of LgBiT-TMDs using Western Blot showed minor differences in size for BAX-TMD, BAK-TMD and BOK-TMD as expected from the varying TMD sequences (protein size ~20 kDa, Figure 11, lower panel). While abundance of LgBiT-BAK-TMD was in general slightly higher than for BAX-TMD or BOK-TMD, expression level among samples with the same LgBiT-TMD were similar. In addition, mTurq2 expression level (as surrogate for SmBiT-TMD) was mostly comparable among samples with slightly elevated levels for combination BAX-/BAX-TMD, BAK-/BAK-TMD and BOK-/TOM5-TMD. Importantly, expression was hence successful and robust for all plasmids used.

In summary, the NanoBiT assay revealed strong homotypic interaction for BAX-TMD, BAK-TMD and BOK-TMD, while interaction signals of heterotypic combinations were negligibly low or comparable to negative controls.



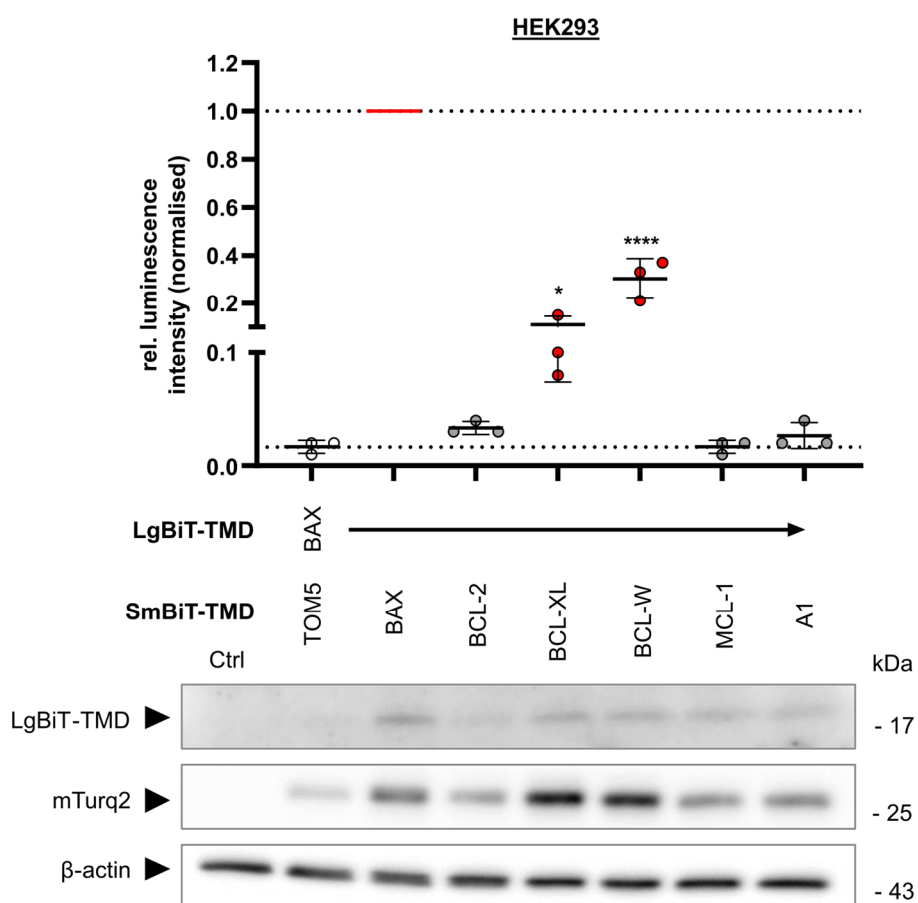
**Figure 11: TMDs of BAX, BAK and BOK show a homotypic interaction pattern.**

NanoBiT interaction data from HEK293 cells co-transfected to express combinations of NanoBiT-TMDs from effector proteins BAX, BAK and BOK. Cells were harvested 24 post transfection and subjected to NanoBiT assay (top) and Western Blot (bottom). For the NanoBiT assay, fluorescence-normalised luminescence intensity is shown relative to positive control (BAX-/BAX-TMD). Mean  $\pm$  sd from three independent experiments. Mean of both negative control (BAX-/TOM5-TMD) and positive control are indicated with a dashed line. Asterisks indicate statistically significant differences compared to negative control. Construct expression was verified via Western Blot (bottom) using antibodies against LgBiT, mTurquoise2 (mTurq2) to indirectly detect SmBiT-TMDs and  $\beta$ -actin as loading control. Ctrl = untransfected cells. Representative Blot from two independent experiments.

### 3.2.2 BAX and BAK TMDs interact both with anti-apoptotic BCL-XL and BCL-W TMDs

The homeostasis of the Bcl-2 interaction network largely depends on the regulating interaction of anti-apoptotic proteins like BCL-2 with effector proteins like BAX (reviewed in (40)). In the next step of the systematic analysis of the Bcl-2 TMD interaction network, interactions of pro-apoptotic BAX and BAK TMDs with TMDs from anti-apoptotic Bcl-2 proteins were thus investigated using the NanoBiT assay.

To this end, HEK293 cells were co-transfected with respective combinations of LgBiT-BAX-TMD or LgBiT-BAK-TMD with SmBiT-TMDs of anti-apoptotic Bcl-2 proteins BCL-2, BCL-XL, BCL-W, MCL-1 and A1. Then, cells were subjected to NanoBiT assay to detect interaction and Western Blot to verify protein expression.



**Figure 12: BAX-TMD interacts moderately with BCL-XL- and BCL-W-TMDs.**

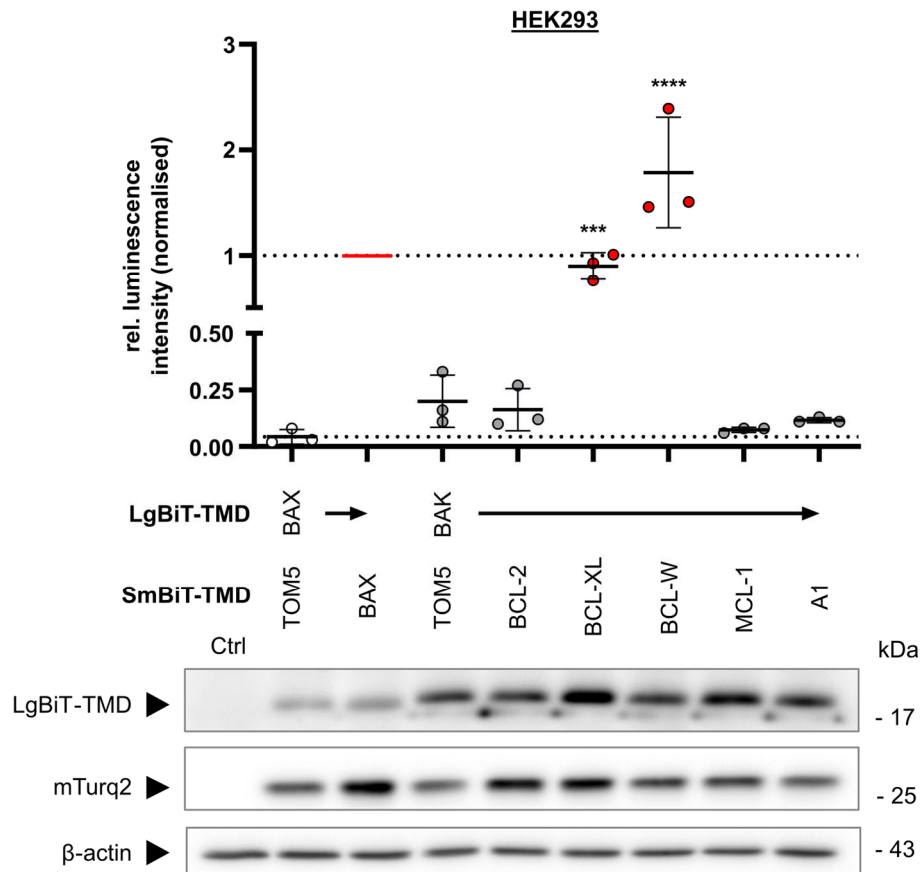
NanoBiT interaction data from HEK293 cells co-transfected to express LgBiT-BAX-TMD in combination with SmBiT-TMDs of antiapoptotic Bcl-2 proteins. Cells were harvested 24 post transfection and subjected to NanoBiT assay (top) and Western Blot (bottom). For the NanoBiT assay, fluorescence-normalised luminescence intensity is shown relative to positive control (BAX-/BAX-TMD). Mean  $\pm$  sd from three independent experiments. Mean of both negative control (BAX-/TOM5-TMD) and positive control are indicated as a dashed line. Asterisks indicate statistically significant differences compared to negative control. Construct expression was verified via Western Blot (bottom) using antibodies against LgBiT, mTurquoise2 (mTurq2) to indirectly detect SmBiT-TMDs and  $\beta$ -actin as loading control. Ctrl = untransfected cells. Representative Blot from two independent experiments.



For BAX-TMD, luminescence relative to BAX-/BAX-TMD positive control (set to 1.00) was elevated for combination with BCL-XL-TMD (0.11) compared to negative control (BAX-/TOM5-TMD, 0.02) which was even more pronounced for combination with BCL-W-TMD (0.30, Figure 12, upper panel). Combinations of BAX-TMD with BCL-2- (0.03), MCL-1- (0.02), and A1-TMD (0.03) resulted in no significant increase in relative luminescence compared to negative control. Moreover, detection of LgBiT-TMDs and mTurq2 using Western Blot verified protein expression for all samples analysed (Figure 12, lower panel). Of note, detected luminescence intensity partially correlated with elevated protein expression, i.e. for combinations BAX-/BAX-TMD, BAX-/BCL-XL-TMD and BAX-/BCL-W-TMD LgBiT-TMD and mTurq2 levels were noticeably higher than for other samples.

For BAK-TMD, combinations with BCL-XL-TMD and BCL-W-TMD led to substantial increase in relative luminescence even more pronounced than for BAX-TMD (0.90 and 1.79 respectively, positive control BAX-/BAX-TMD set to 1.00) compared to BAX-/TOM5-TMD (0.04) and BAK-/TOM5-TMD (0.20) negative control (Figure 13, upper panel). Again, combinations of BAK-TMD with BCL-2- (0.16), MCL-1- (0.07) and A1-TMD (0.11) resulted in relative luminescence comparable to negative controls. Hence, co-expression of LgBiT-BAK-TMD with SmBiT-TMDs of anti-apoptotic Bcl-2 proteins showed a similar interaction pattern as for combinations with LgBiT-BAX-TMD. Western Blot analysis revealed successful expression of both LgBiT-TMDs and mTurq2 with visible but subtle variations in band intensity (Figure 13, lower panel).

Thus, both BAX-TMD and BAK-TMD produced significant interaction signals in combination with BCL-XL-TMD and BCL-W-TMD in the NanoBiT assay. Furthermore, luminescence signals resulting from combinations of BAK-TMD with BCL-XL-TMD and BCL-W-TMD were by a multitude higher than for BAX-TMD.



**Figure 13: BAK-TMD interacts with both BCL-XL- and BCL-W-TMD.**

NanoBiT interaction data from HEK293 cells co-transfected to express LgBiT-BAK-TMD in combination with SmBiT-TMDs of anti-apoptotic Bcl-2 proteins. Cells were harvested 24 post transfection and subjected to NanoBiT assay (top) and Western Blot (bottom). For the NanoBiT assay, fluorescence-normalised luminescence intensity is shown relative to positive control (BAX-/BAX-TMD). Mean  $\pm$  sd from three independent experiments. Mean of both negative control (BAX-/TOM5-TMD) and positive control are indicated as a dashed line. Asterisks indicate statistically significant differences compared to negative control. Construct expression was verified via Western Blot (bottom) using antibodies against LgBiT, mTurquoise2 (mTurq2) to indirectly detect SmBiT-TMDs and  $\beta$ -actin as loading control. Ctrl = untransfected cells. Representative Blot from two independent experiments.

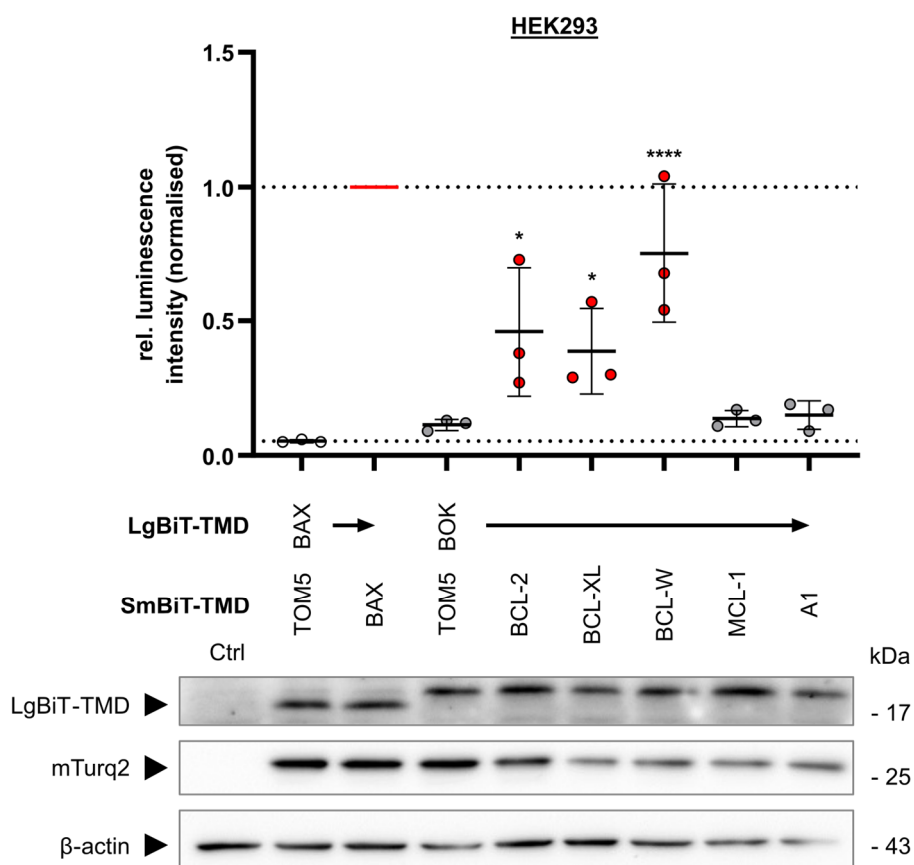
### 3.2.3 NanoBiT assay reveals a unique TMD interaction of BOK and BCL-2

Since function and mode of action for BOK are still a matter of dispute, further unravelling the TMD interaction network of BOK might grant new insights into BOK's regulatory role in apoptosis and other cellular functions. Thus, interaction of BOK-TMD with TMDs of anti-apoptotic Bcl-2 proteins was assessed next in the NanoBiT assay.

Similar to BAX-TMD and BAK-TMD in 3.2.2, HEK293 cells were co-transfected to express LgBiT-BOK-TMD in combination with SmBiT-TMDs of anti-apoptotic Bcl-2 proteins BCL-2, BCL-XL, BCL-W, MCL-1 and A1. Cells were both analysed with the NanoBiT assay to detect interaction and Western Blot to verify protein expression. As observed for BAX-TMD and BAK-TMD, luminescence relative to BAX-/BAX-TMD positive control (set to 1.00) in cells co-expressing LgBiT-BOK-TMD and SmBiT-BCL-XL-TMD or SmBiT-BCL-W-TMD was significantly increased (0.39 or 0.75 respectively) compared to the BAX-/TOM5-TMD negative control (0.05, Figure 14, upper panel). Contradicting references in literature (291, 333), combination of BOK-TMD with MCL-1-TMD produced relative luminescence (0.14) comparable to BAX-/TOM5-TMD and BOK-/TOM5-TMD (0.11) negative control. Also, for the combination of BOK-TMD with A1-TMD a similarly low relative luminescence of 0.15 was detected. Unexpectedly, cells co-expressing LgBiT-BOK-TMD and SmBiT-BCL-2-TMD exerted noticeably elevated relative luminescence (0.46) compared to BAX-/TOM5-TMD negative control. Moreover, robust expression of LgBiT-TMDs and mTurq2 was confirmed by Western Blot analysis (Figure 14, lower panel). Of note, also in MCF-7 cells co-expression of LgBiT-BOK-TMD and SmBiT-BCL-2-TMD led to an increased relative luminescence (0.30) compared to BAX-/TOM5-TMD negative control (0.05) indicating a cell line-independent phenomenon (Supplementary Figure S3B).

To exclude the possibility of device-based variations in NanoBiT luminescence experiments were repeated in another multimode plate reader system (Victor Nivo, Supplementary Figure S3C). Also with the Victor Nivo system elevated relative luminescence compared to the negative control was confirmed for combinations of effector TMDs with BCL-W-TMD, BAK-TMD or BOK-TMD with BCL-XL-TMD and for BOK-/BCL-2-TMD. However, no increase in relative luminescence was found for BAX-/BCL-XL-TMD as previously observed with the ENspire multimode plate reader.

Consequently, the NanoBiT assay suggests not only heterotypic interaction of BOK-TMD with BCL-XL-TMD and BCL-W-TMD (as seen for BAX-TMD and BAK-TMD), but also a yet unidentified and unique interaction with BCL-2-TMD.



**Figure 14: BOK-TMD interacts with BCL-2-, BCL-XL- and BCL-W-TMDs.**

NanoBiT interaction data from HEK293 cells co-transfected to express LgBiT-BOK-TMD in combination with SmBiT-TMDs of antiapoptotic Bcl-2 proteins. Cells were harvested 24 post transfection and subjected to NanoBiT assay (top) and Western Blot (bottom). For the NanoBiT assay, fluorescence-normalised luminescence intensity is shown relative to positive control (BAX-/BAX-TMD). Mean  $\pm$  sd from three independent experiments. Mean of both negative control (BAX-/TOM5-TMD) and positive control are indicated with a dashed line. Asterisks indicate statistically significant differences compared to negative control. Construct expression was verified via Western Blot (bottom) using antibodies against LgBiT, mTurquoise2 (mTurq2) to indirectly detect SmBiT-TMDs and  $\beta$ -actin as loading control. Representative Blot from two independent experiments.

3.2.4 BAX- and BAK-TMD localise to Mitochondria, while BOK-TMD is ER-localised

Protein expression of NanoBiT plasmids can be verified via Western Blot for the NanoBiT assay. However, plasmids were not designed to analyse subcellular localisation of LgBiT- and SmBiT-TMD fusion proteins and hence the subcellular site of interaction. Nevertheless, subcellular localisation of TMD peptides would provide an important insight in which membranes detected TMD interactions could occur.

TMDs of Bcl-2 family proteins are bona fide targeting-sequences which shuttle fluorophores such as GFP to their specific target membranes (172). Aiming to identify subcellular localisation of TMDs, new plasmids based on the pEGFP-C1 backbone (Clontech) were generated which encode the fluorophore mTurq2 Ct-fused to a TMD sequence via a 14 AA hydrophilic linker. MCF-7 cells expressing EYFP-fused subcellular marker for ER (EYFP-ER, Calreticulin ER-targeting/retrieval sequence, Clontech) or Mitochondria (EYFP-Mito, cytochrome C oxidase subunit VIII, Clontech) respectively were transfected with the generated plasmids for expression of mTurq2 fused with BAX-, BAK-, or BOK-TMD. mTurq2-TOM5-TMD and mTurq2 fused to the TMD of ER-resident Cytochrome b5 (cb5) were used as Mitochondria and ER control respectively. After transfection, cells were fixed and subcellular localisation was analysed using cLSM.

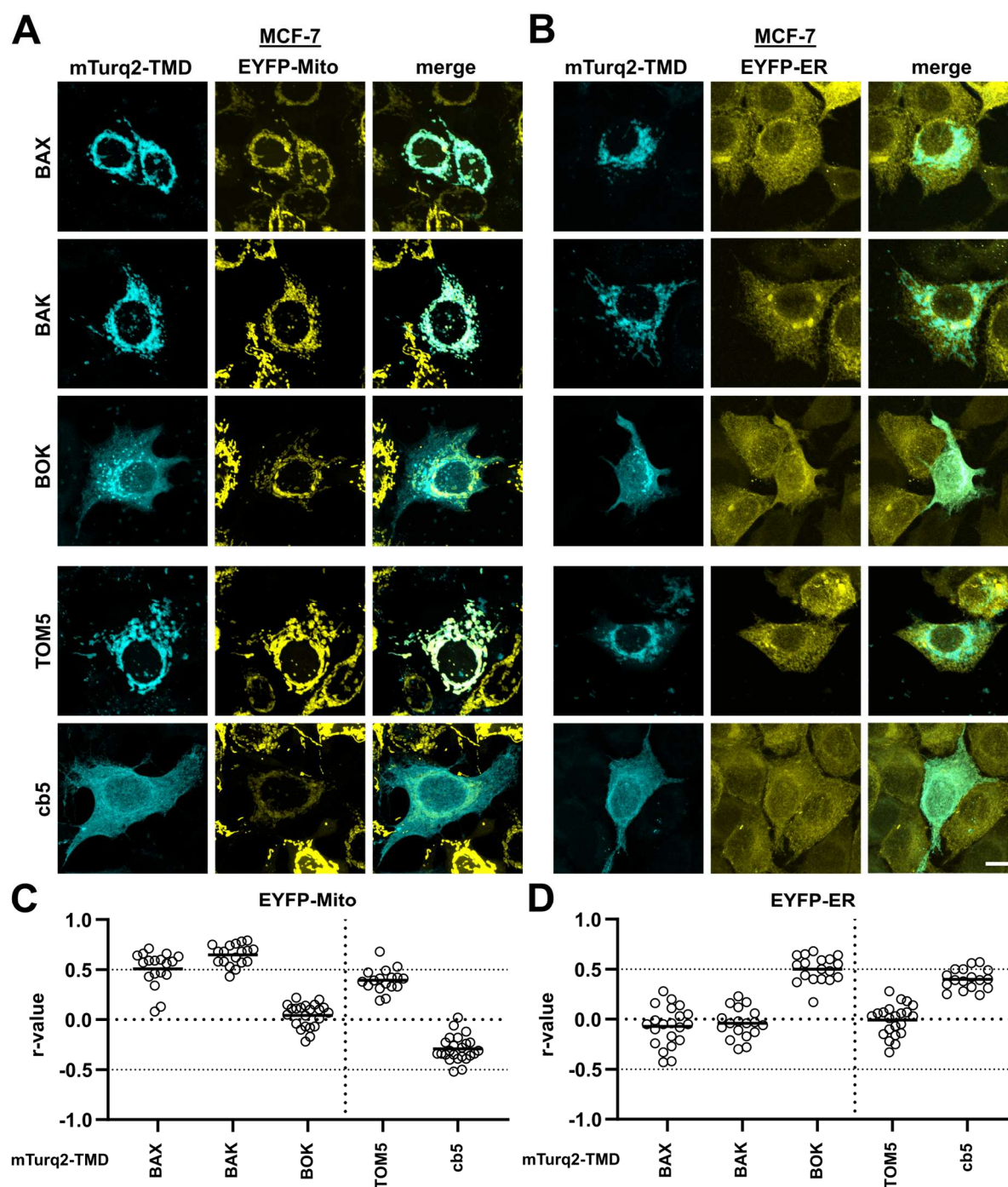
As can be seen in Figure 15, mTurq2-BAX-TMD and mTurq2-BAK-TMD colocalise with EYFP-Mito (Figure 15A) rather than EYFP-ER signal (Figure 15B). In contrast, mTurq2-BOK-TMD prominently colocalised with EYFP-ER rather than EYFP-Mito. For some cells, bright perinuclear clusters were observed in addition to the ER-like distribution of mTurq2-BOK-TMD. In addition, mTurq2-TOM5-TMD colocalised well with EYFP-Mito, while mTurq2-cb5-TMD colocalised well with EYFP-ER confirming specific targeting of mTurq2 by the fused TMD sequence. Of note, analogue localisations could be observed in MCF-7 cells expressing mCitr-fused TMD peptides (Supplementary Figure S4A). In line with the findings in MCF-7 cells, mitochondrial localisation of mTurq2-BAX-TMD and mTurq2-BAK-TMD and ER localisation of mTurq2-BOK-TMD was confirmed in HEK293 cells (Supplementary Figure S4B).

To verify the observations from cLSM images, randomly chosen MCF-7 cells were used for calculation of Pearson's correlation coefficients ( $r$ -values) between mTurq2-TMD and EYFP marker signal as a software-based quantification of colocalisation (Figure 15C, D).

For EYFP-Mito, average Pearson's  $r$ -value of mTurq2-BAX-TMD indicated positive correlation ( $r_{\text{BAX-TMD+Mito}} = 0.51$ ) which was even higher than the  $r$ -value of the Mitochondria control mTurq2-TOM5-TMD with EYFP-Mito ( $r_{\text{TOM5-TMD+Mito}} = 0.39$ ). For mTurq2-BAK-TMD, the highest  $r$ -value with EYFP-Mito among TMDs analysed was calculated ( $r_{\text{BAK-TMD+Mito}} = 0.64$ ). On the other hand,  $r$ -value of mTurq2-BOK-TMD and EYFP-Mito indicated no correlation ( $r_{\text{BOK-TMD+Mito}} = 0.04$ ). ER control mTurq2-cb5-TMD showed a moderate negative correlation with EYFP-Mito ( $r_{\text{cb5-TMD+Mito}} = -0.29$ ). For EYFP-ER,  $r$ -values showed poor colocalisation with mTurq2-BAX-TMD and mTurq2-BAK-TMD ( $r_{\text{BAX-TMD+ER}} = -0.07$  and  $r_{\text{BAK-TMD+ER}} = -0.04$  respectively, Figure 15D) similar to colocalisation with mitochondria control mTurq2-TOM5-TMD ( $r_{\text{TOM5-TMD+ER}} = -0.01$ ). mTurq2-BOK-TMD, however, showed clear positive correlation ( $r_{\text{BOK-TMD+ER}} = 0.50$ ) exceeding EYFP-ER colocalisation of mTurq2-cb5-TMD ( $r_{\text{cb5-TMD+ER}} = 0.40$ ). ER colocalisation for BOK-TMD was further confirmed in MCF-7 cells expressing ER-mCarmine marker (mCarmine fused to a calreticulin-targeting sequence, (366)) in combination with mCitr-BOK-TMD (Supplementary Figure S4C).

The CMV promoter used in the pEGFP backbone can induce strong overexpression of encoded proteins with the risk of artificial subcellular distribution (364). Therefore, cDNA encoding for mTurq2-TMDs was re-cloned into the pBiT vector backbone with HSV TK promoter (as used for NanoBiT-TMD expression) and transfected into MCF-7 cells to analyse mTurq2-TMD subcellular localisation under HSV TK promoter-controlled expression (Supplementary Figure S4D). Exemplarily shown for mTurq2-BAX-TMD<sub>HSV TK</sub>, similar mitochondria-like distribution was observed as for mTurq2-BAX-TMD<sub>CMV</sub> in Figure 15A. Comparing integrated density of fluorescence signal in MCF-7 cells expressing either mTurq2/(mCitr)-BAX-TMD<sub>CMV</sub> or mTurq2/(mCitr)-BAX-TMD<sub>HSV TK</sub>, indeed, higher fluorescence was detected in cells with CMV-controlled expression of fluorophore-fused TMDs (Supplementary Figure S4E). Hence, despite higher expression level compared to the HSV TK promoter, CMV-controlled expression does not affect subcellular localisation of TMDs.

Collectively, analysis of effector TMD subcellular localisation shows foremost mitochondrial localisation for BAX-TMD and BAK-TMD, whereas BOK-TMD, though poorly colocalising with mitochondria, localises to the ER. Moreover, subcellular localisation of effector TMD peptides remained unchanged with regard to changing fluorophore, cell line and promoter.



**Figure 15: BAX and BAK TMDs predominantly localise to mitochondria, TMDs of BOK to the ER.**

**A, B** – cLSM images of MCF-7 cells expressing either EYFP-Mito (**A**) or EYFP-ER (**B**) which were transfected to express indicated mTurq2-TMD fusion proteins. Representative images out of three independent experiments are maximum projections of z-stacks. Scale bar = 10  $\mu$ m. **C, D** – Quantification of colocalisation from MCF-7 cells imaged as in **A** or **B**. Pearson's r-values reflecting colocalisation between EYFP-Mito (**C**) or EYFP-ER (**D**) with mTurq2-TMD signals were determined for middle sections of in total  $n \geq 15$  cells from three independent experiments using Fiji software. Means are indicated with horizontal lines. Colocalisation quantification was performed together with Lynn Barber.

### 3.2.5 TMDs of anti-apoptotic Bcl-2 proteins show distinct subcellular localisation

As performed for effector TMDs in 3.2.4, subcellular localisation of TMD fusion proteins from anti-apoptotic Bcl-2 proteins is to be determined in the next step. To this end, plasmids encoding for mTurq2 Ct-fused to TMD sequences were transfected into MCF-7 cells expressing EYFP-ER or EYFP-Mito. After 24 h, cells were fixed and subcellular localisation analysed by cLSM.

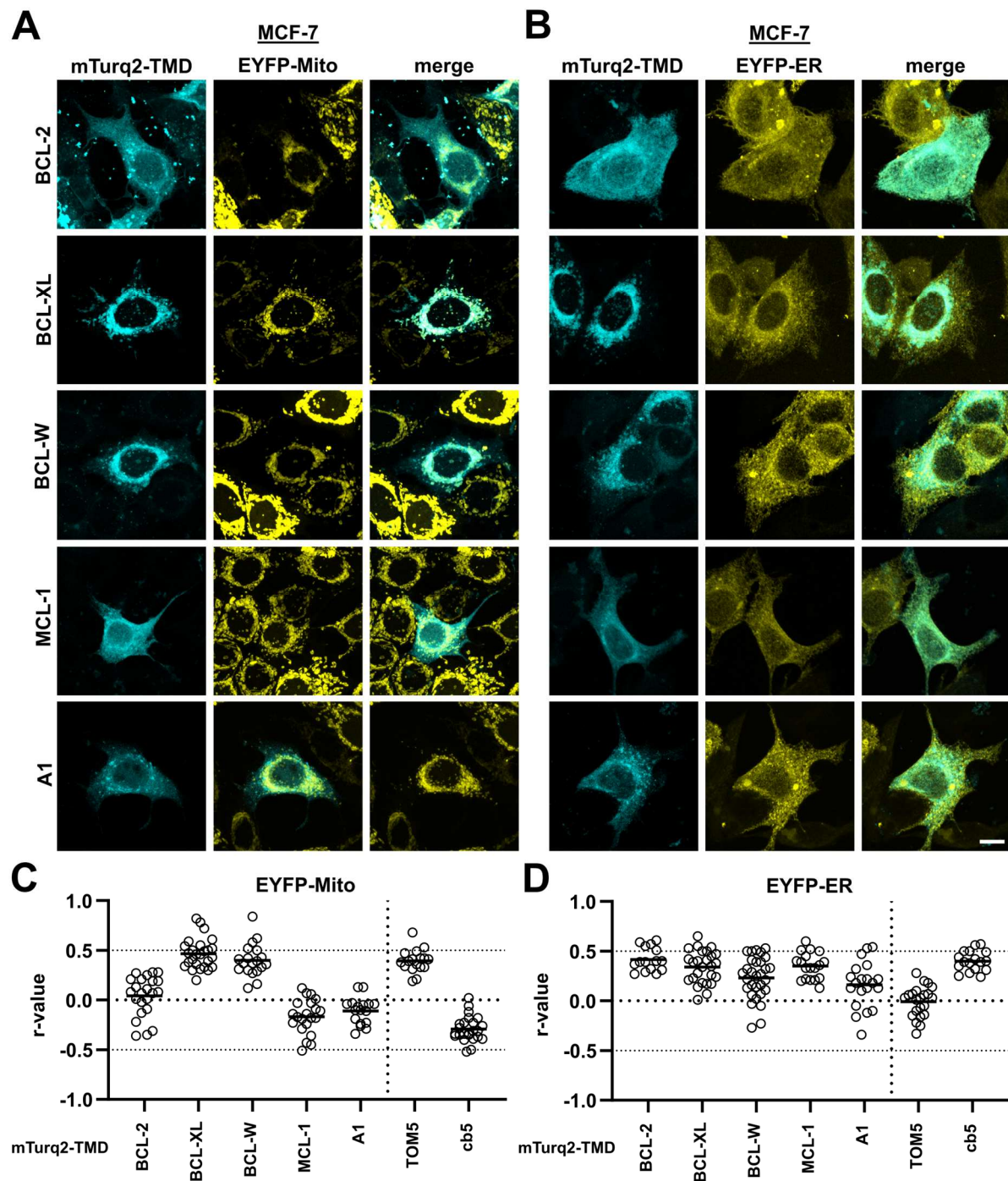
For mTurq2-BCL-2-TMD, fluorescence showed a perinuclear distribution poorly overlapping with EYFP-Mito signals, but colocalised with EYFP-ER (Figure 16A, B). Fluorescence signals of mTurq2-BCL-XL-TMD, however, rather overlapped with EYFP-Mito and only partially with EYFP-ER signals. mTurq2-BCL-W-TMD signals were foremost colocalised with EYFP-Mito although some signal was distributed throughout the whole cell. Interestingly, mTurq2-MCL-1-TMD signals were distributed similar to BCL-2-TMD with foremost EYFP-ER colocalisation. Cells expressing mTurq2-A1-TMD showed diffuse distribution of mTurq2 signals with bright perinuclear clusters that neither co-localised with EYFP-Mito nor EYFP-ER. Thus, it was assumed that mTurq2-A1-TMD is localised foremost at other perinuclear membranes, such as the Golgi apparatus. To check for a possible Golgi localisation of A1-TMD, MCF-7 cells expressing mTurq2-A1-TMD were IF-stained for *cis*-Golgi marker GM130 (367). Indeed, mTurq2-A1-TMD bright perinuclear signal clearly colocalised with Golgi marker (Supplementary Figure S5A). Intriguingly, Golgi localisation was also found for full-length A1 in MCF-7 cells expressing EGFP-A1. Moreover, Subcellular localisation of anti-apoptotic TMD peptides in MCF-7 cells was corroborated in HEK293 cells transfected to express mTurq2-TMD fusion proteins (Supplementary Figure S5B).

Next, also for anti-apoptotic Bcl-2 TMDs, observed colocalisation of mTurq2-TMDs with EYFP-Mito or EYFP-ER (Figure 16A, B) was sought to be validated by quantifying colocalisation in form of Pearson's correlation coefficients (Figure 16C, D). Quantification of EYFP-Mito colocalisation with mTurq2-TMDs resulted in low Pearson's correlation coefficients for mTurq2-BCL-2-TMD ( $r_{\text{BCL-2-TMD+Mito}} = 0.04$ ), mTurq2-MCL-1-TMD ( $r_{\text{MCL-1-TMD+Mito}} = -0.17$ ) and mTurq2-A1-TMD ( $r_{\text{A1-TMD+Mito}} = -0.11$ ). However, colocalisation analysis of mTurq2-BCL-XL-TMD and mTurq2-BCL-W-TMD with EYFP-Mito resulted in r-values comparable to TOM5-TMD mitochondrial control ( $r_{\text{BCL-XL-TMD+Mito}} = 0.46$  and  $r_{\text{BCL-W-TMD+Mito}} = 0.40$  respectively).



Confirming the observations in cLSM images, mTurq2-BCL-2-TMD colocalised well with EYFP-ER according to the r-value of  $r_{\text{BCL-2-TMD+ER}} = 0.42$ . Surprisingly, mitochondria-localised mTurq2-BCL-XL-TMD and mTurq2-BCL-W-TMD showed also high positive correlation with the ER marker ( $r_{\text{BCL-XL-TMD+ER}} = 0.34$  and  $r_{\text{BCL-W-TMD+ER}} = 0.23$  respectively). Also for mTurq2-MCL-1-TMD localisation, positive correlation with EYFP-ER was obtained ( $r_{\text{MCL-1-TMD+ER}} = 0.35$ ). However, EYFP-ER colocalisation was substantially lower for mTurq2-A1-TMD ( $r_{\text{A1-TMD+ER}} = 0.16$ ) in line with predominant Golgi colocalisation.

Taken together, TMDs of anti-apoptotic Bcl-2 proteins individually localised to mitochondria, the ER or the Golgi. TMD peptides of both BCL-XL and BCL-W were visibly and quantifiably colocalised with mitochondria and, in addition, partially localised to the ER. BCL-2 and MCL-1 TMD peptides were predominantly ER-localised, whereas poor colocalisation with mitochondria was observed. Interestingly, A1-TMD as well as A1 full-length protein showed a yet unknown tendency to accumulate at the Golgi apparatus.



**Figure 16: Anti-apoptotic Bcl-2 TMDs have distinct subcellular localisation patterns.**

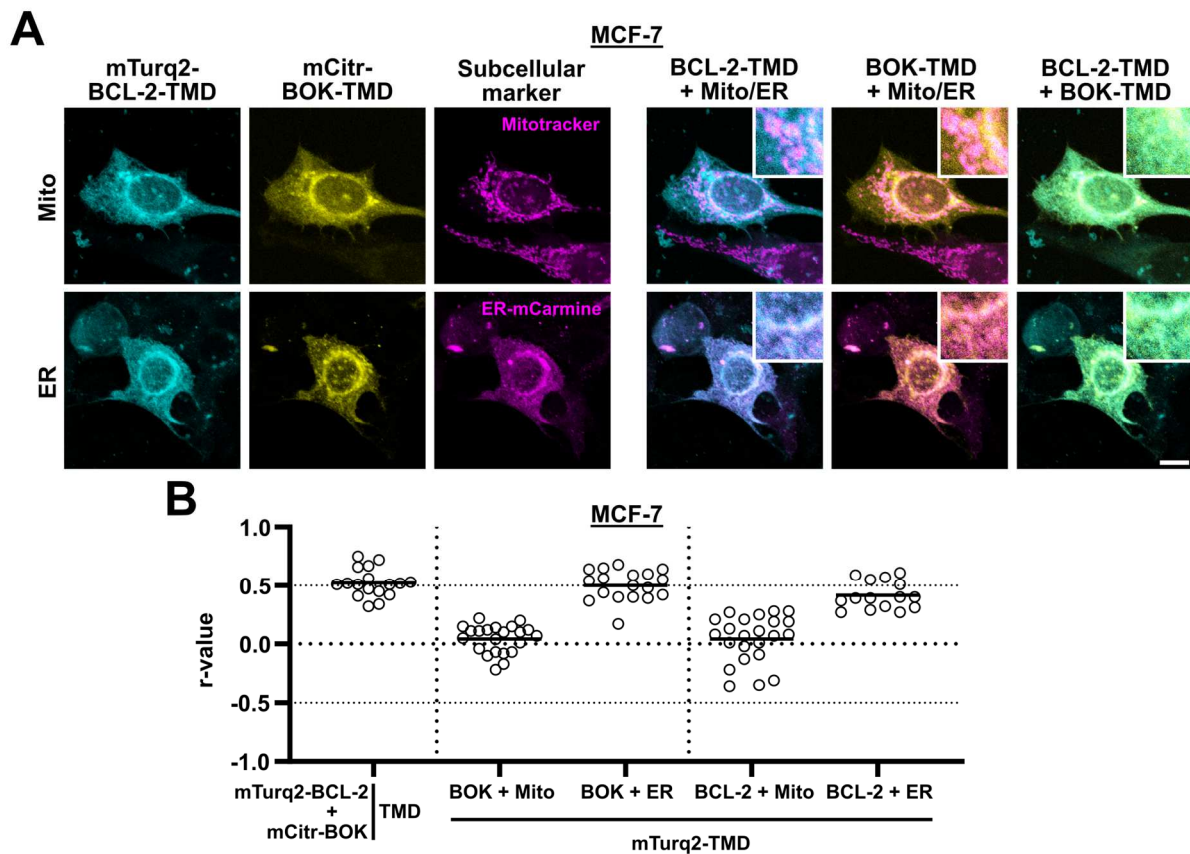
**A, B** –cLSM images of MCF-7 cells expressing either EYFP-Mito (**A**) or EYFP-ER (**B**) which were transfected to express indicated anti-apoptotic Bcl-2 mTurq2-TMD fusion proteins. Representative images out of three independent experiments are maximum projections of z-stacks. Scale bar = 10  $\mu$ m. **C, D** – Quantification of colocalisation from MCF-7 cells imaged as in **A** or **B**. Pearson's r-values reflecting colocalisation between EYFP-Mito (**C**) or EYFP-ER (**D**) with mTurq2-TMD signals were determined for middle sections of in total  $n \geq 15$  cells from three independent experiments using Fiji software. Means are indicated with horizontal lines. Colocalisation quantification was performed together with Lynn Barber.

### 3.2.6 BOK-TMD and BCL-2-TMD colocalise at ER membranes

Since the NanoBiT assay revealed a yet unknown and unique interaction of BOK-TMD and BCL-2-TMD (3.2.3), the subcellular site of this interaction was chosen to be further investigated. Both BOK-TMD and BCL-2-TMD were found to be predominantly ER-localised, while colocalisation with mitochondria marker was rather negligible (Figure 15, Figure 16). However, these findings neither confirm nor rule out any compartment as site for BOK-TMD and BCL-2-TMD interaction.

To further pinpoint the subcellular membranes in which the identified interaction of BOK-TMD and BCL-2-TMD takes place, MCF-7 cells were co-transfected to express both mCitr-BOK-TMD and mTurq2-BCL-2-TMD and subcellular localisation was analysed by cLSM with respect to Mitotracker red staining or co-express ER-mCarmine. In cells co-expressing mCitr-BOK-TMD and mTurq2-BCL-2-TMD, staining with Mitotracker revealed once again negligible colocalisation of TMD peptides with mitochondria (Figure 17A). Colocalisation of co-expressed mCitr-BOK-TMD and mTurq2-BCL-2-TMD with ER-mCarmine, however, was clearly visible. Importantly, also mCitr-BOK-TMD and mTurq2-BCL-2-TMD were colocalised fulfilling the requirement for interaction. Colocalisation was confirmed by calculation of  $r$ -values between mCitr-BOK-TMD and mTurq2-BCL-2-TMD which indicated a clearly positive correlation ( $r_{\text{BOK-TMD+BCL-2-TMD}} = 0.52$ ) comparable with colocalisation of either mTurq2-BOK-TMD or mTurq2-BCL-2-TMD with EYFP-ER ( $r_{\text{BOK-TMD+ER}} = 0.50$  or  $r_{\text{BCL-2-TMD+ER}} = 0.42$  respectively) from previous experiments (Figure 15B, Figure 16B). To substantiate BOK-TMD and BCL-2-TMD colocalisation at the ER, mCitr-BOK-TMD and mTurq2-BCL-2 in combination with Mitotracker staining or ER-mCarmine were also expressed in HeLa cells (Supplementary Figure S5C). In HeLa cells, mCitr-BOK-TMD and mTurq2-BCL-2-TMD were also colocalising with ER-mCarmine suggesting a cell line-independent site of TMD interaction.

Hence, interaction of BOK-TMD with BCL-2-TMD is likely situated in ER membranes. In contrast, colocalisation and, thus, interaction at mitochondria, the most prominent platform for Bcl-2 protein interactions, cannot be concluded from the results obtained.



**Figure 17: TMDs of BOK and BCL-2 colocalise at the ER, not mitochondria.**

**A** – cLSM images of MCF-7 cells transfected to express mTurq2-BOK-TMD and mCitrine-BCL-2-TMD. Cells were either stained with Mitotracker red 24 h after transfection and then fixed (top row) or co-transfected with ER marker ER-mCarmine (bottom row) and fixed 24 post transfection. Representative images from three independent experiments are maximum projections of z-stacks. Zoomed-in insets are in 3x magnification. **B** – Quantification of colocalisation from MCF-7 cells imaged as in A. Colocalisation data of BOK/BCL-2-TMD with Mito/ER are from MCF-7 cells expressing EYFP-Mito/ER transfected to express BOK-/BCL-2-TMD fusion proteins. Pearson's r-values were determined for middle sections of in total  $n \geq 15$  cells from three independent experiments using Fiji software. Means are indicated with horizontal lines.

### 3.3 Impact of TMD interactions on apoptosis signalling

Classically, TMDs of Bcl-2 proteins are recognised as mere membrane anchors. However, as pieces of evidence which suggested TMD-TMD interactions of Bcl-2 proteins stirred new discussions about the impact of Bcl-2 TMD interactions on apoptosis regulation. Already some publications postulate clear correlations of TMD interaction and modulation of apoptosis, for example, a MOMP-stimulating effect of TMD peptides (321), interaction of BAX-TMD with anti-apoptotic proteins (171) or cancer-specific mutations of MCL-1-TMD that modulate apoptosis signalling (333). The here revealed insights into TMD interactions by the NanoBiT assay spark new possibilities how TMD interactions such as of BOK-TMD with BCL-2-TMD might influence apoptosis signalling.

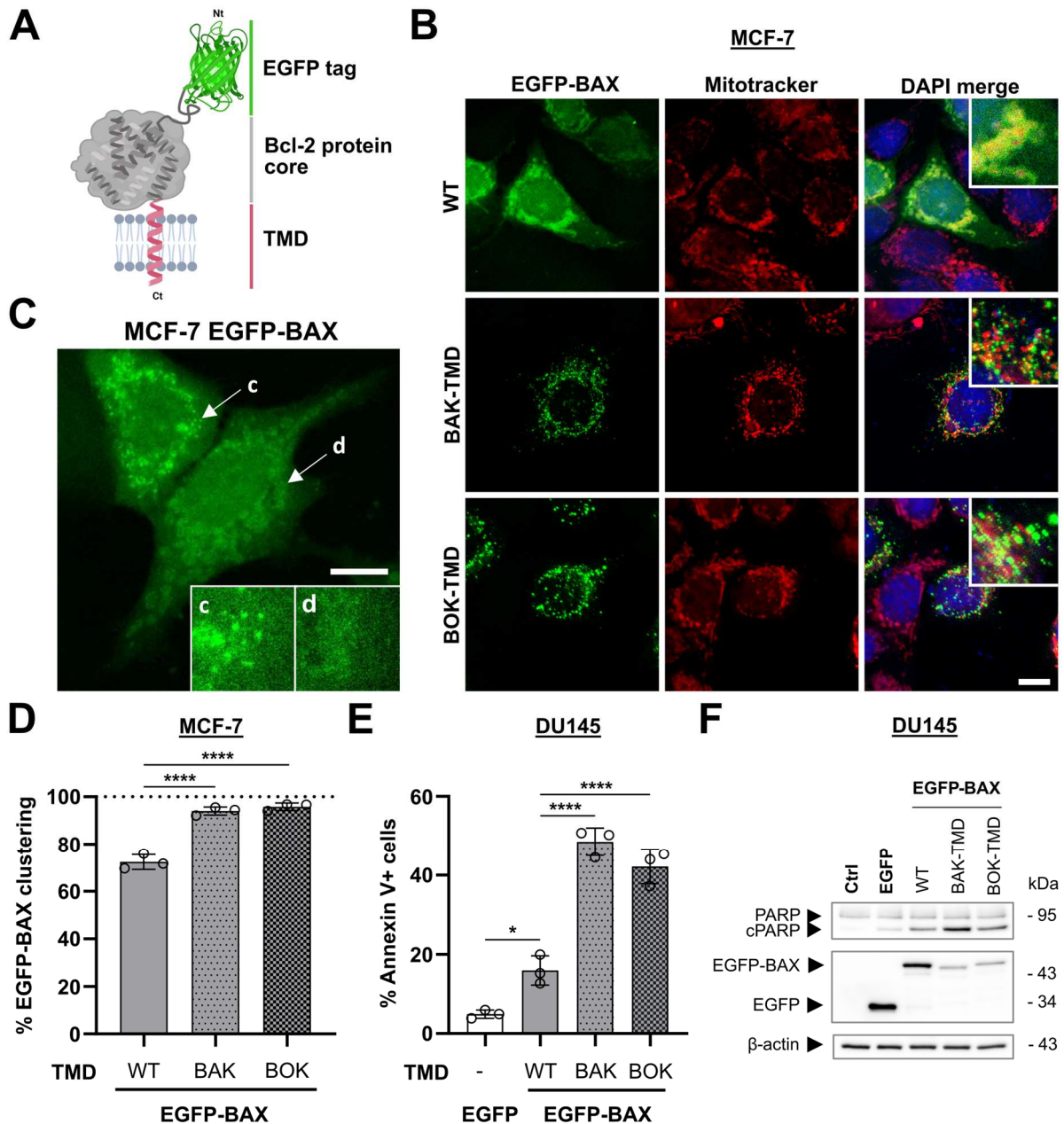
The third and last chapter of the result part in this thesis comprises all studies performed to reveal the functional relevance of TMD interactions found in the NanoBiT assay. Concerning the homotypic interaction pattern of effector TMDs, specific functionality of BAX-TMD is analysed by experiments with TMD chimeric proteins, so-called BAX TMD chimeras. Also, mutations of BAX-TMD and their impact on BAX function and inhibition are investigated. Similarly, the importance of BAK-TMD for BAK-mediated cell death induction and interaction with BCL-2 is analysed using BAK TMD chimeras. Regarding the third effector protein BOK, TMD-dependency of BOK and BCL-2 colocalisation is studied using TMD chimeras. Also, the functional relevance of the unveiled BOK- and BCL-2-TMD interaction in BOK-induced apoptosis is determined by knockdown experiments and application of TMD chimeras. Finally, the mode of BOK-TMD and BCL-2-TMD interaction is enlightened on the molecular level by application of molecular dynamics (MD) simulation followed by the investigation of clinically relevant mutations of BCL-2-TMD and, lastly, BOK-induced ER-stress.

#### 3.3.1 The TMD of BAX is crucial for BAX auto-inhibition

In its inactive state, BAX resides mainly in the cytosol with the TMD folded back to the protein centre (133). Once activated, a conformation change leads to insertion of the TMD into the MOM and allows for BAX pore formation triggering MOMP (135, 137, 140). The specific structure and activation process give BAX a special position among the effector proteins, but also suggest a specific function of its TMD within the BAX activation procedure.

To further investigate how BAX-TMD regulates BAX function, the TMD sequence of BAX in EGFP-BAX expression vectors previously described (158) was exchanged to the sequence of BAK and BOK resulting in plasmids encoding for BAX TMD chimeras comprising a N-terminal EGFP tag, the BAX “protein core” and an effector TMD sequence (Figure 18A). MCF-7 cells were then transfected with BAX TMD chimera-encoding plasmids, cells were stained with Mitotracker red and subcellular localisation was investigated by cLSM. Here, wild-type (WT) EGFP-BAX showed cytosolic but also mitochondrial localisation and formed bright clusters at mitochondria in many, but not all, cells examined indicating BAX oligomerisation (Figure 18B). Interestingly, for expression of BAX TMD chimeras, EGFP-BAX<sup>BAK-TMD</sup> and EGFP-BAX<sup>BOK-TMD</sup>, virtually all cells displayed bright BAX clusters at mitochondria. Hence, the percentage of cells with clusters was subsequently determined by differentiating between cells with clusters and cells with diffuse BAX distribution exemplarily shown in Figure 18C. Quantification of EGFP-BAX clustering resulted in 72% of WT EGFP-BAX-expressing cells displaying clusters, while for BAX TMD chimeras percentage of cells with BAX clusters was significantly increased to 94% for EGFP-BAX<sup>BAK-TMD</sup> and 96% for EGFP-BAX<sup>BOK-TMD</sup> (Figure 18D).

To examine apoptosis induction by BAX TMD chimeras, BAX- and BCL-2-deficient DU145 prostate carcinoma cells (Supplementary Figure S1A) were transfected to express WT EGFP-BAX or BAX TMD chimeras. After 18 h, cell death was analysed for EGFP positive (EGFP+) cells using APC-conjugated Annexin V which binds exposed phosphatidylserine and enables detection of apoptotic cells cells by flow cytometry (Figure 18E). As expected, DU145 cells transfected to express WT EGFP-BAX showed increased rates of apoptosis (16% Annexin V positive (Annexin V+) cells) compared to transfection with an EGFP-encoding control plasmid (5% Annexin V+ cells). Strikingly, expression of EGFP-BAX<sup>BAK-TMD</sup> and EGFP-BAX<sup>BOK-TMD</sup> drastically increased number of Annexin V+ cells to 49% and 42% respectively. Repetition in HEK293 cells confirmed increased apoptotic activity of EGFP-BAX<sup>BAK-TMD</sup> (85% Annexin V+ cells) and EGFP-BAX<sup>BOK-TMD</sup> (76% Annexin V+ cells) compared to WT EGFP-BAX (60% Annexin V+ cells, Supplementary Figure S6A). To further corroborate increased apoptotic activity of BAX TMD chimeras, whole cell lysates of DU145 cells transfected to express EGFP, WT EGFP-BAX or BAX TMD chimeras were analysed by Western Blot (Figure 18F).



**Figure 18: Exchange of TMD in BAX to BAK- or BOK-TMD enhances BAX pro-apoptotic activity.**

**A** – Sketch of EGFP-tagged Bcl-2 protein TMD chimera. Created with Biorender. **B** – cLSM images of MCF-7 transfected to express EGFP-BAX TMD chimeras or wild-type (WT). 18 h post transfection, cells were stained with Mitotracker red and subsequently fixed. Representative images from three independent experiments are maximum projections of z-stacks. Zoomed-in insets are in 3x magnification. Scale bar = 10  $\mu$ m. **C** – Representative cLSM image of MCF-7 cells transfected as in B to express EGFP-BAX demonstrating clustered (c) and diffuse (d) BAX signals used for cell classification and quantification of BAX clustering (D). Zoomed-in insets show marked regions (white arrows) in 3x magnification. Scale bar = 10  $\mu$ m. **D** – Quantification of EGFP-BAX clustering from MCF-7 cells in B. Shown is the percentage of EGFP-BAX-expressing cells containing EGFP-BAX clusters. Mean  $\pm$  sd from three independent experiments including  $\geq$  100 cells per experiment. **E** – Flow cytometric analysis of DU145 cells transfected to express indicated EGFP-BAX variants or EGFP as a control. Cells were harvested 18 h post transfection and stained with Annexin V-APC to detect dead cells (Annexin V+). Mean  $\pm$  sd from three independent experiments. **F** – Western Blot analysis of whole cell lysates from DU145 cells transfected as in E and harvested 18 h post transfection. Cell death and EGFP(-BAX) expression level were detected using antibodies against (cleaved) PARP and EGFP respectively.  $\beta$ -actin was used as loading control. Representative Blot from three independent experiments.

Detection of PARP, a substrate of caspases upon apoptosis execution (13), revealed increased levels of cleaved PARP (cPARP, indicating caspase activity) for cells expressing BAX TMD chimeras compared to WT BAX. Expression of EGFP-fused BAX proteins was verified with bands at expected size of ~50 kDa. Surprisingly, expression levels of EGFP-BAX<sup>BAK-TMD</sup> and EGFP-BAX<sup>BOK-TMD</sup>, however, were much lower compared to WT EGFP-BAX. Similar results were obtained for lysates from HEK293 cells transfected to express EGFP, WT EGFP-BAX or BAX TMD chimeras (Supplementary Figure S6B).

BAX-induced cell death is vigorously inhibited by anti-apoptotic BCL-2 (139). Hence, after assessing BAX pro-apoptotic activity, inhibition of BAX TMD chimeras by BCL-2 was examined to further unravel the role of the TMD in inhibition of BAX by BCL-2. To this end, DU145 cells were left untransfected or co-transfected with EGFP, WT EGFP-BAX or BAX TMD chimeras in combination with mCherry-conjugated BCL-2 (mC-BCL-2) or an empty vector control. Western Blot analysis showed effective PARP cleavage for expression of BAX proteins alone in contrast to untransfected or EGFP-expressing control cells (Figure 19A). Intriguingly, co-transfection with mC-BCL-2 abolished PARP cleavage in WT EGFP-BAX and EGFP-BAX<sup>BOK-TMD</sup>-expressing cells, but not in EGFP-BAX<sup>BAK-TMD</sup>-expressing cells. Again, BAX TMD chimera expression level was much lower than for WT EGFP-BAX – also with co-expression of mC-BCL-2. Of note, co-expression of mC-BCL-2 slightly increased expression levels for all BAX proteins which could be confirmed by densitometry (Supplementary Figure S6C). To normalise for the varying BAX levels in Figure 19A, cPARP and EGFP(-BAX) band intensities were determined using densitometry and set in relation to reflect induced cell death in relation to EGFP expression level (cPARP/EGFP ratio, Figure 19B). cPARP/EGFP ratio relative to EGFP-expressing control cells was 6.5-fold higher for expression of WT EGFP-BAX alone, which was reduced to control levels with co-expression of mC-BCL-2. In agreement with increased Annexin V positivity, relative cPARP/EGFP ratio for expression of BAX TMD chimeras was approx. ten times higher than for WT EGFP-BAX – 64-fold for EGFP-BAX<sup>BAK-TMD</sup> and 85-fold for EGFP-BAX<sup>BOK-TMD</sup>. cPARP/EGFP ratio for expression of EGFP-BAX<sup>BAK-TMD</sup> in combination with mC-BCL-2 was only slightly lower (45-fold) than for expression of EGFP-BAX<sup>BAK-TMD</sup> alone. In contrast, co-expression of EGFP-BAX<sup>BOK-TMD</sup> with mC-BCL-2 led to substantial reduction of relative cPARP/EGFP ratio (4-fold) compared to expression of EGFP-BAX<sup>BOK-TMD</sup> alone.



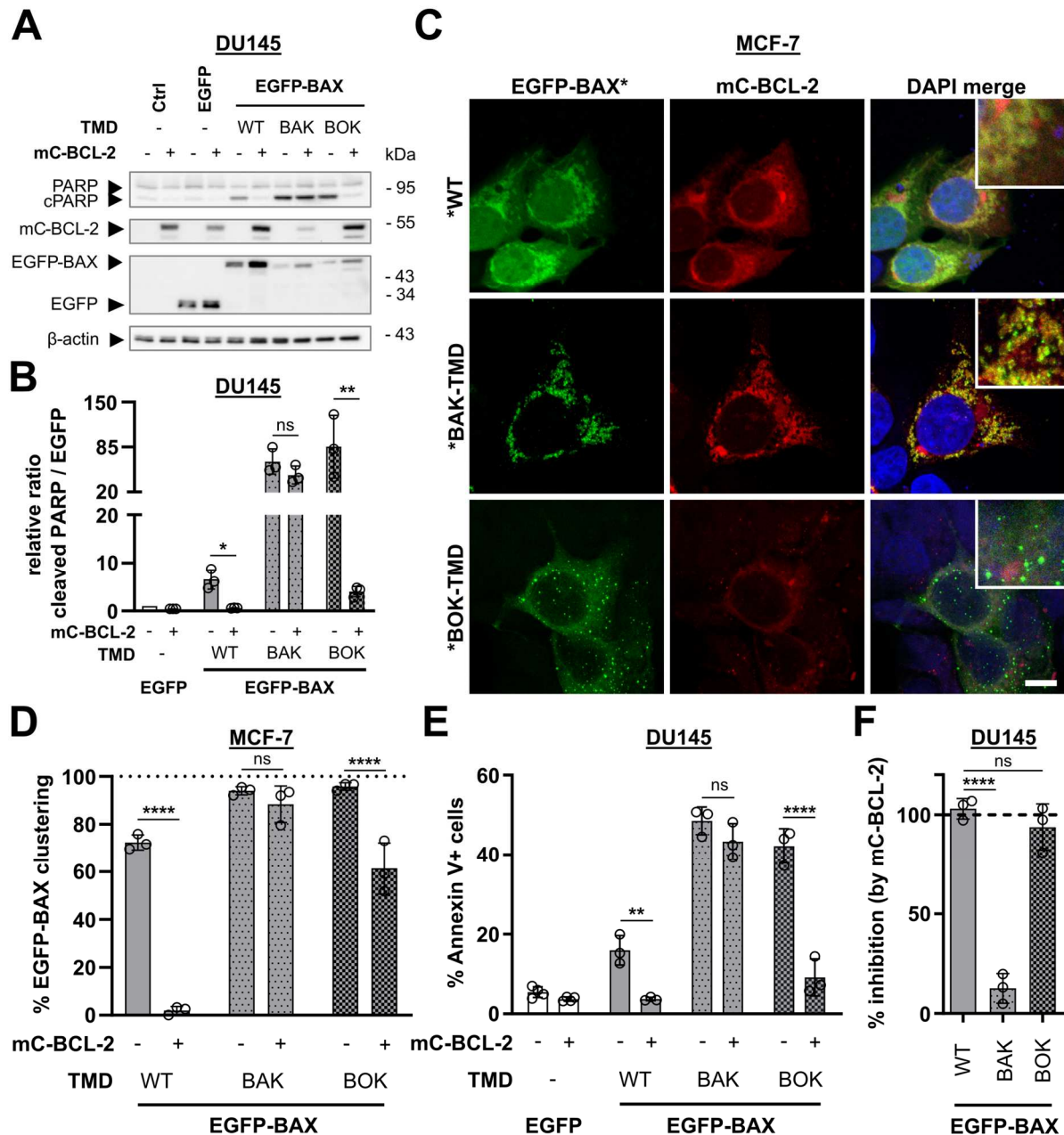
Subcellular localisation of BAX and BCL-2 was analysed in MCF-7 cells co-expressing WT EGFP-BAX or BAX TMD chimeras and mC-BCL-2 using cLSM. Interestingly, WT EGFP-BAX and BAX TMD chimeras colocalised with mC-BCL-2 (Figure 19C). However, WT EGFP-BAX co-expressed with mC-BCL-2 did not form clusters while exerting a partially mitochondrial, but also cytosolic, localisation. In line, quantification of BAX clustering for co-expression of WT EGFP-BAX and mC-BCL-2 yielded less than 2% cells with BAX clusters (Figure 19D). In contrast, 88% of EGFP-BAX<sup>BAK-TMD</sup> and mC-BCL-2-co-expressing cells displayed BAX clusters to which mC-BCL-2 colocalised (Figure 19C, D). EGFP-BAX<sup>BOK-TMD</sup> co-expressed with mC-BCL-2 display a diffuse perinuclear localisation. However, BAX clusters were still visible in many cells, so that about 61% of EGFP-BOK<sup>BOK-TMD</sup> and mC-BCL-2 co-expressing cells contained BAX clusters. Inhibition of BAX-induced cell death was analysed in DU145 cells expressing WT EGFP-BAX or BAX TMD chimeras in combination with mC-BCL-2 or an empty vector control using Annexin V-APC staining and flow cytometry (Figure 19E). Increased cell death after WT EGFP-BAX expression (16% Annexin V+ cells) was effectively reduced to control levels by co-expression of mC-BCL-2 (4% Annexin V+ cells, EGFP control: 5% Annexin V+ cells). Cell death induction by EGFP-BAX<sup>BAK-TMD</sup> of 49% Annexin V+ cells was barely reduced by co-expression of mC-BCL-2 to 43% Annexin V+ cells. Cell death induction by EGFP-BAX<sup>BOK-TMD</sup> (42% Annexin V+ cells) noticeably decreased upon mC-BCL-2 co-expression to 9% Annexin V+ cells.

Based on cell death reduction by mC-BCL-2 in Figure 19E, a theoretical % inhibition value can be calculated for each BAX protein as follows:

$$\% \textit{ inhibition} = \frac{\% \textit{ dead cells (BAX alone)} - \% \textit{ dead cells (BAX+BCL-2)}}{\% \textit{ dead cells (BAX alone)} - \% \textit{ dead cells (EGFP control)}} \cdot 100 \quad (1)$$

Using equation (1), % inhibition of WT EGFP-BAX-induced cell death by mC-BCL-2 was calculated to a theoretical value of 103% (Figure 19F, i.e. cell death was slightly lower than for EGFP control cells). Likewise, for EGFP-BAX<sup>BOK-TMD</sup> a theoretical inhibition of 94% was obtained. Calculations with EGFP-BAX<sup>BAK-TMD</sup> resulted in poor inhibition of EGFP-BAX<sup>BAK-TMD</sup> by mC-BCL-2 (13%).

In summary, exchange of BAX-TMD to BAK- or BOK-TMD promotes BAX oligomerisation as well as BAX pro-apoptotic activity. While inhibition of BAX-induced cell death by BCL-2 is only slightly impaired for BAX<sup>BOK-TMD</sup>, BCL-2 was not capable to counteract cell death caused by EGFP-BAX<sup>BAK-TMD</sup> overexpression.



**Figure 19: BAX inhibition by BCL-2 is abolished for BAX with BAK-TMD.**

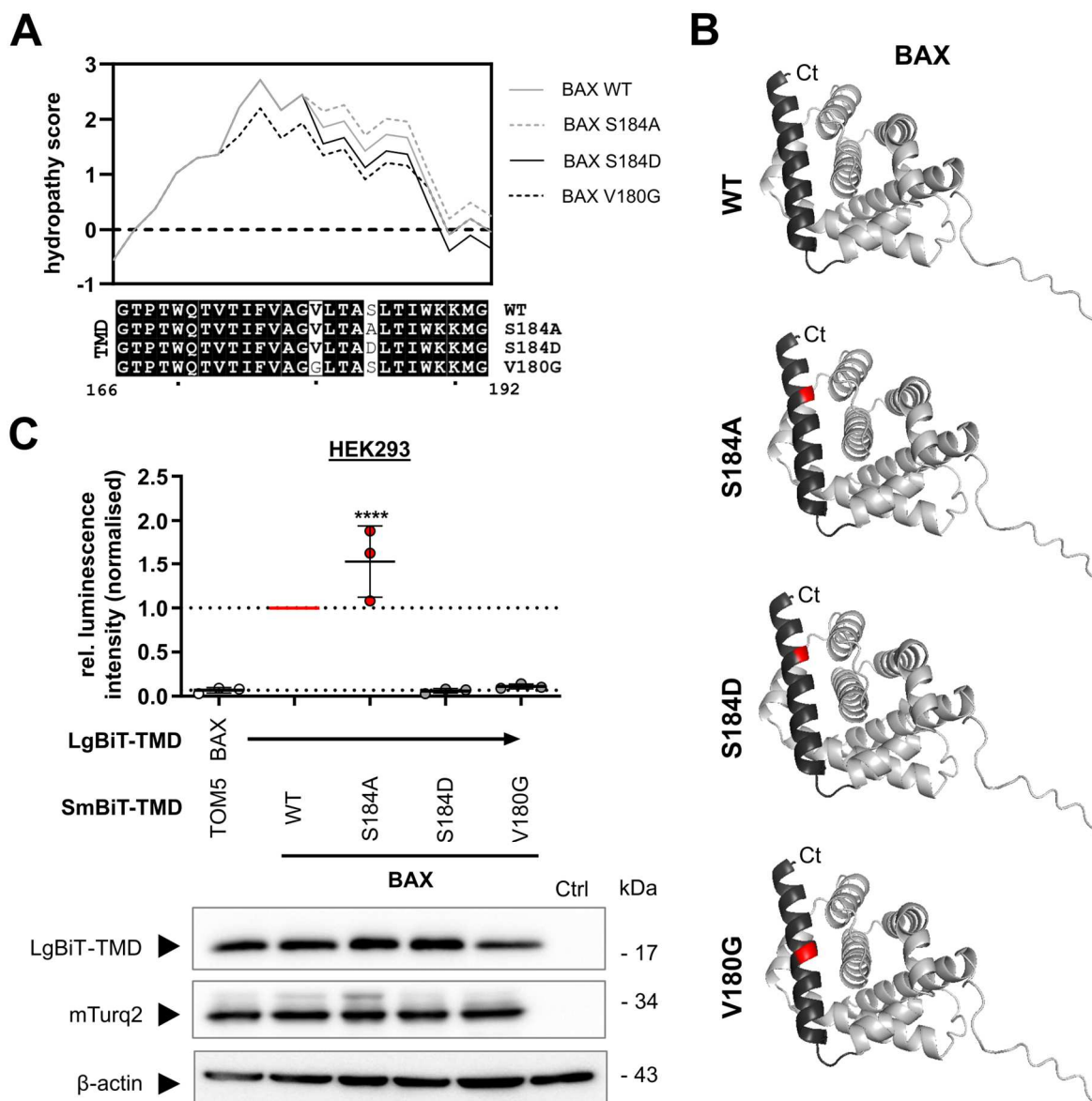
**A** – Western Blot analysis of whole cell lysates from DU145 cells transfected to express EGFP-fused BAX TMD chimeras, wild-type (WT) or EGFP only with co-transfection of mCherry-BCL-2-encoding plasmid (mC-BCL-2) or an empty vector control. Cells were harvested 18 h post transfection and cell death (PARP/cPARP), EGFP(-BAX) and mC-BCL-2 levels were detected.  $\beta$ -actin was used as loading control. Representative Blot from three independent experiments. **B** – Densitometric analysis of Western Blot data shown in A showing cleaved PARP-to-EGFP ratio (cell death per EGFP expression). Mean  $\pm$  sd from three independent experiments is shown in relation to EGFP empty vector control. **C** – cLSM images of MCF-7 transfected to express EGFP-fused BAX TMD chimeras or wild-type (WT) in combination with mC-BCL-2 or an empty vector control. Cells were fixed 18 h post transfection. Representative images from three independent experiments are maximum projections of z-stacks. Zoomed-in insets are in 3x magnification. Scale bar = 10  $\mu$ m. **D** – Quantification of EGFP-BAX clustering from MCF-7 cells in C. Shown is the percentage of EGFP-BAX-expressing cells containing EGFP-BAX clusters. Mean  $\pm$  sd from three independent experiments including  $\geq$  100 cells per experiment. **E** – Flow cytometric analysis of DU145 cells transfected as in A, harvested 18 h post transfection and stained with Annexin V-APC to detect dead cells (Annexin V+). Mean  $\pm$  sd from three independent experiments. **F** – Percent inhibition of BAX by BCL-2 as calculated from cell death data in E. Complete inhibition (100%) equals cell death reduction to EGFP control levels, while no inhibition (0%) equals no cell death reduction at all. Mean  $\pm$  sd from three independent experiments.

### 3.3.2 BAX-TMD mutation crucially interferes with BAX function

After investigating the functional impact of TMD exchange in BAX, the impact of mutating individual amino acids within the TMD sequence on BAX-TMD homotypic interaction as well as BAX localisation was evaluated in the next step.

Serine at position 184 in BAX is a target for BAX phosphorylation by Akt kinase (292). While phosphorylation was shown to abrogate BAX mitochondrial localisation and reduce BAX cell death-inducing activity, constitutive mitochondrial localisation of BAX as well as enhanced pro-apoptotic activity were described for the mutant BAX S184A for which S184 phosphorylation is blocked (293, 302). Thus, (de-)phosphorylation-mimicking mutants BAX S184A and S184D respectively were selected for further investigation. In addition, the “catalogue of somatic mutations in cancer” (COSMIC, [cancer.sanger.ac.uk/cosmic](http://cancer.sanger.ac.uk/cosmic)) harbours numerous mutations in the background of cancer – also within the TMDs of Bcl-2 family proteins. Interestingly, in the BAX-TMD half a dozen mutations from different cancers are listed in COSMIC potentially influencing BAX function in cancer cells. The yet undescribed mutation V180G (COSMIC genome ID: COSV53168900) was found in six independent samples of head and neck cancer and was hence selected as a third BAX-TMD mutation.

BAX-TMD mutations were first analysed *in silico* to gain possible insights into their impact on TMD hydrophobicity as well as protein folding. For that, hydropathy score for TMD sequences of BAX S184A, S184D and V180G as well as BAX wild-type (WT) was calculated for each AA position using the algorithm described by Kyte and Doolittle (346). Here, a hydropathy score (reflecting hydrophobicity) is defined as hydrophilic for values < 0, while values > 0 indicate a hydrophobic character. The score ranges from -4.5 (Arginine) to 4.5 (Isoleucine). As can be seen in Figure 20A, generally hydrophobic hydropathy scores of BAX-TMD mutants and wild-type TMD start to differ at position 173 with BAX V180G exerting lower hydrophobicity than WT until position 188. For BAX S184D, hydropathy score was also reduced compared to WT from position 179 on. Conversely, BAX S184A showed higher hydrophobicity than the WT from position 179 on. Analysis of protein folding using AlphaFold Colab (340) demonstrated, however, that observed changes in hydrophobicity have no impact on BAX protein structure (Figure 20B). The Ct  $\alpha$ 9 helix, key element of the TMD in Bcl-2 proteins (shown in dark grey), was predicted in almost exact same size and orientation for all BAX molecules examined.



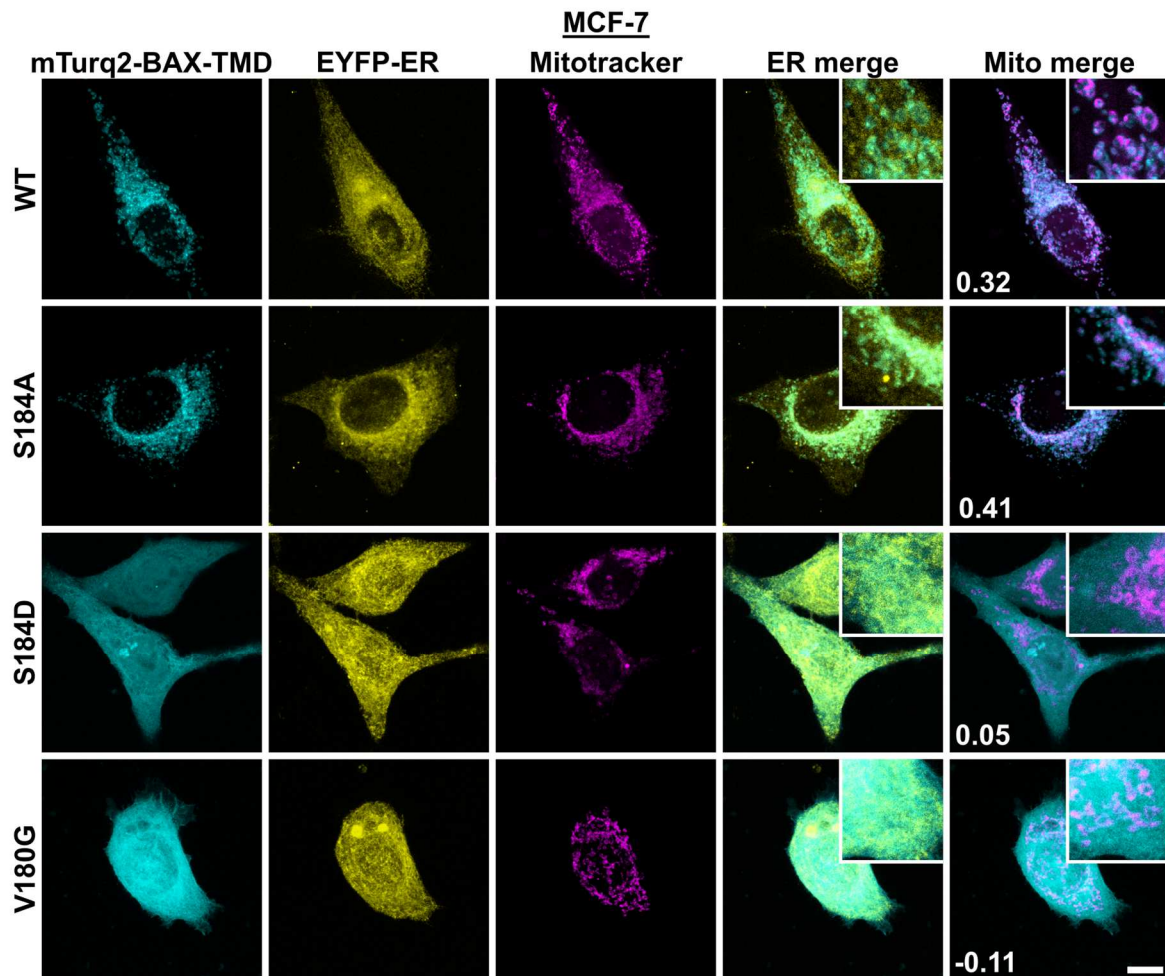
**Figure 20: BAX TMD mutation modulates interaction capacity with wild-type BAX-TMD.**

**A** – Hydropathy scores for indicated BAX TMD sequences according to Kyte and Doolittle (Kyte and Doolittle 1982). **B** – AlphaFold prediction (340) of BAX protein structure. TMD ( $\alpha$ 9-helix) in dark grey, Mutation site in red. Ct = C-terminus. **C** - NanoBiT interaction data from HEK293 cells co-transfected to express LgBiT-BAX-TMD in combination with indicated SmBiT-TMDs. Cells were harvested 24 post transfection and subjected to NanoBiT assay (top) and Western Blot (bottom). For the NanoBiT assay, fluorescence-normalised luminescence intensity is shown relative to positive control (BAX-/BAX-TMD). Mean  $\pm$  sd from three independent experiments. Mean of both negative control (BAX-/TOM5-TMD) and positive control are indicated with a dashed line. Asterisks indicate statistically significant differences compared to negative control. Construct expression was verified via Western Blot (bottom) using antibodies against LgBiT, mTurquoise2 (mTurq2) to indirectly detect SmBiT-TMDs and  $\beta$ -actin as loading control. Representative Blot from two independent experiments. WT = wild-type. Experiments were performed by Alexander Paul.

Next, interaction capacity of BAX-TMD mutants with WT BAX-TMD was assessed. To this end, SmBiT-BAX-TMD-encoding plasmids were subjected to site-directed mutagenesis to introduce desired mutations in BAX-TMD (S184A, S184D, V180G). HEK293 cells were then transfected with mutated plasmids in combination with LgBiT-BAX-TMD-encoding plasmid and subsequently analysed by NanoBiT assay and Western Blot (Figure 20C). Relative luminescence of combination WT BAX-TMD and BAX-TMD S184A was 1.5-fold increased compared to BAX-/BAX-TMD positive control (Figure 20C, upper panel). In contrast, interaction signals for combination of WT BAX-TMD with BAX-TMD S184D or V180G, were reduced to the level of the BAX-/TOM5-TMD negative control (0.06-fold or 0.11-fold respectively). Expression of LgBiT-TMD and mTurq2 were verified using Western Blot revealing similar expression levels across all samples tested (Figure 20C, lower panel). Thus, interaction between WT BAX-TMD and BAX-TMD S184D or BAX-TMD V180G were abolished, while for BAX-TMD S184A interaction with WT BAX-TMD was enhanced compared to homotypic interaction of WT BAX-TMDs.

As the NanoBiT assay revealed an impact of TMD mutation on BAX-TMD homotypic interaction, subcellular localisation of BAX-TMD peptides was sought to be further investigated. To pinpoint subcellular localisation of mutant BAX-TMD peptides, MCF-7 cells expressing EYFP-ER were transfected to express mTurq2-fused BAX TMD peptides, stained with Mitotracker red, fixed and analysed using cLSM (Figure 21). mTurq2-BAX-TMD as well as mTurq2-BAX-TMD S184A were predominantly localised to mitochondria confirmed by representative r-value between mTurq2-TMD signal and Mitotracker signal of  $r_{\text{BAX-TMD+Mito}} = 0.32$  and  $r_{\text{BAX-TMD S184A+Mito}} = 0.41$ . Interestingly, mTurq2-BAX-TMD S184D and mTurq2-BAX-TMD V180G were both diffusely distributed throughout the cell. In consequence, no colocalisation with mitochondria was observable ( $r_{\text{BAX-TMD S184D+Mito}} = 0.05$  and  $r_{\text{BAX-TMD V180G+Mito}} = -0.11$ ) congruent to abolished interaction with mitochondria-localised WT BAX-TMD.

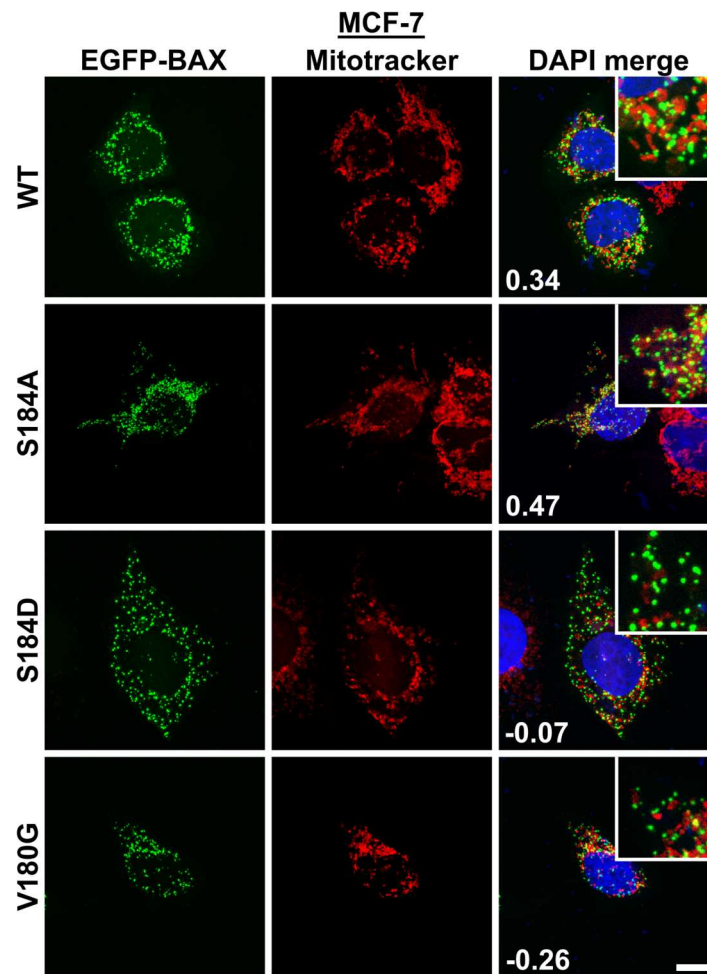
To recapitulate the impact of mutation on functionality of the full-length BAX protein, localisation of full-length BAX mutants was examined subsequently. MCF-7 cells were transfected to express EGFP-fused full-length BAX (mutants). Cells were stained with Mitotracker and fixed followed by cLSM (Figure 22).



**Figure 21: BAX TMD mutation drastically influences subcellular localisation of TMD peptides.**

cLSM images of MCF-7 cells expressing EYFP-ER marker and transfected to express indicated mTurquoise2-BAX-TMD fusion proteins. Cells were stained with Mitotracker red 24 h post transfection and subsequently fixed for imaging. Representative images from three independent experiments are maximum projections of z-stacks. Numbers are Pearson's r-value for merged channels obtained using Fiji software. Zoomed-in insets are in 3x magnification. Scale bar = 10  $\mu$ m. WT = wild-type. Experiments were performed by Alexander Paul.

As observed for BAX-TMD chimeras (Figure 18), cLSM of MCF-7 cells expressing EGFP-BAX mutants revealed BAX clustering in most cells (Figure 22). BAX clusters in cells expressing WT EGFP-BAX or EGFP-BAX S184A were primarily localised to mitochondria. Moreover, colocalisation with mitochondria was slightly increased for EGFP-BAX S184A ( $r_{\text{BAX S184A+Mito}} = 0.47$ ) compared to WT EGFP-BAX ( $r_{\text{BAX+Mito}} = 0.34$ ). On the other hand, expression of EGFP-BAX S184D and EGFP-BAX V180G produced clusters which were evenly distributed in the whole cell. In accordance, colocalisation with mitochondria was abrogated for both EGFP-BAX S184D ( $r_{\text{BAX S184D+Mito}} = -0.07$ ) and EGFP-BAX V180G ( $r_{\text{BAX V180G+Mito}} = -0.26$ ).



**Figure 22: BAX TMD mutation modulates localisation but not clustering of BAX.**

cLSM images of MCF-7 cells transfected to express EGFP-fused BAX wild-type (WT) or mutants. Cells were stained with Mitotracker red 24 h post transfection and subsequently fixed for imaging. DAPI-containing mounting medium was used to stain nuclei. Representative images from three independent experiments are maximum projections of z-stacks. Numbers are Pearson's  $r$ -values for merged channels obtained using Fiji software. Zoomed-in insets are in 3x magnification. Scale bar = 10  $\mu\text{m}$ . Experiments were performed by Alexander Paul.

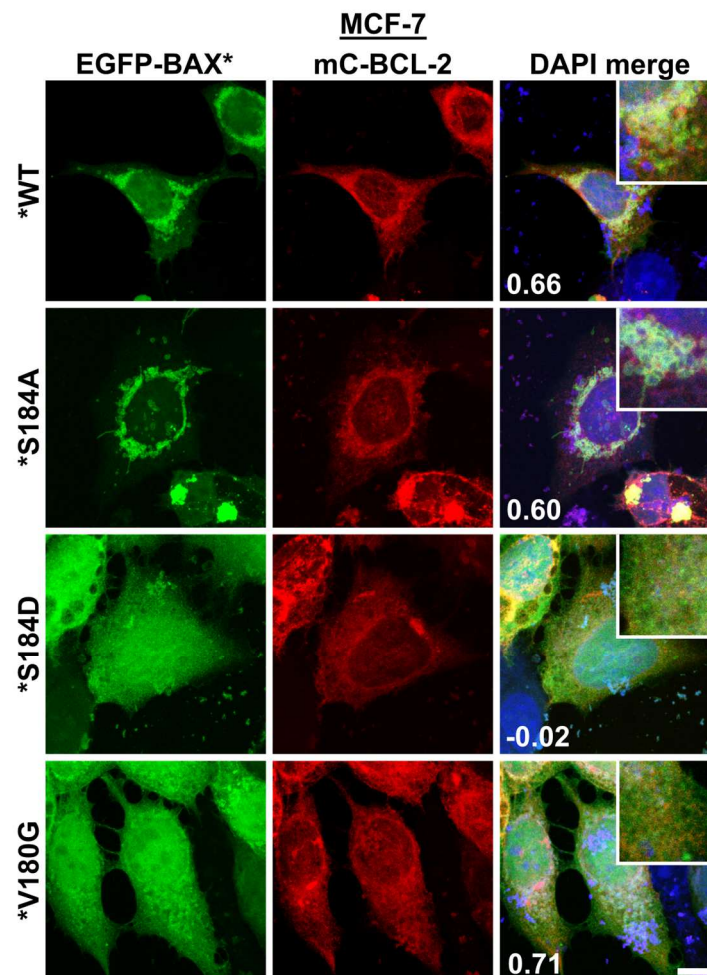
Anti-apoptotic BCL-2 was previously shown to inhibit BAX-induced apoptosis which partially depended on BAX TMD sequence (Figure 19). Therefore, impact of BAX-TMD mutations on inhibition by BCL-2 was analysed to determine the role of individual TMD residues in inhibition by BCL-2. As a first step, colocalisation of BAX mutants with BCL-2 was analysed in MCF-7 cells transfected to express EGFP-BAX (mutants) in combination with mC-BCL-2 using cLSM (Figure 23). In agreement with previous observations (Figure 19C), mC-BCL-2 colocalised well with EGFP-BAX ( $r_{\text{BAX+BCL-2}} = 0.66$ ) and blocked BAX cluster formation. In fact, BAX cluster formation was effectively abrogated for all BAX mutants.

In contrast to partially cytosolic WT EGFP-BAX, EGFP-BAX S184A co-expressed with mC-BCL-2 was exclusively localised to mitochondria colocalising with mC-BCL-2 ( $r_{\text{BAX S184A+BCL-2}} = 0.60$ ). Co-expression of EGFP-BAX S184D with mC-BCL-2, however, led to diffuse cytosolic distribution of EGFP-BAX S184D resembling the diffuse localisation of mTurq2-BAX-TMD S184D (Figure 21), whereas mC-BCL-2 displayed a perinuclear ER-like localisation. Thus, colocalisation was notably reduced compared to WT EGFP-BAX ( $r_{\text{BAX S184D+BCL-2}} = -0.02$ ). Moreover, also EGFP-BAX V180G was diffusely distributed throughout the whole cell when co-expressed with mC-BCL-2. However, EGFP-BAX V180G still showed a perinuclear membrane-bound localisation, presumably at mitochondria, where it colocalised with mC-BCL-2 resulting in highly positive signal correlation ( $r_{\text{BAX V180G+BCL-2}} = 0.72$ ).

Finally, the influence of BAX TMD mutations on apoptosis signalling was assessed by overexpression of EGFP-fused BAX TMD mutants in DU145 cells (Figure 24). In the same experiment, inhibition of BAX-induced cell death by anti-apoptotic Bcl-2 proteins was assessed by co-expression of mC-BCL-2, FLAG-tag MCL-1 and mC-BCL-XL. Cell death was analysed 18 h post transfection via Annexin V-APC staining and flow cytometry (Figure 24A). Expression of WT EGFP-BAX alone resulted in 22% Annexin V<sup>+</sup> cells in contrast to 6% Annexin V<sup>+</sup> cells for EGFP control. No significant differences in cell death induction were observed after overexpression of EGFP-BAX mutants in comparison to WT EGFP-BAX (BAX S184A: 26% Annexin V<sup>+</sup> cells, BAX S184D: 21% Annexin V<sup>+</sup> cells, BAX V180G: 19% Annexin V<sup>+</sup> cells). Co-expression of mC-BCL-2 with WT EGFP-BAX reduced cell death to 3% Annexin V<sup>+</sup> cells. The same inhibitory effect was observed for cells expressing mC-BCL-2 together with EGFP-BAX S184D and V180G (3% and 4% Annexin V<sup>+</sup> cells). Intriguingly, EGFP-BAX S184A-induced cell death was less inhibited by mC-BCL-2 compared to WT BAX resulting in 7.5% Annexin V<sup>+</sup> cells. For cells co-expressing FLAG-tag MCL-1 in combination with WT EGFP-BAX, cell death induction was inhibited to a lesser extent than by co-expression of BCL-2 resulting in 11% Annexin V<sup>+</sup> cells. Also, cell death induced by EGFP-BAX S184D and EGFP-BAX V180G was reduced by FLAG-tag MCL-1 co-expression to the same level as for WT EGFP-BAX (8% and 10% Annexin V<sup>+</sup> cells). However, inhibition by FLAG-tag MCL-1 was virtually abolished for EGFP-BAX S184A (22% Annexin V<sup>+</sup> cells). In contrast to co-expression of BAX (mutants) with BCL-2 and MCL-1, co-expression of mC-BCL-XL reduced cell death levels for all BAX mutants to 3-4% Annexin V<sup>+</sup> cells.



Using Western Blot, specific expression of EGFP-BAX proteins was verified revealing bands of similar size for WT EGFP-BAX and all mutants at ~50 kDa (Figure 24B). BAX protein levels among samples slightly varied for co-expression of MCL-1 and BCL-2. Here, EGFP-BAX S184A showed higher expression level compared to other BAX proteins. Levels of anti-apoptotic proteins BCL-2, MCL-1 and BCL-XL were similar among samples tested. Also, PARP cleavage reflected the differences in cell death induction observed for Annexin V positivity in Figure 24A. However, especially for expression of BAX proteins alone unexpected variations in PARP cleavage were observed which were subsequently analysed with densitometry.

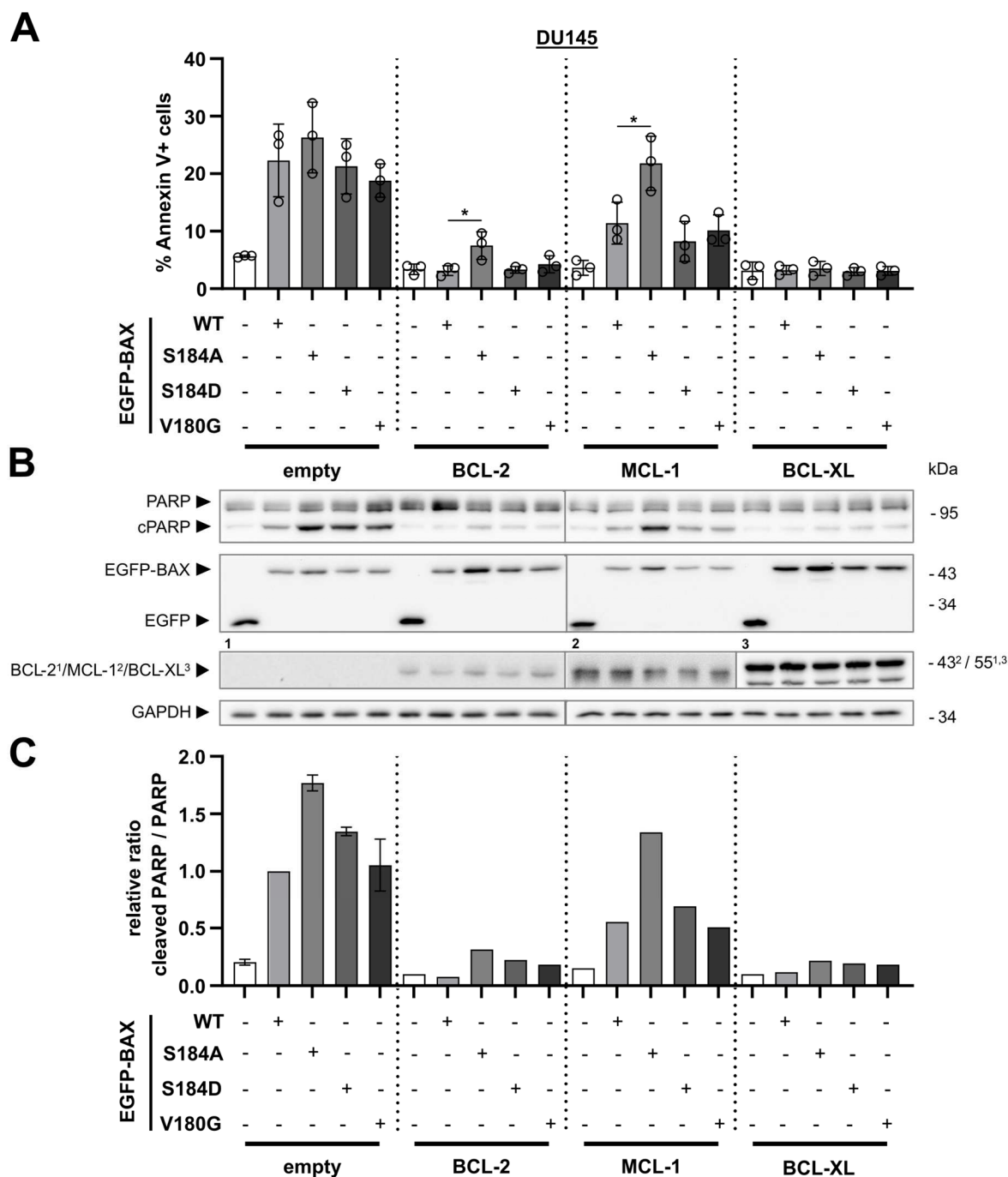


**Figure 23: BAX S184D mutation abolishes colocalisation with BCL-2.**

cLSM images of MCF-7 cells transfected to express EGFP-BAX wild-type (WT) or mutants in combination with mCherry-BCL-2 (mC-BCL-2). Cells were fixed for imaging 24 h post transfection. DAPI-containing mounting medium was used to stain nuclei. Representative images from three independent experiments are maximum projections of z-stacks. Numbers are Pearson's r-values for merged channels obtained using Fiji software. Zoomed-in insets are in 3x magnification. Scale bar = 10  $\mu$ m. Experiments were performed by Alexander Paul.

Densitometric analysis of cPARP-to-PARP ratio (indicating cell death) in Figure 24B revealed an increased relative ratio for expression of EGFP-BAX S184A alone (1.76-fold) compared to WT EGFP-BAX alone (set to 1.00). Surprisingly, cPARP/PARP ratio was also increased 1.35-fold for expression of EGFP-BAX S184D alone. cPARP/PARP ratio for expression of EGFP-BAX V180G alone was comparable to WT EGFP-BAX (1.05-fold). Of note, relative cPARP/PARP ratio for EGFP control was 0.20-fold. Co-expression of mC-BCL-2 revealed effective reduction of relative cPARP/PARP ratio for EGFP-BAX (0.07-fold). A slight increase (0.31-fold) for co-expression of mC-BCL-2 and EGFP-BAX S184A corroborates slightly impaired inhibition of EGFP-BAX S184A from Figure 24A. However, also slight increase was detected for combination of mC-BCL-2 with EGFP-BAX S184D (0.22-fold) and EGFP-BAX V180G (0.18-fold) compared to WT EGFP-BAX. cPARP/PARP ratios for samples with co-expressed FLAG-tag MCL-1 also underpinned the findings from flow cytometry: moderate cell death reduction for co-expression of FLAG-tag MCL-1 with WT EGFP-BAX (0.55-fold), EGFP-BAX S184D (0.69-fold) or EGFP-BAX V180G (0.51-fold), while the ratio for co-expression with EGFP-BAX S184A was only slightly reduced (1.33-fold) compared to expression of EGFP-BAX S184A alone. Finally, co-expression of mC-BCL-XL with EGFP-BAX (mutants) also recapitulated cell death rates from flow cytometry with robust reduction of relative cPARP/PARP ratio to control levels ranging from 0.12-fold (WT EGFP-BAX) to 0.21-fold (EGFP-BAX S184A).

To sum up the findings for the analysed BAX TMD mutants, BAX S184A, BAX S184D and BAX V180G, clear differences in TMD hydrophobicity were observed depending on the exchanged AA – increased hydrophobicity for S184A and reduced hydrophobicity for S184D and V180G. Although no visible alterations in protein structure were revealed by folding prediction, mutations enhanced (S184A) or abolished (S184D, V180G) homotypic interaction with BAX-TMD. While S184A mutation led to an apparently constitutive mitochondrial localisation of BAX, mutations S184D and V180G led to diffuse localisation of BAX which did not prevent BAX oligomerisation. Strikingly, cell death assays revealed slightly reduced and abolished inhibition of BAX S184A-induced cell death by BCL-2 or MCL-1 respectively. Detection of PARP cleavage also suggests increased apoptotic potential of not only BAX S184A, but also BAX S184D.



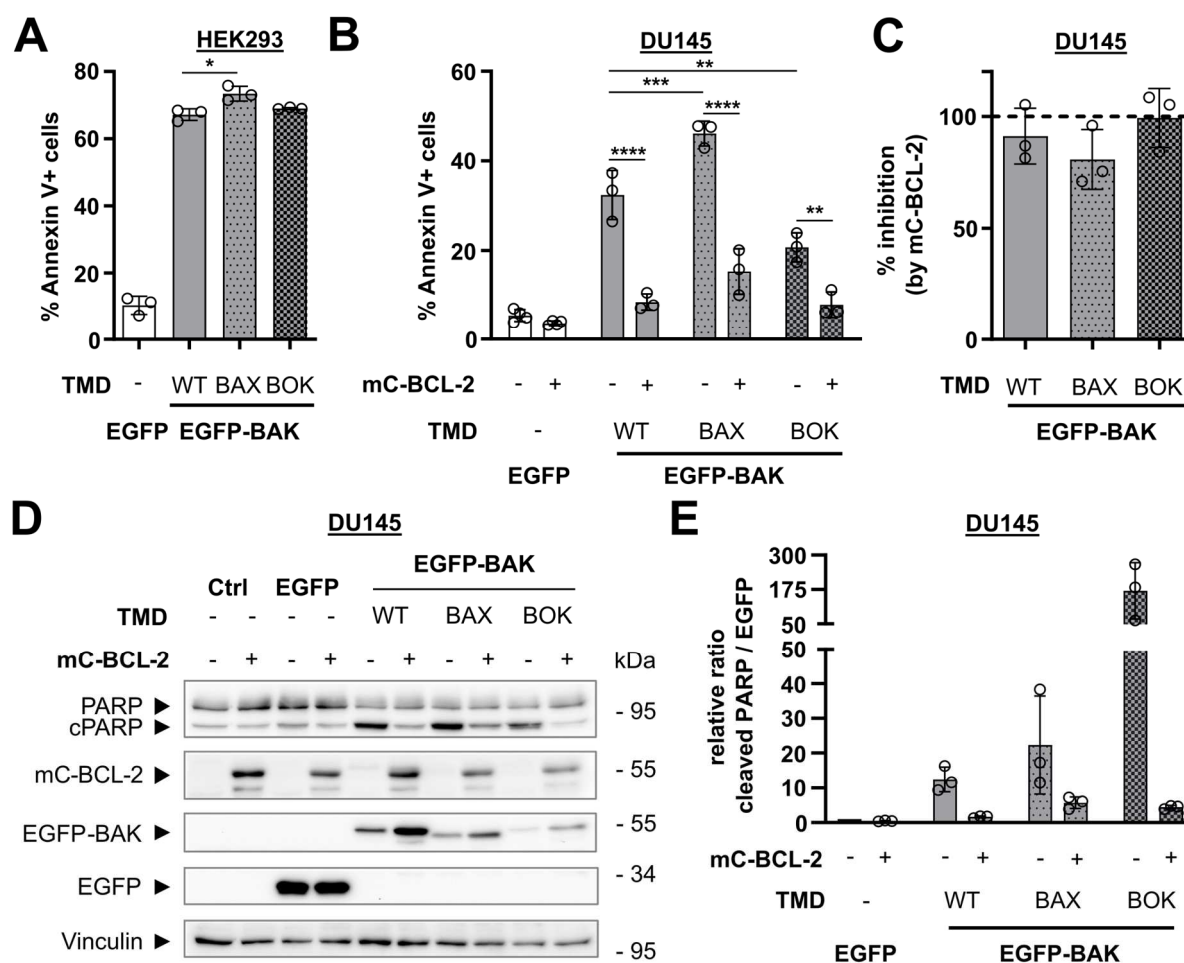
**Figure 24: BAX TMD mutation modulates apoptosis and inhibition by anti-apoptotic proteins.**

**A** – Flow cytometric cell death assessment in DU145 cells transfected to express indicated EGFP-BAX proteins or EGFP alone in combination with mCherry-BCL-2, FLAG-tag MCL-1, mCherry-BCL-XL or an empty vector control respectively. Cells were harvested 18 h post transfection and stained with Annexin V-APC to detect dead cells (Annexin V+) using flow cytometry. Mean  $\pm$  sd from three independent experiments. **B** – DU145 cells transfected as in A were subjected to Western Blot 18 h post transfection. Whole cell lysates were analysed using antibodies against (cleaved) PARP to detect cell death and EGFP, BCL-2, MCL-1 and BCL-XL to verify protein expression. GAPDH was used as a loading control. Blot from one independent experiment. **C** – Densitometric analysis of PARP band intensities out of B showing cleaved PARP-to-PARP ratio (cell death). Mean  $\pm$  range from two independent experiments (EGFP-BAX (mutants) + empty vector control) or ratios from one independent experiments (EGFP-BAX (mutants) + anti-apoptotic BCL-2 proteins) are shown in relation to EGFP-BAX empty vector control. WT = wild-type. Experiments were performed by Alexander Paul.

### 3.3.3 Inhibition of BAK by BCL-2 is TMD-independent

With highest sequence similarity to BAX, BAK is another bona fide pro-apoptotic effector protein which can be inhibited by anti-apoptotic BCL-2 (151). Thus, after investigating the impact of TMD exchange and mutation in BAX, it was sought to be elucidated if the TMD sequence in BAK plays a role in BAK function and inhibition. Likewise, the BAK TMD sequence was exchanged for the sequence of BAX or BOK respectively. As a first step to determine pro-apoptotic activity of these BAK TMD chimeras, HEK293 cells were transfected with plasmids encoding for WT EGFP-BAK, EGFP-BAK TMD chimeras or EGFP as a control and phosphatidylserine exposure was analysed with Annexin V-APC using flow cytometry (Figure 25A). Cell death was substantially increased in cells expressing WT EGFP-BAK (67% Annexin V+ cells) compared to EGFP control (10% Annexin V+ cells). For EGFP-BAK<sup>BAX-TMD</sup>, Annexin V positivity was slightly but significantly increased compared to WT EGFP-BAK (73% Annexin V+ cells). For EGFP-BAK<sup>BOK-TMD</sup>, cell death was not significantly altered compared to WT EGFP-BAK (69% Annexin V+ cells). In line with increased apoptotic activity of EGFP-BAK<sup>BAX-TMD</sup>, MCF-7 cells stained with Mitotracker red and transfected to express EGFP-BAK<sup>BAX-TMD</sup> showed a higher tendency of mitochondria-localised BAK clusters than cells expressing WT EGFP-BAK (Supplementary Figure S7A).

To consolidate these findings in a second cell line and to analyse the effect of the TMD exchange on BAK inhibition by BCL-2, DU145 prostate carcinoma cells were co-transfected to express EGFP, WT EGFP-BAK or EGFP-BAK TMD chimeras in combination with mC-BCL-2 or an empty vector control. Again, cells were stained with Annexin V-APC and percentage of dead cells was assessed using flow cytometry. Cell death was increased in cells expressing EGFP-BAK<sup>BAX-TMD</sup> (46% Annexin V+ cells) compared to WT EGFP-BAK (32% Annexin V+ cells, Figure 25B). In contrast, expression of EGFP-BAK<sup>BOK-TMD</sup> led to a reduction in cell death compared to WT EGFP-BAK (20% Annexin V+ cells). Interestingly, TMD exchange did not prevent cell death inhibition by co-expression of mC-BCL-2 (EGFP-BAK<sup>BAX-TMD</sup>: 15% Annexin V+ cells, EGFP-BAK<sup>BOK-TMD</sup>: 8% Annexin V+ cells, WT EGFP-BAK: 8% Annexin V+ cells). However, cell death was not completely reduced to levels of EGFP control (5% Annexin V+ cells). As a consequence, calculation of % inhibition by BCL-2 (as for BAX, equation (1), 3.3.1) results in similarly effective inhibition of 91% for WT EGFP-BAK, 81% for EGFP-BAK<sup>BAX-TMD</sup> and 99% for EGFP-BAK<sup>BOK-TMD</sup> (Figure 25C).



**Figure 25: TMD exchange in BAK to BAX- or BOK-TMD has no influence on inhibition by BCL-2.**

**A** – Flow cytometry of HEK293 cells transfected to express EGFP-fused BAK TMD chimeras, wild-type (WT) or EGFP as a control. Cells were harvested 18 h post transfection and stained with Annexin V-APC to detect dead cells (Annexin V+). Mean  $\pm$  sd from three independent experiments. **B** - Flow cytometry of DU145 cells transfected to express EGFP-fused BAK TMD chimeras, WT or EGFP in combination with mCherry-BCL-2 (mC-BCL-2) or an empty vector control. Cells were harvested 18 h post transfection and stained with Annexin V-APC to detect Annexin V+ cells. Mean  $\pm$  sd from three independent experiments. **C** – Inhibition of EGFP-BAK (TMD chimeras) by mC-BCL-2 as calculated from cell death data in B. Complete inhibition (100%) equals cell death reduction to EGFP control levels, while no inhibition (0%) equals no cell death reduction. Mean  $\pm$  sd from three independent experiments. **D** - Western Blot analysis of whole cell lysates from DU145 cells transfected as in B. Cells were harvested 18 h post transfection and cell death, EGFP(-BAK) and mC-BCL-2 expression levels were detected using antibodies against (cleaved) PARP, EGFP and BCL-2 respectively. Vinculin was used as loading control. Representative Blot from three independent experiments. **E** –Densitometric analysis of Western Blot data shown in D showing cleaved PARP-to-EGFP ratio (cell death per EGFP expression). Mean  $\pm$  sd from three independent experiments is shown in relation to EGFP control.

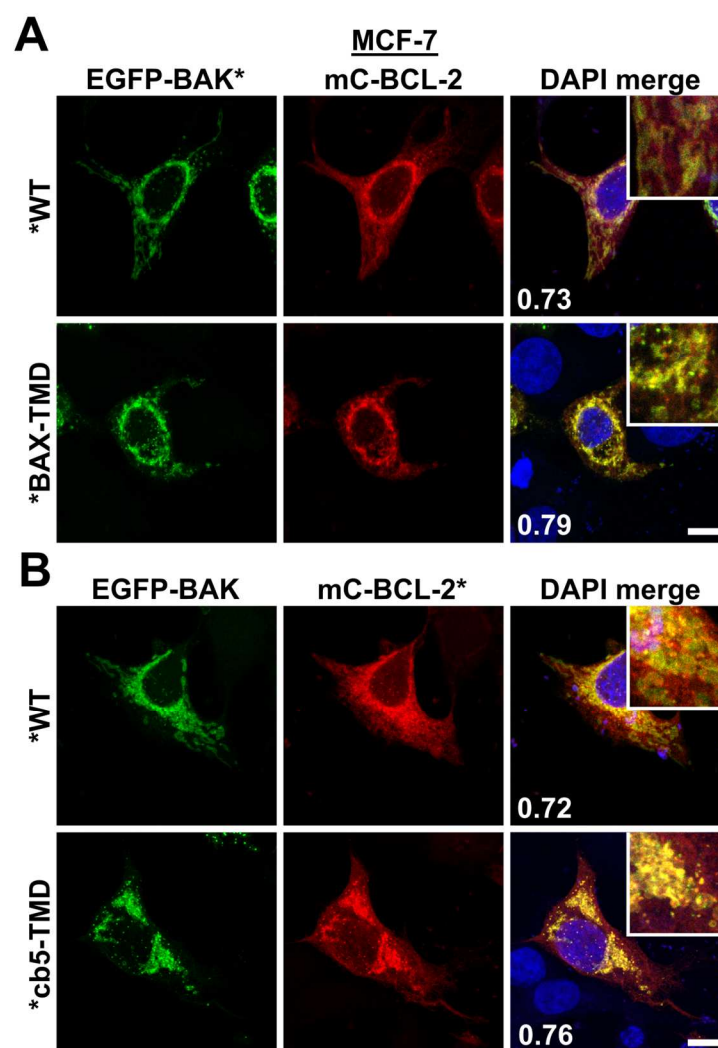
To verify protein expression of BAK TMD chimeras, whole cell lysates of DU145 cells transfected as in Figure 25B were analysed using Western Blot (Figure 25D). Expression level of BAK TMD chimeras was lowered, especially for EGFP-BAK<sup>BOK-TMD</sup>, compared to WT EGFP-BAK which could also be quantified by densitometry (Supplementary Figure S10C). Co-expression of mC-BCL-2, however, visibly increased expression level of all EGFP-BAK proteins.

Additionally, expression level of mC-BCL-2 was similar among samples analysed (Figure 25D). Increased PARP cleavage could be observed for expression of EGFP-BAK proteins alone which was reduced upon mC-BCL-2 co-expression. Densitometric analysis of cPARP/EGFP ratio (Figure 25E) yielded an increased relative cPARP/EGFP ratio for expression of WT EGFP-BAX (12-fold), EGFP-BAK<sup>BAX-TMD</sup> (22-fold) and especially EGFP-BAK<sup>BOK-TMD</sup> (170-fold) compared to EGFP control. Co-expression of mC-BCL-2 effectively reduced relative cPARP/EGFP ratio for all BAK proteins (WT EGFP-BAK: 2-fold, EGFP-BAK<sup>BAX-TMD</sup>: 6-fold, EGFP-BOK<sup>BOK-TMD</sup>: 4-fold).

In order to confirm that TMD exchange in BAK or BCL-2 does not affect BAK inhibition by BCL-2, colocalisation as a prerequisite for interaction and, thus, inhibition was investigated next. MCF-7 cells were transfected to express WT EGFP-BAK or EGFP-BAK<sup>BAX-TMD</sup> in combination with mC-BCL-2, cells were fixed and analysed by cLSM (Figure 26A). Both, WT EGFP-BAK or EGFP-BAK<sup>BAX-TMD</sup> colocalised with mC-BCL-2 ( $r_{\text{BAK+BCL-2}} = 0.73$ ,  $r_{\text{BAK-BAX-TMD+BCL-2}} = 0.79$ ). Additionally, MCF-7 cells were transfected to co-express EGFP-BAK with BCL-2 TMD chimeras carrying the TMD of cb5-TMD or TOM5-TMD (Figure 26B, Supplementary Figure S7B,C). cLSM analysis of cells expressing EGFP-BAK and mC-BCL-2<sup>cb5-TMD</sup> revealed that BAK was colocalising with BCL-2<sup>cb5-TMD</sup> only in cells with comparably high BAK expression and occurrence of BAK clusters ( $r_{\text{BAK(high)+BCL-2-cb5-TMD}} = 0.76$ , Figure 26B). Colocalisation was also found for co-expressed EGFP-BAK and mC-BCL-2<sup>TOM5-TMD</sup> (Supplementary Figure S7B). However, in cells expressing comparably low amounts of EGFP-BAK colocalisation of BAK and mC-BCL-2<sup>cb5-TMD</sup> was dampened ( $r_{\text{BAK(low)+BCL-2-cb5-TMD}} = 0.26$ , Supplementary Figure S7C).

Of note, the same localisation phenomena observed for co-expression of EGFP-BAK with mC-BCL-2<sup>cb5-TMD</sup> and mC-BCL-2<sup>TOM5-TMD</sup> were found for co-expression of EGFP-BAX with these BCL-2 TMD chimeras in MCF-7 cells (Supplementary Figure S7B,C). mC-BCL-2<sup>TOM5-TMD</sup> and EGFP-BAX colocalised well at mitochondria ( $r_{\text{BAX+BCL-2-TOM5-TMD}} = 0.70$ ). mC-BCL-2<sup>cb5-TMD</sup> only colocalised with EGFP-BAX in cells with high amounts of BAX (bright BAX clusters,  $r_{\text{BAX(high)+BCL-2-cb5-TMD}} = 0.39$ ) in contrast to a lack of colocalisation between mC-BCL-2<sup>cb5-TMD</sup> and EGFP-BAX in cells with low BAX expression level ( $r_{\text{BAX(low)+BCL-2-cb5-TMD}} = -0.04$ ).

Taken together, although pro-apoptotic activity was slightly modulated by TMD exchange in BAK to BAX- or BOK-TMD, BAK-induced cell death was not altered by TMD exchange. Also, inhibition of BAK by BCL-2 was comparable for BAK TMD chimeras and WT BAK indicating TMD-independence. TMD independency was also shown for colocalisation of BAK with BCL-2, since neither TMD exchange in BAK to BAX-TMD nor TMD exchange in BCL-2 to cb5-TMD fully prevented colocalisation of BAK and BCL-2. Therefore, obtained results suggest BAK's mode of action and regulation by BCL-2 to be dictated by features other than the TMD.



**Figure 26: Colocalisation of BAK and BCL-2 is not affected by changes in TMD sequence.**

cLSM images of MCF-7 cells transfected to co-express EGFP-BAK wild-type (WT) or EGFP-BAK<sup>BAX-TMD</sup> with mCherry-BCL-2 (mC-BCL-2) (A) or EGFP-BAK with mC-BCL-2 WT or mCherry-BCL-2<sup>cb5-TMD</sup> (B). Cells were fixed 24 h post transfection and mounted using DAPI-containing mounting medium. Representative images are maximum projections of z-stacks from two independent experiments. Numbers indicate Pearson's r-values for merged channels obtained using Fiji software. Scale bar = 10 µm.

### 3.3.4 The TMD, not BH3 region, influences BOK and BCL-2 colocalisation

Following up on the identified TMD interaction of BOK-TMD and BCL-2-TMD at the ER, the following chapters will focus on the functional relevance of the interaction between BOK-TMD and BCL-2-TMD.

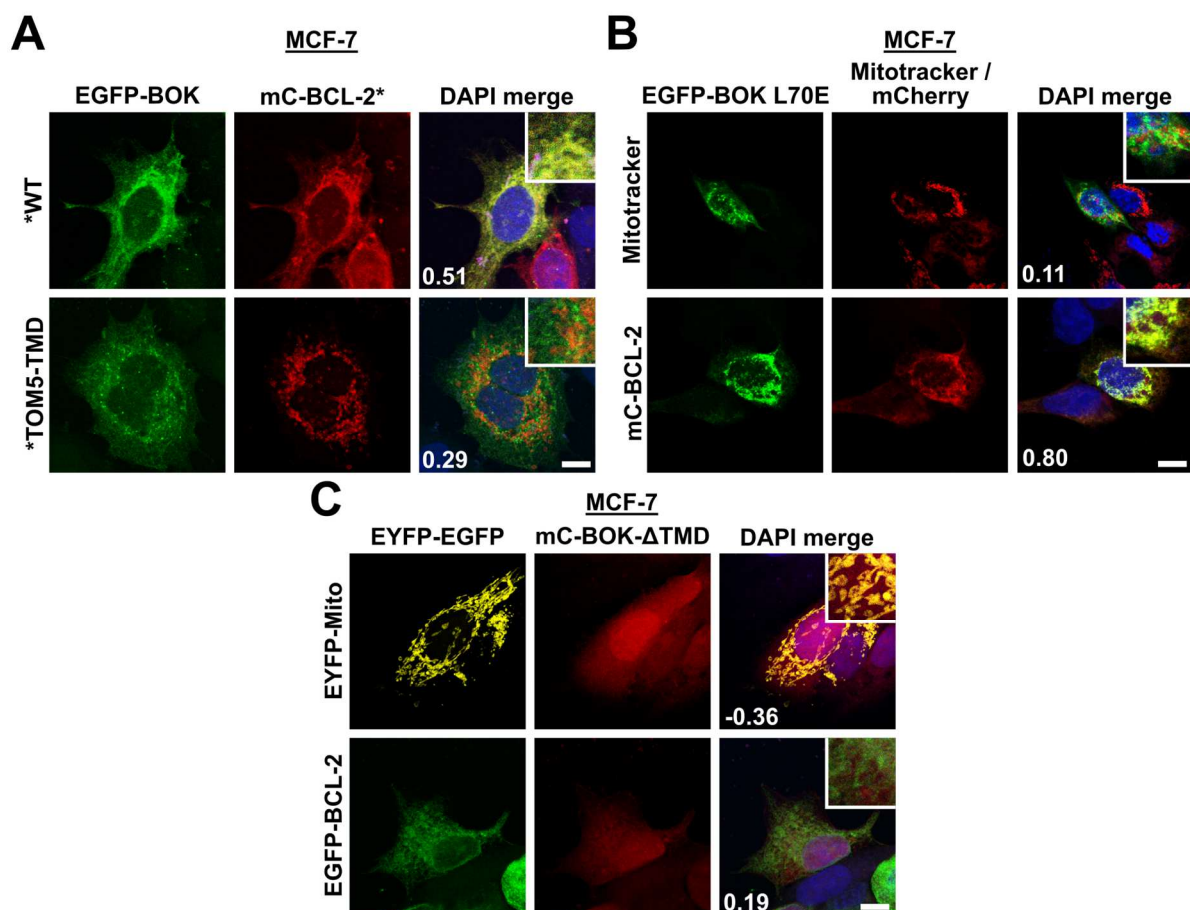
Predominant ER localisation dictated by the TMD was already described for full-length BOK and BCL-2 (157, 172). To confirm ER colocalisation of TMD peptides (Figure 17) of BOK and BCL-2 in full-length proteins, colocalisation of full-length BOK and BCL-2 was investigated in MCF-7 cells co-expressing EGFP-BOK and mC-BCL-2 using cLSM (Figure 27A). Indeed, colocalisation of both BOK and BCL-2 was comparable to their TMD peptides ( $r_{\text{BOK+BCL-2}} = 0.51$ ). In line with literature, BOK and BCL-2 predominant ER localisation was also confirmed by cLSM (Supplementary Figure S8A,B). It is worth mentioning that in cells with visible and especially with strong overexpression of BOK ER marker signals were barely visible or diffusely distributed. Application of different luminal ER markers (PDI or EYFP-ER) confirmed that overexpression of BOK dispersed ER marker signals (Supplementary Figure S9). However, this effect was not observed for membrane-bound, ER-targeted mCitrine-cb5-TMD (Supplementary Figure S8B).

Challenging the suggested TMD dependency of their interaction, the influence of TMD exchange in BCL-2 to TMD of BOK, cb5 or TOM5 on colocalisation with BOK was analysed next. Co-expression EGFP-BOK and mC-BCL-2<sup>BOK-TMD</sup> or mC-BCL-2<sup>cb5-TMD</sup> in MCF-7 cells revealed no change in colocalisation compared to WT BCL-2 ( $r_{\text{BOK+BCL-2-BOK-TMD}} = 0.51$ ,  $r_{\text{BOK+BCL-2-cb5-TMD}} = 0.56$ , Supplementary Figure S8C). Strikingly, TMD exchange in BCL-2 to TOM5-TMD disrupted colocalisation with EGFP-BOK ( $r_{\text{BOK+BCL-2-TOM5-TMD}} = 0.29$ , Figure 27A). In order to exclude that the BH3 region of BOK plays a key role in colocalisation with BCL-2, BOK with the conserved leucine L70 mutated to glutamate for functional inactivation of the BH3 region was applied in the next step. In MCF-7 cells transfected to express EGFP-BOK L70E and stained with Mitotracker, poor colocalisation of BOK L70E with mitochondria was observed ( $r_{\text{BOK L70E + Mito}} = 0.11$ , Figure 27B). In contrast, co-expressed EGFP-BOK L70E and mC-BCL-2 colocalised well in perinuclear regions ( $r_{\text{BOK L70E + Mito}} = 0.80$ ). Finally, the importance of the TMD in colocalisation of BOK and BCL-2 was sought to be underlined by co-expression of Ct truncated BOK without a TMD (BOK- $\Delta$ TMD) and BCL-2.



mCherry-fused BOK- $\Delta$ TMD (mC-BOK- $\Delta$ TMD) was distributed diffusely in the cytosol when expressed in MCF-7 cells with EYFP-Mito marker as revealed by cLSM in Figure 27C. The cytosolic distribution of mC-BOK- $\Delta$ TMD did not change for co-expression of EGFP-fused BCL-2 in MCF-7 cells resulting in abolished colocalisation of Ct truncated BOK and BCL-2 ( $r_{\text{BOK-}\Delta\text{TMD+BCL-2}} = 0.19$ ).

In sum, while TMD exchange in BCL-2 was sufficient to abrogate colocalisation with BOK, BOK with mutated BH3 motif further colocalised with BCL-2. Removing the TMD in BOK, however, not only caused cytosolic localisation of BOK, but also abolished colocalisation with BCL-2. Hence, colocalisation of BOK and BCL-2 at the ER was found to be regulated by interaction of their TMDs rather than BH3:groove interaction.

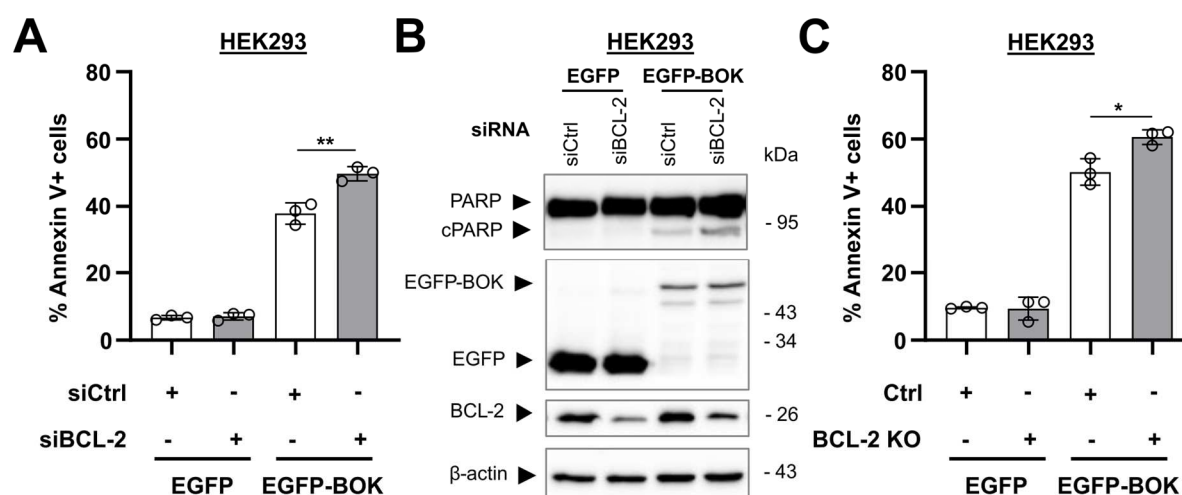


**Figure 27: Colocalisation of BOK and BCL-2 is dictated by their TMD sequences.**

**A** - cLSM images of MCF-7 cells transfected to express EGFP-BOK with mCherry-BCL-2 (mC-BCL-2) wild-type or mC-BCL-2<sup>TOM5-TMD</sup>. Cells were fixed 24 h post transfection and mounted with DAPI-containing mounting medium. Representative images are maximum projections of z-stacks from two independent experiments. Numbers indicate Pearson's  $r$ -values for merged channels obtained using Fiji software. Scale bar = 10  $\mu\text{m}$ . **B** - cLSM images of MCF-7 cells transfected to express EGFP-BOK L70E and either stained with Mitotracker red prior to fixation or co-transfected to express mC-BCL-2. Cells were processed as in A. Scale bar = 10  $\mu\text{m}$ . **C** - cLSM images of MCF-7 transfected to express mCherry (mC)-BOK- $\Delta$ TMD with either EYFP-Mito marker or EGFP-BCL-2. Cells were processed as in A. Scale bar = 10  $\mu\text{m}$ .

3.3.5 BOK-induced cell death is inhibited by BCL-2 which is influenced by their TMDs  
Full-length BOK and BCL-2 were shown to colocalise TMD-dependently at the ER (3.3.4). Thus, the question arises whether BCL-2 could influence cell death induced by BOK and if affirmative, whether this was due to TMD interaction with BOK.

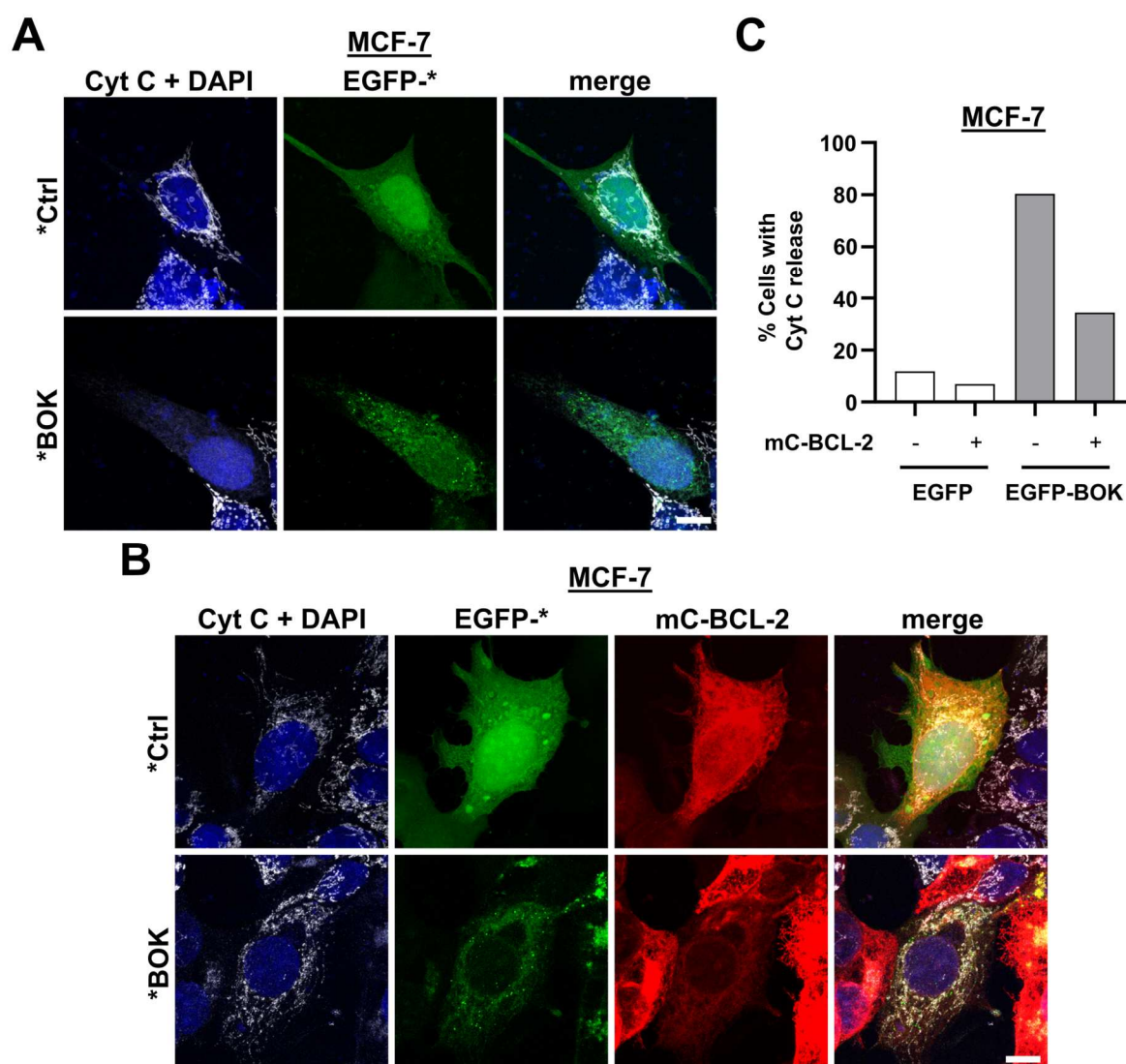
To analyse BOK-induced cell death in the presence and absence of BCL-2, siRNA-mediated knockdown was performed in HEK293 cells by transfection with siRNA targeting the *BCL-2* gene (siBCL-2) or control siRNA (siCtrl). BOK-induced cell death commenced by a second transfection with plasmid encoding EGFP-BOK or EGFP as a control and cell death was analysed after 18 h by flow cytometry (Annexin V-APC). As can be seen in Figure 28A, expression of EGFP-BOK after BCL-2 knockdown significantly increased cell death (50% Annexin V+ cells) compared to transfection with siCtrl (38% Annexin V+ cells). Of note, for expression of EGFP, siBCL-2 and siCtrl led to similarly low cell death levels (7% Annexin V+ cells). Moreover, HEK293 cells transfected as in Figure 28A were analysed using Western Blot to validate BOK and BCL-2 protein levels as well as cell death induction (Figure 28B). Increased levels of cPARP confirmed pronounced BOK overexpression-induced cell death after BCL-2 knockdown compared to siCtrl, while EGFP-BOK levels were similar in both samples.



**Figure 28: BOK-induced cell death is pronounced in absence of BCL-2.**

**A** - Flow cytometric analysis of HEK293 cells which were subjected to siRNA-mediated knockdown of BCL-2 (siBCL-2) or transfected with non-targeted control siRNA (siCtrl). Subsequently, cells were transfected to express EGFP-BOK or EGFP, harvested 18 h post transfection and stained with Annexin V-APC to detect dead cells (Annexin V+). Mean  $\pm$  sd from three independent experiments. **B** - Western Blot analysis of whole cell lysates from cells as in A using antibodies against (cleaved) PARP to detect cell death and EGFP as well as BCL-2 to verify protein expression.  $\beta$ -actin was used as loading control. Representative blot from two independent experiments. **C** - Flow cytometric analysis of HEK293 cells which were transfected with plasmid encoding for the CRISPR/Cas9 system targeting *BCL-2* or an empty vector and plasmids for expression of EGFP-BOK or EGFP. Cells were harvested 18 h post transfection and stained with Annexin V-APC to detect dead cells (Annexin V+). Mean  $\pm$  sd from three independent experiments.

Although BCL-2 levels were reduced upon siRNA-mediated knockdown, Western Blot analysis revealed still detectable levels of BCL-2 indicating only a partial knockdown. Hence, a second experimental approach was conducted in which HEK293 cells were transfected with a plasmid encoding for a CRISPR/Cas9 system targeting the *BCL-2* gene (BCL-2 KO) or a non-targeting control plasmid (Ctrl KO). Simultaneously, cells were transfected to express EGFP-BOK or EGFP. Cell death was subsequently analysed using flow cytometry (Annexin V-APC, Figure 28C). In line with findings from BCL-2 knockdown, BCL-2 KO led to a pronounced cell death induction after EGFP-BOK expression (61% Annexin V+ cells) compared to Ctrl KO (50% Annexin V+ cells).

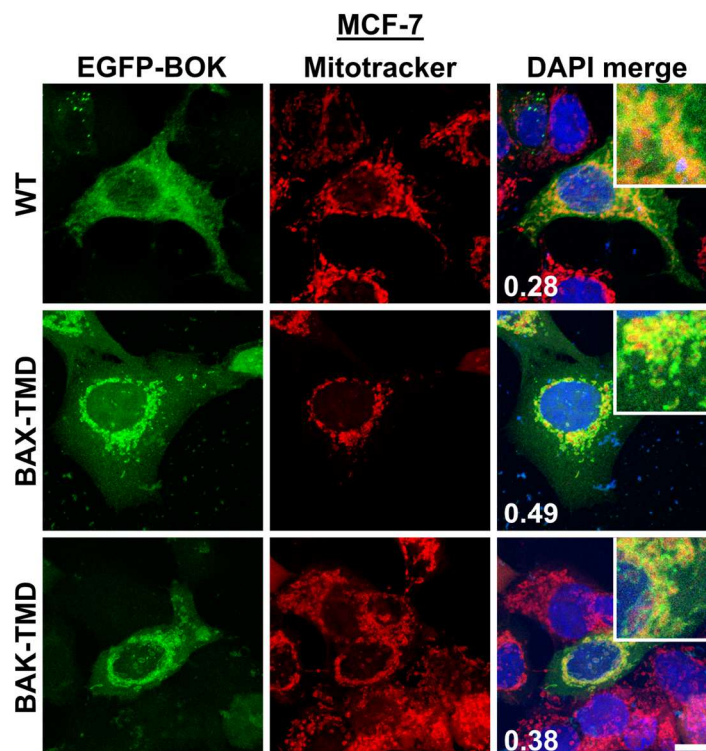


**Figure 29: BOK-induced Cytochrome C release is dampened by BCL-2 co-expression.**

**A** – cLSM images of MCF-7 cells transfected to express EGFP or EGFP-BOK, fixed 18 h post transfection and IF-stained with antibodies against Cytochrome C (Cyt C). Cells were mounted using DAPI-containing mounting medium. Representative images are maximum projections of z-stacks from one independent experiment. **B** – cLSM images of MCF-7 cells transfected to express EGFP or EGFP-BOK and mCherry-BCL-2 (mC-BCL-2). Cells were processed as in A. Representative images from one independent experiment. **C** – Quantification of Cyt C release in cells shown in A,B. Data include  $\geq 50$  cells from one independent experiment.

To study the BOK-induced cell death regulation by BCL-2 in more detail, the role of BCL-2 in guarding BOK-dependent Cytochrome C (CytC) release from mitochondria was analysed using cLSM. MCF-7 cells were transfected to express either EGFP or EGFP-BOK in combination with mC-BCL-2 or an empty vector control. Subsequently, cells were fixed and IF stained for Cytochrome C. Expectedly, most cells expressing EGFP-BOK alone showed diffuse localisation of CytC indicating CytC release from mitochondria upon MOMP exemplarily shown in Figure 29A. In contrast, expression of EGFP alone was not sufficient to induce CytC release so that CytC showed a bright mitochondria-like distribution. Likewise, co-expression of EGFP with mC-BCL-2 revealed mitochondria-localised CytC (Figure 29B). Strikingly, also cells co-expressing EGFP-BOK and mC-BCL-2 frequently possessed mitochondria-localised CytC indicating a reduction of CytC release due to presence of BCL-2. Quantification of the diffuse (released) CytC phenotype recapitulated the observation from cLSM as in 80% of EGFP-BOK-expressing cells CytC was released, whereas co-expression of EGFP-BOK and mC-BCL-2 led to CytC release in only 35% of cells (Figure 29C).

After confirming an influence of BCL-2 on BOK-induced apoptosis, TMD-dependency of this influence was put to the test. As for BAX and BAK, thus, BOK TMD chimeras in which the TMD sequence was exchanged for BAX-TMD or BAK-TMD were analysed. First, BOK TMD chimera localisation was studied in MCF-7 cells which were transfected to express EGFP-fused BOK or BOK TMD chimeras and stained with Mitotracker (Figure 30). As observed previously, colocalisation of EGFP-BOK and mitochondria was rather poor ( $r_{\text{BOK+Mito}} = 0.28$ ). However, both EGFP-BOK<sup>BAX-TMD</sup> as well as EGFP-BOK<sup>BAK-TMD</sup> colocalised notably better with mitochondria ( $r_{\text{BOK-BAX-TMD+Mito}} = 0.49$ ,  $r_{\text{BOK-BAK-TMD+Mito}} = 0.38$ ) indicating a shift of BOK to mitochondria due to the TMD exchange. As a second step, pro-apoptotic activity of BOK TMD chimeras was analysed by flow cytometry in HEK293 cells which were transfected to express EGFP-BOK or EGFP-fused BOK TMD chimeras (Figure 31A). Flow cytometric analysis of Annexin V positivity revealed a potent cell death induction by overexpression of WT EGFP-BOK (58% Annexin V<sup>+</sup> cells) in contrast to EGFP alone (8% Annexin V<sup>+</sup> cells). Interestingly, EGFP-BOK<sup>BAX-TMD</sup> overexpression-induced cells death surpassed cell death induced by WT EGFP-BOK (69% Annexin V<sup>+</sup> cells). Expression of EGFP-BOK<sup>BAK-TMD</sup> caused cell death comparable to WT EGFP-BOK (58% Annexin V<sup>+</sup> cells).



**Figure 30: TMD exchange in BOK to BAX-TMD or BAK-TMD shifts localisation to Mitochondria.**

cLSM images of MCF-7 cells transfected to express EGFP-fused BOK TMD chimeras or wild-type (WT). Cells were stained with Mitotracker red 18 h post transfection, subsequently fixed and mounted using DAPI-containing mounting medium. Representative images from two independent experiments are maximum projections of z-stacks. Numbers indicate Pearson's r-values for merged channels obtained using Fiji software. Zoomed-in insets are in 3x magnification. Scale bar = 10  $\mu$ m.

Corroborating BOK pro-apoptotic activity, relative caspase-3/7 activity was similarly increased for WT EGFP-BOK (79-fold) and EGFP-BOK<sup>BAK-TMD</sup> (70-fold) compared to EGFP control (set to 1), while EGFP-BOK<sup>BAX-TMD</sup> expression caused an even higher level of caspase activation (117-fold, Supplementary Figure S10A). Next, regulation of BOK TMD chimera activity by BCL-2 was investigated in DU145 cells co-transfected with plasmids for expression of EGFP, WT EGFP-BOK or EGFP-fused BOK TMD chimeras in combination with mC-BCL-2 or an empty vector control using flow cytometry (Annexin V-APC, Figure 31B). In line with findings in HEK293 cells, expression of WT EGFP-BOK led to an increase in Annexin V+ cells (12.3% Annexin V+ cells) compared to expression of EGFP alone (5.4% Annexin V+ cells). While EGFP-BOK<sup>BAX-TMD</sup> expression again caused significantly higher cell death compared to WT EGFP-BOK (20.0% Annexin V+ cells), EGFP-BOK<sup>BAK-TMD</sup>-induced cell death was similar to WT EGFP-BOK (10.3% Annexin V+ cells). Co-expression of mC-BCL-2 reduced cell death induction for both WT EGFP-BOK (5.7% Annexin V+ cells) and EGFP-BOK<sup>BAK-TMD</sup> (5.3% Annexin V+ cells) to control levels.

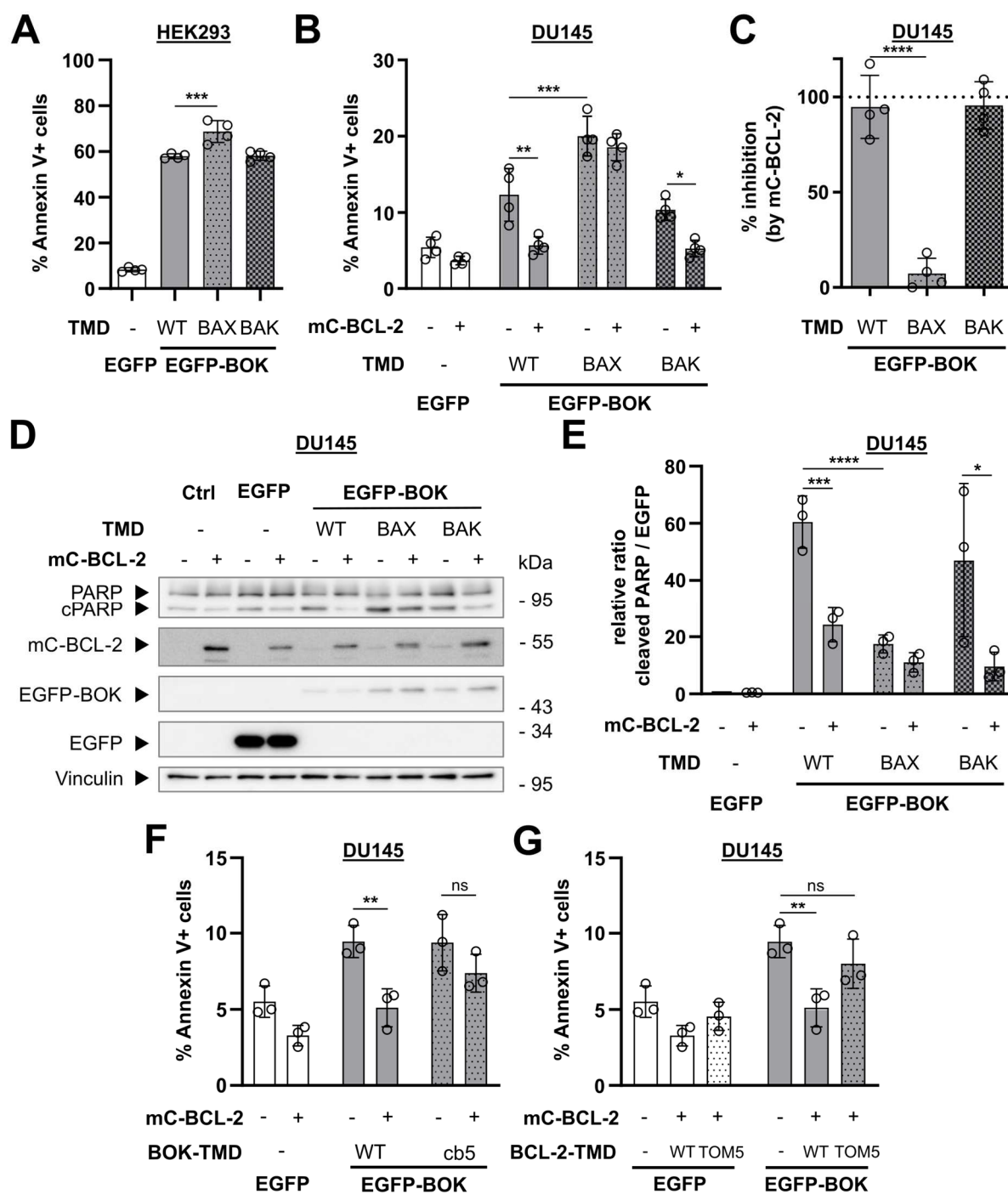
Intriguingly, cell death remained unchanged for co-expression of EGFP-BOK<sup>BAX-TMD</sup> and mC-BCL-2 (18.5% Annexin V<sup>+</sup> cells) compared to expression of EGFP-BOK<sup>BAX-TMD</sup> alone. Accordingly, calculated inhibition of BOK by BCL-2 (as for BAX, equation (1), 3.3.1) was negligible for EGFP-BOK<sup>BAX-TMD</sup> (7.3% inhibition, Figure 31C). On the other hand, for WT EGFP-BOK and EGFP-BOK<sup>BAK-TMD</sup> inhibition by mC-BCL-2 of 94.8% and 95.5% was obtained. Again, caspase-3/7 activity was detected in same samples to verify flow cytometry data (Supplementary Figure S10B). WT EGFP-BOK as well as BOK TMD chimera expression led to a detectable increase in caspase activity. Hereof, WT EGFP-BOK showed the highest increase of +32% caspase activity compared to the EGFP control (set to 0%). Expression of EGFP-BOK<sup>BAX-TMD</sup> and EGFP-BOK<sup>BAK-TMD</sup> increased caspase activity to a lesser extent (+20.8% and +13.8% respectively). In agreement with Annexin V positivity, change in caspase activity was effectively reversed by co-expression of mC-BCL-2 for WT EGFP-BOK (-17%) and EGFP-BOK<sup>BAK-TMD</sup> (-9.6%), whereas for EGFP-BOK<sup>BAX-TMD</sup> caspase activity was only negligibly reduced (+10.6%). Of note, analysing MCF-7 cells transfected to express WT EGFP-BOK or EGFP-fused BOK TMD chimeras in combination with mC-BCL-2 by cLSM, colocalisation of mC-BCL-2 with BOK was persistent for all BOK TMD chimeras (Supplementary Figure S10C).

To further validate protein expression and cell death induction in DU145 cells, samples used for flow cytometry in Figure 31B were analysed using Western Blot (Figure 31D). Interestingly, detection of EGFP-fused BOK TMD chimeras showed a higher expression level compared to WT EGFP-BOK. However, co-expression of mC-BCL-2 had only minor influence on BOK levels, which was confirmed by densitometric analysis (Supplementary Figure S10E). Also, mC-BCL-2 expression levels remained unchanged among samples analysed. cPARP levels were visibly elevated for expression of all BOK variants, while co-expression of mC-BCL-2 reduced cPARP band intensity only for WT EGFP-BOK and EGFP-BOK<sup>BAK-TMD</sup> resembling the same pattern for cell death as observed for Annexin V staining and caspase activity. Again, cell death induction (cPARP) with respect to BOK expression level (EGFP) in Figure 31D was assessed densitometrically (cPARP/EGFP ratio, Figure 31E). cPARP/EGFP ratio relative to EGFP control (set to 1) was found to be similarly increased for expression of WT EGFP-BOK (60-fold) and EGFP-BOK<sup>BAK-TMD</sup> (45-fold).

Co-expression of mC-BCL-2 substantially lowered cPARP/EGFP ratio for both EGFP-BOK (24-fold) and EGFP-BOK<sup>BAK-TMD</sup> (10-fold). For expression of EGFP-BOK<sup>BAX-TMD</sup>, however, relative cPARP/EGFP ratio was only increased by 17-fold compared to EGFP control and remained unchanged upon co-expression of mC-BCL-2 (11-fold) further underpinning the previous finding that cell death induced by EGFP-BOK<sup>BAX-TMD</sup> is not inhibited by BCL-2 co-expression.

To exclude that abrogated inhibition of BOK by BCL-2 is an isolated case for the TMD exchange in BOK<sup>BAX-TMD</sup>, additional TMD chimeras were applied in the next step. As shown for flow cytometric analysis of Annexin V staining in Figure 31F, DU145 cells transfected to express EGFP-BOK with the TMD of cb5 underwent cell death to a comparable extent (9.4% Annexin V+ cells) as for the transfection with WT EGFP-BOK (9.5% Annexin V cells). While co-expression of mC-BCL-2 reduced cell death induction for WT EGFP-BOK (5.1% Annexin V+ cells), no significant change in Annexin V positivity was obtained for EGFP-BOK<sup>cb5-TMD</sup> (7.4% Annexin V+ cells). In the same experiment, DU145 cells were also transfected to express EGFP-BOK in combination with a BCL-2 TMD chimera carrying the mitochondria-localised TOM5-TMD (Figure 31G). Co-expression of EGFP-BOK and mC-BCL-2<sup>TOM5-TMD</sup> led to an increase in cell death (8% Annexin V+ cells) compared to co-expression of EGFP-BOK with WT mC-BCL-2 (5.1% Annexin V+ cells) comparable to cell death induced by EGFP-BOK alone (9.5% Annexin V+ cells). Thus, results from additional TMD chimeras confirmed an influence of the TMD sequence on regulation of BOK-induced cell death by BCL-2.

Taken together, knockdown/knockout experiments in HEK293 cells revealed that BOK-induced cell death is enhanced upon downregulation of BCL-2. CytC release in MCF-7 cells after BOK overexpression can be blocked by co-expression of BCL-2. Also, cell death assessment in DU145 cells applying TMD chimeras of BOK but also BCL-2 showed that inhibition of BOK-induced cell death by BCL-2 is impaired after exchanging the TMD in BOK to BAX-TMD or cb5-TMD as well as exchanging the TMD in BCL-2 to TOM5-TMD thus suggesting BCL-2-mediated regulation of BOK-induced cell death to be dependent on the TMD sequence.



**Figure 31: BOK-induced apoptosis is inhibited by BCL-2 in a TMD-dependent manner.**

**A** – Flow cytometric analysis of HEK293 cells transfected to express EGFP-fused BOK TMD chimeras, wild-type (WT) or EGFP. Cells were harvested 18 h post transfection and stained with Annexin V-APC to detect dead cells (Annexin V+). Mean  $\pm$  sd from three independent experiments. **B** - Flow cytometric analysis of DU145 cells transfected as in A in combination with mCherry-BCL-2 (mC-BCL-2) or an empty vector control. Cells were harvested and analysed as in A. Mean  $\pm$  sd from three independent experiments. **C** – Percent inhibition of EGFP-BOK (TMD chimeras) by mC-BCL-2 as calculated from cell death data in B. Mean  $\pm$  sd from three independent experiments. **D** - Western Blot analysis of whole cell lysates from DU145 cells transfected as in B. Cells were harvested 18 h post transfection and (cleaved) PARP, EGFP(-BOK) and mC-BCL-2 levels were detected. Vinculin was used as loading control. Representative Blot from three independent experiments. **E** –Densitometric analysis of data shown in D showing cleaved PARP-to-EGFP ratio (cell death per EGFP expression). Mean  $\pm$  sd from three independent experiments is shown in relation to EGFP empty vector control. **F, G** - Flow cytometric analysis of DU145 cells transfected to express (F) EGFP-BOK<sup>cb5-TMD</sup>, WT or EGFP in combination with mC-BCL-2 or an empty vector control or (G) EGFP-BOK or EGFP in combination with mC-BCL-2, mC-BCL-2<sup>TOM5-TMD</sup> or an empty vector control. Cells were harvested 18 h post transfection and stained with Annexin V-APC to detect Annexin V+ cells. Mean  $\pm$  sd from three independent experiments.



### 3.3.6 BOK-TMD and BCL-2-TMD interact in molecular dynamics simulations

Since the interaction of BOK and BCL-2 via their TMDs was shown to play a functional role in apoptosis signalling (3.3.5), unravelling the molecular basis of this interaction was pursued next. In collaboration with Thomas Fellmeth and Kristyna Pluhackova from the Stuttgart Research Center Systems Biology, high-throughput multiscaling MD simulations were performed to study BOK-TMD and BCL-2-TMD interactions in a mimic of the ER membrane. In the following only the most prominent structures are discussed in more detail to not go beyond the scope of this thesis.

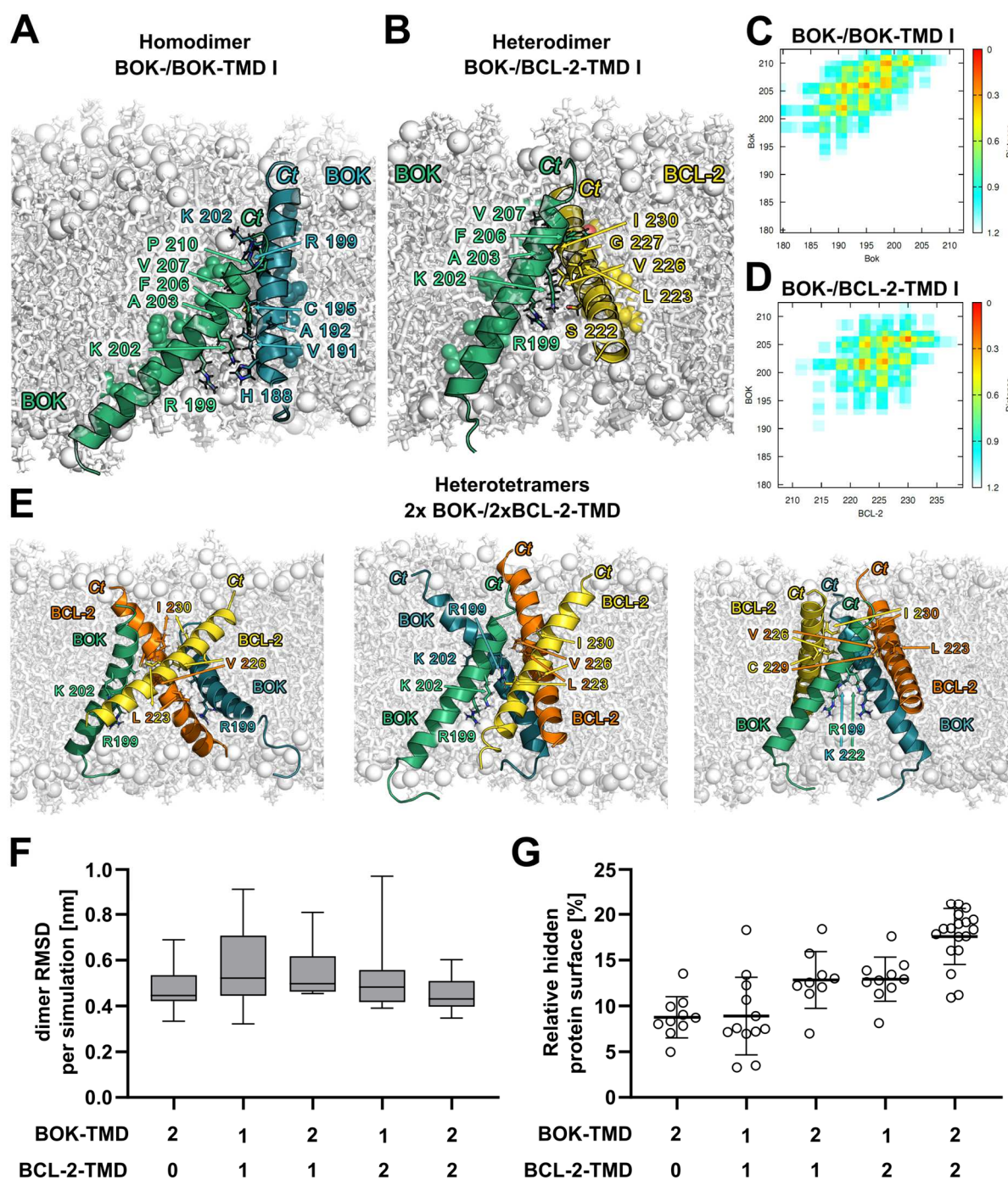
As a first step, modelling of BOK-/BOK-TMD homotypic interaction was recapitulated using two BOK TMDs (Figure 32A, B). Coarse-grained (CG) resolution simulation resulted in three main clusters of which the most prominent cluster (BOK/BOK-TMD I) occurred in 55% of all simulations (Figure 32A). For BOK/BOK-TMD I, most prominent interactions occurred between K202, A203, F206, V207, P210 (from one BOK-TMD) and H188, V191, A192, C195, R199 (from second BOK-TMD, Figure 32B). Conformation of BOK-TMDs was stable over the time of subsequent all-atom resolution simulations indicating specific interaction. Next, BOK-/BCL-2-TMD heterodimerisation was simulated at CG resolution and resulted in four main clusters of which the most prominent cluster (BOK-/BCL-2-TMD I) was formed in 44% of cases (Figure 32C). TMDs contacted each other most frequently at L201<sup>BOK</sup>, K202<sup>BOK</sup>, F205<sup>BOK</sup>, F206<sup>BOK</sup> and L223<sup>BCL-2</sup>, V226<sup>BCL-2</sup> or I230<sup>BCL-2</sup> (Figure 32D). However, simulations at all-atom resolution revealed that conformation was more flexible than for BOK-/BOK-TMD homodimers. Of note, for both BOK-/BOK-TMD homodimers and BOK-/BCL-2-TMD heterodimers snorkeling of positively charged AA residues (R199<sup>BOK</sup>, K202<sup>BOK</sup>, K212<sup>BCL-2</sup>) to lipid head groups was observed leading to local membrane indentation (Figure 32A, C).

Since obtained heterodimer structures displayed high conformational flexibility and several interacting residues, BOK and BCL-2 TMD interaction might preferentially take place in form of higher order oligomers (368). Therefore, simulations were performed comprising two BOK-TMDs and two BCL-2-TMDs. Indeed, CG simulations revealed the preferred formation of tetramers in 50% of simulations, while 36% led to trimer formation and only 7% to formation of hetero- or homodimers.

For tetramerization of BOK-TMDs and BCL-2-TMDs, the most prominent conformation was a slightly twisted, right-handed structure which occurred in 27% of tetramers. This shape allowed for interaction at multiple sites as shown in Figure 32E. Simulations at all-atom resolution confirmed that the twisted tetramers are the most favoured structure as it was formed in over 60% of cases and remained stable over the time of simulation. Trimers formed after CG simulations are split in 72% trimers consisting of one BOK-TMD and two BCL-2-TMDs and 28% trimers in which two BOK-TMD interact with one BCL-2-TMD. At all-atom resolution, formation of trimers albeit being compact in shape was similarly flexible as for heterodimers during 1  $\mu$ s of simulation (Supplementary Figure S11). Interestingly, quantifying peptide-lipid interactions between TMD peptides in the tetramers and lipids of the ER membrane mimic, negatively charged POPI was strongly enriched at both BOK-TMD and BCL-2-TMD compared to the expected frequency by proportion and random distribution (Supplementary Figure S11C). In contrast, MOPC was strongly depleted at both TMDs, while Cholesterol abundance was mediocly reduced.

Assessing stability of the obtained structures, for dimers, trimers and tetramers from all all-atom simulations, the RMSD (root mean square deviation) was calculated on a per dimer basis (Figure 32F). RMSD is a numerical measurement reflecting the change (deviation in distance) over time of the target structure compared to the reference structure at the beginning of the simulation. In line with the observations from the all-atom simulations, lowest RMSD (highest stability) was obtained for tetramers (median RMSD = 0.43 nm) followed by stable BOK-/BOK-TMD dimers (0.45 nm). High conformational flexibility observed for BOK-/BCL-2-TMD heterodimers and heterotrimers is reflected by the increased RMSD (heterodimer 0.52 nm, 2xBOK-/1xBCL-2-TMD trimer 0.50 nm, 1xBOK-/2xBCL-2-TMD trimer 0.48nm).

In addition to RMSD, SASA (solvent accessible surface area) was determined for obtained structures as a measure for hidden protein surface due to non-solvent interactions. As shown in Figure 32G, relative hidden protein surface was elevated with increasing structure complexity: homo- and heterodimers harboured approx. 9% of relative hidden protein surface, which increased to about 13% for trimeric structures. Most relative hidden protein surface (18%) was reached by tetramers reflecting the tightly packed conformation with multiple interaction sites.



**Figure 32: BOK-TMD and BCL-2-TMD form stable heterotetramers in an ER membrane mimic.**

**A** – Snapshot of BOK-/BOK-TMD I homodimer after 1  $\mu$ s all-atom resolution simulation in mimic of ER membrane. **B** - Snapshot of BOK-/BCL-2-TMD I heterodimer after 1  $\mu$ s all-atom resolution simulation in mimic of ER membrane. **C** – Contact map of BOK-/BOK-TMD I homodimer as shown in **A**. **D** – Contact map of BOK-/BCL-2-TMD I heterodimer as shown in **B**. **E** – Snapshots of 2xBOK-TMD/2xBCL-2-TMD heterotetramers after 1  $\mu$ s all-atom simulation in ER membrane mimic. Shown are representative, right-handed and stable tetramer structures of either altering heterotetramers with central BCL-2-TMD and BOK-TMD homodimers arranged symmetrically (left, right) or heterotetramers in which both BOK-TMDs are followed by BCL-2-TMDs (middle). **F** – Root mean square deviation (RMSD) per dimer and simulation from all-atom simulations relative to backmapped CG structure. Boxes represent IQR with median marked as a line. **G** – Solvent accessible surface area (SASA) plot shows the hidden protein surface relative to total peptide surface. Single dots indicate values from simulations in **F**. Mean  $\pm$  sd is indicated with a horizontal line. Ct = C-terminus. Experiments were performed and analysed by Thomas Fellmeth and Kristyna Pluhackova.

As an exemplary effort to evaluate the importance of an identified interaction site, K202 in BOK was picked for mutation to alanine *in vitro*, since it was not only a frequent contact site for homo- and heterodimers but also involved in membrane indentation by snorkeling to lipid head groups. However, analysis of subcellular localisation using cLSM as well as flowcytometric cell death analysis of BOK K202A did not reveal any differences in colocalisation with BCL-2 or cell death inhibition by BCL-2 compared to WT BOK (Supplementary Figure S12)

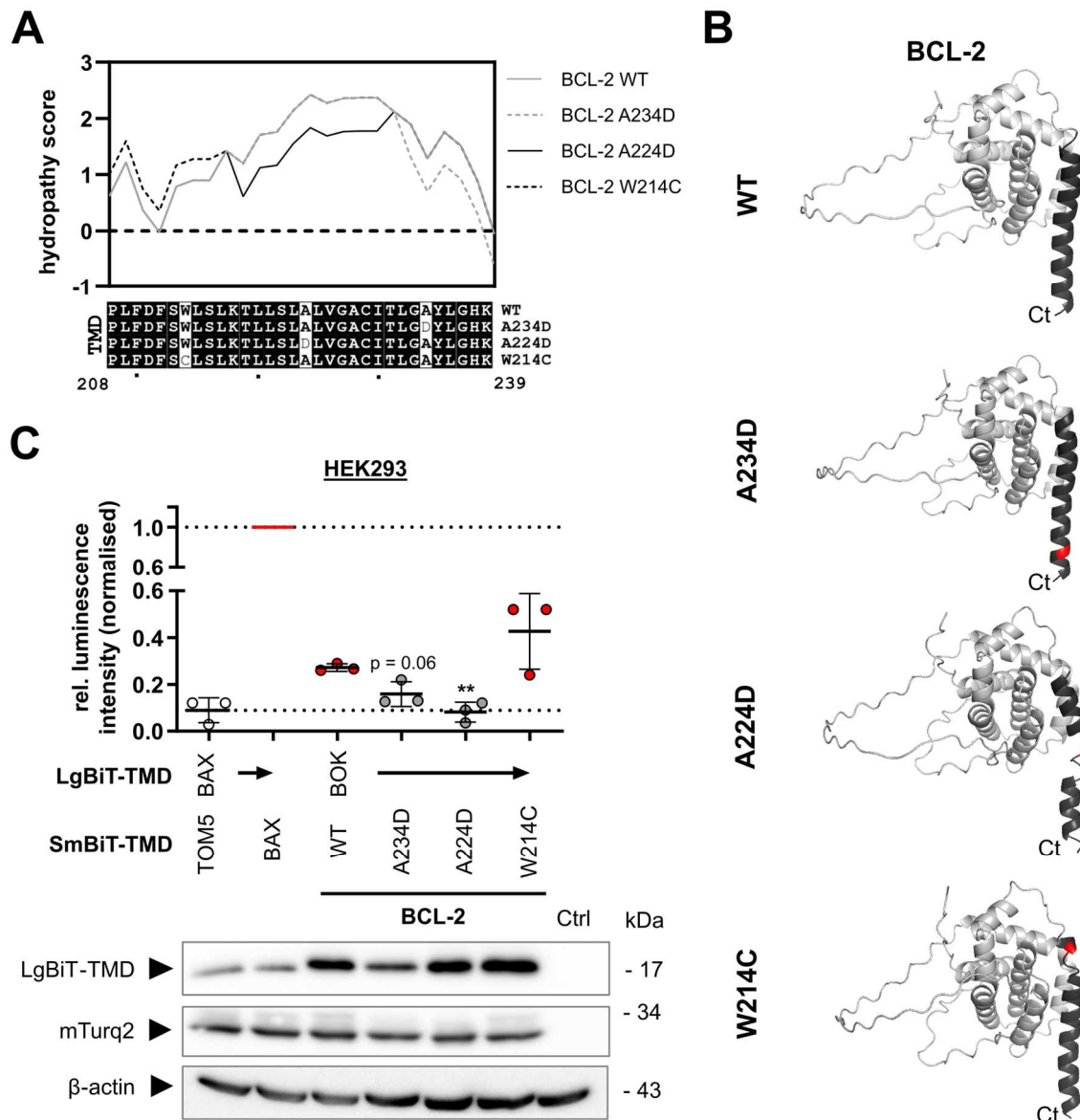
To sum up the findings from MD simulations exploring BOK-TMD and BCL-2-TMD interaction, simulations corroborated BOK-TMD and BCL-2-TMD interaction in an *in silico* ER membrane environment. Especially formation of heterotetramers out of two BOK-TMD and two BCL-2-TMD appeared to be stable indicating the tendency of BOK-TMD and BCL-2-TMD to prefer interaction in higher order oligomers. Hereby, interaction of TMDs with certain ER lipids was enriched (POPI) or depleted (MOPC). In addition, BOK-/BCL-2-TMD interaction was characterised by multiple interaction sites in dimers as well as trimers and tetramers. However, mutation of one of these interaction sites, K202 in BOK, *in vitro* did neither influence BOK's colocalisation with BCL-2 nor abrogate BCL-2's inhibitory capacity in BOK-induced cell death.

### 3.3.7 BCL-2 TMD mutation impairs its ability to counteract cell death induction

Previous results have shown a role of the TMD sequence for both BCL-2-mediated inhibition of BAX and BOK (3.3.1, 3.3.5). Hence, following experiments will focus on the functional basis of the BCL-2 TMD sequence for effector protein inhibition. Aiming to define the functional basis more precisely, mutation of the TMD and its impact on protein function, as it was already performed for BAX, was investigated for BCL-2.

In general, mutation of anti-apoptotic BCL-2 is a common feature of several cancer types underlining a vital influence of these mutations in oncogenesis and apoptotic dysregulation (369, 370). In COSMIC, numerous (> 20) mutations across different cancer entities can be found in the BCL-2 TMD. Three of these mutations covering the Ct, central and Nt part of the TMD respectively were picked to be analysed in more detail based on their drastic influence on amino acid size and charge: The BCL-2 TMD mutation A234D (COSMIC genome ID: COSV61376029) from ovary carcinoma, A224D (COSMIC genome ID: COSV61390472) from a liver neoplasm and W214C (COSMIC genome ID: COSV100384309) from a lung carcinoma patient.

As for BAX-TMD mutants in 3.3.2, BCL-2-TMD mutants were firstly analysed *in silico* regarding hydrophobicity and protein folding. Hydropathy scores according to Kyte and Doolittle (346) reflecting hydrophobicity were reduced for mutants A234D and A224D compared to the WT in large parts of the TMD sequence (position 231 – 239 and position 217 – 231 respectively, Figure 33A). In contrast, an increased hydropathy score compared to the WT was obtained for BCL-2 W214C from the Nt part of the TMD to position 217. Interestingly, the range of hydrophobicity changes did not overlap for the three mutations which highlights that the chosen mutations (and their functional impact) are representative for different TMD sections (Ct, central, Nt). Intriguingly, protein folding prediction using AlphaFold Colab (340) unveiled that the TMD  $\alpha$ 9-helix is disrupted for mutants BCL-2 A224D (position 222 - 227) and to a smaller extent for W214C (position 214 – 216, Figure 33B). BCL-2 A234D was predicted with an intact  $\alpha$ 9-helix similar to WT BCL-2. To analyse whether the introduced mutations have an influence on the interaction ability of BCL-2-TMD, possible alteration of the interaction with BOK-TMD was determined using the NanoBiT assay. For that, HEK293 cells were transfected to express LgBiT-BOK-TMD in combination with WT or mutant SmBiT-BCL-2-TMDs and cells were subjected to the NanoBiT assay as well as Western Blot analysis.

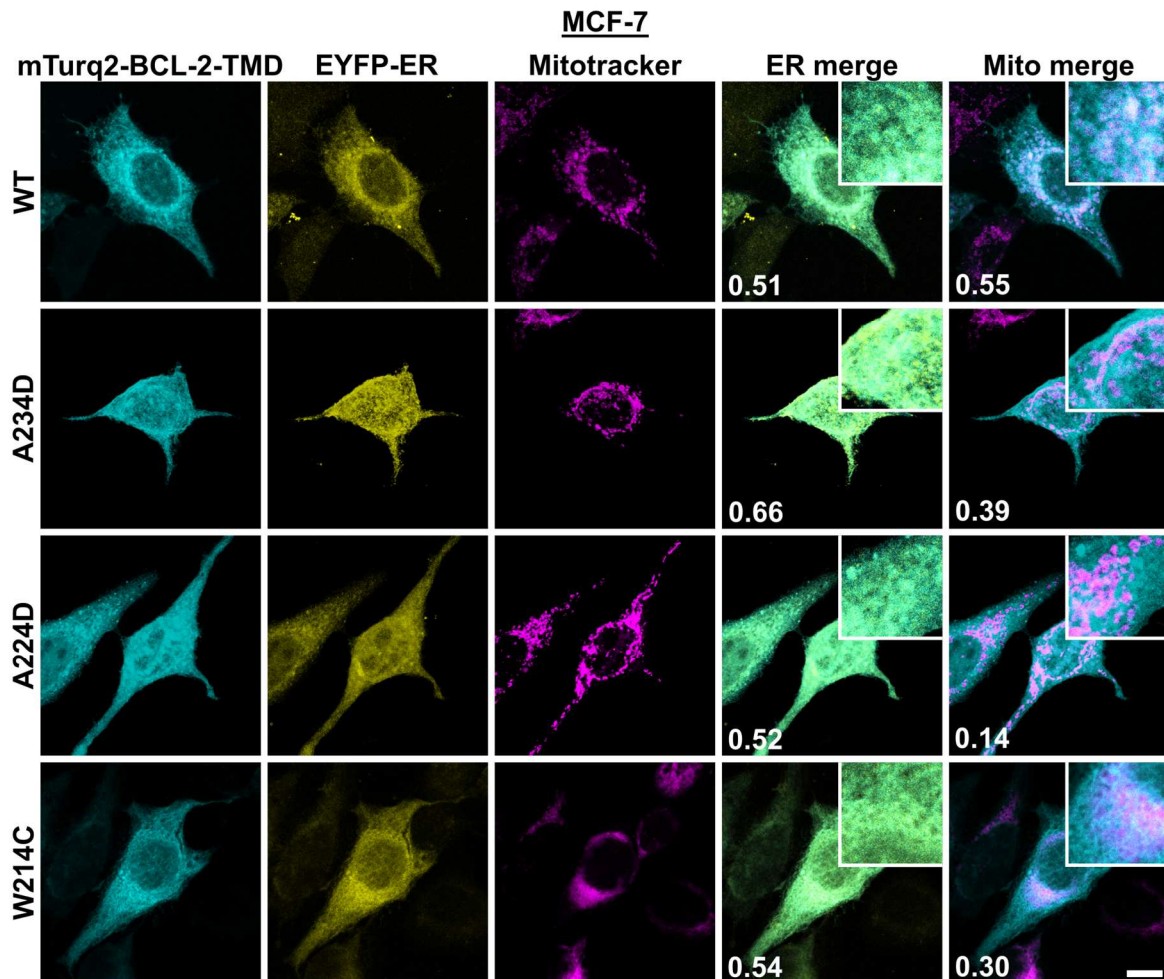


**Figure 33: Patient-derived BCL-2 TMD mutations abolish interaction with BOK-TMD.**

**A** – Hydropathy scores for indicated BCL-2 TMD sequences according to Kyte and Doolittle (Kyte and Doolittle 1982). **B** – AlphaFold prediction (340) of BCL-2 protein structure. TMD ( $\alpha$ 9-helix) in dark grey, Mutation site in red. Ct = C-terminus. **C** - NanoBiT interaction data from HEK293 cells co-transfected to express LgBiT-BOK-TMD in combination with indicated SmBiT-BCL-2-TMDs. Cells were harvested 24 post transfection and subjected to NanoBiT assay (top) and Western Blot (bottom). For the NanoBiT assay, fluorescence-normalised luminescence intensity is shown relative to positive control (BAX-/BAX-TMD). Mean  $\pm$  sd from three independent experiments. Mean of both negative control (BAX-/TOM5-TMD) and positive control are indicated with a dashed line. Asterisks indicate statistically significant differences compared to BOK-/BCL-2-TMD (WT). Construct expression was verified via Western Blot (bottom) using antibodies against LgBiT, mTurquoise2 (mTurq2) to indirectly detect SmBiT-TMDs and  $\beta$ -actin as loading control. Representative Blot from two independent experiments. WT = wild-type. Experiments were performed by Alexander Paul.

Interestingly, relative luminescence i.e. interaction of LgBiT-BOK-TMD and SmBiT-BCL-2-TMD (relative luminescence 0.27) was reduced for BCL-2-TMD mutations A234D (0.16) and A224D (0.08) to the level of the BAX-/TOM5-TMD negative control (0.09, Figure 33C upper panel). Combination of BOK-TMD and BCL-2-TMD W214C, however, resulted in similarly high if not higher relative luminescence (0.43) as for WT BCL-2-TMD. Western Blot analysis revealed homogeneous expression of SmBiT-BCL-2-TMDs according to indirect detection via mTurq2 (Figure 33C lower panel).

Subcellular localisation of TMD peptides was subsequently studied in MCF-7 cells expressing EYFP-ER marker. Cells were transfected to express mTurq2-fused BCL-2-TMDs, stained with Mitotracker red and fixed for cLSM analysis (Figure 34). Previously described localisation of WT BCL-2-TMD at the ER was not only confirmed ( $r_{\text{BCL-2-TMD+ER}} = 0.51$ ) but also not visibly altered by BCL-2 mutations ( $r_{\text{BCL-2-TMD A234D+ER}} = 0.66$ ,  $r_{\text{BCL-2-TMD A224D+ER}} = 0.52$ ,  $r_{\text{BCL-2-TMD W214C+ER}} = 0.54$ ). Unexpectedly, ER-like distribution of WT BCL-2-TMD correlated substantially better with Mitotracker signal compared to virtually no correlation with EYFP-Mito signal shown in Figure 16C ( $r_{\text{BCL-2-TMD+Mitotracker}} = 0.55$ ). However, colocalisation with Mitotracker was slightly reduced for BCL-2-TMD A234D ( $r_{\text{BCL-2-TMD A234D+Mitotracker}} = 0.39$ ) and BCL-2 W214C ( $r_{\text{BCL-2-TMD W214C+Mitotracker}} = 0.30$ ) compared to WT BCL-2-TMD. BCL-2-TMD A224D showed lowest colocalisation with Mitotracker ( $r_{\text{BCL-2-TMD A224D+Mitotracker}} = 0.14$ ) compared to all other BCL-2-TMD mutants. In addition, BCL-2-TMD A224D and A234D displayed a slightly more homogeneous distribution of signals, also within the nucleus, while BCL-2-TMD A224D peptides also formed bright subcellular clusters throughout the cells. After evaluation of peptide localisation, the impact of BCL-2 TMD mutation on full-length protein localisation was investigated in MCF-7 cells expressing EYFP-ER marker. For this purpose, cells were transfected with plasmids for expression of mC-BCL-2, subsequently fixed and analysed by cLSM (Figure 35). In line with expected ER localisation, mC-BCL-2 co-localised well with EYFP-ER signals ( $r_{\text{BCL-2+ER}} = 0.50$ ). Although mC-BCL-2 A234D and mC-BCL-2 W214C displayed a similar localisation, detected EYFP-ER colocalisation was lower than for WT mC-BCL-2 ( $r_{\text{BCL-2 A234D+ER}} = 0.21$ ,  $r_{\text{BCL-2 W214C+ER}} = 0.40$ ). Intriguingly, mC-BCL-2 A224D displayed a diffuse, presumably cytosolic as well as nuclear localisation.



**Figure 34: BCL-2 TMD mutation A224D affects TMD peptide localisation.**

cLSM images of MCF-7 cells expressing EYFP-ER marker and transfected to express indicated mTurquoise2-BCL-2-TMD fusion proteins. Cells were stained with Mitotracker red 24 h post transfection and subsequently fixed for imaging. Representative images from three independent experiments are maximum projections of z-stacks. Numbers are Pearson's r-value for merged channels obtained using Fiji software. Zoomed-in insets are in 3x magnification. Scale bar = 10  $\mu$ m. WT = wild-type. Experiments were performed by Alexander Paul.

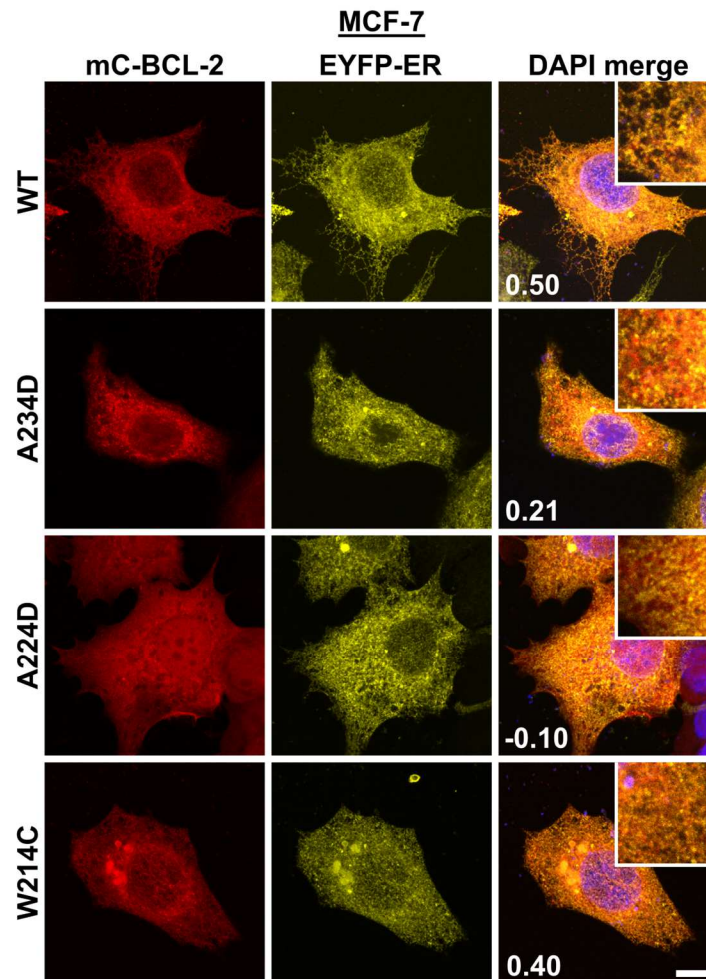
Moreover, same diffuse localisation of mC-BCL-2 A224D was observed in MCF-7 cells expressing EYFP-Mito (Supplementary Figure S13). In general, none of the analysed BCL-2 proteins colocalised well with Mitochondria ( $r_{\text{BCL-2+Mito}} = 0.18$ ,  $r_{\text{BCL-2 A234D+Mito}} = -0.13$ ,  $r_{\text{BCL-2 A224D+Mito}} = -0.23$ ,  $r_{\text{BCL-2 W214C+Mito}} = 0.09$ ).

Finally, the impact of the patient-derived BCL-2 TMD mutations on anti-apoptotic function of BCL-2 was evaluated in DU145 cells (with no expression of endogenous BCL-2). Cells were co-transfected with plasmids for expression of EGFP or EGFP-fused effectors (BAX, BAK and BOK) and mC-BCL-2 (mutants) or an empty vector control. After 18 h, cell death was analysed by Annexin V-APC staining and flow cytometry (Figure 36A).



Overexpression of EGFP-BAX and EGFP-BAK without BCL-2 co-expression expectedly induced cell death in 23% and 35% of EGFP-expressing DU145 cells (Annexin V<sup>+</sup> cells). Expression of EGFP-BOK alone, however, did not lead to significant induction of cell death compared to EGFP control in this setting (data not shown) and, hence, could not be used for evaluation of changes in anti-apoptotic capacity of BCL-2 TMD mutants. Of note, basal cell death after co-expression of EGFP with mC-BCL-2 (mutants) did also not differ from cell death induced by expression of EGFP alone (3% Annexin V<sup>+</sup> cells). Cell death induced by EGFP-BAX overexpression was notably reduced by co-expression of all mC-BCL-2 mutants. Co-expression of EGFP-BAX and WT mC-BCL-2 virtually abolished BAX-induced cell death to levels of the EGFP control (4% Annexin V<sup>+</sup> cells). Also for co-expression of EGFP-BAX with mC-BCL-2 A234D and mC-BCL-2 W214C, cell death was insignificantly higher than for co-expression with WT mC-BCL-2 (7% Annexin V<sup>+</sup> cells). For mC-BCL-2 A224D, however, a slightly higher increase in Annexin V positivity was detected for co-expression with EGFP-BAX compared to WT mC-BCL-2 (10% Annexin V<sup>+</sup> cells). Intriguingly, co-expression of mC-BCL-2 A224D with EGFP-BAK also revealed impaired cell death inhibition compared to WT mC-BCL-2 (24% Annexin V<sup>+</sup> cells) so that BAK-induced cell death was only slightly reduced in contrast to the strong inhibition by co-expression of WT mC-BCL-2 (7% Annexin V<sup>+</sup> cells). In addition, also co-expression of mC-BCL-2 A234D with EGFP-BAK yielding 13% Annexin V<sup>+</sup> cells slightly, but not significantly, increased cell death compared to co-expression of WT mC-BCL-2 with EGFP-BAK. Cell death induced by co-expression of mC-BCL-2 W214C with EGFP-BAK was comparable to cell death for co-expression of WT mC-BCL-2 with EGFP-BAK (10% Annexin V<sup>+</sup> cells).

In the next step, DU145 cells co-transfected to express EGFP-effectors and mC-BCL-2 mutants as in Figure 36A were subjected to Western Blot (Figure 36B). Across all samples expression of mC-BCL-2 mutants at the expected size of ~50 kDa differed notably with visibly higher expression level of mC-BCL-2 W214C compared to the other two mutants of which mC-BCL-2 A224D showed the lowest expression level. Expression level of EGFP-BAX was comparable between samples, but slightly increased in samples with mC-BCL-2 overexpression except for co-expression with mC-BCL-2 A224D. Moreover, expression level of EGFP-BAK was slightly increased for co-expression with mC-BCL-2 (mutants) – most noticeable for co-expression with WT mC-BCL-2.



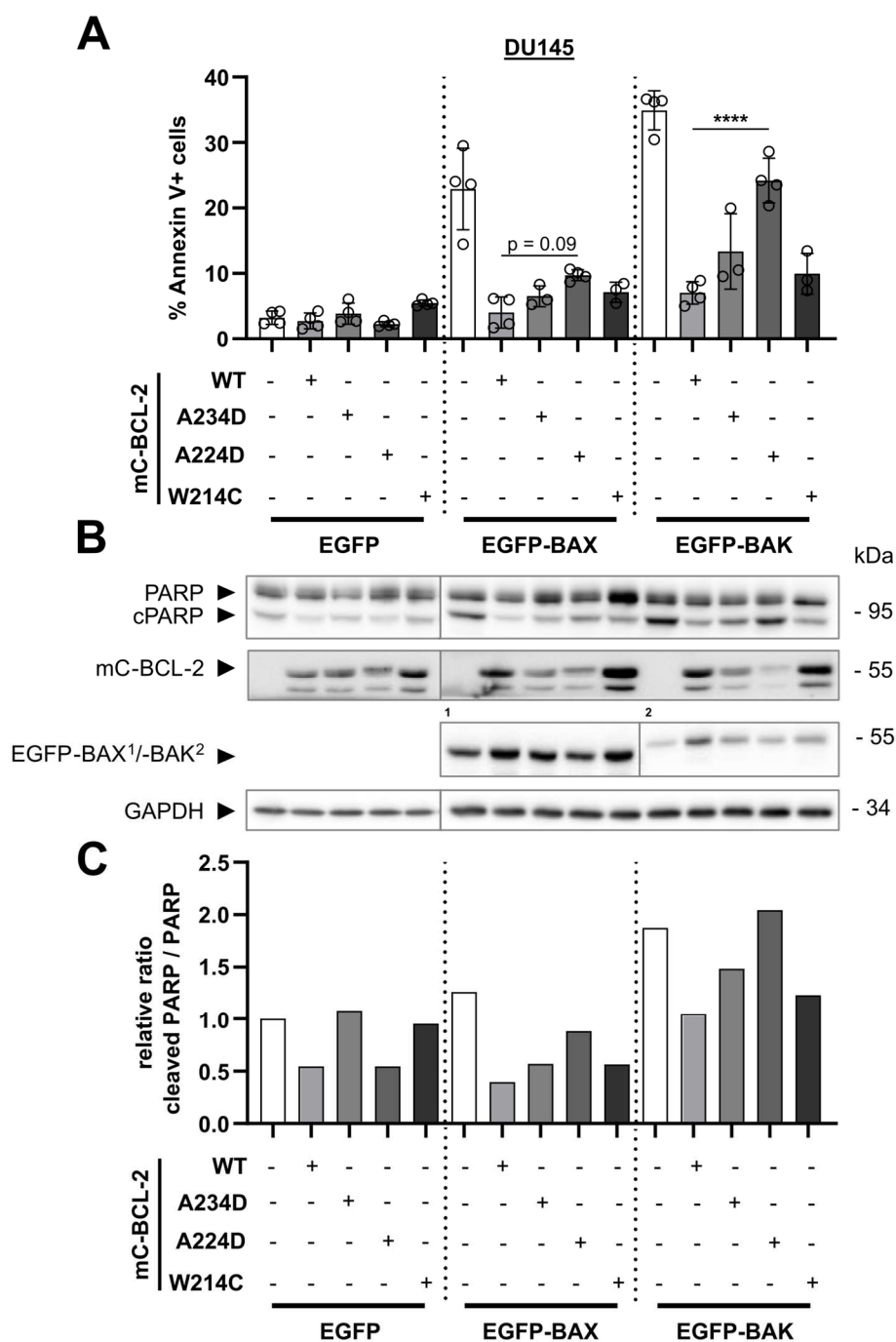
**Figure 35: BCL-2 TMD mutation A224D leads to diffuse localisation of full-length BCL-2.**

cLSM images of MCF-7 cells expressing EYFP-ER and transfected to express mCherry-BCL-2 (mC-BCL-2) wild-type (WT) or mutants. Cells were fixed for imaging 24 h post transfection. DAPI-containing mounting medium was used to stain nuclei. Representative images from three independent experiments are maximum projections of z-stacks. Numbers are Pearson's r-values for merged channels obtained using Fiji software. Zoomed-in insets are in 3x magnification. Scale bar = 10  $\mu\text{m}$ . Experiments were performed by Alexander Paul.

Detection of cPARP generally resembled cell death data from flow cytometry. However, cPARP/PARP ratio (Figure 36C) was reduced by half for co-expression of WT mC-BCL-2 or mC-BCL-2 A224D with EGFP (0.54-fold) compared to expression of EGFP alone (set to 1.00), while the ratio was constant for co-expression of mC-BCL-2 A234D (1.08-fold) and mC-BCL-2 W214C (0.95-fold) with EGFP. Overexpression of EGFP-BAX or EGFP-BAK alone resulted in a relative cPARP/PARP ratio increased by 1.26-fold for BAX and 1.87-fold for BAK compared to expression of EGFP alone in line with previously detected cell death induction,

Congruent to flow cytometry data, co-expression of WT mC-BCL-2 effectively reduced cPARP/PARP ratio to 0.40-fold for EGFP-BAX and to 1.05-fold for EGFP-BAK. Additionally, co-expression of EGFP-BAX or EGFP-BAK with mC-BCL-2 A234D or mC-BCL-2 W214C reduced cPARP/PARP ratio likewise, however, to a slightly lesser extent than the respective samples with WT mC-BCL-2. For mC-BCL-2 A224D, cPARP/PARP ratio was less reduced for co-expression with EGFP-BAX than for other mC-BCL-2 mutants (0.88-fold) and even increased for co-expression with EGFP-BAK compared to expression of EGFP-BAK alone (2.04-fold).

In sum, investigations of patient-derived TMD mutations in anti-apoptotic BCL-2 showed increased hydrophobicity of mutant TMD W214C compared to WT in contrast to more hydrophilic TMDs of the A234D and A224D mutant. In addition, TMD  $\alpha$ 9-helices of both W214C and A224D are disrupted according to folding prediction via AlphaFold Colab. Interaction studies using the NanoBiT assay revealed abolished interaction of BCL-2-TMD with BOK-TMD for both aspartate-carrying mutants (A234D, A224D), despite of minor visible changes in subcellular localisation of TMD peptides. Full-length mC-BCL-2 A224D, however, exhibited a diffuse subcellular localisation in contrast to the ER-like localisation of WT mC-BCL-2. Assessing the functionality of the mutated proteins, again mC-BCL-2 A224D was distinguished by its inability to counteract BAK-induced cell death as well as an impaired reduction of BAX-induced cell death. Both other mutants, BCL-2 A234D and W214C, however, remained comparably functional as WT BCL-2 regarding anti-apoptotic activity.



**Figure 36: BCL-2 TMD mutation A224D interferes with BCL-2 anti-apoptotic function.**

**A** – Flow cytometric analysis of DU145 cells transfected with to express mCherry-BCL-2 (mC-BCL-2) or an empty vector control in combination with EGFP, EGFP-BAX or EGFP-BAK respectively. Cells were harvested 18 h post transfection and stained with Annexin V-APC to detect dead cells (Annexin V+). Mean  $\pm$  sd from three or four independent experiments. **B** – DU145 cells transfected as in A were subjected to Western Blot 18 h post transfection. Whole cell lysates were analysed using antibodies against (cleaved) PARP to detect cell death and BCL-2 as well as EGFP to verify protein expression. GAPDH was used as a loading control. Blot from one independent experiment. **C** – Densitometric analysis of PARP band intensities out of B showing cleaved PARP-to-PARP ratio (cell death). Ratios from one independent are shown in relation to EGFP empty vector control. WT = wild-type. Experiments were performed together with (A) or by (B,C) Alexander Paul.

### 3.3.8 BOK-dependent ER stress response is modulated by the presence of BCL-2

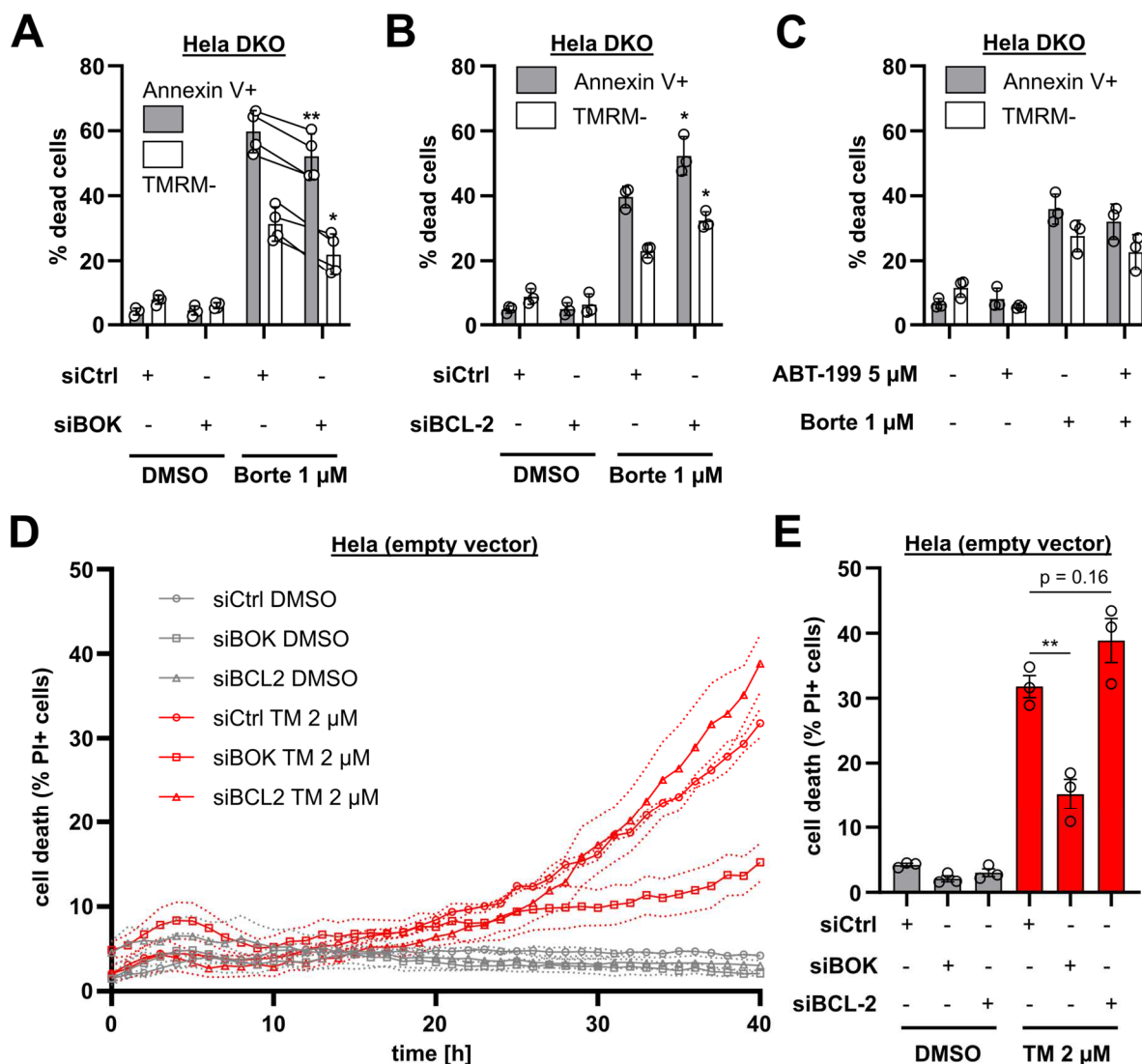
In the final chapter of this section, the interaction of BOK and BCL-2 via the TMDs was examined in the physiological context of the ER-stress response. Both BOK and BCL-2 were postulated to regulate ER stress at the level of calcium signalling at the ER or MAMs (167, 174). While BOK is thought to mediate ER stress-induced cell death, BCL-2 was shown to abrogate  $\text{Ca}^{2+}$ -dependent cell death. To investigate a possible interplay of BOK and BCL-2 in ER stress signalling, the FDA-approved drug Bortezomib (Velcade) was applied. Bortezomib is a potent proteasome inhibitor which induces ER stress indirectly through accumulation of proteins destined for proteasomal degradation promoting the unfolded protein response (UPR) (371, 372). Also, to get a more isolated view on BOK's pro-apoptotic activity, HeLa cells with genetic deletion of BAX and BAK (HeLa DKO) were used (Supplementary Figure S1B).

Analysing the role of BOK in Bortezomib-dependent cell death, HeLa DKO cells were transfected with siRNA targeting the *BOK* gene (siBOK) or control siRNA (siCtrl). Afterwards, cells were incubated with 1  $\mu\text{M}$  Bortezomib. Of note, 1  $\mu\text{M}$  Bortezomib was previously determined to induce noticeable amounts of cell death in HeLa DKO cells after 48 h rather than 24 h (Supplementary Figure S14A, Supplementary Figure S14B). Thus, cell death was analysed after 48 h simultaneously as phosphatidylserine exposure via Annexin V-APC (Annexin V+ cells) and as loss of mitochondrial membrane potential ( $\Delta\Psi_m$ ) via TMRM staining (TMRM- cells) using flow cytometry. For siCtrl transfection, Bortezomib caused an approx. 15-fold (59.8 % Annexin V+ cells) and 4-fold (31.3% TMRM- cells) increase in phosphatidylserine exposure and loss of  $\Delta\Psi_m$  respectively compared to DMSO control (Figure 37A). Interestingly, knockdown of BOK in combination with Bortezomib reduced cell death in all samples compared to siCtrl despite high inter-sample heterogeneity (52.1% Annexin V+, 21.9% TMRM- cells). For DMSO control, cell death after siBOK (4.4% Annexin V+, 5.9% TMRM- cells) remained similar to siCtrl (4.1% Annexin V+, 7.8% TMRM- cells). Next, involvement of BCL-2 was assessed likewise by siRNA-mediated knockdown of BCL-2 (siBCL-2) followed by Bortezomib incubation and flow cytometry. As shown in Figure 37B, cell death of HeLa DKO cells incubated with Bortezomib for 48 h was significantly increased for siBCL-2 (52% Annexin V+, 32.4% TMRM- cells) compared to siCtrl (40% Annexin V+, 23.0% TMRM- cells). Moreover, DMSO control did not yield any differences for siBCL-2 (5% Annexin V+, 8% TMRM- cells) and siCtrl (5% Annexin V+, 6% TMRM- cells).

Of note, an ER stress response in Hela DKO cells caused by Bortezomib was verified by Western Blot detection of phosphorylated c-Jun N-Terminal kinase (pJNK1) and expression of C/EBP homologous protein (CHOP) as ER stress markers. Moreover, BCL-2 expression level remained unchanged, while BOK expression level was slightly decreased after 48 h Bortezomib incubation (Supplementary Figure S14D).

To challenge if the cell death inhibitory effect of BCL-2 upon Bortezomib incubation is mediated by the classically involved BH3:groove interaction, the specific BCL-2 inhibitor ABT-199 (Venetoclax) was applied which effectively and specifically binds the groove of BCL-2 and blocks its interaction ability (244). Hence, Hela DKO cells were either incubated with ABT-199 or Bortezomib alone or in combination followed by flow cytometric cell death analysis (Figure 37C). After 48 h, incubation with 5  $\mu$ M ABT-199 alone resulted in similar Annexin V positivity as for DMSO control (8% Annexin V+ cells), while TMRM levels were slightly reduced (5.5% TMRM- cells) compared to DMSO control (11.3% TMRM- cells). In line with previous findings, incubation with Bortezomib alone visibly increased cell death induction (36% Annexin V+, 28% TMRM- cells). Strikingly, concomitant incubation with ABT-199 and Bortezomib resulted in comparable cell death as for incubation with Bortezomib alone (32% Annexin V+, 23% TMRM- cells).

As a second ER stress-inducing drug, Tunicamycin (TM), an inhibitor of N-linked glycosylation resulting in UPR and ER stress (reviewed in (373)), was applied. However, incubation with 2  $\mu$ M TM for 48 h in Hela DKO cells revealed only moderate cell death induction (14% Annexin V+, 19% TMRM- cells) compared to DMSO-incubated cells (8% Annexin V+, 9% TMRM- cells, Supplementary Figure S14C). Even at 10  $\mu$ M TM for 48 h, cell death did not exceed 22% Annexin V+ cells. Therefore, Hela (empty vector) cells which underwent the identical knockout procedure as Hela DKO cells with an empty vector were used instead, since incubation with 2  $\mu$ M TM killed approx. 50 % of cells (50% Annexin V+, 34% TMRM- cells) enabling the detection of possible cell death differences in subsequent experiments.



**Figure 37: BCL-2 reduces ER stress-induced cell death mediated by BOK.**

**A, B** – Flow cytometric analysis of HeLa  $BAX^{-/-}/BAK^{-/-}$  (DKO) cells transfected with siRNA targeting (A) BOK (siBOK) or (B) BCL-2 (siBCL-2) or control siRNA (siCtrl). After 24 h, cells were incubated with 1  $\mu$ M Bortezomib (Borte) or DMSO for another 48 h. Then, cells were stained with TMRM and Annexin V-APC to detect dead cells. Percentage of Annexin V+/TMRM- cells is shown as mean  $\pm$  sd from four (A) or three (B) independent experiments. Statistical significance of differences is shown in comparison to siCtrl + Borte. In A, statistical significance was tested using a paired t-test with paired samples indicated with horizontal connection lines. **C** – Flow cytometric analysis of HeLa DKO cells incubated with 5  $\mu$ M ABT-199, 1  $\mu$ M Bortezomib or both for 48 h. DMSO was used as control. Cells were stained with TMRM and Annexin V-APC to detect dead cells. Percentage of Annexin V+/TMRM- cells is shown as mean  $\pm$  sd from three independent experiments. **D** – Time-lapse imaging to assess cell death in HeLa (empty vector) cells transfected with siRNA targeting BOK (siBOK), BCL-2 (siBCL-2) or control siRNA (siCtrl). After 24 h, Cells were incubated with 2  $\mu$ M Tunicamycin (TM) or DMSO and 0.67  $\mu$ g/ml Propidium Iodide (PI). Cells were imaged every hour for 40 h. PI positive (PI+) area (reflecting cell death) was set in relation to PI+ area after digitonin-mediated permeabilization (= 100% cell death) and is shown as % PI+ cells. Symbols reflect means of triplicates from one independent experiment. Dashed lines indicate SEM. **E** – Cell death data from time-lapse imaging in D plotted for t = 40 h.

With the aim to evaluate the role of BOK and BCL-2 and their possible interplay in TM-induced ER stress, HeLa (empty vector) cells were subjected to siRNA-mediated knockdown of BOK or BCL-2. Non-targeting siRNA was used as control (siCtrl). Afterwards, cells were incubated with DMSO or 2  $\mu$ M TM and Propidium Iodide (PI) to stain dead cells followed by Incucyte time-lapse imaging (Figure 37D). Percentage of PI positive (PI+) cells hardly reached 10% for all samples in the first 20 h of imaging. However, after approximately 20 h, cell death in TM-incubated samples began to differ from DMSO control samples. Cell death in DMSO control samples regardless of transfected siRNA stayed below 5% PI+ cells until the end of the imaging period. In TM-incubated cells, however, cell death continuously climbed until final imaging at  $t = 40$  h. Intriguingly, cell death in TM-incubated cells transfected with siBOK increased more slowly compared to siBCL-2 and siCtrl. In fact, at  $t = 30$  h cell death for siBOK was notably lower than other TM-incubated samples and this gap increased steadily until the end of the experiment. Moreover, for PI positivity of siBCL-2-transfected cells a clear tendency to surpass cell death marks from siCtrl occurred at approx.  $t = 34$  h and was henceforth continuously observed until  $t = 40$  h. Therefore, at the final time point of  $t = 40$  h TM-induced cell death in combination with siBOK transfection was substantially decreased (15% PI+ cells) compared to siCtrl transfection (32% PI+ cells, Figure 37E). Also in representative images shown in Supplementary Figure S14E decreased number of PI+ cells is clearly visible by the naked eye. Furthermore, the observed tendency of increased PI positivity in TM-incubated samples with knockdown of BCL-2 compared to control siRNA resulted in 39% PI+ cells after 40 h. However, sample-to-sample variations were too high to result in a significant difference to cell death in siCtrl samples.

Altogether, it could be shown that, on the one hand, presence of BOK promotes and, on the other hand, presence of BCL-2 reduced cell death in HeLa DKO cells caused by Bortezomib incubation which verifiably led to an ER stress response. Interestingly, BCL-2's anti-apoptotic function in Bortezomib-induced cell death was not dictated by its ability to interact via the BH3:groove interaction. Finally, TM-induced cell death was largely dependent on BOK expression in HeLa (empty vector) cells indicating a key role of BOK to mediate TM-dependent cell death. Knockdown of BCL-2, however, noticeably, but not significantly, increased cell death in TM-incubated HeLa (empty vector) cells.



## 4 Discussion

The research on Bcl-2 protein interaction has reached new heights in the recent years. Over the course of more than three decades intensive studies led from the discovery of BCL-2 as an important oncogene to the structural illumination of BH3 motif-mediated inhibition. In 2016, these scientific efforts culminated in the clinical approval of a specific inhibitor for BCL-2, Venetoclax, as an anti-cancer agent (253) highlighting that i) interactions of Bcl-2 proteins are critical targets for cancer therapy and ii) profound understanding of these interactions is imperative for their successful exploitation.

Intriguingly, Venetoclax was the first-ever drug approved for clinical use which directly targets components of the apoptosis pathway underlining the spearheading role of anti-cancer drugs which specifically target the Bcl-2 interaction network. Also, numerous clinical trials and promising pre-clinical results herald the great potential of Venetoclax and other BH3 mimetic drugs (reviewed in (374)). Next to evaluation of specific BCL-XL and MCL-1 inhibitors, a promising new approach is the combination of BH3 mimetics with other drugs sensitizing cancer cells to apoptosis such as BET or kinase inhibitors (256–258). On the other hand, recent advances indicate that BH3 mimetics can have unintentional additional implications in cells independent of their original purpose to specifically inhibit anti-apoptotic Bcl-2 proteins. For example, Venetoclax reportedly activated the integrated stress response and caused metabolic reprogramming due to inhibition of mitochondrial respiration (375, 376). These unexpected off-target functions further underline that much more studies are necessary to fully understand and be able to harness the potential of BH3 mimetics.

Nevertheless, finding efficient and tolerable treatments remains challenging: anti-apoptotic adaptation of tumours is highly individual so that few cancer entities are homogeneously dependent on the same anti-apoptotic Bcl-2 proteins such as individual addiction of lymphomas to BCL-XL, MCL-1 or BCL-2 (246, 377, 378). In addition, expression of many Bcl-2 proteins undergoes highly dynamic changes throughout development, cell differentiation or in response to treatment (379–381). Moreover, tissue-specific epigenetic regulation of BCL-2 and MCL-1 by BAP1 described by He *et al.* adds another facet to the highly dynamic expression of Bcl-2 proteins (382). Another recent study which postulates that BH3-only protein BID can function as a MOMP-inducer independent of BAX and BAK further stresses a more detailed and individual investigation of family members (383).

Concludingly, our understanding of the Bcl-2 interaction network still undergoes a highly dynamic development. There is furthermore a pressing need to resolve the persisting inconsistencies and unravel the elusive molecular details on how the Bcl-2 interaction network is fine-tuned. A growing body of evidence supports a functional relevance of Bcl-2 TMD interactions for regulation of apoptosis signalling in addition to the BH3-mimetic-targeted BH3:groove interaction interface (171, 291, 333). However, the bigger picture of the Bcl-2 TMD interactome largely remains in the dark.

This thesis, therefore, aims to shed light on the composition of the Bcl-2 TMD interactome and deepen the understanding how TMD interactions fine-tune cell death decisions.

Starting with the development, optimisation and validation of a plasmid-based bimolecular split luciferase assay, the TMD interactome of BH multi-domain proteins was systematically analysed. Enlightening the subcellular localisation of these interactions, cellular distribution of fluorophore-conjugated TMDs was investigated by cLSM. To assess functional implications of the revealed TMD interactions, the impact of TMD exchange and mutation on apoptosis induced by effector protein overexpression was investigated with focus on BAX, BAK and BOK. Finally, the role of the newly identified interaction between the TMDs of BOK and BCL-2 in the regulation of apoptosis was further dissected by use of chimeric proteins with exchanged TMDs, MD simulations and by studying the role of BCL-2 in the background of BOK-mediated ER stress.

## 4.1 Harnessing NanoBiT for the detection of TMD interactions

### 4.1.1 NanoBiT assay parameters and fluorescence normalisation

As suitable substrate for the NanoBiT luciferase, coelenterazine-h was selected and the detection time point set to  $t = 30$  min after substrate addition with a measurement duration of 1 s/well (Figure 8, Table 25, Supplementary Figure S2).

Expectedly, all analysed NanoBiT substrates (Vivazine, Endurazine and Coelenterazine-h) produced detectable luminescence signals for the control assay used in Figure 8 since they are all structurally related to the NanoLuc substrate Furimazine. The selected Coelenterazine-h is a synthetic derivate of the native form with improved efficiency of substrate availability (384). The high initial but slowly declining luminescence detected for Coelenterazine-h, thus, indicates the increased bioavailability leading to an accelerated turn-over and loss of signal in comparison to 'caged' Vivazine and Endurazine which first need to be hydrolysed by cellular esterases (363). Of note, final concentrations of Vivazine and Endurazine are unknown since substrate concentrations are not specified by the manufacturer (used as 1x solution). Coelenterazine-h 1x concentration of 5  $\mu$ M was selected from reviewed literature (385). Hence, repetition of the assay with adjusted concentrations would likely produce different results since higher/lower substrate concentrations increase/decrease NanoBiT luminescence (Supplementary Figure S2B). The detection time point of  $t = 30$  min was selected since changes in signal intensity were higher at earlier time points (Figure 8A). Also, a detection after 30 min ensures a still sufficiently high signal-to-noise ratio and unjeopardized viability of analysed cells. The integration time of 1 s/well is in accordance with the manufacturer's recommendation of 0.25 – 2 s/well for NanoBiT assays (NanoGlo live cell assay system protocol, Promega, Madison, WI, USA). In sum, adjusting these parameters is expected to generate visible but negligible differences in the subsequent luminescence acquisition.

Next, expression plasmids had been designed to simultaneously express LgBiT-/SmBiT-TMDs and a fluorescent protein (mCitr/mTurq2) with the purpose to use fluorescence as a marker for transfection efficiency and to normalize luminescence signal. Plasmid functionality was confirmed by cLSM and flow cytometry as mCitr/mTurq2 were specifically expressed from plasmids for LgBiT-/SmBiT-TMD expression respectively (Figure 9B-D). Simultaneous, but separate, expression of fluorophore and NanoBiT-TMD from the same plasmid was ensured by introduction of

a self-cleaving T2A sequence (Figure 9A). The diffuse cytosolic distribution of fluorescence signal in Figure 9B confirms separate expression of fluorophores from membrane-bound NanoBiT-TMDs i.e. functionality of the T2A sequence causing ribosome skipping before the Ct proline of the T2A peptide. However, it is possible that in rare cases translation of the subsequent NanoBiT-TMD is skipped or ribosome skipping is unsuccessful producing a fluorophore-NanoBiT-TMD fusion protein (386).

Ribosome skipping mistakes are expected to occur at the same rate for different plasmids since the T2A sequence is identical in all plasmids used. Thus, ribosome skipping mistakes will not affect data normalisation. To be able to directly compare the absolute number of fluorophores per cell with that of NanoBiT-TMDs, a more specialized methodology like quantitative western blots or mass spectroscopy-based proteomics would be necessary. Flow cytometry revealed that transfection efficiency (approx. 30% fluorescent cells) was comparable among plasmids analysed (Figure 9C). However, the flow cytometry data indicate bleed-through of mTurq2 signal into the mCitr detection channel visible as an alleged increase of mCitr fluorescence in mTurq2-expressing cells (Figure 9C, Figure 9D). Since flow cytometry was only used for verification of fluorophore expression, the observed bleed-through did not have significance in the subsequent interaction assay in which a multimode plate reader was used for fluorescence acquisition. Here, no crosstalk was observed (Figure 10B).

Co-transfection with equal amounts of plasmids for LgBiT-TMD and SmBiT-TMD expression resulted in similar fluorescence intensities and expression of either fluorophore (Figure 9 B, C, D). Therefore, normalisation of luminescence data over either fluorophore is comparable as confirmed in Figure 9E. Plasmid DNA is mixed in a ratio of 1:1 before liposome packaging leading to a highly correlated amount of plasmid per liposome. Although the amount of total DNA per cell can vary substantially, the fraction of different plasmids per cell is expected to be identical given the encoded proteins are expressed with the same efficiency (387). Normalisation via mTurq2 and mCitr fluorescence yielded qualitatively identical results (Figure 9E) so that normalisation via solely mTurq2 fluorescence was assumed to be sufficient. Supplementary Figure S2D and Figure 9E also demonstrate, however, that there are subtle variations in the relative fluorescence of mTurq2 and mCitr across a panel of samples. This can most likely be attributed to workflow-dependent technical variations, for example, in plasmid concentrations, quality of plasmid preparations (e.g. influenced by number of freeze-thaw cycles) or plasmid handling during transfection.

Hence, it can't be ruled out that normalisation over mCitr instead of mTurq2 can produce minor inconsistencies with the current interaction data. However, as demonstrated by Figure 9E these variations are assumed to be qualitatively negligible over several repetitions.

#### 4.1.2 NanoBiT assay validation

After design of the NanoBiT assay, fluorescence and luminescence acquisition was analysed with appropriate controls to validate assay functionality and specificity (Figure 10). The similar luminescence of technical controls with either untransfected cells or cells transfected with a single plasmid encoding LgBiT-BAX-TMD or SmBiT-BAX-TMD indicates, that absence of one NanoBiT subunit completely abolishes its enzymatic activity (Figure 10C). More importantly, it was critical that also the functional negative control (BAX-/TOM5-TMD) yielded a near background luminescence signal. TOM5 is associated with the high-molecular TOM complex as part of the translocase machinery for mitochondrial import and belongs to the group of tail-anchored proteins (280, 365). Although Bcl-2 proteins such as BAX and BAK are known to interact with unrelated MOM-residing protein complexes such as VDAC2 (323, 338), no evidence indicates BAX interaction with the TOM complex. The here acquired luminescence data also attest that TOM5-TMD is not interacting with BAX-TMD and, thus, is a suitable candidate for a functional negative control. In light of the tremendous increase in luminescence (~80-fold) for combination of LgBiT-BAX-TMD with SmBiT-BAX-TMD (BAX-/BAX-TMD) compared to untransfected cells, homotypic interaction of BAX-TMD as found in literature (171, 332) was successfully confirmed and is a specific functional positive control for the NanoBiT assay. Although these controls were deemed sufficient to attest the validity of the NanoBiT assay, additional controls could be added to further support its functionality. For example, next to MOM-specific TOM5-TMD also negative controls for each other subcellular compartment might be worth establishing such as ER-targeted cb5-TMD as a possible control for the ER membrane (279).

Western Blot analysis of LgBiT-TMD and mTurq2 (as a surrogate marker for SmBiT-TMD) expression confirmed specific expression of proteins with expected molecular weight (Figure 10C). The expression level of mTurq2 assumingly reflects expression level of SmBiT-TMDs due to identical expression based on the T2A sequence as discussed in 4.1.1.

However, it has to be kept in mind that the expression level of SmBiT-TMDs might differ from detected mTurq2 expression level, for example, by TMD-specific differences in expression efficiency or degradation. Hence, these factors might be worth exploring, for example, looking at stability of detectable TMD-tagged proteins by using cycloheximide chase assays, in order to judge the credibility of the indirect detection via Western Blot. Cycloheximide chase assays are based on ribosome inhibition by cycloheximide. Since protein synthesis comes to a standstill, protein half-life i.e. the rate of protein degradation can be determined by the subsequent decrease in protein level (388).

In order to find the optimal LgBiT/SmBiT ratio for the NanoBiT assay, titration of SmBiT-BAX-TMD-encoding plasmid with constant amount of LgBiT-BAX-TMD-encoding plasmid resulted in a LgBiT/SmBiT ratio of 1:1 to be optimal for luminescence generation i.e. TMD interaction (Figure 10D). Stoichiometrically, TMD-TMD interaction thus forms in the ratio 1:1 i.e. as dimers, tetramers etc. Indeed, empirical data and models of BAX oligomerisation agree that BAX-TMD homotypic interaction forms dimer-dimer interfaces in which BAX-TMDs interact in an either parallel or anti-parallel dimeric fashion (140, 332). Also, dimerization is frequently found for other Bcl-2 protein interactions and structures mainly based on the dimeric nature of the BH3:groove interaction. Examples are numerous including sequestration of effector proteins by anti-apoptotic Bcl-2 proteins (e.g. BAX and BCL-XL) or BH3-only protein binding to BH multi-domain proteins (e.g. BID and BCL-XL) (184, 286, 389). Also TMD dimerization is considered a reoccurring feature of Bcl-2 protein interaction and was studied as such (171, 332, 333). Hence, it was presumed that the majority of the here assessed TMD interactions most efficiently interact in a 1:1 ratio. As a consequence, plasmids were always used at a LgBiT/SmBiT ratio of 1:1 for co-transfections during assessment of TMD interactions using the NanoBiT assay.

## 4.2 Identification of novel and known TMD interactions

As described in chapters 3.2.1, 3.2.2 and 3.2.3, the developed NanoBiT luciferase assay was used to systematically analyse TMD interactions of i) effector TMDs and ii) interaction of effector TMDs with TMDs of anti-apoptotic Bcl-2 proteins. The summary of identified interactions is shown in Table 26. Subsequently, the localisation of fluorophore-conjugated TMDs was assessed using cLSM. The results of the subcellular localisation analyses are depicted in Table 27.

**Table 26: Summary of TMD interactions identified via the NanoBiT luciferase assay.**

TMD interactions obtained from assessed combinations in the NanoBiT assay from Figure 11-14.

SmBiT-TMD LgBiT-TMD	BAX	BAK	BOK	BCL-2	BCL-XL	BCL-W	MCL-1	A1
BAX	✓	X	X	X	✓	✓	X	X
BAK		✓	X	X	✓	✓	X	X
BOK			✓	✓	✓	✓	X	X

First of all, some general considerations about the here discussed interaction data are given in the following. Presence and intensity of interaction signals (NanoBiT luminescence) are influenced by a number of factors which are independent of TMD affinity. Also, some of these factors are difficult to assess with the given system. TMDs are membrane-anchors and target the attached protein to a specific subcellular compartment (172, 283). For example, while TOM5-TMD is exclusively targeted to the MOM, cb5-TMD is ER-targeted resulting in a spatially separated cellular distribution of both TMDs (279, 280). Hence, some TMDs are more likely to share the same subcellular localisation than others which inevitably pre-selects for possible interaction partners. Addressing this, interaction data in light of subsequently assessed subcellular localisation of TMD peptides is discussed in 4.2.4. Moreover, interaction data are likely individually biased by the used cell system. The endogenously expressed Bcl-2 proteins might sequester NanoBiT-TMDs to a varying extent which would suppress interaction of LgBiT- and SmBiT-TMD resulting in reduced NanoBiT luminescence. For instance, HEK293 cells express lower amounts of BCL-2 than MCF-7 cells (Supplementary Figure S1A) so that BCL-2-interacting TMDs might be more intercepted in MCF-7 than in HEK293 cells.

Additionally, transfection and expression efficiency of the used vectors and encoded proteins, the degree of posttranslational modification and rate of degradation are most likely divergent in different cell systems. To minimise a potential bias from the cell system some TMD combinations were assessed in HEK293, Hela and MCF-7 cells (Supplementary Figure S3). However, repetition in various additional cell lines would render interaction data even more reliable and should be considered in future experiments. In addition, technical aspects like the plasmid design likely affects NanoBiT complementation upon TMD interaction. For example, length and composition of the hydrophilic linker between TMD and NanoBiT subunit in combination with the adjacent TMD sequence might result in varying orientations and flexibility of the NanoBiT subunit (390, 391). Although it would demand a substantial amount of additional cloning effort, analysis of different linkers for all assessed TMD combinations, thus, could reveal interactions veiled by sterical hindrance or unfavourable orientation.

In general, all of the above-mentioned factors render the NanoBiT assay more prone to false negative signals than false positive signals. However, a residual possibility for false positive signals remains as well, for example, by unspecific NanoBiT constitution through random collisions of expressed NanoBiT-TMDs. Despite low affinity of NanoBiT subunits, interaction signal is likely proportional to collision rate as shown for FRET-FLIM interaction assays (392). Adding to this, it cannot be ruled out that seemingly interacting TMDs are brought into close proximity by binding to the same subcellular complex or adapter proteins generating interaction signals without direct TMD interaction. Switching to an artificial membrane environment such as large, unilamellar vesicles (LUVs) with recombinant NanoBiT-TMDs might be an alternative – however, it might introduce artificial conditions concerning, for example, lipid composition or pH value (393). To further boost validity of NanoBiT-TMD interaction data, findings should be independently verified with additional methods such as FRET-based interaction assays. For example, the already implemented combination of mTurq2 (functioning as FRET donor) and mCitr (functioning as FRET acceptor) represents a FRET-compatible pair of fluorophores that allows analysis of TMD interaction using acceptor photobleaching or FRET-FLIM assays (392, 394). However, since also these assays come with similar or other limitations, both congruent and incongruent interaction data should be furthermore critically considered and interpreted accordingly.



#### 4.2.1 Homotypic interaction of effector TMDs

The TMDs of BAX, BAK and BOK were found to interact in a strict homotypic manner (Figure 11). Homotypic interaction of BAX-TMD and BAK-TMD during oligomerisation was already described in form of dimer-dimer interaction (331, 332). Thus, the positive interaction signal i.e. luminescence in the NanoBiT assay was expected and, in the case of BAX, served as the positive control of the NanoBiT system. Intriguingly, no experimental evidence for BOK-TMD homotypic interaction was found in literature. But, Lucendo *et al.* demonstrated formation of stable BOK-TMD dimers in MD simulations (333). In addition, the recently unveiled mode of BOK pore formation was shown to have structural similarities to that of BAX and BAK (160). Hence, it can be hypothesized that BOK-TMD homotypic interaction is likewise involved in BOK oligomerisation. Also for anti-apoptotic Bcl-2 proteins such as BCL-2, BCL-XL and MCL-1, homotypic TMD interaction was already shown (171, 333). Taken together, homotypic TMD interaction seems to be a common pattern in the Bcl-2 protein family. However, further studies including the current thesis are needed to define affinities and physiological impact of homotypic TMD interactions.

The degree of redundancy among effectors, especially BAX and BAK, is still a matter of debate albeit BAX and BAK hetero-oligomerisation via the BH3:groove interaction was shown to be possible to a minor extent (137). Just recently, a study by Consentino *et al.* found recruitment of BAK and BAX to hetero-oligomers at mitochondria using super resolution microscopy and SMALP pull-down assays (149). In contrast, the interaction data in this thesis point out a molecular mechanism which clearly differentiates between BAX and BAK molecules for oligomerisation and rather corroborate unique, not redundant, structure and function. It can be speculated that the here found preference for TMD homotypic interaction drastically impacts on effector oligomerisation, so that, for example, formation of BAX/BAK hetero-oligomers is impeded in comparison to homo-oligomerisation via the TMD-dictated dimer-dimer interface. On the other hand, the absence of heterotypic interaction between BOK-TMD and BAX- or BAK-TMD might primarily result from differences in subcellular localisation (Figure 15). Since BOK-TMD was foremost localised to the ER, while BAX- and BAK-TMDs resided at mitochondria, putative interaction could be masked by spatial separation.

#### 4.2.2 BCL-XL and BCL-W – universal TMD-scavengers of effector proteins?

All combinations of effector TMDs with BCL-W-TMD and, less pronounced, BCL-XL-TMD produced a noticeable luminescence signal indicating interaction (Figure 12, Figure 13, Figure 14). Interestingly, functional implications of the Ct TMD in anti-apoptotic activity can be found in literature for both BCL-W and BCL-XL: the BCL-XL-TMD is reportedly involved in homodimerization of cytosolic BCL-XL (326). Moreover, Todt and coworkers found an involvement of the BCL-XL-TMD in BAX retrotranslocation since exchange or deletion of the BCL-XL-TMD hampered retrotranslocation and led to BAX accumulation at the mitochondria (329). Thus, it is plausible that the BCL-XL-TMD can interact with effector TMDs of both BAX and BAK in order to facilitate retrotranslocation since also BAK undergoes retrotranslocation by BCL-XL (395). In case of BAX-TMD, however, the interaction signal with BCL-XL-TMD was rather low compared to BAX-/BAX-TMD homotypic interaction (Figure 12). Therefore, TMD interaction might represent a necessary, but secondary step in retrotranslocation compared to the BH3:groove interaction. Although for the TMD of BCL-W no role in interaction with other Bcl-2 proteins was suggested yet, the BCL-W-TMD is a crucial element of BCL-W regulation by occupying its hydrophobic groove in cytosolic monomers (396). Thus, TMD-TMD interaction might become relevant once the protein is inserted into the MOM adding another layer of BCL-W regulation.

In line with the similar TMD interaction pattern of BCL-W and BCL-XL found here, structural analysis revealed more similar features of both proteins than previously anticipated in addition to their high sequence similarity (193). Consequently, it can be speculated that both proteins are capable to bind active BAX and BAK molecules simultaneously via TMD and BH3:groove to counteract apoptosis. Dual binding might inhibit dimer-dimer and intra-dimer interactions of the effectors simultaneously. How the interaction of both proteins with BOK-TMD fits in the regulatory framework of Bcl-2 proteins is less natural to determine since BOK-TMD was primarily found at the ER and barely colocalises with MOM-localised BCL-W-TMD and BCL-XL-TMD (Figure 16). However, BCL-XL-TMD and BCL-W-TMD partially colocalised with the ER and BCL-XL exerts some of its anti-apoptotic functions at the ER, for example, binding to IP3Rs to maintain ER Ca<sup>2+</sup> homeostasis (397). On the other hand, under the assumption that BOK also forms pores in the MOM similar to BAX and BAK, BOK oligomerisation in the MOM might be likewise inhibited by BCL-XL and BCL-W.

Challenging this hypothesis, no evidence in literature supports association of BOK with BCL-XL or BCL-W underlining the need for further studies confirming the identified TMD interactions with BOK (160, 161). Of note, combination of BCL-W-TMD with BAK-TMD produced the strongest interaction signal in the NanoBiT assay (Figure 13). Hence, this interaction is a promising candidate for further functional studies how TMD interaction impacts apoptosis signalling. In general, capacity of BCL-XL and BCL-W to interact via the TMD and the cellular impact of TMD interaction would be worth to be further explored by means of cell death assays such as co-expression of TMD-chimeric proteins with effector proteins.

#### 4.2.3 A newly identified Interaction of BOK and BCL-2 via their TMDs

The here developed interaction assay brought to light a yet unknown interaction of BOK-TMD and BCL-2-TMD (Figure 14). This interaction is especially interesting since BCL-2-TMD did not show interaction with any other tested effector TMD. To date, no interaction of BOK via BH3:groove binding was demonstrated hinting at an even more important role of the TMD as an interaction site and, thus, as a regulatory element for BOK pro-apoptotic activity. Hence, further elucidation of BOK-TMD interactions might shift the still prevailing view that BOK is not inhibited by any other Bcl-2 protein (161, 160). In favour of a functional relevance of BOK-TMD interaction, Lucendo *et al.* revealed interaction of BOK with anti-apoptotic MCL-1 via their TMDs which regulates BOK-dependent apoptosis (333). However, interaction of BOK-TMD and MCL-1-TMD could not be confirmed with the here developed interaction assay. According to Lucendo *et al.* interaction of BOK-TMD and MCL-1-TMD occurs at mitochondria or MAMs respectively to which ER-localised BOK-TMD is tethered by MCL-1-TMD. In contrast, cLSM analysis indicates predominant localisation of both BOK-TMD and MCL-1-TMD at the ER, rather than mitochondria (Figure 16). Subcellular localisation data, hence, let neither conclude mitochondria-targeting by MCL-1-TMD nor a putative interaction with BOK-TMD. Several publications already confirmed interaction of BOK with MCL-1 (153, 161, 291). Moreover, a recent study investigating the BOK interactome using proximity labelling also found the presence of BOK-TMD crucial for interaction with MCL-1, while no interaction of BOK with any other Bcl-2 protein including BCL-2 was found (398). In the background of these apparent contradictions, the found interaction of BOK-TMD and BCL-2-TMD was further investigated (further discussed in 4.3.4).

Possible reasons for no interaction of BOK-TMD and MCL-1-TMD in the NanoBiT assay are sterical hindrance or unfavourable orientation of NanoBiT subunits or cell system-dependent factors such as sequestering of MCL-1-TMD by endogenous Bcl-2 proteins. Therefore, combination of BOK-TMD and MCL-1-TMD could be analysed with different NanoBiT-TMD linker length and composition as well as cell systems.

#### 4.2.4 Subcellular localisation of TMD interactions












In addition to TMD interaction, TMD subcellular localisation was assessed in MCF-7 cells using fluorophore-conjugated TMD peptides (Figure 15, Figure 16). Fluorophore-conjugated TMD peptides were found to either localise predominantly to mitochondria (BAX, BAK, BCL-XL, BCL-W) or the ER (BOK, BCL-2, MCL-1). For A1-TMD, additional experiments revealed a predominant colocalisation with the Golgi apparatus (Supplementary Figure S5A, summarised in Table 27).

The subcellular localisation of fluorophore-conjugated TMD peptides often resembles localisation of Bcl-2 full-length proteins under normal (non-apoptotic) conditions (Table 27) underlining the dominant role of the TMD for specific subcellular targeting. TMDs of BAK, BOK, BCL-2 and BCL-XL effectively targeted mTurq2 to the Bcl-2 protein-specific localisation within the cell. For BAX and BCL-W, mitochondrial TMD localisation was expected as well since the full-length proteins only reside in the cytosol as long as their TMD is sequestered in their binding groove (134, 194). Only for A1 and MCL-1, the found TMD localisation did not reflect expectations from literature.

However, the markers for the performed colocalisation analysis, namely EYFP-Mito and EYFP-ER, naturally limit the differentiation of subcellular localisation to these two compartments. In the case of BAX-TMD or BCL-2-TMD which are known to localise to mitochondria or ER respectively this is completely sufficient and subcellular localisation easier to be recognised as for other less thoroughly studied family members such as A1-TMD. Therefore, additional co-stainings as done for A1 with the Golgi marker GM130 (Supplementary Figure S5A) might reveal additional compartments to which TMD peptides are localised such as endosomes, lysosomes, nuclear envelope or the plasma membrane. Nevertheless, the site of homotypic TMD interactions of effector TMDs can clearly be allocated to their published predominant subcellular localisation – the mitochondria for BAX- and BAK-TMD and the ER for BOK-TMD.

**Table 27: Summary of TMD subcellular localisation found for mTurq2-conjugated TMD peptides.**

Predominant localisation of mTurq2-fused TMD peptides obtained from Figure 15 and Figure 16. Localisation of full-length proteins under normal conditions (healthy cells) is retrieved from Table 1.

Sub-type	Protein TMD	Predominant localisation (TMD peptide)			Localisation of full-length protein (normal conditions)
		 Mito	 ER	 Others	
Effector	BAX				Cytosol
	BAK				Mitochondria
	BOK				ER
Anti-apoptotic Bcl-2-like	BCL-2				ER
	BCL-XL				Mito/Cytosol
	BCL-W				Cytosol
	MCL-1				Mitochondria
	A1				Mitochondria

Additionally, based on the high colocalisation with mitochondria it can be assumed that interaction of BAX- and BAK-TMD with BCL-XL-TMD and BCL-W-TMD occurs foremost at mitochondria (Figure 15, Figure 16). This would be in line with literature in which the MOM is in the spotlight for interactions of these proteins (184, 191, 329, 331). As mentioned, interaction of BOK-TMD and BCL-XL-TMD or BCL-W-TMD could occur at the ER since both anti-apoptotic Bcl-2 TMDs were at least partially colocalising with the ER as well.

The newly identified interaction of BOK-TMD and BCL-2-TMD is localised at the ER since colocalisation of both TMDs was found at the ER (Figure 17). This finding implies that a putative functional relevance of BOK and BCL-2 interaction is implicated at the ER. In line, both BCL-2 and BOK perform apoptosis-regulating functions at the ER (166, 174). However, further discussion about the impact of BOK-TMD and BCL-2-TMD interaction at the ER on apoptosis signalling is provided in section 4.3.4 alongside the respective functional experiments. In contrast, the lack of interaction between BCL-2-TMD and BAX- or BAK-TMD in the NanoBiT assay (Figure 12, Figure 13) might be caused by the spatial separation of TMD peptides (BCL-2-TMD at ER, BAX-/BAK-TMD at mitochondria).

However, it is possible that BCL-2, which's inhibitory capacity towards BAX and BAK (via BH3:groove interaction) is well-known (170, 169), is capable of interaction with BAX or BAK via its TMD once BCL-2 translocated to mitochondria. Corroborating this, Andreu-Fernández *et al.* reported TMD interaction of BAX-TMD and BCL-2-TMD in *E.coli* membranes (171).

Also localisation of MCL-1-TMD was different than published data: literature clearly states mitochondrial localisation of MCL-1(-TMD) (205, 333) whereas in the present study MCL-1-TMD neither clearly localised to the ER nor mitochondria (Figure 16). Visual evaluation of cLSM images indicated an ER-like subcellular distribution of mTurq2-MCL-1 with signals partially diffusely distributed throughout the whole cell indicating a cytosolic localisation. Of note, this diffuse cytosolic background was also observed for other TMD peptides, for example, A1-TMD and BCL-W-TMD (Figure 16). Thus, spatial separation of MCL-1-TMD and BAX- or BAK-TMD might prevent TMD interaction, while the lack of interaction with BOK-TMD, an interaction which was repeatedly published (291, 333, 398), remains elusive as discussed in 4.2.3.

The unique localisation of A1-TMD at the Golgi might be the underlying reason why no interaction of A1-TMD and effector TMDs was found. However, the A1-TMD has anyway an unique structure and function among Bcl-2 TMDs (213, 216). Due to its comparably truncated, not membrane-spanning character it might not take part in TMD-TMD interactions as detected with the here developed assay. Intriguingly, the here found predominant Golgi localisation of A1 was not found in literature. On the contrary, A1 was postulated to localise to mitochondria dependent on its Ct sequence (213). Therefore, further studies about the subcellular localisation of A1 including additional cell lines and staining of endogenous A1 protein are needed to determine whether the observed Golgi localisation is indeed a novel, yet undefined feature of A1 or merely a cell system or overexpression-dependent phenomenon.

Taken together, the here described subcellular localisation of TMD peptides is mostly congruent with published data. Observed discrepancies such as for MCL-1-TMD and A1-TMD could be further analysed by additional methods to determine their subcellular localisation and membrane insertion like advanced subcellular fractionation after expression of TMD peptides followed by detection of the fused fluorophore in the respective membrane fractions using Western blot (399).

### 4.3 Investigating the functional relevance of TMD interactions

Experiments in the last part of this thesis aimed to shed light on yet uncharacterised roles of Bcl-2 TMDs in apoptosis signalling. Next to over-expression of effector proteins with an exchanged TMD sequence, so-called TMD chimeras, also the impact of TMD mutations in BAX and BCL-2 and the functional importance of the identified interaction of BOK-TMD with BCL-2-TMD is discussed.

Generally, it has to be noted that the majority of the functional data was obtained by means of transient transfection and vector-based overexpression of Bcl-2 proteins. Protein expression from used vectors (Table 11, Table 12) is controlled by strong CMV promoters known to produce vast amounts of encoded protein (364). Although few studies directly measured Bcl-2 protein concentrations within the cell, members of the Bcl-2 protein family are assumed to be present in concentrations of low nanomolar range (reviewed in (40)). BAX is one of the few examples for which valid data is present describing a physiological BAX concentration reaching from 3 nM to 170 nM (400, 401). Thus, it is likely that here observed mechanisms comprise protein concentrations far beyond physiological relevance of the Bcl-2 interaction network. On the one hand, high expression of exogenous proteins ensures neglectable influence of the cellular 'background', i.e. endogenous Bcl-2 proteins, on readout such as cell death. On the other hand, overexpression beyond physiologically relevant concentrations might create an unnatural, distorted situation and bears the risk of artifact formation like protein aggregation (reviewed in (402)). Hence, drawn conclusions are to be taken with caution and are best confirmed with experiments utilizing only endogenous Bcl-2 proteins such as knockout/knockdown experiments. Nevertheless, overexpression phenotypes are frequently used as starting points to reveal cellular mechanisms (reviewed in (403)). Another important aspect for the subsequent interpretations, is the versatile function of TMDs. Since TMD-targeting, membrane insertion as well as interaction specificity are inherently coupled and encoded by the TMD sequence, it is virtually impossible to influence one of these functions independently. Thus, modifying the TMD sequence in order to study its impact on the cellular system always requires a holistic view on TMD functions. However, this also complicates to pinpoint the underlying mechanisms how TMDs regulate apoptosis signalling.

#### 4.3.1 The TMD has a crucial role for regulation of BAX activity

In a first approach to unravel a functional relevance of the BAX TMD sequence, overexpression of chimeric proteins BAX<sup>BAK-TMD</sup> and BAX<sup>BOK-TMD</sup> revealed an increase in cell death and BAX cluster formation at mitochondria compared to overexpression of WT BAX (Figure 18). In addition, co-expression of BAX TMD chimeras with BCL-2 showed no inhibition of BAX<sup>BAK-TMD</sup> pro-apoptotic activity by BCL-2, while cluster formation and cell death were blocked for WT BAX and BAX<sup>BOK-TMD</sup> (Figure 19).

BAX overexpression induces apoptosis as the excess in BAX molecules exceeds the retrotranslocation capacity leading to BAX accumulation at mitochondria, followed by spontaneous BAX activation, oligomerisation and pore-formation (130–132). This process is nicely reflected by the here presented data as BAX overexpression effectively led to BAX accumulation at mitochondria in form of bright EGFP(-BAX) clusters and cell death (Figure 18). The exchange of the BAX-TMD to BAK- or BOK-TMD might accelerate this process since a higher percentage of cells displayed BAX accumulation at mitochondria when expressing BAX<sup>BAK-TMD</sup> or BAX<sup>BOK-TMD</sup> compared to WT BAX (Figure 18D). The increase in cell death is especially remarkable with regard to the reduced abundance of BAX<sup>BAK-TMD</sup> and BAX<sup>BOK-TMD</sup> after overexpression (Figure 18F) which might either be based on a less efficient expression or reduced stability compared to WT BAX. Suggesting the latter, the impact of the TMD sequence on protein stability was reported for other Bcl-2 proteins (216, 294). TMD exchange in BAX could also increase misfolding and thereby accelerate BAX degradation. Thus, analysing stability of BAX TMD chimeras, for example, using cycloheximide chase assays could confirm if TMD exchange altered BAX stability. An auto-inhibitory role of the BAX-TMD sequence when folded back onto the BAX groove might explain enhanced activation of BAX TMD chimeras. Association of TMD and groove presumably maintains the inactive form of BAX as displacement of the TMD, for example, by BH3-only proteins promotes BAX activation (134). Simultaneously, an exposed BAX-TMD in turn promotes membrane-insertion in mitochondria as demonstrated by reports studying its MOM-targeting function (302, 331, 395). Therefore, maintaining the affinity of TMD and groove is vital for regulation of BAX conformation and activity – an equilibrium naturally dictated by the interaction of TMD and groove residues. TMD exchange likely leads to repulsion of the BAK-TMD or BOK-TMD from the BAX centre and promotes active, membrane-targeting BAX conformation.



Supporting the auto-inhibitory role of the BAX-TMD, Schinzel and colleagues confirmed that BAX-TMD is sufficient to regulate BAX activation and mitochondrial targeting (404). However, the authors showed that P168, a residue upstream of the TMD, controlled BAX conformation. Moreover, Garner *et al.* described formation of inactive BAX homodimers in the cytosol for which displacement of the TMD plays a crucial role (131). Hence, it is not surprising that both BAX TMD chimeras accelerate cell death despite of the different targeting functions of BAK-TMD and BOK-TMD. In fact, the increased pro-apoptotic activity of BAX carrying BAK-TMD was previously reported by Todt and coworkers (395) who explain the increased pro-apoptotic capacity of BAX<sup>BAK-TMD</sup> with reduction of the BAX retrotranslocation to the rate of BAK. Thus, the TMD sequence dictates BAX retrotranslocation hinting at anti-apoptotic Bcl-2 proteins to be another important factor. TMD-dependent retrotranslocation by anti-apoptotic Bcl-2 proteins fits well to the observation that BAX<sup>BAK-TMD</sup> cluster formation and cell death induction is no longer inhibited by BCL-2 (Figure 19). It can be hypothesized that TMD-TMD interactions are directly involved underlined by the reported importance of BCL-XL-TMD in retrotranslocation (329). As mentioned, the here revealed interactions of BCL-XL-TMD with effector TMDs might also be linked to a function in retrotranslocation (Figure 12 - 14). Intriguingly, switching the TMD in BAX to BCL-XL-TMD abolishes BAX apoptotic function, while maintaining its mitochondrial localisation further indicating a TMD function beyond mere membrane-targeting (405).

However, current data as well as results from literature are still insufficient to judge whether TMD-TMD interaction, TMD hydrophobicity (i.e. TMD-membrane interaction) or a combination of both is the key regulator of the retrotranslocation process. The striking difference in inhibition of BAX TMD chimeras could, therefore, be based on either the reduced hydrophobicity of BOK-TMD compared to BAK-TMD or differences in TMD-TMD interaction capacity of BCL-2-TMD with BAK-TMD and BOK-TMD. The latter is supported by the here acquired interaction data showing interaction of BOK-TMD with BCL-2-TMD, while no interaction of BCL-2-TMD with BAK-TMD was found (Figure 13, Figure 14). Despite of the lack in cell death inhibition, BCL-2 and BAX<sup>BAK-TMD</sup> colocalise at mitochondria (Figure 19C). It's likely that this is due to the BH3:groove interaction of both proteins. Consequently, BH3:groove interaction is necessary but not sufficient for retrotranslocation and, counterintuitive to the classical dogma, counteraction of BAX activation.

#### 4.3.2 BAK-TMD has limited influence on BAK activity and regulation

In contrast to BAX, TMD exchange in BAK to BAX-TMD or BOK-TMD had a minor impact on BAK inhibition by or colocalisation with BCL-2 (Figure 25, Figure 26). While BAK<sup>BAX-TMD</sup> exerted increased pro-apoptotic activity, cell death induction by BAK<sup>BOK-TMD</sup> was similar compared to WT BAK.

Also under non-apoptotic physiological conditions, BAK is targeted to the MOM by the BAK-TMD sequence (296). But, BAK activation requires conformational changes similar to BAX including unfolding of the N-terminus and exposure of BH3 region (406). Exchange of the TMD in BAK to BAX-TMD, hence, does not affect BAK subcellular localisation and seems to rather promote than abrogate BAK activation corroborated by cell death data and the observation of increased mitochondrial BAK cluster formation for BAK<sup>BAX-TMD</sup> compared to WT BAK (Supplementary Figure S7A). Intriguingly, Ferrer *et al.* also studied the exchange of parts of the BAK-TMD to the corresponding BAX-TMD sequences and found partial cytosolic localisation of BAK carrying only the four final Ct residues of BAX-TMD (KKMG). The authors demonstrated that the TMD in this BAK variant is likewise folded back onto the BAK centre similar to BAX (407). Also, Todt and colleagues observed a shift of BAK to the cytosol when equipped with the BAX-TMD correlating with a decreased pro-apoptotic activity of BAK (395). Thus, both references rather draw a picture of an inactivating function of BAX-TMD or parts thereof on the BAK protein. The apparent discrepancy with the data acquired here could result from differences in methodology, for example, the use of different cell systems, time points and expression vectors. At least for the study by Ferrer *et al.*, the exchange of the four final AA is in large contrast to the exchange of the final 23 AA in the present study. Therefore, further studies with focus on BAK<sup>BAX-TMD</sup> inhibition or localisation are necessary to determine a possible context-specific influence on pro-apoptotic activity of BAK. However, similar inhibition of BAK TMD chimeras by BCL-2 and maintained colocalisation let assume a fundamental different regulation of BAK compared to BAX: while BAX is mainly regulated by retrotranslocation which is crucially influenced by the TMD (as discussed in 4.3.1), the TMD sequence and, hence, TMD interaction seems obsolete for effective inhibition of BAK by BCL-2. The TMD-independent colocalisation of BAK and BCL-2 (Figure 26) indicates that the BH3:groove interaction is sufficient to tether both proteins to the same localisation and confer inhibition of BAK.

Of note, comparison of cells expressing low or high amounts of BAK or BAX respectively (Supplementary Figure S7C) demonstrates that recruitment of BCL-2 carrying a cb5-TMD to effector proteins takes place above a certain threshold of effector protein concentration and is likely triggered by accumulation and activation of BAK or BAX respectively since only in the active conformation their BH3 motif becomes exposed (137, 408). Additional experiments should focus on confirming the decisive role of the BH3 region for regulation of BAK activity, for example, by usage of BH3-mutated BAK or BCL-2 variants.

#### 4.3.3 Cancer-related TMD mutations shift the Bcl-2 network homeostasis

Mutations in the TMD of pro-apoptotic BAX and anti-apoptotic BCL-2 were investigated to evaluate the impact of the mutations on interaction, subcellular localisation and cell death regulation. In BAX, (de-)phosphorylation mimicking mutations S184A and S183D as well as the cancer-derived mutation V180G were analysed. In BCL-2, all chosen mutations were derived from the COSMIC database and comprised mutations A234D, A224D and W214C.

##### 4.3.3.1 BAX TMD mutations

In the NanoBiT assay, BAX mutation S184A increased BAX homotypic TMD interaction with WT BAX-TMD (Figure 20C). In contrast, mutations S184D and V180G completely abolished interaction with WT BAX-TMD. The observed interaction capacities fit well with the observed subcellular localisation of TMD peptides as WT BAX TMD and S184A were localised to mitochondria, while S184D and V180G were diffusely localised throughout the cytosol indicating their inability to integrate into membranes (Figure 21). This is in line with published data demonstrating constitutive MOM localisation of BAX S184A and abolished membrane integration of phospho-mimicking BAX S184D or S184E respectively (293, 302). Hydrophobicity of the TMD helix in tail-anchored proteins is known as a crucial factor for membrane integration and protein subcellular localisation (reviewed in (278)). Thus, the decrease in hydrophobicity of S184D and V180G is vital for their inability to integrate into membranes (Figure 20A). In turn, increased hydrophobicity of S184A causes higher affinity to the MOM. However, why increased hydrophobicity increases interaction with WT BAX-TMD remains unclear. Nevertheless, interaction data indicate that BAX phosphorylation at S184 by Akt not only modulates BAX localisation, but also TMD interaction.

It would be worth exploring homotypic interactions of BAX mutant TMDs (e.g. BAX-TMD V180G with another BAX-TMD V180G) to estimate the BAX oligomerisation potential in, for example, cancer cells only possessing BAX V180G. Despite of missing membrane integration, full-length BAX mutants S184D and V180G were still able to form BAX clusters, i.e. BAX oligomers, as observed in Figure 22. However, missing colocalisation with mitochondria (in contrast to WT BAX and BAX S184A clusters) indicates that these clusters are cytosolic BAX aggregates. Since BAX activation and oligomerisation usually occurs at mitochondria, cytosolic BAX aggregates are likely a consequence of a massive overexpression (402). Co-expression of mC-BCL-2 confirmed that BAX S184A constitutively localises to mitochondria where it colocalises with BCL-2 (Figure 23). In contrast, BAX S184D displays a similar cytosolic localisation as observed for the TMD peptide and, intriguingly, is not co-localised with BCL-2, while BAX V180G visibly associates with membranes (presumably mitochondria). Thus, these changes in localisation caused by BCL-2 suggest a similarly deactivating regulation of BAX mutants as for WT BAX. In case of BAX S184D and V180G, this seems to be vastly achieved by retrotranslocation to the cytosol which, by contrast, seems to be abolished for the S184A mutation.

Indeed, BCL-2-mediated inhibition of cell death caused by BAX S184A is less efficient compared to WT BAX and barely inhibited by MCL-1 (Figure 24). PARP cleavage after BAX S184A overexpression also indicates increased pro-apoptotic activity compared to WT BAX (Figure 24B). Hence, it can be hypothesized that BAX S184A functions similar to the already studied BAX<sup>BAK-TMD</sup> (discussed in 4.3.1). In contrast to WT BAX, both BAX S184A and BAX<sup>BAK-TMD</sup> possess an increased TMD hydrophobicity, show constitutive mitochondrial localisation, increased pro-apoptotic potential and impaired inhibition by anti-apoptotic Bcl-2 proteins. The constant inhibition of all BAX mutants by BCL-XL is consistent to findings in literature for S184A (302) and suggests that tested BAX TMD mutations do not interfere with BCL-XL's ability to retrotranslocate BAX. It would be interesting to analyse cell death induction for co-expression of BCL-XL with BAX TMD chimeras such as BAX<sup>BAK-TMD</sup> and whether BAX TMD mutation alters TMD interaction with BCL-XL. Despite of abolished mitochondrial localisation of BAX-TMD S184D and V180G, both BAX mutants induced cell death similar to WT BAX (Figure 24). Also, cell death inhibition by anti-apoptotic Bcl-2 proteins did not differ from WT BAX. Thus, BAX S184D or V180G are similarly functional as WT BAX.

Protein folding prediction comparable to WT BAX corroborates that S184D or V180G are no loss-of-function mutations in BAX (Figure 20B). However, structure prediction likely reflects solely cytosolic BAX structure lacking information of membrane-inserted conformation. In contrast, other studies found that phosphorylation of S184, mimicked by S184D or S184E, abrogated BAX pro-apoptotic activity due to the cytosolic localisation of BAX (293, 302). Interestingly, in a study by Simonyan *et al.* BAX activation is stimulated by phosphorylation through Akt reflected by increased cell death induction for the phosphorylation-mimicking mutant BAX S184D (409). However, the authors found exactly opposite localisations of BAX S184 mutants compared to the here presented data as BAX S184A was localised to the cytosol, while BAX S184D constitutively associated with mitochondria. Also, BAX S184D was found to be sensitive to proteasomal degradation which was blocked by BCL-XL interaction in line with the here observed inhibition of BAX S184D by BCL-XL. Taken together, more evidence is necessary to determine how phosphorylation of BAX at S184 regulates cell death. The inconsistent results from literature indicate a context-specific function.

Since the cancer-specific BAX V180G mutant yielded similar results to BAX S184D in most experiments, BAX V180G is less associated with membranes and, thus, has a lowered pro-apoptotic potential in tumours. In general, tumours frequently develop resistance to pro-apoptotic stimuli by downregulation, inhibition and/or loss-of-function of pro-apoptotic proteins like BAX (94, 95, 97). Substantiating a promoting role of BAX V180G in apoptosis resistance, a close-by TMD mutation, namely BAX G179E, was reported to confer resistance to the BH3 mimetic Venetoclax in human lymphoma cells (410). BAX G179E was likewise unable to integrate into membranes and remained cytosolic in cells incubated with ABT-199. However, flow cytometric cell death analysis after BAX overexpression suggests maintained pro-apoptotic function of BAX V180G (Figure 24). It can be speculated that the impaired function of BAX V180G depends on the cellular context not given in the used cell system. Unfortunately, the information from COSMIC is not sufficient to make reliable statements about, for example, other mutations in the same samples. Hence, the impact of the clearly visible phenotypic differences between WT BAX and BAX V180G on cell death signalling should be assessed in more detail, for example, by investigating BAX dynamics, cell death induction at different time points and by using cell lines closer related to the original oncogenic background (head and neck cancer).

#### 4.3.3.2 BCL-2 TMD mutations

BCL-2-TMD mutations A234D and A224D reduced interaction of BCL-2-TMD with BOK-TMD (Figure 33C). In contrast, mutation W214C insignificantly increased BCL-2-TMD interaction with BOK-TMD. As for BAX TMD mutations, this is in line with changes in hydrophobicity as A234D and A224D decreased hydrophobicity of the BCL-2-TMD, while W214C increased hydrophobicity (Figure 33A). Changes in TMD hydrophobicity give rise to the hypothesis that BCL-2 A234D and A224D membrane association might be reduced compared to W214C. Although a more homogenous distribution of BCL-2-TMD A234D and A224D indicated a partially cytosolic localisation, BCL-2-TMD A234D, A224D and W214C colocalised with the ER comparable to WT BCL-2-TMD (Figure 34). However, also visible cluster formation by BCL-2-TMD A224D indicated an increased cytosolic abundance of TMD peptides. Nevertheless, also full-length BCL-2 A234D and W214C displayed similar subcellular localisation compared to WT BCL-2 (Figure 35). In contrast, BCL-2 A224D was localised to the cytosol cementing the hypothesis that A224D mutation hampers membrane integration.

One vital factor for the impaired functionality of the A224D mutant might have a structural component as a kinked TMD structure with a disrupted  $\alpha$ -helix around the A224 mutation was predicted by Alphafold (Figure 33B). Membrane insertion of a disrupted  $\alpha$ -helix can be speculated to be less feasible compared to integration of the WT helix. Proper integration might as well be not possible at all given that the general  $\alpha$ -helical TMD structure with foremost hydrophobic AA in the central part of the TMD is essential for membrane integration (278). However, also W214C caused a helix disruption as predicted by Alphafold (Figure 33B). Either the predicted helix disruption in BCL-2 W214C does not interfere with membrane insertion or obtained changes in structure prediction do not reflect structural changes *in vitro*.

Cytosolic localisation of BCL-2 A224D likely contributes to the impaired counteraction of BAX- and BAK-induced apoptosis (Figure 36). Decreased membrane association of BCL-2 A224D might reduce its affinity for BAX and BAK since the membrane is an important binding platform for Bcl-2 protein interactions as suggested by the 'embedded together' model (123). Moreover, presence of membrane lipids crucially affects Bcl-2 proteins exemplified by a study in which cholesterol inhibited BAX activation, while membrane integration of BID depended on the mitochondria-exclusive anionic phospholipid cardiolipin (CL) (411).

On the other hand, BCL-2 has other anti-apoptotic functions, for example, binding to IP3Rs in a TMD-dependent manner to regulate  $\text{Ca}^{2+}$  flux from and into the ER lumen (337). Hence, BCL-2 A224D might be less capable to interact with IP3Rs and reduce apoptosis-promoting  $\text{Ca}^{2+}$  efflux from the ER. Concludingly, it would be worth to perform Interaction studies of IP3Rs and BCL-2 after TMD mutation with methods such as proximity ligation or immunoprecipitation assays. In addition, lower abundance of BCL-2 A234D and A224D compared to WT BCL-2 after overexpression (Figure 36B) indicates that reduced TMD hydrophobicity (i.e. membrane integration) reduces protein stability and, thus, BCL-2 anti-apoptotic capacity. The question, if TMD-TMD interactions are involved in the observed differences in effector inhibition by BCL-2 due to TMD mutation presupposes a possible interaction of BCL-2-TMD with BAX- or BAK-TMD discussed in sections 4.2.4, 4.3.1 and 4.3.2. Although experimental data suggested a crucial role of the TMD for BAX inhibition by BCL-2 (4.3.1) and TMD interaction of BCL-2 and BAX were described in literature (171), it remains unclear whether the mutations in BCL-2-TMD reduce its ability of putative TMD interaction with BAX-TMD and if the lack of this interaction causes increased BAX-induced apoptosis. Again, the general issue arises that changes in the TMD sequence inherently influence both TMD-TMD interaction and protein localisation. For instance, inability of BCL-2 A224D to integrate into membranes abolishes interaction with any membrane-bound TMDs. Also, the drastic impact of TMD mutation in BCL-2 on inhibition of BAK-induced apoptosis (Figure 36) is in stark contrast to TMD-independent inhibition of BAK-induced apoptosis by BCL-2 (discussed in 4.3.2). However, this dilemma is resolvable by the hypothesis that the ability of Bcl-2 proteins to integrate into membranes is a dominant regulatory factor over membrane-bound interactions. Investigated BAK TMD chimeras integrated into membranes (Figure 26), while BCL-2 A224D did not (Figure 35). Consequently, the BH3:groove interaction is not sufficient to tether BCL-2 to the membrane to inhibit BAK. Nevertheless, subcellular localisation of co-expressed BAK and BCL-2 A224D as well as additional BAK variants with different membrane-binding affinities should be investigated to further solve this conundrum.

Initially, all BCL-2 mutations were selected because of the large impact on side-chain size and charge. In the case of A224D, the exchange of the small hydrophobic alanine to large negatively charged aspartate, results indeed suggest crucially influenced protein structure, localisation and function (Figure 33 - 36). Similar results could have been expected for the identical exchange A234D.

However, phenotypes as observed for A224D were either reduced (impaired anti-apoptotic activity) or not visible at all (cytosolic localisation) for A234D. Confirmed by similar structure prediction for WT BCL-2 and A234D (Figure 33B), it seems that aspartate at the Ct end of the TMD has a lower impact on function compared to the central A224D mutation. The same is true for W214C since no changes in subcellular localisation or cell death regulation were detected. Thus, TMD mutations affects function very individually depending on position, charge and size of the introduced residue. For example, mutation of W214 in the Nt part of the TMD might generally affect TMD function less than mutation of the central A224. Also, exchanging W214 with a cysteine (small, no charge) is expected to impact on TMD structure and function differently compared to exchanging W214 to aspartate (large, charged). Concludingly, individual assessment of cancer-specific TMD mutations is vital to estimate the impact on protein functionality and, thus, the impact on apoptosis signalling in cancer cells. Since BCL-2's anti-apoptotic function is often essential for oncogenesis, for example, in haematological malignancies (241, 244), identified mutations are less expected to disturb the tumour-promoting function of BCL-2. Preserved anti-apoptotic function of BCL-2 A234D and W214C, thus, speaks in favour of an important role in the respective tumours of origin. On the other hand, loss-of-function mutations such as A224D are not expected to facilitate tumorigenesis. However, impaired function of BCL-2 A224D could be buffered by other anti-apoptotic proteins or apoptosis could be blocked by completely unrelated means such as downregulation of pro-apoptotic proteins (95, 96). A more fine-tuneable system, for example, with inducible expression of BCL-2 or expression of transgenic BCL-2 at endogenous level might reveal implications of BCL-2 TMD mutations undetected in the here utilized overexpression model.

All this considered, TMD mutation confirms a vital role of the TMD in BAX and BCL-2 function. Point mutation is sufficient to disturb localisation and modulate pro- and anti-apoptotic function of Bcl-2 proteins highlighting the importance to understand the impact of individual Bcl-2 TMD mutations on apoptosis signalling and diseases such as cancer. The investigated mutations represent a mere fraction of mutations found in the COSMIC database which contains a multitude of yet uncharacterised mutations in TMDs of Bcl-2 proteins such as BCL-XL (>20 mutations) or MCL-1 (12 mutations). Thus, further studies are required to unravel the exact role of these TMD mutations in apoptosis signalling. It can be assumed that many TMD mutations impact apoptosis regulation and, hence, are worth further investigation.



#### 4.3.4 Functional characterisation of the newly identified BOK-/BCL-2-TMD interaction

##### 4.3.4.1 TMD-dictated colocalisation of full-length BOK and BCL-2 at the ER

Similar to their TMD peptides, BOK and BCL-2 full-length proteins were found to colocalise at the ER (Figure 27A) in line with TMD-dependent ER-targeting of BCL-2 and BOK (157, 172). Intriguingly, co-stainings of full-length BOK with luminal localised ER markers resulted in abolished or diffuse ER marker localisation as if markers were released from the ER lumen (Supplementary Figure S9). Thus, it can be speculated that BOK overexpression disrupts ER homeostasis or ER membrane integrity. Supporting a severe membrane disruption by BOK, MD simulations demonstrated membrane indentation by R199 and K202 in BOK-TMD (Figure 32). Also, Walter *et al.* found an increase of KDEL peptide, the ER targeting sequence in the EYFP-ER marker, in neurons of BOK-deficient mice compared to BOK-expressing neurons (166). Kanekura *et al.* found ER permeabilization by BAX and BAK in response to ER stress which is regulated by IRE1 (412). Since also BOK plays an essential role in ER stress-mediated apoptosis (163), BOK-induced ER stress might lead to the observed ER permeabilization. The mechanism of BOK-induced ER permeabilization should be further analysed, for example, using live-cell imaging of a fluorescent probe in the ER lumen during induced BOK expression.

Interestingly, BCL-2<sup>TOM5-TMD</sup> is not colocalised with BOK (Figure 27A), while BH3-mutation of BOK did not affect colocalisation with BCL-2 (Figure 27B). Additionally, removing the TMD from BOK resulted in cytosolic BOK localisation and abolished colocalisation with BCL-2 (Figure 27C). Exclusively mitochondrial localisation of BCL-2<sup>TOM5-TMD</sup> suggests that BCL-2 and BOK do not interact via BH3:groove. This is in clear contrast to colocalisation of BAX and BAK with ER-targeted BCL-2<sup>cb5-TMD</sup>. In cells with strong BAX or BAK expression BCL-2<sup>cb5-TMD</sup> associates with BAX and BAK at mitochondria (Supplementary Figure S7C). Thus, BCL-2<sup>cb5-TMD</sup> is recruited to mitochondria despite the ER-targeting function of cb5-TMD. Consequently, BH3:groove binding is the dominant factor of BCL-2 interaction with BAX or BAK and causes their colocalisation. In contrast, colocalisation of BCL-2 and BOK solely depends on the TMD. Since no interactions of the BOK BH3 motif are known from literature (160, 161), interactions of BOK and other Bcl-2 proteins via the TMD might be all the more important for regulation of BOK pro-apoptotic activity.

Nevertheless, it must be borne in mind that colocalisation is not synonymous with interaction and, hence, not a bona fide proof of the TMD interaction obtained in the NanoBiT assay. This is especially important for interpretation of colocalisation of BOK with BCL-2<sup>cb5-TMD</sup> (Supplementary Figure S8C). Although BCL-2<sup>cb5-TMD</sup> might interact with BOK, colocalisation could originate from localisation of both proteins in the ER. Along these lines, colocalisation does not allow to differentiate between concomitant presence in a distinct compartment and interaction as long as both BOK and BCL-2 are targeted to the same compartment. Likewise, both proteins may also be targeted to the same subcellular complex without interaction, for example, IP3Rs to which both BOK and BCL-2 are able to bind (164, 174). However, as colocalisation is a prerequisite for interaction, TMD-dictated colocalisation of BOK and BCL-2 is an important indicator for TMD interaction of BOK and BCL-2 at the ER. Whether colocalisation of BOK and BCL-2 occurs through TMD interaction, close proximity in a complex or the mere ER-targeting function of the TMD does not annihilate the fact that BOK and BCL-2 colocalisation is clearly TMD-dependent.

#### *4.3.4.2 BCL-2-mediated regulation of BOK overexpression-induced cell death*

Analysing the influence of BCL-2 in BOK overexpression-induced cell death, knockdown/knockout of BCL-2 promoted BOK overexpression-induced apoptosis (Figure 28). Consistently, BOK overexpression caused CytC release which was inhibited by BCL-2 co-expression (Figure 29). Apoptosis induction by BOK overexpression is the long-known basis of BOK's pro-apoptotic character (413). However, data on BOK-induced cell death are interpreted controversially since BOK's mode of action itself and dependency on BAX/BAK for cell death induction is still controversial. Some studies confirm a BAX/BAK-independent role of BOK as a pore-forming effector which implicates that cell death is caused by CytC release from mitochondrial BOK pores (158–161). Others report a role of BOK upstream of BAX and BAK postulating that BOK overexpression induces BAX/BAK pore formation (157, 163). In addition, recent insights revealed that BOK can induce apoptosis by mediating pro-apoptotic Ca<sup>2+</sup> flux into mitochondria by binding to IP3R receptors (167). Major mitochondrial Ca<sup>2+</sup> influx leads to formation of the permeability transitions pore (PTP), a large conductance channel in the mitochondrial inner membrane (MIM) which's composition is still controversial. In addition, mitochondrial Ca<sup>2+</sup> influx disrupts the respiratory chain, for example, by Ca<sup>2+</sup>-dependent oxidation of CL leading to disintegration of respiratory chain complex II (414).

Both PTP and damage in the respiratory chain cause loss of  $\Delta\Psi_m$ , release of CytC and cell death (reviewed in (415)). Thus,  $Ca^{2+}$ -dependent cell death represents a third mechanism by which BOK induces apoptosis. Interestingly, inhibition of BOK-induced apoptosis by BCL-2 was not found in literature. On the contrary, many studies postulated that BOK pro-apoptotic activity is not regulated by any anti-apoptotic Bcl-2 protein (160, 161, 413). Both HEK293 and MCF-7 cells used for BOK overexpression in Figure 28 and Figure 29 express detectable levels of BAX and BAK (Supplementary Figure S1A) so that involvement of BAX and BAK in BOK overexpression-induced cell death cannot be ruled out. Accordingly, it is possible that BCL-2 binds and inhibits BAX and BAK to attenuate cell death independent of direct interaction with BOK. On the other hand, considering the possibility of BAX/BAK-independent cell death induction by BOK, cell death inhibition by BCL-2 is consistent with cell death regulation by direct interaction of BOK and BCL-2 via the TMD.

Further trying to pinpoint the TMD as the decisive regulatory feature, cell death was analysed after overexpression of BOK TMD chimeras carrying TMDs of BAX or BAK. In line with the previously observed MOM-targeting, BAX-TMD and BAK-TMD expectedly targeted BOK TMD chimeras to mitochondria (Figure 30). In HEK293 as well as DU145 cells, BOK<sup>BAX-TMD</sup> was more potent in inducing cell death than WT BOK, while BOK<sup>BAK-TMD</sup> induced cell death comparable to WT BOK (Figure 31A, B). Since Western Blot analysis of DU145 cells revealed increased levels of BOK<sup>BAX-TMD</sup> compared to WT BOK or BOK<sup>BAK-TMD</sup> (Figure 31D, Supplementary Figure S10D), BAX-TMD or mitochondrial localisation might stabilise BOK. In accordance, densitometry of PARP cleavage and EGFP signal (reflecting BOK abundance) resulted in a lower cPARP/EGFP ratio (reflecting cell death/BOK molecule) for BOK<sup>BAX-TMD</sup> compared to WT BOK (Figure 31E). Thus, increased pro-apoptotic activity of BOK<sup>BAX-TMD</sup> might be based on its increased abundance. Stabilisation, however, should be confirmed with additional experiments such as cycloheximide chase assays. Intriguingly, BCL-2-mediated inhibition of BOK overexpression-induced cell death was abolished for BOK<sup>BAX-TMD</sup>, but not BOK<sup>BAK-TMD</sup> (Figure 31B-E). Although this finding provides evidence that inhibition of BOK by BCL-2 is TMD-dependent, it remains elusive why cell death inhibition by BCL-2 is blocked for BOK<sup>BAX-TMD</sup>. As discussed for BAX TMD chimeras (4.3.1) and mutants (4.3.3.1), BAX-TMD is vital for BAX inhibition and retrotranslocation by BCL-2.

In line with TMD-TMD interaction of BAX and BCL-2 found by Andreu-Fernández *et al.* (171), presence of BAX-TMD in BOK should facilitate, not abrogate, inhibition by BCL-2. On the other hand, interaction of BAX- and BCL-2-TMD was not found with the NanoBiT assay (Figure 12) consistent with abolished inhibition of BOK<sup>BAX-TMD</sup> by BCL-2. However, following this line of reasoning, inhibition of BOK<sup>BAK-TMD</sup> by BCL-2 is inconclusive since also BAK-TMD did not interact with BCL-2-TMD in the NanoBiT assay (Figure 13). In addition, cell death induction by BAK TMD chimeras suggested a TMD-independent inhibition of BAK by BCL-2 (Figure 25). Given these contradictions, it could be hypothesized that inhibition of BOK is not solely dependent on direct interaction of BOK-TMD and BCL-2-TMD. DU145 cells are BAX-deficient, but still express visible amounts of BAK (Supplementary Figure S1A). Hence, detected cell death could be BAK-dependent which can be inhibited by direct binding of BCL-2 to BAK (151). Nevertheless, if BOK<sup>BAX-TMD</sup> overexpression induced BAK-dependent cell death it would be expected to be blocked by BCL-2 similar to WT BOK which was not the case (Figure 31B-E). Therefore, BAK dependency of BOK-induced cell death cannot be fully excluded but is highly unlikely. However, it cannot be ruled out that TMD exchange in BOK influences cell death inhibition by BCL-2 independent of TMD interaction between BOK and BCL-2 since TMD exchange in BOK could alter interaction of BOK with BAK and other (Bcl-2) proteins like MCL-1 which was recently reported to interact with BOK via the TMD to regulate cell death (333).

Both BOK and BCL-2 bind IP3R channels in the ER via their BH4 motif at different sites (AAs 1389 – 1408 for BCL-2 BH4 and AA ~1900 for BOK BH4) (165, 174). At least in the case of BCL-2 additional binding of the TMD to IP3R's Ct domain (AAs 2512 – 2749) is necessary to inhibit IP3R-mediated Ca<sup>2+</sup> release (337). In contrast, BOK promotes pro-apoptotic Ca<sup>2+</sup> release from IP3R to mitochondria and simultaneously facilitates formations of MAMs through IP3R complexation (167). Therefore, competitive binding of BOK and BCL-2 to IP3Rs could represent another possible mechanism explaining TMD-dependent inhibition of BOK-induced cell death by BCL-2. The opposing roles in apoptosis of BOK and BCL-2 are reflected in their IP3R binding-dependent functions in Ca<sup>2+</sup> signalling. Consequently, it seems conclusive that both proteins compete for IP3R binding to regulate Ca<sup>2+</sup> release and apoptosis. Assuming a similar role of the BOK-TMD in IP3R binding as BCL-2-TMD, the TMD sequence might be a key feature of competitive binding.

Along these lines, displacement of BOK by BCL-2 from IP3Rs in a TMD-dependent manner would contribute to the observed inhibition of BOK-induced cell death. Furthermore, TMD exchange in BOK to BAX-TMD might hamper displacement from IP3Rs leading to the observed abolished inhibition by BCL-2. Although mitochondrial localisation of BOK<sup>BAX-TMD</sup> and BOK<sup>BAK-TMD</sup> (Figure 30) might speak against this theory, BOK<sup>BAX-TMD</sup> and BOK<sup>BAK-TMD</sup> could still be localised to MAMs in which BOK evidently binds to IP3Rs to facilitate mitochondrial Ca<sup>2+</sup> influx (167). Moreover, BAX/BAK-deficient cells were found more sensitive to IP3 activation resulting in reduced Ca<sup>2+</sup> amounts in the ER and a lower pro-apoptotic burden by Ca<sup>2+</sup> influx to mitochondria (416) suggesting overlapping functions of BAX, BAK and BOK at the ER. Thus, TMD exchange in BOK to BAX-TMD and BAK-TMD not necessarily interferes with BOK's function at the ER such as binding to IP3Rs. Also, IP3R regulation by other Bcl-2 proteins such as BCL-XL and MCL-1 supports the role of IP3Rs as a central hub for Bcl-2 interactions in addition to the MOM (203, 417). However, additional experiments are needed to consolidate this hypothesis. TMD-dependent binding of BOK to IP3Rs and reduced interaction of BOK with IP3Rs upon presence of BCL-2 could be analysed using methods such as immunoprecipitation or proximity ligation assays. More importantly, direct detection of subcellular Ca<sup>2+</sup> pools might reveal a contribution to the cell death in the here presented experimental settings.

Additionally, exchange of the TMD in BOK to cb5-TMD and in BCL-2 to TOM5-TMD both impaired inhibition of BOK overexpression-induced cell death by BCL-2 confirming the dependency of cell death inhibition on both BOK- and BCL-2-TMD (Figure 31G, H). Results of both TMD chimeras corroborate the ER as the main site for BOK pro-apoptotic activity, since BOK<sup>cb5-TMD</sup> is localised to the ER and BCL-2<sup>TOM5-TMD</sup> to mitochondria without notable colocalisation with BOK at the ER (Figure 27). The latter might explain why BCL-2<sup>TOM5-TMD</sup> does not inhibit BOK overexpression-induced cell death. Of course, cell death induced by BOK pore formation in mitochondria cannot be ruled out either since BOK<sup>BAX-TMD</sup> and BOK<sup>BAK-TMD</sup> mainly localised to mitochondria (Figure 30). As studies postulated proteasomal degradation of BOK via the ERAD pathway to be decisive for BOK regulation (161, 165) BOK pore formation at mitochondria might be sensitive to a certain threshold of BOK expression. Supported by the observed increase on the protein level after the TMD exchange to BAX-TMD (Figure 31D, Supplementary Figure S10E) the BOK-TMD might be vital for BOK stability in line with degradation-dependent regulation of BOK.

A putative increase in stability for BOK<sup>BAX-TMD</sup> might not only enhance pore formation by BOK leading to the observed increase in cell death, but also exhaust inhibitory capacity of BCL-2. Thus, the role of the TMD interaction of BOK and BCL-2 at the ER would comprise the sequestration of BOK at the ER to avoid BOK shuttling to MOM and mitochondrial pore formation. The impact of the TMD exchange in BOK<sup>cb5-TMD</sup> partially disagrees with this model since BOK<sup>cb5-TMD</sup> is neither more toxic than WT BOK nor expected to localise to mitochondria (Figure 31G). However, how BOK is shuttled to mitochondria is yet to be defined and might not depend on the TMD. Instead, abolished TMD interaction with BCL-2 could explain impaired inhibition of BOK<sup>cb5-TMD</sup>. In the case of BCL-2<sup>TOM5-TMD</sup>, BCL-2 might be incapable to tether BOK to the ER to avoid BOK pore formation as it is constitutively localised to mitochondria. Here, investigation of the TOM20-dependent BCL-2 translocation between ER and mitochondria might be interesting with respect to the localisation of BCL-2 TMD chimeras (173).

Taken together, experiments with TMD chimeras corroborate that the regulation of BOK overexpression-induced cell death by BCL-2 is dictated by their TMDs. However, since acquired cell death data are not fully consistent, the underlying mechanism cannot be resolved into detail. In the recent years, light was shed on multiple additional functions of BOK of which most remain poorly understood. For example, BOK was found as a positive regulator of uridine metabolism controlling sensitivity to 5-fluorouracil-induced cell death (418). Also, an involvement of BOK in membrane modulation such as mitochondrial fission and fusion (168) or MAM organization was reported (167). Since TMD exchange in BOK likely influences various aspects of BOK function, especially those at membranes, TMD exchange in BOK could modulate yet unrecognised interactions and aspects of BOK function.

#### *4.3.4.3 Molecular dynamics simulations uncover molecular details of TMD interaction*

MD simulations propose formation of stable BOK-/BOK-TMD homodimers as well as flexible BOK-/BCL-2-TMD heterodimers (Figure 32A-D). MD simulations indicated a tendency of BOK-TMD and BCL-2-TMD to form higher order oligomers which was confirmed by formation of stable heterotetramers using two BOK-TMDs and two BCL-2-TMDs (Figure 32E). In the same simulations, also formation of trimers was observed to a lesser extent (Supplementary Figure S11A,B).

Formation of stable homodimers is in line with preferential homotypic interaction of BOK-TMDs in the NanoBiT interaction assay (Figure 11). Consequently, BOK TMD dimerization could represent an important step in BOK pore formation similar to BAX and BAK (331, 332). Also, Lucendo *et al.* postulate stable formation of BOK-TMD homodimers in MD simulations (333). Involvement of AA residues V191, C195, R199 and K202 in homodimerization coincides with the here acquired *in silico* data. However, a total of 10 non-consistent AA residues at the homodimer interface indicates that BOK-TMD homodimerization allows at least some degree of flexibility. Of note, simulations by Lucendo *et al.* were performed in a generic phospholipid bilayer that is substantially different from the lipid composition in simulations presented here. The ER-specific lipid composition derived from Scrima *et al.* (357) which was used here might explain the differences in BOK dimer formation compared to Lucendo *et al.* Strikingly, formation of heterodimers, -trimers and -tetramers provides evidence for the TMD interaction between BOK-TMD and BCL-2-TMD at the molecular level. Participation of multiple AAs in heterodimerization (Figure 32D) and observed conformational flexibility (reflected by RMSD values in Figure 32F) already suggested formation of higher order oligomers as previously described, for example, for oligomerisation of synaptobrevin (368). Relative stability of the tetramers compared to dimers and trimers is even higher than anticipated by the RMSD which intrinsically increases with the size of the assessed structure (419). The likewise increased flexibility of formed trimers (Figure 32F) indicates that BOK-/BCL-2-TMD dimers and trimers are less stable intermediate structures. Thus, BCL-2 recruitment to BOK or BOK dimers via the TMD at the ER might constitute a mechanism of inhibiting BOK oligomerisation and preventing BOK pore formation in the MOM. Also, the tight packing of BOK-/BCL-2-TMD tetramers reflected by the increase in relative hidden protein surface (Figure 32G) further supports stability of such heterooligomeric structures.

Membrane lipids are not only vital components for Bcl-2 protein function and interactions, but also well known to influence TMD-TMD interaction (275–277). For Bcl-2 protein interaction, Shamas-Din *et al.* demonstrated that membranes with high content of cholesterol hindered BAX membrane insertion and oligomerisation (411) in line with depletion of cholesterol in the BOK-/BCL-2-TMD tetramer (Supplementary Figure S11C). Moreover, negatively charged CL regulates specific targeting of tBID to the MOM and is required for BAX insertion and oligomerization, while it preferentially interacts with positively charged residues (420, 421).

Similar to the role of CL in BAX oligomerisation, enrichment of negatively charged POPI at positively charged residues in BOK-/BCL-2-TMD tetramers (R199<sup>BOK</sup>, K202<sup>BOK</sup> and K218<sup>BCL-2</sup>) could facilitate oligomerisation (Supplementary Figure S11C). Positively charged residues were involved in TMD-TMD interaction, namely R199<sup>BOK</sup> and K202<sup>BOK</sup>. Interestingly, in rare cases positively charged residues can represent important intermolecular locks in helix-helix interaction (269). However, mutation of K202<sup>BOK</sup> to alanine did neither disturb colocalisation with BCL-2 nor influenced BOK inhibition by BCL-2 (Supplementary Figure S12). Moreover, MD simulations suggested that interaction of BOK-TMD and BCL-2-TMD depends on multiple residues stressing a more systematic approach to reveal all vital residues for interaction. Thus, systematic mutations of residues involved in TMD-TMD interaction could provide evidence about the importance of residues for the interaction. More often, other, mostly small and hydrophobic, residues participate in distinct interaction motifs for helix-helix interaction such as glycine, alanine, serine and threonine (reviewed in (270, 271)). Some of these motifs are indeed present in the BCL-2-TMD, namely the VI<sub>4</sub> (pos. 227 - 230) and GG<sub>4</sub> (pos. 234 – 237) motif. Indeed, AAs most often identified in the TMD-TMD interface of BOK-/BCL-2-TMD heterodimers are found in the region of the VI<sub>4</sub> motif (e.g. L223, V226 and I230) rendering the motif a hot candidate for further mutation studies. Although BOK-TMD does not harbour common interaction motifs, it contains an intriguingly high number of phenylalanine residues (F197, F200, F205, F206). Indeed, some of the phenylalanines were frequently found at the interaction interface of BOK-/BOK-TMD homodimers and BOK-/BCL-2-TMD heterodimers (F205, F206). Interestingly, phenylalanine evidently promotes interactions of TMDs in certain cases, for example, in proximity to GxxxG motifs or the TMD of syndecans (422, 423). Hence, phenylalanines in BOK-TMD might be a vital factor for TMD oligomerisation worth to be studied with mutation experiments *in vitro* or *in silico*.

#### 4.3.4.4 Role of BCL-2 and BOK interplay in ER stress

To investigate the functional link between BOK-/BCL-2-TMD interaction and BOK-dependent apoptosis signalling, Hela DKO cells were incubated with the proteasome inhibitor Bortezomib (Figure 37A-C). Bortezomib-induced cell death was shown to be partially dependent on the presence of BOK (Figure 37A), while absence of BCL-2 exacerbated Bortezomib toxicity (Figure 37B). Proteasome inhibition by Bortezomib has been linked to induction of ER-stress and UPR (424).



Indeed, multiple studies already recognised a role of BOK in ER stress signalling: Carpio and coworkers observed attenuated ER stress response in BOK-deficient cells after incubation with several ER stress-inducing drugs including Bortezomib (163). BOK stabilisation as a result of proteasome inhibition was postulated by Llambi *et al.* who concluded that proteasomal degradation of BOK controls pro-apoptotic activity of constitutively active BOK (161). By contrast, Western blot analysis of BOK in Hela DKO cells did not indicate an increase in BOK level after incubation with Bortezomib (Supplementary Figure S14D). Thus, the role of BOK in ER stress might be more versatile than its regulation via the ERAD pathway. The reports of BOK binding to IP3Rs and thereby regulating mitochondrial  $\text{Ca}^{2+}$  influx to mitochondria at MAMs is another important link of BOK to ER-stress since  $\text{Ca}^{2+}$  regulates ER stress signalling, for example, as a co-factor of chaperones (425). Recently, Walter *et al.* demonstrated that presence of BOK promotes motility of the ER chaperone GRP78 enhancing all three branches of the ER stress pathway via PERK, ATF6 and IRE1 (166). However, Bortezomib-induced cell death was reduced but not blocked by BOK knockdown. Likewise, knockdown of BCL-2 only slightly increased Bortezomib-induced cell death (Figure 37A, B). Since Bortezomib indirectly induces ER stress via proteasome inhibition, it is likely that cell death is promoted by additional pathways independent of BOK, for example, involving pro-apoptotic proteins regulated by ubiquitination and degradation such as stabilisation of BH3-only protein NOXA (426). However, siRNA-mediated knockdown of BOK could have been incomplete as observed for BCL-2 in Figure 28B. Therefore, Western Blot analysis of BOK levels after knockdown is the next mandatory step to analyse BOK dependency of Bortezomib-induced cell death. Interestingly, inhibition of Bortezomib-induced cell death by BCL-2 was not dependent on interaction ability via its BH3 motif as demonstrated by specific inhibition using ABT-199 (Figure 37C). Thus, the anti-apoptotic effect of BCL-2 on Bortezomib-induced cell death in Hela DKO cells is not based on BH3:groove interaction of BCL-2 suggesting importance of a secondary interaction interface, for example, the TMD.

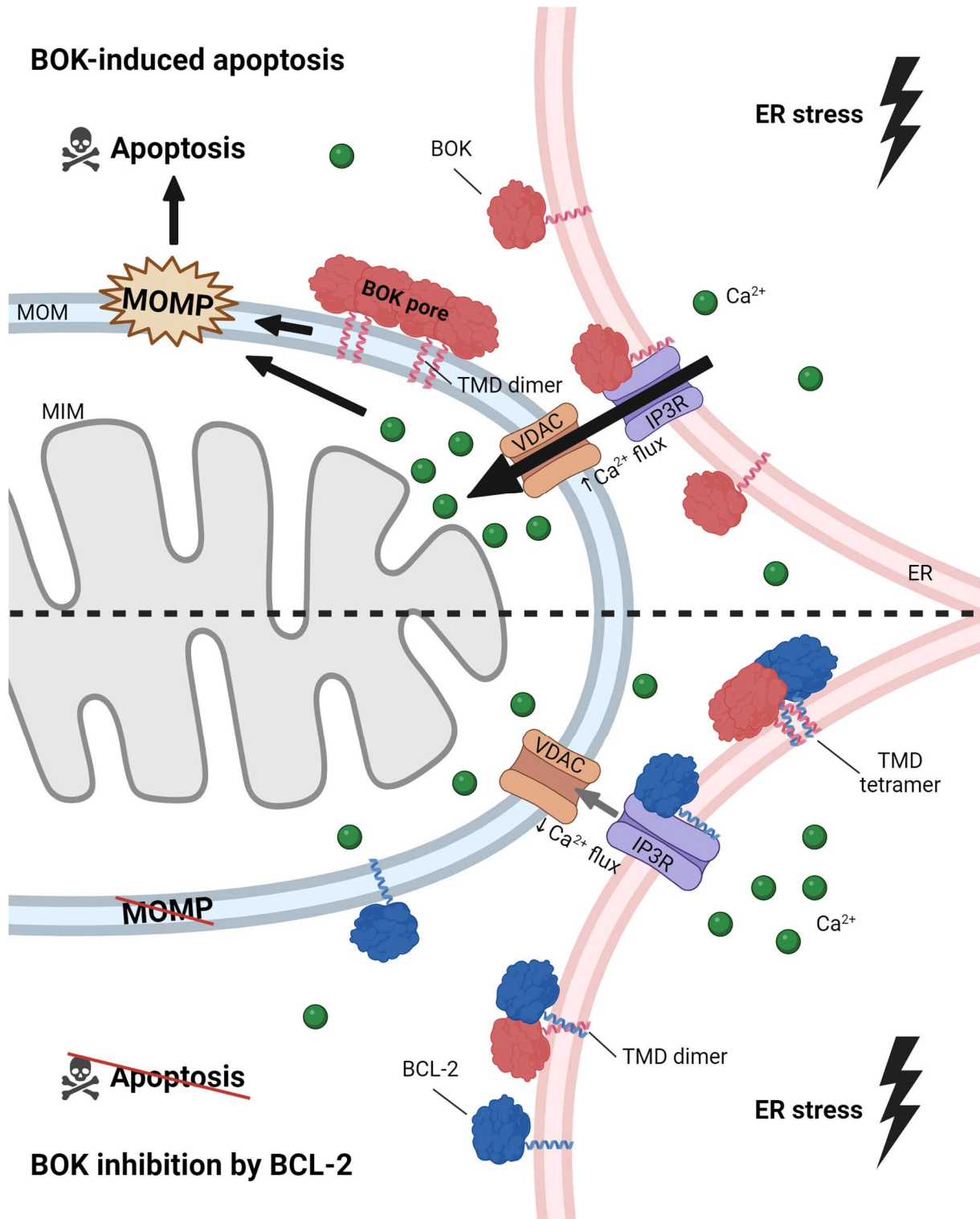
Interestingly, after knockdown of BOK in HeLa cells time lapse imaging revealed reduced cell death of HeLa (empty vector) cells incubated with Tunicamycin (TM) compared to control cells confirming an essential function of BOK in TM-induced cell death (Figure 37D, E). TM effectively blocks protein N-glycosylation in the ER leading to accumulation of misfolded proteins in the ER lumen and, hence, triggers the UPR and ER stress (reviewed in (373)).

Since aberrant glycosylation frequently occurs in cancer (427), TM's anti-cancer potential which can sensitize cancer cells to apoptosis could largely depend on BOK. This is in line with results from Walter *et al.* rendering BOK vital for a TM-dependent ER stress response (166). In contrast, time-lapse imaging after knockdown of BCL-2 showed a slight, but insignificant, increase in cell death upon TM incubation compared to control cells (Figure 37D, E). Since the deviation in cell death increased towards later time points, BCL-2 knockdown could enhance TM-induced cell death significantly at time points beyond the analysed time scale of 40 h. Opposing roles of BOK and BCL-2 in TM-dependent ER stress and cell death would then again indicate that the regulatory role of their TMD interaction is situated at the ER, more precisely in ER stress signalling. However, since time-lapse imaging in Figure 37 was only performed once in technical triplicates experiments should be repeated to consolidate obtained results. Furthermore, massively reduced TM sensitivity in BAX/BAK-deficient HeLa DKO cells (Supplementary Figure S14C) suggest a clear BAX/BAK-dependency of TM-induced cell death in HeLa (empty vector) cells used in Figure 37D,E. A possible reason for BAX/BAK-dependency of BOK-mediated cell death in HeLa DKO cells could be low endogenous levels of BOK too low for efficient cell death induction independent of BAX and BAK. Nevertheless, BAX/BAK-dependency of TM-induced cell death further complicates to draw conclusions about interaction of BOK and BCL-2 since cell death inhibition could also be based on interaction of BCL-2 with BAX and BAK. Thus, analysing TM-induced cell death in BAX/BAK-deficient cells in presence of BOK (or BCL-2) TMD chimeras could further unravel the functional role of the BOK-/BCL-2-TMD interaction in ER stress signalling.

In conclusion, the functional investigation of TMD interaction between BOK and BCL-2 in this thesis revealed not only a regulatory function of BCL-2 in cell death induced by BOK overexpression, but also demonstrates dependency on the TMD sequences of both proteins. Supported by MD simulations, TMD-dependent sequestration of BOK by BCL-2 likely takes place in form of higher order oligomers in the ER membrane. Accordingly, TMD-dependent BOK sequestration by BCL-2 could influence apoptosis at the level of BOK pore formation in the MOM or IP3R-binding and Ca<sup>2+</sup> signalling at the ER as summarized in Figure 38. However, physiological importance and a detailed mechanism needs further elaboration in future studies. The opposing roles of BOK and BCL-2 on ER-stress-induced cell death indicate that modulation of apoptotic signalling by interaction of their TMDs might be crucial in an ER-stress context.

In the bigger picture, fine-tuning of apoptosis by the BOK-/BCL-2-TMD interaction could influence therapies targeted on the ER signalling pathways and therapeutic outcomes of such. For instance, FDA-approved Bortezomib (for treatment of multiple myeloma/mantle cell lymphoma, (428)), valproic acid (epilepsy, (429)) or arsenic trioxide (acute promyelocytic leukaemia, (430)) all induce ER stress and, thus, might be affected by BOK-dependent alterations in ER stress signalling. Further studies, therefore, should focus on the mechanistic details of the BOK-/BCL-2-TMD interaction to further elucidate its role in ER stress signalling. Detection of  $\text{Ca}^{2+}$  flux from the ER, live-cell imaging of BOK and BCL-2 molecules or MD simulations of BOK pore-forming behaviour upon apoptosis induction are just a few examples how the TMD-dependency of BOK and BCL-2 functions could be further enlightened.

Although the debate about the physiological significance of BOK has been ongoing for decades, a growing body of evidence reveals that BOK is indeed performing increasingly important and versatile cellular functions including regulation of uridine metabolism (418), control of mitochondrial dynamics (168) and promotion of apoptosis via  $\text{Ca}^{2+}$  signalling and ER stress (163). With regard to recent events in history, even a role of BOK in mediating cell death induced by the SARS-CoV-2 membrane protein was published representing another clear indication that the role of BOK in the context of disease is far more vital than previously anticipated (431). Along these lines, a role of BOK in cancer has long been neglected despite frequent deletion of *BOK* in cancer (156). In the meantime, however, some findings point to a substantial influence of BOK in oncogenesis and promote BOK as a worthwhile target of anti-cancer therapy. For example, while BOK facilitates tumour progression in *KRAS*-driven lung cancer (432), BOK was assigned a tumour suppressor role in non-small cell lung cancer by inhibiting epithelial-to-mesenchymal transition (433). With regard to the findings in this thesis, interaction of BOK and BCL-2 via the TMD, therefore, might be an important lever for cancer cells to regulate BOK function, for example, by upregulation of BCL-2. Similar to pharmacological targeting of the BH3:groove interaction with BH3 mimetics, pharmacological targeting of the BOK-/BCL-2-TMD interaction might offer a novel tool, for example, to increase pro-apoptotic activity of BOK in cancer. Thus, BOK-TMD and BCL-2-TMD interaction might be another important fragment of the newly identified and yet uncharacterised roles of BOK.



**Figure 38: Summary of hypothesized BOK mode of action and inhibition by BCL-2 via the TMD.**

Upper panel shows postulated pro-apoptotic functions of BOK. Lower panel shows possible regulation of BOK-induced cell death by TMD interaction with BCL-2. MOM = Mitochondrial outer membrane. MOMP = MOM permeabilization. MIM = Mitochondrial inner membrane. Created with biorender.com.

#### 4.3.5 TMD interaction of Bcl-2 proteins – a new drug target?

Small-molecule inhibitors counteracting BH3:groove interaction of Bcl-2 proteins, BH3 mimetics, were successfully established as highly-effective anti-cancer drugs spearheaded by the FDA-approved specific inhibitor of BCL-2, Venetoclax/ABT-199 (434). Thus, targeting of Bcl-2 protein interactions is an important strategy to counteract the anti-apoptotic defence of cancers. However, the increasing use of BH3 mimetics is naturally accompanied by emerging resistance mechanisms since therapy inevitably creates a bottleneck for cancer cells resistant to BH3 mimetic-induced apoptosis. Resistance-mechanisms are versatile including, for example, resistance-promoting mutations or downregulation of pro-apoptotic proteins (435–437). Thus, new ways to target cancer cells are all the more important.

The vast majority of therapeutics binds proteins in solvated regions outside the lipid bilayer. In fact, presence of a solvent-accessible hydrophobic pocket is classically considered a hallmark of druggability so that drug design categorically excluded druggability of protein TMDs (reviewed in (438)). In recent years, new technologies substantially improved the possibilities to analyse TMD regions for druggability. For example, methods like cryoelectron microscopy enable structural analysis of transmembrane regions in their natural environment and facilitate acquisition of underrepresented membrane protein structures (439). Furthermore, novel computational approaches refine prediction of TMD structures such as the Evolutionary-guided Fold and Dock of TransMembrane proteins (EFDOCK-TM) tool (440). EFDOCK-TM could generate more detailed models, for example, of the BOK-/BCL-2-TMD interaction serving as a basis for drug development targeting the interaction. Based on cryoelectron microscopy and *in silico* structures computational tools like CHAMP promote rational design of molecules antagonizing TMD interactions (441). Hence, given a detailed model of two interacting TMDs CHAMP might be able to predict molecules counteracting the interaction – drug candidates, which then could be analysed *in vitro*. Some rare examples like the FDA-approved ivacaftor already demonstrate that also TMDs embedded in membranes are targetable by small-molecule drugs: Ivacaftor promotes the ion flux of mutant cystic fibrosis transmembrane conductance regulator (CFTRs) by binding at the protein-lipid interface to the TMD region of CFTR (442).

On the other hand, TMD targeting not necessarily needs to take place in membranes since, for example, this thesis corroborates a vital auto-inhibitory role of the BAX-TMD (as discussed in 4.3.1). Development of drugs which directly activate BAX, thus, inherently involves removal of the BAX-TMD from the protein core. Indeed, several molecules directly activating BAX are currently under investigation as a promising strategy to treat chemo- and radioresistant cancers (reviewed in (443)). Also, other findings in this thesis promote the TMD as a potential drug target as results indicate interaction of anti-apoptotic Bcl-2-like proteins such as BCL-2, BCL-XL and BCL-W via the TMD (discussed in 4.2.2, 4.3.4). Thus, it is possible that the TMD interactions of Bcl-2 proteins are druggable targets for cancer therapy, for example, by use of anti-TMD peptides (444). Anti-TMD peptides are peptides which specifically bind to a certain TMD interfering with TMD interaction. Based on the insights into the Bcl-2 TMD interactome presented here, for example, the identification of an apoptosis-regulating BOK-TMD and BCL-2-TMD interaction (discussed in 4.3.4), such anti-TMD peptides could be developed to specifically interfere with TMD interaction, for example, releasing BOK from BCL-2 to promote apoptosis. Therefore, development of small-molecule drugs based on anti-TMD peptides could be valuable to abolish apoptosis regulation and enhance apoptosis in cancer cells. Similar approaches could target TMD interactions of BCL-XL or BCL-W with pro-apoptotic Bcl-2 proteins. Of course, further investigations are necessary to define the physiological context in which such a therapy would be promising. That said, systematic data collection of Bcl-2 protein copy number and expression level in cancer samples as well as analysis of mutations in Bcl 2 TMDs might be valuable biomarkers for future clinical interventions.

BH3 mimetics were originally designed based on BH3 peptides of BH3-only proteins which bind the hydrophobic groove of anti-apoptotic Bcl-2 proteins (244, 248). However, recent advances reveal that at least some BH3-only proteins such as BIM and PUMA bind their targets not only via the BH3 motif. In fact, high affinity binding of BIM and PUMA is ensured by the so-called 'double-bolt' locking including both BH3 motif and TMD interaction interface (334–336). Thus, mimicking the mode of action of these proteins as precisely as possible to maximise specificity and efficacy, inevitably leads to a drug design that includes TMD-TMD interaction. Therefore, findings in this thesis are expected to contribute to the development of a 2<sup>nd</sup> generation of BH3-mimetics capable of BH3-TMD 'double-bolt' locking increasing specificity and efficacy.

## 5 Conclusion

The Bcl-2 interaction network is fundamental for our understanding of apoptosis dysregulation in diseases such as cancer. This intricate interaction network is defined by BH3:groove interactions which instigated the development of highly-specific anti-cancer drugs, while the regulatory impact of the TMD as a secondary interaction site remained in the dark. In this thesis, new insights into the understudied Bcl-2 TMD interactome were brought to light creating the basis for further in-depth studies how TMD-TMD interactions fine-tune the Bcl-2 interaction network and apoptosis signalling.

The NanoBiT assay developed to identify Bcl-2 TMD interactions could become a pivotal tool for discovery and investigation of TMD interactions in living cells given verification by other state-of-the-art assays. Several yet unidentified interactions were revealed such as the interaction of BOK-TMD and BCL-2-TMD at the ER. Functional Investigation of Bcl-2 TMD chimeras highlighted individual roles of the TMD in BAX and BAK regulation, while TMD-dependent inhibition of BOK by BCL-2 points out an intriguing new aspect of BOK regulation. Nonetheless, the unveiled TMD interactions are only the first step to the elucidation of the full spectrum of Bcl-2 TMD interactions. Advances in this thesis revealed several paths which could be pursued in future studies such as TMD interactions of BCL-XL and BCL-W. Also, TMD interactions of BH3-only proteins will be especially interesting in light of the recently reported ‘double-bolt’ locking of BIM and PUMA with simultaneous interaction via BH3 region and TMD (334–336). In addition, the functional impact of TMD mutations in BAX and BCL-2 characterised here outlines a potential of TMD mutation and modification to regulate apoptosis and contribute to apoptosis dysregulation in disease. Along these lines, TMD mutations should be considered as therapeutic markers and further evaluated to predict their influence on resistance mechanisms. Concludingly, the presented findings stress the need for a holistic view on the Bcl-2 interaction network including the TMD interactome. Especially for disease-specific targeting of Bcl-2 proteins the TMD interactome harbours a transformative potential yet to be unlocked, for example, by creation of anti-cancer drugs capable of ‘double-bolt’-locking increasing binding specificity and therapeutic effect. Thus, enlightenment of the TMD interactome will not only enhance our understanding of the multifaceted regulation of Bcl-2 proteins but also open new avenues for development of specifically tailored therapeutic solutions in diseases marked by apoptosis dysregulation.

## 6 References

1. Y. Fuchs, H. Steller, Live to die another way: modes of programmed cell death and the signals emanating from dying cells. *Nat Rev Mol Cell Biol* **16**, 329–344 (2015).
2. J. F. Kerr, A. H. Wyllie, A. R. Currie, Apoptosis: a basic biological phenomenon with wide-ranging implications in tissue kinetics. *British journal of cancer* **26**, 239–257 (1972).
3. I. K. H. Poon, C. D. Lucas, A. G. Rossi, K. S. Ravichandran, Apoptotic cell clearance: basic biology and therapeutic potential. *Nature reviews. Immunology* **14**, 166–180 (2014).
4. Z. A. Radi, Z. S. Stewart, S. P. O'Neil, Accidental and Programmed Cell Death in Investigative and Toxicologic Pathology. *Current protocols in toxicology* **76**, e51 (2018).
5. L. Galluzzi, I. Vitale, S. A. Aaronson, J. M. Abrams, D. Adam, P. Agostinis, E. S. Alnemri, L. Altucci, I. Amelio, D. W. Andrews, et al., Molecular mechanisms of cell death: recommendations of the Nomenclature Committee on Cell Death 2018. *Cell Death Differ* **25**, 486–541 (2018).
6. X. Song, S. Zhu, Y. Xie, J. Liu, L. Sun, D. Zeng, P. Wang, X. Ma, G. Kroemer, D. L. Bartlett, et al., JTC801 Induces pH-dependent Death Specifically in Cancer Cells and Slows Growth of Tumors in Mice. *Gastroenterology* **154**, 1480–1493 (2018).
7. P. Tsvetkov, S. Coy, B. Petrova, M. Dreishpoon, A. Verma, M. Abdusamad, J. Rossen, L. Joesch-Cohen, R. Humeidi, R. D. Spangler, et al., Copper induces cell death by targeting lipoylated TCA cycle proteins. *Science (New York, N.Y.)* **375**, 1254–1261 (2022).
8. R. K. S. Malireddi, S. Kesavardhana, T.-D. Kanneganti, ZBP1 and TAK1: Master Regulators of NLRP3 Inflammasome/Pyroptosis, Apoptosis, and Necroptosis (PAN-optosis). *Front. Cell. Infect. Microbiol.* **9**, 406 (2019).
9. O. Julien, J. A. Wells, Caspases and their substrates. *Cell Death Differ* **24**, 1380–1389 (2017).
10. G. Ichim, S. W. G. Tait, A fate worse than death: apoptosis as an oncogenic process. *Nature reviews. Cancer* **16**, 539–548 (2016).
11. S. J. Martin, D. M. Finucane, G. P. Amarante-Mendes, G. A. O'Brien, D. R. Green, Phosphatidylserine externalization during CD95-induced apoptosis of cells and cytoplasts requires ICE/CED-3 protease activity. *The Journal of biological chemistry* **271**, 28753–28756 (1996).
12. S. Nagata, DNA degradation in development and programmed cell death. *Annual review of immunology* **23**, 853–875 (2005).
13. S. H. Kaufmann, S. Desnoyers, Y. Ottaviano, N. E. Davidson, G. G. Poirier, Specific proteolytic cleavage of poly(ADP-ribose) polymerase: an early marker of chemotherapy-induced apoptosis. *Cancer research* **53**, 3976–3985 (1993).
14. G. Koopman, C. P. Reutelingsperger, G. A. Kuijten, R. M. Keehnen, S. T. Pals, M. H. van Oers, Annexin V for flow cytometric detection of phosphatidylserine expression on B cells undergoing apoptosis. *Blood* **84**, 1415–1420 (1994).
15. G. V. Chaitanya, A. J. Steven, P. P. Babu, PARP-1 cleavage fragments: signatures of cell-death proteases in neurodegeneration. *Cell Commun Signal* **8**, 31 (2010).



16. I. Vitale, F. Pietrocola, E. Guilbaud, S. A. Aaronson, J. M. Abrams, D. Adam, M. Agostini, P. Agostinis, E. S. Alnemri, L. Altucci, et al., Apoptotic cell death in disease-Current understanding of the NCCD 2023. *Cell death and differentiation* **30**, 1097–1154 (2023).
17. C. M. Zmasek, A. Godzik, Evolution of the animal apoptosis network. *Cold Spring Harbor Perspectives in Biology* **5**, a008649 (2013).
18. S. Pankow, C. Bamberger, The p53 tumor suppressor-like protein nvp63 mediates selective germ cell death in the sea anemone *Nematostella vectensis*. *PLOS ONE* **2**, e782 (2007).
19. A. Ashkenazi, V. M. Dixit, Death receptors: signaling and modulation. *Science (New York, N.Y.)* **281**, 1305–1308 (1998).
20. B. B. Aggarwal, S. C. Gupta, J. H. Kim, Historical perspectives on tumor necrosis factor and its superfamily: 25 years later, a golden journey. *Blood* **119**, 651–665 (2012).
21. M. Redza-Dutordoir, D. A. Averill-Bates, Activation of apoptosis signalling pathways by reactive oxygen species. *Biochimica et biophysica acta* **1863**, 2977–2992 (2016).
22. W. P. Roos, B. Kaina, DNA damage-induced cell death by apoptosis. *Trends in molecular medicine* **12**, 440–450 (2006).
23. R. Sano, J. C. Reed, ER stress-induced cell death mechanisms. *Biochimica et biophysica acta* **1833**, 3460–3470 (2013).
24. G. Brumatti, M. Salmanidis, P. G. Ekert, Crossing paths: interactions between the cell death machinery and growth factor survival signals. *Cellular and molecular life sciences : CMLS* **67**, 1619–1630 (2010).
25. K. Schleich, J. H. Buchbinder, S. Pietkiewicz, T. Kähne, U. Warnken, S. Öztürk, M. Schnölzer, M. Naumann, P. H. Krammer, I. N. Lavrik, Molecular architecture of the DED chains at the DISC: regulation of procaspase-8 activation by short DED proteins c-FLIP and procaspase-8 prodomain. *Cell Death Differ* **23**, 681–694 (2016).
26. N. Fricker, J. Beaudouin, P. Richter, R. Eils, P. H. Krammer, I. N. Lavrik, Model-based dissection of CD95 signaling dynamics reveals both a pro- and antiapoptotic role of c-FLIPL. *The Journal of Cell Biology* **190**, 377–389 (2010).
27. M. A. Hughes, I. R. Powley, R. Jukes-Jones, S. Horn, M. Feoktistova, L. Fairall, J. W. R. Schwabe, M. Leverkus, K. Cain, M. MacFarlane, Co-operative and Hierarchical Binding of c-FLIP and Caspase-8: A Unified Model Defines How c-FLIP Isoforms Differentially Control Cell Fate. *Molecular cell* **61**, 834–849 (2016).
28. Z. You, H. Ouyang, D. Lopatin, P. J. Polver, C. Y. Wang, Nuclear factor-kappa B-inducible death effector domain-containing protein suppresses tumor necrosis factor-mediated apoptosis by inhibiting caspase-8 activity. *The Journal of biological chemistry* **276**, 26398–26404 (2001).
29. H. Wajant, D. Siegmund, TNFR1 and TNFR2 in the Control of the Life and Death Balance of Macrophages. *Frontiers in Cell and Developmental Biology* **7**, 91 (2019).
30. P. Gough, I. A. Myles, Tumor Necrosis Factor Receptors: Pleiotropic Signaling Complexes and Their Differential Effects. *Frontiers in immunology* **11**, 585880 (2020).
31. H. Wajant, K. Pfizenmaier, P. Scheurich, Non-apoptotic Fas signaling. *Cytokine & Growth Factor Reviews* **14**, 53–66 (2003).
32. D. de Miguel, J. Lemke, A. Anel, H. Walczak, L. Martinez-Lostao, Onto better TRAILs for cancer treatment. *Cell Death Differ* **23**, 733–747 (2016).

33. M. Brisset, M. Grandin, A. Bernet, P. Mehlen, F. Hollande, Dependence receptors: new targets for cancer therapy. *EMBO Molecular Medicine* **13**, e14495 (2021).
34. J. Fombonne, P.-A. Bissey, C. Guix, R. Sadoul, C. Thibert, P. Mehlen, Patched dependence receptor triggers apoptosis through ubiquitination of caspase-9. *Proceedings of the National Academy of Sciences of the United States of America* **109**, 10510–10515 (2012).
35. H. Li, H. Zhu, C. J. Xu, J. Yuan, Cleavage of BID by caspase 8 mediates the mitochondrial damage in the Fas pathway of apoptosis. *Cell* **94**, 491–501 (1998).
36. P. Paoli, E. Giannoni, P. Chiarugi, Anoikis molecular pathways and its role in cancer progression. *Biochimica et biophysica acta* **1833**, 3481–3498 (2013).
37. A. Hafner, M. L. Bulyk, A. Jambhekar, G. Lahav, The multiple mechanisms that regulate p53 activity and cell fate. *Nat Rev Mol Cell Biol* **20**, 199–210 (2019).
38. H. Yamaguchi, H.-G. Wang, CHOP is involved in endoplasmic reticulum stress-induced apoptosis by enhancing DR5 expression in human carcinoma cells. *Journal of Biological Chemistry* **279**, 45495–45502 (2004).
39. H.-H. Choi, D.-M. Shin, G. Kang, K.-H. Kim, J. B. Park, G. M. Hur, H.-M. Lee, Y.-J. Lim, J.-K. Park, E.-K. Jo, et al., Endoplasmic reticulum stress response is involved in Mycobacterium tuberculosis protein ESAT-6-mediated apoptosis. *FEBS letters* **584**, 2445–2454 (2010).
40. J. Kale, E. J. Osterlund, D. W. Andrews, BCL-2 family proteins: changing partners in the dance towards death. *Cell death and differentiation* **25**, 65–80 (2018).
41. M. P. A. Luna-Vargas, J. E. Chipuk, Physiological and Pharmacological Control of BAK, BAX, and Beyond. *Trends in cell biology* **26**, 906–917 (2016).
42. T. C. Cheng, C. Hong, I. V. Akey, S. Yuan, C. W. Akey, A near atomic structure of the active human apoptosome. *eLife* **5** (2016).
43. C.-C. Wu, S. Lee, S. Malladi, M.-D. Chen, N. J. Mastrandrea, Z. Zhang, S. B. Bratton, The Apaf-1 apoptosome induces formation of caspase-9 homo- and heterodimers with distinct activities. *Nature communications* **7**, 13565 (2016).
44. Y. Li, M. Zhou, Q. Hu, X.-C. Bai, W. Huang, S. H. W. Scheres, Y. Shi, Mechanistic insights into caspase-9 activation by the structure of the apoptosome holoenzyme. *Proceedings of the National Academy of Sciences of the United States of America* **114**, 1542–1547 (2017).
45. F. L. Scott, J.-B. Denault, S. J. Riedl, H. Shin, M. Renatus, G. S. Salvesen, XIAP inhibits caspase-3 and -7 using two binding sites: evolutionarily conserved mechanism of IAPs. *The EMBO journal* **24**, 645–655 (2005).
46. T. V. Lee, Y. Fan, S. Wang, M. Srivastava, M. Broemer, P. Meier, A. Bergmann, Drosophila IAP1-mediated ubiquitylation controls activation of the initiator caspase DRONC independent of protein degradation. *PLoS genetics* **7**, e1002261 (2011).
47. E. Varfolomeev, T. Goncharov, A. V. Fedorova, J. N. Dynek, K. Zobel, K. Deshayes, W. J. Fairbrother, D. Vucic, c-IAP1 and c-IAP2 are critical mediators of tumor necrosis factor alpha (TNFalpha)-induced NF-kappaB activation. *The Journal of biological chemistry* **283**, 24295–24299 (2008).
48. C. Du, M. Fang, Y. Li, L. Li, X. Wang, Smac, a mitochondrial protein that promotes cytochrome c-dependent caspase activation by eliminating IAP inhibition. *Cell* **102**, 33–42 (2000).

49. A. M. Verhagen, P. G. Ekert, M. Pakusch, J. Silke, L. M. Connolly, G. E. Reid, R. L. Moritz, R. J. Simpson, D. L. Vaux, Identification of DIABLO, a mammalian protein that promotes apoptosis by binding to and antagonizing IAP proteins. *Cell* **102**, 43–53 (2000).
50. Y. Kushnareva, D. D. Newmeyer, Bioenergetics and cell death. *Annals of the New York Academy of Sciences* **1201**, 50–57 (2010).
51. Y. Wang, X. Ning, P. Gao, S. Wu, M. Sha, M. Lv, X. Zhou, J. Gao, R. Fang, G. Meng, et al., Inflammasome Activation Triggers Caspase-1-Mediated Cleavage of cGAS to Regulate Responses to DNA Virus Infection. *Immunity* **46**, 393–404 (2017).
52. X. Ning, Y. Wang, M. Jing, M. Sha, M. Lv, P. Gao, R. Zhang, X. Huang, J.-M. Feng, Z. Jiang, Apoptotic Caspases Suppress Type I Interferon Production via the Cleavage of cGAS, MAVS, and IRF3. *Molecular cell* **74**, 19-31.e7 (2019).
53. H. Jiang, P. He, C. H. Adler, H. Shill, T. G. Beach, R. Li, Y. Shen, Bid signal pathway components are identified in the temporal cortex with Parkinson disease. *Neurology* **79**, 1767–1773 (2012).
54. W. Kudo, H.-P. Lee, M. A. Smith, X. Zhu, S. Matsuyama, H.-G. Lee, Inhibition of Bax protects neuronal cells from oligomeric A $\beta$  neurotoxicity. *Cell Death Dis* **3**, e309 (2012).
55. R. Akhter, S. Saleem, A. Saha, S. C. Biswas, The pro-apoptotic protein Bmf co-operates with Bim and Puma in neuron death induced by  $\beta$ -amyloid or NGF deprivation. *Molecular and cellular neurosciences* **88**, 249–257 (2018).
56. L. Zhang, Y. Qian, J. Li, X. Zhou, H. Xu, J. Yan, J. Xiang, X. Yuan, B. Sun, S. S. Sisodia, et al., BAD-mediated neuronal apoptosis and neuroinflammation contribute to Alzheimer's disease pathology. *iScience* **24**, 102942 (2021).
57. A. Quintana, M. Giralt, S. Rojas, M. Penkowa, I. L. Campbell, J. Hidalgo, A. Molinero, Differential role of tumor necrosis factor receptors in mouse brain inflammatory responses in cryolesion brain injury. *Journal of neuroscience research* **82**, 701–716 (2005).
58. F. Locatelli, S. Corti, D. Papadimitriou, F. Fortunato, R. Del Bo, C. Donadoni, M. Nizzardo, M. Nardini, S. Salani, S. Ghezzi, et al., Fas small interfering RNA reduces motoneuron death in amyotrophic lateral sclerosis mice. *Annals of neurology* **62**, 81–92 (2007).
59. J. M. Harder, R. T. Libby, Deficiency in Bim, Bid and Bbc3 (Puma) do not prevent axonal injury induced death. *Cell Death Differ* **20**, 182 (2013).
60. A. Krishnan, A. J. Kocab, D. N. Zacks, A. Marshak-Rothstein, M. Gregory-Ksander, A small peptide antagonist of the Fas receptor inhibits neuroinflammation and prevents axon degeneration and retinal ganglion cell death in an inducible mouse model of glaucoma. *J Neuroinflammation* **16**, 184 (2019).
61. A. V. Kristen, K. Ackermann, S. Buss, L. Lehmann, P. A. Schnabel, A. Haunstetter, H. A. Katus, S. E. Hardt, Inhibition of apoptosis by the intrinsic but not the extrinsic apoptotic pathway in myocardial ischemia-reperfusion. *Cardiovascular pathology : the official journal of the Society for Cardiovascular Pathology* **22**, 280–286 (2013).
62. P. Boisguérin, A. Covinhas, L. Gallot, C. Barrère, A. Vincent, M. Busson, C. Piot, J. Nargeot, B. Lebleu, S. Barrère-Lemaire, A novel therapeutic peptide targeting myocardial reperfusion injury. *Cardiovascular research* **116**, 633–644 (2020).

63. N. Weisleder, G. E. Taffet, Y. Capetanaki, Bcl-2 overexpression corrects mitochondrial defects and ameliorates inherited desmin null cardiomyopathy. *Proceedings of the National Academy of Sciences of the United States of America* **101**, 769–774 (2004).
64. H. Fauvel, P. Marchetti, C. Chopin, P. Formstecher, R. Nevière, Differential effects of caspase inhibitors on endotoxin-induced myocardial dysfunction and heart apoptosis. *American journal of physiology. Heart and circulatory physiology* **280**, H1608-14 (2001).
65. E. Thorp, Y. Li, L. Bao, P. M. Yao, G. Kuriakose, J. Rong, E. A. Fisher, I. Tabas, Brief report: increased apoptosis in advanced atherosclerotic lesions of Apoe<sup>-/-</sup> mice lacking macrophage Bcl-2. *Arteriosclerosis, thrombosis, and vascular biology* **29**, 169–172 (2009).
66. B. A. Di Bartolo, S. P. Cartland, H. H. Harith, Y. V. Bobryshev, M. Schoppet, M. M. Kavurma, TRAIL-deficiency accelerates vascular calcification in atherosclerosis via modulation of RANKL. *PLOS ONE* **8**, e74211 (2013).
67. S. Papathanasiou, S. Rickelt, M. E. Soriano, T. G. Schips, H. J. Maier, C. H. Davos, A. Varela, L. Kaklamanis, D. L. Mann, Y. Capetanaki, Tumor necrosis factor- $\alpha$  confers cardioprotection through ectopic expression of keratins K8 and K18. *Nature medicine* **21**, 1076–1084 (2015).
68. B. Mundt, T. Wirth, L. Zender, M. Waltemathe, C. Trautwein, M. P. Manns, F. Kühnel, S. Kubicka, Tumour necrosis factor related apoptosis inducing ligand (TRAIL) induces hepatic steatosis in viral hepatitis and after alcohol intake. *Gut* **54**, 1590–1596 (2005).
69. J. Gracia-Sancho, N. Manicardi, M. Ortega-Ribera, R. Maeso-Díaz, S. Guixé-Muntet, A. Fernández-Iglesias, D. Hide, H. García-Calderó, Z. Boyer-Díaz, P. C. Contreras, et al., Emricasan Ameliorates Portal Hypertension and Liver Fibrosis in Cirrhotic Rats Through a Hepatocyte-Mediated Paracrine Mechanism. *Hepatology Communications* **3**, 987–1000 (2019).
70. A. Kahraman, J. L. Mott, S. F. Bronk, N. W. Werneburg, F. J. Barreyro, M. E. Guicciardi, Y. Akazawa, K. Braley, R. W. Craig, G. J. Gores, Overexpression of mcl-1 attenuates liver injury and fibrosis in the bile duct-ligated mouse. *Digestive diseases and sciences* **54**, 1908–1917 (2009).
71. A. Krishnan, T. Katsumi, M. E. Guicciardi, A. I. Azad, N. B. Ozturk, C. E. Trussoni, G. J. Gores, Tumor Necrosis Factor-Related Apoptosis-Inducing Ligand Receptor Deficiency Promotes the Ductular Reaction, Macrophage Accumulation, and Hepatic Fibrosis in the Abcb4<sup>-/-</sup> Mouse. *The American journal of pathology* **190**, 1284–1297 (2020).
72. F. Isayama, S. Moore, I. N. Hines, M. D. Wheeler, Fas Regulates Macrophage Polarization and Fibrogenic Phenotype in a Model of Chronic Ethanol-Induced Hepatocellular Injury. *The American journal of pathology* **186**, 1524–1536 (2016).
73. Q. Wei, G. Dong, J.-K. Chen, G. Ramesh, Z. Dong, Bax and Bak have critical roles in ischemic acute kidney injury in global and proximal tubule-specific knockout mouse models. *Kidney international* **84**, 138–148 (2013).
74. L. Hou, G. Chen, B. Feng, X.-S. Zhang, X.-F. Zheng, Y. Xiang, G.-Y. Zhao, W.-P. Min, Small interfering RNA targeting TNF- $\alpha$  gene significantly attenuates renal ischemia-reperfusion injury in mice. *Journal of Huazhong University of Science and Technology. Medical sciences = Hua zhong ke ji da xue xue bao. Yi xue Ying De wen ban = Huazhong keji daxue xuebao. Yixue Yingdewen ban* **36**, 634–638 (2016).

75. S. Mei, L. Li, Q. Wei, J. Hao, Y. Su, C. Mei, Z. Dong, Double knockout of Bax and Bak from kidney proximal tubules reduces unilateral urethral obstruction associated apoptosis and renal interstitial fibrosis. *Sci Rep* **7**, 44892 (2017).
76. L. Duplomb, N. Droin, O. Bouchot, C. Thauvin-Robinet, A.-L. Bruel, J. Thevenon, P. Callier, G. Meurice, N. Pata-Merci, R. Loffroy, et al., A constitutive BCL2 down-regulation aggravates the phenotype of PKD1-mutant-induced polycystic kidney disease. *Human molecular genetics* **26**, 4680–4688 (2017).
77. D. Cheng, R. Liang, B. Huang, J. Hou, J. Yin, T. Zhao, L. Zhou, R. Wu, Y. Qian, F. Wang, Tumor necrosis factor- $\alpha$  blockade ameliorates diabetic nephropathy in rats. *Clinical kidney journal* **14**, 301–308 (2021).
78. C. S. Moore, A. L. O. Hebb, M. M. Blanchard, C. E. Crocker, P. Liston, R. G. Korneluk, G. S. Robertson, Increased X-linked inhibitor of apoptosis protein (XIAP) expression exacerbates experimental autoimmune encephalomyelitis (EAE). *Journal of neuroimmunology* **203**, 79–93 (2008).
79. M. Razmara, B. Hilliard, A. K. Ziarani, R. Murali, S. Yellayi, M. Ghazanfar, Y. H. Chen, M. L. Tykocinski, Fn14-TRAIL, a chimeric intercellular signal exchanger, attenuates experimental autoimmune encephalomyelitis. *The American journal of pathology* **174**, 460–474 (2009).
80. C. Lutz, M. Mozaffari, V. Tosevski, M. Caj, P. Cippà, B. L. McRae, C. L. Graff, G. Rogler, M. Fried, M. Hausmann, Increased lymphocyte apoptosis in mouse models of colitis upon ABT-737 treatment is dependent upon BIM expression. *Clinical and experimental immunology* **181**, 343–356 (2015).
81. B. Krishnamurthy, J. Chee, G. Jhala, P. Trivedi, T. Catterall, C. Selck, E. N. Gurzov, T. C. Brodnicki, K. L. Graham, J. A. Wali, et al., BIM Deficiency Protects NOD Mice From Diabetes by Diverting Thymocytes to Regulatory T Cells. *Diabetes* **64**, 3229–3238 (2015).
82. S. A. White, L. S. Zhang, D. J. Pasula, Y. H. C. Yang, D. S. Luciani, Bax and Bak jointly control survival and dampen the early unfolded protein response in pancreatic  $\beta$ -cells under glucolipotoxic stress. *Sci Rep* **10**, 10986 (2020).
83. B. Tummers, D. R. Green, The evolution of regulated cell death pathways in animals and their evasion by pathogens. *Physiological Reviews* **102**, 411–454 (2022).
84. M. Kvensakul, S. Caria, M. G. Hinds, The Bcl-2 Family in Host-Virus Interactions. *Viruses* **9** (2017).
85. M. M. Rahman, G. McFadden, Modulation of NF- $\kappa$ B signalling by microbial pathogens. *Nature reviews. Microbiology* **9**, 291–306 (2011).
86. M. K. Balcewicz-Sablinska, J. Keane, H. Kornfeld, H. G. Remold, Pathogenic Mycobacterium tuberculosis evades apoptosis of host macrophages by release of TNF-R2, resulting in inactivation of TNF- $\alpha$ . *Journal of immunology (Baltimore, Md. : 1950)* **161**, 2636–2641 (1998).
87. W. S. Hambricht, R. S. Fonseca, L. Chen, R. Na, Q. Ran, Ablation of ferroptosis regulator glutathione peroxidase 4 in forebrain neurons promotes cognitive impairment and neurodegeneration. *Redox biology* **12**, 8–17 (2017).
88. M. J. Koper, E. van Schoor, S. Ospitalieri, R. Vandenberghe, M. Vandenbulcke, C. A. F. von Arnim, T. Tousseyn, S. Balusu, B. de Strooper, D. R. Thal, Necrosome complex detected in granulovacuolar degeneration is associated with neuronal loss in Alzheimer's disease. *Acta neuropathologica* **139**, 463–484 (2020).

89. T. Kuriakose, S. M. Man, R. K. S. Malireddi, R. Karki, S. Kesavardhana, D. E. Place, G. Neale, P. Vogel, T.-D. Kanneganti, ZBP1/DAI is an innate sensor of influenza virus triggering the NLRP3 inflammasome and programmed cell death pathways. *Science immunology* **1** (2016).
90. T. Oltean, E. van San, T. Divert, T. Vanden Berghe, X. Saelens, J. Maelfait, N. Takahashi, P. Vandenabeele, Viral dosing of influenza A infection reveals involvement of RIPK3 and FADD, but not MLKL. *Cell Death Dis* **12**, 471 (2021).
91. D. Hanahan, R. A. Weinberg, Hallmarks of cancer: the next generation. *Cell* **144**, 646–674 (2011).
92. A. Strasser, A. W. Harris, M. L. Bath, S. Cory, Novel primitive lymphoid tumours induced in transgenic mice by cooperation between myc and bcl-2. *Nature* **348**, 331–333 (1990).
93. A. Finch, J. Prescott, K. Shchors, A. Hunt, L. Soucek, T. B. Dansen, L. B. Swigart, G. I. Evan, Bcl-xL gain of function and p19 ARF loss of function cooperate oncogenically with Myc in vivo by distinct mechanisms. *Cancer cell* **10**, 113–120 (2006).
94. K. Höglstrand, E. Hejll, B. Sander, B. Rozell, L.-G. Larsson, A. Grandien, Inhibition of the intrinsic but not the extrinsic apoptosis pathway accelerates and drives MYC-driven tumorigenesis towards acute myeloid leukemia. *PLOS ONE* **7**, e31366 (2012).
95. C. Yin, C. M. Knudson, S. J. Korsmeyer, T. van Dyke, Bax suppresses tumorigenesis and stimulates apoptosis in vivo. *Nature* **385**, 637–640 (1997).
96. M. A. Shibata, M. L. Liu, M. C. Knudson, E. Shibata, K. Yoshidome, T. Bandey, S. J. Korsmeyer, J. E. Green, Haploid loss of bax leads to accelerated mammary tumor development in C3(1)/SV40-TAg transgenic mice: reduction in protective apoptotic response at the preneoplastic stage. *The EMBO journal* **18**, 2692–2701 (1999).
97. I. Garcia, A. J. Crowther, V. Gama, C. R. Miller, M. Deshmukh, T. R. Gershon, Bax deficiency prolongs cerebellar neurogenesis, accelerates medulloblastoma formation and paradoxically increases both malignancy and differentiation. *Oncogene* **32**, 2304–2314 (2013).
98. C. L. Buchheit, B. L. Angarola, A. Steiner, K. J. Weigel, Z. T. Schafer, Anoikis evasion in inflammatory breast cancer cells is mediated by Bim-EL sequestration. *Cell Death Differ* **22**, 1275–1286 (2015).
99. R. R. Rayavarapu, B. Heiden, N. Pagani, M. M. Shaw, S. Shuff, S. Zhang, Z. T. Schafer, The role of multicellular aggregation in the survival of ErbB2-positive breast cancer cells during extracellular matrix detachment. *The Journal of biological chemistry* **290**, 8722–8733 (2015).
100. F. J. Barreyro, S. Holod, P. V. Finocchietto, A. M. Camino, J. B. Aquino, A. Avagnina, M. C. Carreras, J. J. Poderoso, G. J. Gores, The pan-caspase inhibitor Emricasan (IDN-6556) decreases liver injury and fibrosis in a murine model of non-alcoholic steatohepatitis. *Liver international : official journal of the International Association for the Study of the Liver* **35**, 953–966 (2015).
101. J. Mersmann, P. A. Zacharowski, I. Schmitz, K. Zacharowski, Caspase inhibitor zVAD.fmk reduces infarct size after myocardial ischaemia and reperfusion in rats but not in mice. *Resuscitation* **79**, 468–474 (2008).
102. J. S. Braun, K. Prass, U. Dirnagl, A. Meisel, C. Meisel, Protection from brain damage and bacterial infection in murine stroke by the novel caspase-inhibitor Q-VD-OPH. *Experimental neurology* **206**, 183–191 (2007).
103. S. Dhani, Y. Zhao, B. Zhivotovsky, A long way to go: caspase inhibitors in clinical use. *Cell Death Dis* **12**, 949 (2021).

104. G. Cantarella, G. Di Benedetto, D. Puzzo, L. Privitera, C. Loreto, S. Saccone, S. Giunta, A. Palmeri, R. Bernardini, Neutralization of TNFSF10 ameliorates functional outcome in a murine model of Alzheimer's disease. *Brain : a journal of neurology* **138**, 203–216 (2015).
105. R. Souktani, S. Pons, C. Guegan, O. Bouhidel, P. Bruneval, R. Zini, C. Mandet, B. Onteniente, A. Berdeaux, B. Ghaleh, Cardioprotection against myocardial infarction with PTD-BIR3/RING, a XIAP mimicking protein. *Journal of molecular and cellular cardiology* **46**, 713–718 (2009).
106. D. Zhao, L. Yang, P. Han, H. Zhang, F. Wang, Z. Meng, H. Gan, Z. Wu, W. Sun, C. Chen, et al., Blocking TRAIL-DR5 signaling pathway with soluble death receptor 5 fusion protein mitigates radiation-induced injury. *Frontiers in pharmacology* **14**, 1171293 (2023).
107. W. M. C. van den Boogaard, D. S. J. Komninos, W. P. Vermeij, Chemotherapy Side-Effects: Not All DNA Damage Is Equal. *Cancers* **14** (2022).
108. J. Wiezorek, P. Holland, J. Graves, Death receptor agonists as a targeted therapy for cancer. *Clinical cancer research : an official journal of the American Association for Cancer Research* **16**, 1701–1708 (2010).
109. L. Chen, S.-M. Park, A. V. Tumanov, A. Hau, K. Sawada, C. Feig, J. R. Turner, Y.-X. Fu, I. L. Romero, E. Lengyel, et al., CD95 promotes tumour growth. *Nature* **465**, 492–496 (2010).
110. K. A. Charles, H. Kulbe, R. Soper, M. Escorcio-Correia, T. Lawrence, A. Schultheis, P. Chakravarty, R. G. Thompson, G. Kollias, J. F. Smyth, et al., The tumor-promoting actions of TNF-alpha involve TNFR1 and IL-17 in ovarian cancer in mice and humans. *The Journal of clinical investigation* **119**, 3011–3023 (2009).
111. A. Montinaro, H. Walczak, Harnessing TRAIL-induced cell death for cancer therapy: a long walk with thrilling discoveries. *Cell Death Differ* **30**, 237–249 (2023).
112. F. Di Cristofano, A. George, V. Tajiknia, M. Ghandali, L. Wu, Y. Zhang, P. Srinivasan, J. Strandberg, M. Hahn, A. Sanchez Sevilla Uruchurtu, et al., Therapeutic targeting of TRAIL death receptors. *Biochemical Society transactions* **51**, 57–70 (2023).
113. A. Montinaro, I. Areso Zubiaur, J. Saggau, A.-L. Kretz, R. M. M. Ferreira, O. Hassan, E. Kitzig, I. Müller, M. A. El-Bahrawy, S. von Karstedt, et al., Potent pro-apoptotic combination therapy is highly effective in a broad range of cancers. *Cell Death Differ* **29**, 492–503 (2022).
114. E. Morrish, G. Brumatti, J. Silke, Future Therapeutic Directions for Smac-Mimetics. *Cells* **9** (2020).
115. D. Lagares, A. Santos, P. E. Grasberger, F. Liu, C. K. Probst, R. A. Rahimi, N. Sakai, T. Kuehl, J. Ryan, P. Bholra, et al., Targeted apoptosis of myofibroblasts with the BH3 mimetic ABT-263 reverses established fibrosis. *Science translational medicine* **9** (2017).
116. S. T. Diepstraten, M. A. Anderson, P. E. Czabotar, G. Lessene, A. Strasser, G. L. Kelly, The manipulation of apoptosis for cancer therapy using BH3-mimetic drugs. *Nature reviews. Cancer* **22**, 45–64 (2022).
117. Y. Tsujimoto, L. R. Finger, J. Yunis, P. C. Nowell, C. M. Croce, Cloning of the chromosome breakpoint of neoplastic B cells with the t(14;18) chromosome translocation. *Science (New York, N.Y.)* **226**, 1097–1099 (1984).
118. S. Banjara, C. D. Suraweera, M. G. Hinds, M. Kvansakul, The Bcl-2 Family: Ancient Origins, Conserved Structures, and Divergent Mechanisms. *Biomolecules* **10** (2020).

119. L. P. Billen, A. Shamas-Din, D. W. Andrews, Bid: a Bax-like BH3 protein. *Oncogene* **27 Suppl 1**, S93-104 (2008).
120. L. Chen, S. N. Willis, A. Wei, B. J. Smith, J. I. Fletcher, M. G. Hinds, P. M. Colman, C. L. Day, J. M. Adams, D. C. S. Huang, Differential targeting of prosurvival Bcl-2 proteins by their BH3-only ligands allows complementary apoptotic function. *Molecular cell* **17**, 393–403 (2005).
121. S. J. Korsmeyer, J. R. Shutter, D. J. Veis, D. E. Merry, Z. N. Oltvai, Bcl-2/Bax: a rheostat that regulates an anti-oxidant pathway and cell death. *Seminars in cancer biology* **4**, 327–332 (1993).
122. A. Letai, M. C. Bassik, L. D. Walensky, M. D. Sorcinelli, S. Weiler, S. J. Korsmeyer, Distinct BH3 domains either sensitize or activate mitochondrial apoptosis, serving as prototype cancer therapeutics. *Cancer cell* **2**, 183–192 (2002).
123. B. Leber, J. Lin, D. W. Andrews, Embedded together: the life and death consequences of interaction of the Bcl-2 family with membranes. *Apoptosis : an international journal on programmed cell death* **12**, 897–911 (2007).
124. B. Leber, J. Lin, D. W. Andrews, Still embedded together binding to membranes regulates Bcl-2 protein interactions. *Oncogene* **29**, 5221–5230 (2010).
125. F. Llambi, T. Moldoveanu, S. W. G. Tait, L. Bouchier-Hayes, J. Temirov, L. L. McCormick, C. P. Dillon, D. R. Green, A unified model of mammalian BCL-2 protein family interactions at the mitochondria. *Molecular cell* **44**, 517–531 (2011).
126. H.-C. Chen, M. Kanai, A. Inoue-Yamauchi, H.-C. Tu, Y. Huang, D. Ren, H. Kim, S. Takeda, D. E. Reyna, P. M. Chan, et al., An interconnected hierarchical model of cell death regulation by the BCL-2 family. *Nature cell biology* **17**, 1270–1281 (2015).
127. K. L. O'Neill, K. Huang, J. Zhang, Y. Chen, X. Luo, Inactivation of prosurvival Bcl-2 proteins activates Bax/Bak through the outer mitochondrial membrane. *Genes & development* **30**, 973–988 (2016).
128. X. Luo, K. L. O'Neill, K. Huang, The third model of Bax/Bak activation: a Bcl-2 family feud finally resolved? *F1000Research* **9** (2020).
129. Z. N. Oltvai, C. L. Milliman, S. J. Korsmeyer, Bcl-2 heterodimerizes in vivo with a conserved homolog, Bax, that accelerates programmed cell death. *Cell* **74**, 609–619 (1993).
130. F. Edlich, S. Banerjee, M. Suzuki, M. M. Cleland, D. Arnoult, C. Wang, A. Neutzner, N. Tjandra, R. J. Youle, Bcl-x(L) retrotranslocates Bax from the mitochondria into the cytosol. *Cell* **145**, 104–116 (2011).
131. T. P. Garner, D. E. Reyna, A. Priyadarshi, H.-C. Chen, S. Li, Y. Wu, Y. T. Ganesan, V. N. Malashkevich, E. H. Cheng, E. Gavathiotis, An Autoinhibited Dimeric Form of BAX Regulates the BAX Activation Pathway. *Molecular cell* **63**, 485–497 (2016).
132. M. A. Dengler, A. Y. Robin, L. Gibson, M. X. Li, J. J. Sandow, S. Iyer, A. I. Webb, D. Westphal, G. Dewson, J. M. Adams, BAX Activation: Mutations Near Its Proposed Non-canonical BH3 Binding Site Reveal Allosteric Changes Controlling Mitochondrial Association. *Cell reports* **27**, 359-373.e6 (2019).
133. M. Suzuki, R. J. Youle, N. Tjandra, Structure of Bax: coregulation of dimer formation and intracellular localization. *Cell* **103**, 645–654 (2000).
134. S. Bleicken, M. Classen, P. V. L. Padmavathi, T. Ishikawa, K. Zeth, H.-J. Steinhoff, E. Bordignon, Molecular details of Bax activation, oligomerization, and membrane insertion. *The Journal of biological chemistry* **285**, 6636–6647 (2010).



135. P. E. Czabotar, D. Westphal, G. Dewson, S. Ma, C. Hockings, W. D. Fairlie, E. F. Lee, S. Yao, A. Y. Robin, B. J. Smith, et al., Bax crystal structures reveal how BH3 domains activate Bax and nucleate its oligomerization to induce apoptosis. *Cell* **152**, 519–531 (2013).
136. J. M. Brouwer, D. Westphal, G. Dewson, A. Y. Robin, R. T. Uren, R. Bartolo, G. V. Thompson, P. M. Colman, R. M. Kluck, P. E. Czabotar, Bak core and latch domains separate during activation, and freed core domains form symmetric homodimers. *Molecular cell* **55**, 938–946 (2014).
137. G. Dewson, S. Ma, P. Frederick, C. Hockings, I. Tan, T. Kratina, R. M. Kluck, Bax dimerizes via a symmetric BH3:groove interface during apoptosis. *Cell Death Differ* **19**, 661–670 (2012).
138. S. Bleicken, G. Jeschke, C. Stegmüller, R. Salvador-Gallego, A. J. García-Sáez, E. Bordignon, Structural model of active Bax at the membrane. *Molecular cell* **56**, 496–505 (2014).
139. P. J. Dlugosz, L. P. Billen, M. G. Annis, W. Zhu, Z. Zhang, J. Lin, B. Leber, D. W. Andrews, Bcl-2 changes conformation to inhibit Bax oligomerization. *The EMBO journal* **25**, 2287–2296 (2006).
140. S. Bleicken, T. E. Assafa, C. Stegmüller, A. Wittig, A. J. Garcia-Saez, E. Bordignon, Topology of active, membrane-embedded Bax in the context of a toroidal pore. *Cell Death Differ* **25**, 1717–1731 (2018).
141. T. Mandal, S. Shin, S. Aluvila, H.-C. Chen, C. Grieve, J.-Y. Choe, E. H. Cheng, E. J. Hustedt, K. J. Oh, Assembly of Bak homodimers into higher order homooligomers in the mitochondrial apoptotic pore. *Sci Rep* **6**, 30763 (2016).
142. R. Salvador-Gallego, M. Mund, K. Cosentino, J. Schneider, J. Unsay, U. Schraermeyer, J. Engelhardt, J. Ries, A. J. García-Sáez, Bax assembly into rings and arcs in apoptotic mitochondria is linked to membrane pores. *The EMBO journal* **35**, 389–401 (2016).
143. K. McArthur, L. W. Whitehead, J. M. Heddleston, L. Li, B. S. Padman, V. Oorschot, N. D. Geoghegan, S. Chappaz, S. Davidson, H. San Chin, et al., BAK/BAX macropores facilitate mitochondrial herniation and mtDNA efflux during apoptosis. *Science (New York, N.Y.)* **359** (2018).
144. T. Chittenden, E. A. Harrington, R. O'Connor, C. Flemington, R. J. Lutz, G. I. Evan, B. C. Guild, Induction of apoptosis by the Bcl-2 homologue Bak. *Nature* **374**, 733–736 (1995).
145. T. Moldoveanu, C. R. Grace, F. Llambi, A. Nourse, P. Fitzgerald, K. Gehring, R. W. Kriwacki, D. R. Green, BID-induced structural changes in BAK promote apoptosis. *Nature structural & molecular biology* **20**, 589–597 (2013).
146. S. Naghdi, P. Várnai, G. Hajnóczy, Motifs of VDAC2 required for mitochondrial Bak import and tBid-induced apoptosis. *Proceedings of the National Academy of Sciences of the United States of America* **112**, E5590-9 (2015).
147. S. B. Ma, T. N. Nguyen, I. Tan, R. Ninnis, S. Iyer, D. A. Stroud, M. Menard, R. M. Kluck, M. T. Ryan, G. Dewson, Bax targets mitochondria by distinct mechanisms before or during apoptotic cell death: a requirement for VDAC2 or Bak for efficient Bax apoptotic function. *Cell Death Differ* **21**, 1925–1935 (2014).
148. R. T. Uren, S. Iyer, R. M. Kluck, Pore formation by dimeric Bak and Bax: an unusual pore? *Philosophical transactions of the Royal Society of London. Series B, Biological sciences* **372** (2017).
149. K. Cosentino, V. Hertlein, A. Jenner, T. Dellmann, M. Gojkovic, A. Peña-Blanco, S. Dadsena, N. Wajngarten, J. S. H. Danial, J. V. Thevathasan, et al., The interplay between BAX and BAK tunes apoptotic pore growth to control mitochondrial-DNA-mediated inflammation. *Molecular cell* **82**, 933-949.e9 (2022).

150. F. F. S. Ke, H. K. Vanyai, A. D. Cowan, A. R. D. Delbridge, L. Whitehead, S. Grabow, P. E. Czabotar, A. K. Voss, A. Strasser, Embryogenesis and Adult Life in the Absence of Intrinsic Apoptosis Effectors BAX, BAK, and BOK. *Cell* **173**, 1217–1230.e17 (2018).
151. S. N. Willis, L. Chen, G. Dewson, A. Wei, E. Naik, J. I. Fletcher, J. M. Adams, D. C. S. Huang, Proapoptotic Bak is sequestered by Mcl-1 and Bcl-xL, but not Bcl-2, until displaced by BH3-only proteins. *Genes & development* **19**, 1294–1305 (2005).
152. D. Neise, V. Graupner, B. F. Gillissen, P. T. Daniel, K. Schulze-Osthoff, R. U. Jänicke, F. Essmann, Activation of the mitochondrial death pathway is commonly mediated by a preferential engagement of Bak. *Oncogene* **27**, 1387–1396 (2008).
153. S. Y. Hsu, A. Kaipia, E. McGee, M. Lomeli, A. J. Hsueh, Bok is a pro-apoptotic Bcl-2 protein with restricted expression in reproductive tissues and heterodimerizes with selective anti-apoptotic Bcl-2 family members. *Proceedings of the National Academy of Sciences of the United States of America* **94**, 12401–12406 (1997).
154. S. Gao, W. Fu, M. Dürrenberger, C. de Geyter, H. Zhang, Membrane translocation and oligomerization of hBok are triggered in response to apoptotic stimuli and Bnip3. *Cellular and molecular life sciences : CMLS* **62**, 1015–1024 (2005).
155. J. M. Rodriguez, M. A. Glozak, Y. Ma, W. D. Cress, Bok, Bcl-2-related Ovarian Killer, Is Cell Cycle-regulated and Sensitizes to Stress-induced Apoptosis. *The Journal of biological chemistry* **281**, 22729–22735 (2006).
156. R. Beroukhim, C. H. Mermel, D. Porter, G. Wei, S. Raychaudhuri, J. Donovan, J. Barretina, J. S. Boehm, J. Dobson, M. Urashima, et al., The landscape of somatic copy-number alteration across human cancers. *Nature* **463**, 899–905 (2010).
157. N. Echeverry, D. Bachmann, F. Ke, A. Strasser, H. U. Simon, T. Kaufmann, Intracellular localization of the BCL-2 family member BOK and functional implications. *Cell death and differentiation* **20**, 785–799 (2013).
158. S. Einsele-Scholz, S. Malmshemer, K. Bertram, D. Stehle, J. Johanning, M. Manz, P. T. Daniel, B. F. Gillissen, K. Schulze-Osthoff, F. Essmann, Bok is a genuine multi-BH-domain protein that triggers apoptosis in the absence of Bax and Bak. *Journal of cell science* **129**, 3054 (2016).
159. Y. Fernández-Marrero, S. Bleicken, K. K. Das, D. Bachmann, T. Kaufmann, A. J. Garcia-Saez, The membrane activity of BOK involves formation of large, stable toroidal pores and is promoted by cBID. *The FEBS journal* **284**, 711–724 (2017).
160. R. Shalaby, A. Diwan, H. Flores-Romero, V. Hertlein, A. J. Garcia-Saez, Visualization of BOK pores independent of BAX and BAK reveals a similar mechanism with differing regulation. *Cell Death Differ* **30**, 731–741 (2023).
161. F. Llambi, Y.-M. Wang, B. Victor, M. Yang, D. M. Schneider, S. Gingras, M. J. Parsons, J. H. Zheng, S. A. Brown, S. Pelletier, et al., BOK Is a Non-canonical BCL-2 Family Effector of Apoptosis Regulated by ER-Associated Degradation. *Cell* **165**, 421–433 (2016).
162. F. Ke, A. Voss, J. B. Kerr, L. A. O'Reilly, L. Tai, N. Echeverry, P. Bouillet, A. Strasser, T. Kaufmann, BCL-2 family member BOK is widely expressed but its loss has only minimal impact in mice. *Cell Death Differ* **19**, 915–925 (2012).
163. M. A. Carpio, M. Michaud, W. Zhou, J. K. Fisher, L. D. Walensky, S. G. Katz, BCL-2 family member BOK promotes apoptosis in response to endoplasmic reticulum stress. *Proceedings of the National Academy of Sciences of the United States of America* **112**, 7201–7206 (2015).

164. J. J. Schulman, F. A. Wright, T. Kaufmann, R. J. H. Wojcikiewicz, The Bcl-2 protein family member Bok binds to the coupling domain of inositol 1,4,5-trisphosphate receptors and protects them from proteolytic cleavage. *The Journal of biological chemistry* **288**, 25340–25349 (2013).
165. J. J. Schulman, F. A. Wright, X. Han, E. J. Zluhan, L. M. Szczesniak, R. J. H. Wojcikiewicz, The Stability and Expression Level of Bok Are Governed by Binding to Inositol 1,4,5-Trisphosphate Receptors. *The Journal of biological chemistry* **291**, 11820–11828 (2016).
166. F. Walter, B. D'Orsi, A. Jagannathan, H. Dussmann, J. H. M. Prehn, BOK controls ER proteostasis and physiological ER stress responses in neurons. *Frontiers in Cell and Developmental Biology* **10**, 915065 (2022).
167. M. A. Carpio, R. E. Means, A. L. Brill, A. Sainz, B. E. Ehrlich, S. G. Katz, BOK controls apoptosis by Ca<sup>2+</sup> transfer through ER-mitochondrial contact sites. *Cell reports* **34**, 108827 (2021).
168. J. J. Schulman, L. M. Szczesniak, E. N. Bunker, H. A. Nelson, M. W. Roe, L. E. Wagner, D. I. Yule, R. J. H. Wojcikiewicz, Bok regulates mitochondrial fusion and morphology. *Cell death and differentiation* **26**, 2682–2694 (2019).
169. J. Ding, Z. Zhang, G. J. Roberts, M. Falcone, Y. Miao, Y. Shao, X. C. Zhang, D. W. Andrews, J. Lin, Bcl-2 and Bax interact via the BH1-3 groove-BH3 motif interface and a novel interface involving the BH4 motif. *The Journal of biological chemistry* **285**, 28749–28763 (2010).
170. B. Ku, C. Liang, J. U. Jung, B.-H. Oh, Evidence that inhibition of BAX activation by BCL-2 involves its tight and preferential interaction with the BH3 domain of BAX. *Cell research* **21**, 627–641 (2011).
171. V. Andreu-Fernández, M. Sancho, A. Genovés, E. Lucendo, F. Todt, J. Lauterwasser, K. Funk, G. Jahreis, E. Pérez-Payá, I. Mingarro, et al., Bax transmembrane domain interacts with prosurvival Bcl-2 proteins in biological membranes. *Proceedings of the National Academy of Sciences of the United States of America* **114**, 310–315 (2017).
172. T. Kaufmann, S. Schlipf, J. Sanz, K. Neubert, R. Stein, C. Borner, Characterization of the signal that directs Bcl-x(L), but not Bcl-2, to the mitochondrial outer membrane. *The Journal of Cell Biology* **160**, 53–64 (2003).
173. L. Lalier, V. Mignard, M.-P. Joalland, D. Lanoé, P.-F. Cartron, S. Manon, F. M. Vallette, TOM20-mediated transfer of Bcl2 from ER to MAM and mitochondria upon induction of apoptosis. *Cell Death & Disease* **12**, 182 (2021).
174. Y.-P. Rong, G. Bultynck, A. S. Aromolaran, F. Zhong, J. B. Parys, H. de Smedt, G. A. Mignery, H. L. Roderick, M. D. Bootman, C. W. Distelhorst, The BH4 domain of Bcl-2 inhibits ER calcium release and apoptosis by binding the regulatory and coupling domain of the IP<sub>3</sub> receptor. *Proceedings of the National Academy of Sciences of the United States of America* **106**, 14397–14402 (2009).
175. H. He, M. Lam, T. S. McCormick, C. W. Distelhorst, Maintenance of calcium homeostasis in the endoplasmic reticulum by Bcl-2. *The Journal of Cell Biology* **138**, 1219–1228 (1997).
176. P. Pinton, D. Ferrari, P. Magalhães, K. Schulze-Osthoff, F. Di Virgilio, T. Pozzan, R. Rizzuto, Reduced loading of intracellular Ca(2+) stores and downregulation of capacitative Ca(2+) influx in Bcl-2-overexpressing cells. *The Journal of Cell Biology* **148**, 857–862 (2000).
177. G. Monaco, E. Decrock, H. Akl, R. Ponsaerts, T. Vervliet, T. Luyten, M. de Maeyer, L. Missiaen, C. W. Distelhorst, H. de Smedt, et al., Selective regulation of IP<sub>3</sub>-receptor-mediated Ca<sup>2+</sup> signaling and apoptosis by the BH4 domain of Bcl-2 versus Bcl-Xl. *Cell death and differentiation* **19**, 295–309 (2012).

178. E. F. Greenberg, A. R. Lavik, C. W. Distelhorst, Bcl-2 regulation of the inositol 1,4,5-trisphosphate receptor and calcium signaling in normal and malignant lymphocytes: potential new target for cancer treatment. *Biochimica et biophysica acta* **1843**, 2205–2210 (2014).
179. E. M. Kobrinisky, M. A. Kirchberger, Evidence for a role of the sarcoplasmic/endoplasmic reticulum Ca(2+)-ATPase in thapsigargin and Bcl-2 induced changes in *Xenopus laevis* oocyte maturation. *Oncogene* **20**, 933–941 (2001).
180. T. Vervliet, E. Decrock, J. Molgó, V. Sorrentino, L. Missiaen, L. Leybaert, H. de Smedt, N. N. Kasri, J. B. Parys, G. Bultynck, Bcl-2 binds to and inhibits ryanodine receptors. *Journal of cell science* **127**, 2782–2792 (2014).
181. L. Zhu, Y. Yu, B. H. Chua, Y. S. Ho, T. H. Kuo, Regulation of sodium-calcium exchange and mitochondrial energetics by Bcl-2 in the heart of transgenic mice. *Journal of molecular and cellular cardiology* **33**, 2135–2144 (2001).
182. L. E. Robertson, W. Plunkett, K. McConnell, M. J. Keating, T. J. McDonnell, Bcl-2 expression in chronic lymphocytic leukemia and its correlation with the induction of apoptosis and clinical outcome. *Leukemia* **10**, 456–459 (1996).
183. A. Williams, T. Hayashi, D. Wolozny, B. Yin, T.-C. Su, M. J. Betenbaugh, T.-P. Su, The non-apoptotic action of Bcl-xL: regulating Ca(2+) signaling and bioenergetics at the ER-mitochondrion interface. *Journal of bioenergetics and biomembranes* **48**, 211–225 (2016).
184. S. Bleicken, A. Hantusch, K. K. Das, T. Frickey, A. J. Garcia-Saez, Quantitative interactome of a membrane Bcl-2 network identifies a hierarchy of complexes for apoptosis regulation. *Nat Commun* **8**, 73 (2017).
185. B. S. Chang, A. Kelekar, M. H. Harris, J. E. Harlan, S. W. Fesik, C. B. Thompson, The BH3 domain of Bcl-x(S) is required for inhibition of the antiapoptotic function of Bcl-x(L). *Molecular and cellular biology* **19**, 6673–6681 (1999).
186. E. A. Jonas, J. A. Hickman, M. Chachar, B. M. Polster, T. A. Brandt, Y. Fannjiang, I. Ivanovska, G. Basañez, K. W. Kinnally, J. Zimmerberg, et al., Proapoptotic N-truncated BCL-xL protein activates endogenous mitochondrial channels in living synaptic terminals. *Proceedings of the National Academy of Sciences of the United States of America* **101**, 13590–13595 (2004).
187. M. Stevens, S. Oltean, Modulation of the Apoptosis Gene Bcl-x Function Through Alternative Splicing. *Frontiers in genetics* **10**, 804 (2019).
188. L. Campos, O. Sabido, A. Viallet, C. Vasselon, D. Guyotat, Expression of apoptosis-controlling proteins in acute leukemia cells. *Leukemia & lymphoma* **33**, 499–509 (1999).
189. Y. Chen, W. Li, S. Zhang, hnRNP K expression and its clinical significance in human lung cancer tissues. *Zhongguo fei ai za zhi = Chinese journal of lung cancer* **11**, 241–245 (2008).
190. J. C. Shultz, N. Vu, M. D. Shultz, M.-U. U. Mba, B. A. Shapiro, C. E. Chalfant, The Proto-oncogene PKC $\zeta$  regulates the alternative splicing of Bcl-x pre-mRNA. *Molecular cancer research : MCR* **10**, 660–669 (2012).
191. J. Wilson-Annan, L. A. O'Reilly, S. A. Crawford, G. Hausmann, J. G. Beaumont, L. P. Parma, L. Chen, M. Lackmann, T. Lithgow, M. G. Hinds, et al., Proapoptotic BH3-only proteins trigger membrane integration of prosurvival Bcl-w and neutralize its activity. *The Journal of Cell Biology* **162**, 877–887 (2003).

192. G. Moroy, E. Martin, A. Dejaegere, R. H. Stote, Molecular basis for Bcl-2 homology 3 domain recognition in the Bcl-2 protein family: identification of conserved hot spot interactions. *The Journal of biological chemistry* **284**, 17499–17511 (2009).
193. J. Schilling, J. Schöppe, E. Sauer, A. Plückthun, Co-crystallization with conformation-specific designed ankyrin repeat proteins explains the conformational flexibility of BCL-W. *Journal of molecular biology* **426**, 2346–2362 (2014).
194. M. G. Hinds, M. Lackmann, G. L. Skea, P. J. Harrison, D. C. S. Huang, C. L. Day, The structure of Bcl-w reveals a role for the C-terminal residues in modulating biological activity. *The EMBO journal* **22**, 1497–1507 (2003).
195. A. Y. Denisov, G. Chen, T. Sprules, T. Moldoveanu, P. Beauparlant, K. Gehring, Structural model of the BCL-w-BID peptide complex and its interactions with phospholipid micelles. *Biochemistry* **45**, 2250–2256 (2006).
196. C. G. Print, K. L. Loveland, L. Gibson, T. Meehan, A. Stylianou, N. Wreford, D. de Kretser, D. Metcalf, F. Köntgen, J. M. Adams, et al., Apoptosis regulator bcl-w is essential for spermatogenesis but appears otherwise redundant. *Proceedings of the National Academy of Sciences of the United States of America* **95**, 12424–12431 (1998).
197. I. H. Bae, S. H. Yoon, S. B. Lee, J. K. Park, J.-N. Ho, H.-D. Um, Signaling components involved in Bcl-w-induced migration of gastric cancer cells. *Cancer Letters* **277**, 22–28 (2009).
198. E. M. Kim, C.-H. Jung, J. Kim, S.-G. Hwang, J. K. Park, H.-D. Um, The p53/p21 Complex Regulates Cancer Cell Invasion and Apoptosis by Targeting Bcl-2 Family Proteins. *Cancer research* **77**, 3092–3100 (2017).
199. J. Y. Choi, H. J. Shin, I. H. Bae, miR-93-5p suppresses cellular senescence by directly targeting Bcl-w and p21. *Biochemical and biophysical research communications* **505**, 1134–1140 (2018).
200. K. M. Kozopas, T. Yang, H. L. Buchan, P. Zhou, R. W. Craig, MCL1, a gene expressed in programmed myeloid cell differentiation, has sequence similarity to BCL2. *Proceedings of the National Academy of Sciences of the United States of America* **90**, 3516–3520 (1993).
201. V. V. Senichkin, A. Y. Streletskaia, A. S. Gorbunova, B. Zhivotovsky, G. S. Kopeina, Saga of Mcl-1: regulation from transcription to degradation. *Cell Death Differ* **27**, 405–419 (2020).
202. R. M. Perciavalle, D. P. Stewart, B. Koss, J. Lynch, S. Milasta, M. Bathina, J. Temirov, M. M. Cleland, S. Pelletier, J. D. Schuetz, et al., Anti-apoptotic MCL-1 localizes to the mitochondrial matrix and couples mitochondrial fusion to respiration. *Nature cell biology* **14**, 575–583 (2012).
203. E. F. Eckenrode, J. Yang, G. V. Velmurugan, J. K. Foskett, C. White, Apoptosis protection by Mcl-1 and Bcl-2 modulation of inositol 1,4,5-trisphosphate receptor-dependent Ca<sup>2+</sup> signaling. *The Journal of biological chemistry* **285**, 13678–13684 (2010).
204. H. Huang, K. Shah, N. A. Bradbury, C. Li, C. White, Mcl-1 promotes lung cancer cell migration by directly interacting with VDAC to increase mitochondrial Ca<sup>2+</sup> uptake and reactive oxygen species generation. *Cell Death Dis* **5**, e1482 (2014).
205. T. Yang, K. M. Kozopas, R. W. Craig, The intracellular distribution and pattern of expression of Mcl-1 overlap with, but are not identical to, those of Bcl-2. *J Cell Biol* **128**, 1173–1184 (1995).

206. W. Nakajima, K. Sharma, J. Y. Lee, N. T. Maxim, M. A. Hicks, T.-T. Vu, A. Luu, W. A. Yeudall, N. Tanaka, H. Harada, DNA damaging agent-induced apoptosis is regulated by MCL-1 phosphorylation and degradation mediated by the Noxa/MCL-1/CDK2 complex. *Oncotarget* **7**, 36353–36365 (2016).
207. M. D. Haschka, C. Soratroi, S. Kirschnek, G. Häcker, R. Hilbe, S. Geley, A. Villunger, L. L. Fava, The NOXA-MCL1-BIM axis defines lifespan on extended mitotic arrest. *Nat Commun* **6**, 6891 (2015).
208. J.-H. Kim, S.-H. Sim, H.-J. Ha, J.-J. Ko, K. Lee, J. Bae, MCL-1ES, a novel variant of MCL-1, associates with MCL-1L and induces mitochondrial cell death. *FEBS letters* **583**, 2758–2764 (2009).
209. F. Fan, G. Tonon, M. H. Bashari, S. Vallet, E. Antonini, H. Goldschmidt, H. Schulze-Bergkamen, J. T. Opferman, M. Sattler, K. C. Anderson, et al., Targeting Mcl-1 for multiple myeloma (MM) therapy: drug-induced generation of Mcl-1 fragment Mcl-1(128-350) triggers MM cell death via c-Jun upregulation. *Cancer Letters* **343**, 286–294 (2014).
210. H. Widden, W. J. Placzek, The multiple mechanisms of MCL1 in the regulation of cell fate. *Communications Biology* **4**, 1029 (2021).
211. A. B. Werner, E. de Vries, S. W. G. Tait, I. Bontjer, J. Borst, Bcl-2 family member Bfl-1/A1 sequesters truncated bid to inhibit its collaboration with pro-apoptotic Bak or Bax. *The Journal of biological chemistry* **277**, 22781–22788 (2002).
212. J.-K. Ko, K.-H. Choi, H.-J. Kim, H.-Y. Choi, D.-J. Yeo, S.-O. Park, W. S. Yang, Y.-N. Kim, C.-W. Kim, Conversion of Bfl-1, an anti-apoptotic Bcl-2 family protein, to a potent pro-apoptotic protein by fusion with green fluorescent protein (GFP). *FEBS letters* **551**, 29–36 (2003).
213. G. Brien, A.-L. Debaud, X. Robert, L. Oliver, M.-C. Trescol-Biemont, N. Cauquil, O. Geneste, N. Aghajari, F. M. Vallette, R. Haser, et al., C-terminal residues regulate localization and function of the antiapoptotic protein Bfl-1. *Journal of Biological Chemistry* **284**, 30257–30263 (2009).
214. M. J. Simmons, G. Fan, W.-X. Zong, K. Degenhardt, E. White, C. Gélinas, Bfl-1/A1 functions, similar to Mcl-1, as a selective tBid and Bak antagonist. *Oncogene* **27**, 1421–1428 (2008).
215. J. F. Kucharczak, M. J. Simmons, C. S. Duckett, C. Gélinas, Constitutive proteasome-mediated turnover of Bfl-1/A1 and its processing in response to TNF receptor activation in FL5.12 pro-B cells convert it into a prodeath factor. *Cell death and differentiation* **12**, 1225–1239 (2005).
216. M. J. Herold, J. Zeitz, C. Pelzer, C. Kraus, A. Peters, G. Wohlleben, I. Berberich, The stability and anti-apoptotic function of A1 are controlled by its C terminus. *The Journal of biological chemistry* **281**, 13663–13671 (2006).
217. E. P. Harvey, H.-S. Seo, R. M. Guerra, G. H. Bird, S. Dhe-Paganon, L. D. Walensky, Crystal Structures of Anti-apoptotic BFL-1 and Its Complex with a Covalent Stapled Peptide Inhibitor. *Structure (London, England : 1993)* **26**, 153-160.e4 (2018).
218. N. Ke, A. Godzik, J. C. Reed, Bcl-B, a novel Bcl-2 family member that differentially binds and regulates Bax and Bak. *The Journal of biological chemistry* **276**, 12481–12484 (2001).
219. G. Robert, C. Gastaldi, A. Puissant, A. Hamouda, A. Jacquiel, M. Dufies, N. Belhacene, P. Colosetti, J. C. Reed, P. Auberger, et al., The anti-apoptotic Bcl-B protein inhibits BECN1-dependent autophagic cell death. *Autophagy* **8**, 637–649 (2012).

220. M. Krajewska, S. Kitada, J. N. Winter, D. Variakojis, A. Lichtenstein, D. Zhai, M. Cuddy, X. Huang, F. Luciano, C. H. Baker, et al., Bcl-B expression in human epithelial and nonepithelial malignancies. *Clinical cancer research : an official journal of the American Association for Cancer Research* **14**, 3011–3021 (2008).
221. D. Xue, H. R. Horvitz, Caenorhabditis elegans CED-9 protein is a bifunctional cell-death inhibitor. *Nature* **390**, 305–308 (1997).
222. L. Quinn, M. Coombe, K. Mills, T. Daish, P. Colussi, S. Kumar, H. Richardson, Buffy, a Drosophila Bcl-2 protein, has anti-apoptotic and cell cycle inhibitory functions. *The EMBO journal* **22**, 3568–3579 (2003).
223. A. Shamas-Din, H. Brahmabhatt, B. Leber, D. W. Andrews, BH3-only proteins: Orchestrators of apoptosis. *Biochimica et biophysica acta* **1813**, 508–520 (2011).
224. M. Certo, V. Del Gaizo Moore, M. Nishino, G. Wei, S. Korsmeyer, S. A. Armstrong, A. Letai, Mitochondria primed by death signals determine cellular addiction to antiapoptotic BCL-2 family members. *Cancer cell* **9**, 351–365 (2006).
225. S. Dutta, S. Gullá, T. S. Chen, E. Fire, R. A. Grant, A. E. Keating, Determinants of BH3 binding specificity for Mcl-1 versus Bcl-xL. *Journal of molecular biology* **398**, 747–762 (2010).
226. S. Dutta, T. S. Chen, A. E. Keating, Peptide ligands for pro-survival protein Bfl-1 from computationally guided library screening. *ACS chemical biology* **8**, 778–788 (2013).
227. H. Du, J. Wolf, B. Schafer, T. Moldoveanu, J. E. Chipuk, T. Kuwana, BH3 domains other than Bim and Bid can directly activate Bax/Bak. *Journal of Biological Chemistry* **286**, 491–501 (2011).
228. J. Montero, A. Letai, Why do BCL-2 inhibitors work and where should we use them in the clinic? *Cell death and differentiation* **25**, 56–64 (2018).
229. A. Aouacheria, V. Rech de Laval, C. Combet, J. M. Hardwick, Evolution of Bcl-2 homology motifs: homology versus homoplasy. *Trends in cell biology* **23**, 103–111 (2013).
230. S.-Y. Kim, X. Song, L. Zhang, D. L. Bartlett, Y. J. Lee, Role of Bcl-xL/Beclin-1 in interplay between apoptosis and autophagy in oxaliplatin and bortezomib-induced cell death. *Biochemical pharmacology* **88**, 178–188 (2014).
231. J. Yang, H. Vais, W. Gu, J. K. Foskett, Biphasic regulation of InsP3 receptor gating by dual Ca<sup>2+</sup> release channel BH3-like domains mediates Bcl-xL control of cell viability. *Proceedings of the National Academy of Sciences of the United States of America* **113**, E1953-62 (2016).
232. Q. Zhong, W. Gao, F. Du, X. Wang, Mule/ARF-BP1, a BH3-only E3 ubiquitin ligase, catalyzes the polyubiquitination of Mcl-1 and regulates apoptosis. *Cell* **121**, 1085–1095 (2005).
233. D. Lim, S.-H. Choe, S. Jin, S. Lee, Y. Kim, H.-C. Shin, J. S. Choi, D.-B. Oh, S. J. Kim, J. Seo, et al., Structural basis for proapoptotic activation of Bak by the noncanonical BH3-only protein Pxt1. *PLoS Biology* **21**, e3002156 (2023).
234. A. Aouacheria, C. Combet, P. Tompa, J. M. Hardwick, Redefining the BH3 Death Domain as a 'Short Linear Motif'. *Trends in Biochemical Sciences* **40**, 736–748 (2015).
235. T. Oltersdorf, S. W. Elmore, A. R. Shoemaker, R. C. Armstrong, D. J. Augeri, B. A. Belli, M. Bruncko, T. L. Deckwerth, J. Dinges, P. J. Hajduk, et al., An inhibitor of Bcl-2 family proteins induces regression of solid tumours. *Nature* **435**, 677–681 (2005).
236. E. White, Role of the metabolic stress responses of apoptosis and autophagy in tumor suppression. *Ernst Schering Foundation symposium proceedings*. 10.1007/2789\_2008\_087, 23–34 (2007).

237. M. Macheret, T. D. Halazonetis, DNA replication stress as a hallmark of cancer. *Annual review of pathology* **10**, 425–448 (2015).
238. T. Ni Chonghaile, K. A. Sarosiek, T.-T. Vo, J. A. Ryan, A. Tammareddi, V. G. Del Moore, J. Deng, K. C. Anderson, P. Richardson, Y.-T. Tai, et al., Pretreatment mitochondrial priming correlates with clinical response to cytotoxic chemotherapy. *Science (New York, N.Y.)* **334**, 1129–1133 (2011).
239. A. C. Faber, D. Li, Y. Song, M.-C. Liang, B. Y. Yeap, R. T. Bronson, E. Lifshits, Z. Chen, S.-M. Maira, C. García-Echeverría, et al., Differential induction of apoptosis in HER2 and EGFR addicted cancers following PI3K inhibition. *Proceedings of the National Academy of Sciences of the United States of America* **106**, 19503–19508 (2009).
240. A. Bender, D. Opel, I. Naumann, R. Kappler, L. Friedman, D. von Schweinitz, K.-M. Debatin, S. Fulda, PI3K inhibitors prime neuroblastoma cells for chemotherapy by shifting the balance towards pro-apoptotic Bcl-2 proteins and enhanced mitochondrial apoptosis. *Oncogene* **30**, 494–503 (2011).
241. V. Del Gaizo Moore, J. R. Brown, M. Certo, T. M. Love, C. D. Novina, A. Letai, Chronic lymphocytic leukemia requires BCL2 to sequester prodeath BIM, explaining sensitivity to BCL2 antagonist ABT-737. *The Journal of clinical investigation* **117**, 112–121 (2007).
242. S. P. Glaser, E. F. Lee, E. Trounson, P. Bouillet, A. Wei, W. D. Fairlie, D. J. Izon, J. Zuber, A. R. Rappaport, M. J. Herold, et al., Anti-apoptotic Mcl-1 is essential for the development and sustained growth of acute myeloid leukemia. *Genes & development* **26**, 120–125 (2012).
243. V. Peperzak, I. Vikström, J. Walker, S. P. Glaser, M. LePage, C. M. Coquery, L. D. Erickson, K. Fairfax, F. Mackay, A. Strasser, et al., Mcl-1 is essential for the survival of plasma cells. *Nature immunology* **14**, 290–297 (2013).
244. A. J. Souers, J. D. Levenson, E. R. Boghaert, S. L. Ackler, N. D. Catron, J. Chen, B. D. Dayton, H. Ding, S. H. Enschede, W. J. Fairbrother, et al., ABT-199, a potent and selective BCL-2 inhibitor, achieves antitumor activity while sparing platelets. *Nature medicine* **19**, 202–208 (2013).
245. A. Letai, M. D. Sorcinelli, C. Beard, S. J. Korsmeyer, Antiapoptotic BCL-2 is required for maintenance of a model leukemia. *Cancer cell* **6**, 241–249 (2004).
246. G. L. Kelly, S. Grabow, S. P. Glaser, L. Fitzsimmons, B. J. Aubrey, T. Okamoto, L. J. Valente, M. Robati, L. Tai, W. D. Fairlie, et al., Targeting of MCL-1 kills MYC-driven mouse and human lymphomas even when they bear mutations in p53. *Genes & development* **28**, 58–70 (2014).
247. M. J. Morris, W. P. Tong, C. Cordon-Cardo, M. Drobnjak, W. K. Kelly, S. F. Slovin, K. L. Terry, K. Siedlecki, P. Swanson, M. Rafi, et al., Phase I trial of BCL-2 antisense oligonucleotide (G3139) administered by continuous intravenous infusion in patients with advanced cancer. *Clinical cancer research : an official journal of the American Association for Cancer Research* **8**, 679–683 (2002).
248. C. Tse, A. R. Shoemaker, J. Adickes, M. G. Anderson, J. Chen, S. Jin, E. F. Johnson, K. C. Marsh, M. J. Mitten, P. Nimmer, et al., ABT-263: a potent and orally bioavailable Bcl-2 family inhibitor. *Cancer research* **68**, 3421–3428 (2008).
249. S. M. Schoenwaelder, K. E. Jarman, E. E. Gardiner, M. Hua, J. Qiao, M. J. White, E. C. Josefsson, I. Alwis, A. Ono, A. Willcox, et al., Bcl-xL-inhibitory BH3 mimetics can induce a transient thrombocytopenia that undermines the hemostatic function of platelets. *Blood* **118**, 1663–1674 (2011).



250. M. F. van Delft, A. H. Wei, K. D. Mason, C. J. Vandenberg, L. Chen, P. E. Czabotar, S. N. Willis, C. L. Scott, C. L. Day, S. Cory, et al., The BH3 mimetic ABT-737 targets selective Bcl-2 proteins and efficiently induces apoptosis via Bak/Bax if Mcl-1 is neutralized. *Cancer cell* **10**, 389–399 (2006).
251. M. H. Kang, Y. H. Kang, B. Szymanska, U. Wilczynska-Kalak, M. A. Sheard, T. M. Harned, R. B. Lock, C. P. Reynolds, Activity of vincristine, L-ASP, and dexamethasone against acute lymphoblastic leukemia is enhanced by the BH3-mimetic ABT-737 in vitro and in vivo. *Blood* **110**, 2057–2066 (2007).
252. W. H. Wilson, O. A. O'Connor, M. S. Czuczman, A. S. LaCasce, J. F. Gerecitano, J. P. Leonard, A. Tulpule, K. Dunleavy, H. Xiong, Y.-L. Chiu, et al., Navitoclax, a targeted high-affinity inhibitor of BCL-2, in lymphoid malignancies: a phase 1 dose-escalation study of safety, pharmacokinetics, pharmacodynamics, and antitumour activity. *The Lancet. Oncology* **11**, 1149–1159 (2010).
253. A. W. Roberts, M. S. Davids, J. M. Pagel, B. S. Kahl, S. D. Puvvada, J. F. Gerecitano, T. J. Kipps, M. A. Anderson, J. R. Brown, L. Gressick, et al., Targeting BCL2 with Venetoclax in Relapsed Chronic Lymphocytic Leukemia. *The New England journal of medicine* **374**, 311–322 (2016).
254. C. D. DiNardo, K. Pratz, V. Pullarkat, B. A. Jonas, M. Arellano, P. S. Becker, O. Frankfurt, M. Konopleva, A. H. Wei, H. M. Kantarjian, et al., Venetoclax combined with decitabine or azacitidine in treatment-naive, elderly patients with acute myeloid leukemia. *Blood* **133**, 7–17 (2019).
255. S. Kehr, M. Vogler, It's time to die: BH3 mimetics in solid tumors. *Biochimica et biophysica acta. Molecular cell research* **1868**, 118987 (2021).
256. C. Alcon, A. Manzano-Muñoz, E. Prada, J. Mora, A. Soriano, G. Guillén, S. Gallego, J. Roma, J. Samitier, A. Villanueva, et al., Sequential combinations of chemotherapeutic agents with BH3 mimetics to treat rhabdomyosarcoma and avoid resistance. *Cell Death Dis* **11**, 634 (2020).
257. H.-Y. Tseng, J. Dreyer, A. A. Emran, D. Gunatilake, M. Pirozyan, C. Cullinane, K. Dutton-Regester, H. Rizos, N. K. Hayward, G. McArthur, et al., Co-targeting bromodomain and extra-terminal proteins and MCL1 induces synergistic cell death in melanoma. *International journal of cancer* **147**, 2176–2189 (2020).
258. B. Cucarull, A. Tutusaus, M. Subías, M. Stefanovic, T. Hernández-Alsina, L. Boix, M. Reig, P. García de Frutos, M. Marí, A. Colell, et al., Regorafenib Alteration of the BCL-xL/MCL-1 Ratio Provides a Therapeutic Opportunity for BH3-Mimetics in Hepatocellular Carcinoma Models. *Cancers* **12** (2020).
259. L. A. Barclay, T. E. Wales, T. P. Garner, F. Wachter, S. Lee, R. M. Guerra, M. L. Stewart, C. R. Braun, G. H. Bird, E. Gavathiotis, et al., Inhibition of Pro-apoptotic BAX by a noncanonical interaction mechanism. *Molecular cell* **57**, 873–886 (2015).
260. B. Han, D. Park, R. Li, M. Xie, T. K. Owonikoko, G. Zhang, G. L. Sica, C. Ding, J. Zhou, A. T. Magis, et al., Small-Molecule Bcl2 BH4 Antagonist for Lung Cancer Therapy. *Cancer cell* **27**, 852–863 (2015).
261. M. Sancho, M. Orzáez, BOK-MCL1 transmembrane interactions: a challenging target for cancer therapy. *Molecular & cellular oncology* **8**, 1859918 (2021).
262. S. Jayasinghe, K. Hristova, S. H. White, MPTopo: A database of membrane protein topology. *Protein science : a publication of the Protein Society* **10**, 455–458 (2001).
263. L. Fagerberg, K. Jonasson, G. von Heijne, M. Uhlén, L. Berglund, Prediction of the human membrane proteome. *Proteomics* **10**, 1141–1149 (2010).

264. G. C. Brito, W. Schormann, S. K. Gidda, R. T. Mullen, D. W. Andrews, Genome-wide analysis of *Homo sapiens*, *Arabidopsis thaliana*, and *Saccharomyces cerevisiae* reveals novel attributes of tail-anchored membrane proteins. *BMC Genomics* **20**, 835 (2019).
265. D. J. Müller, N. Wu, K. Palczewski, Vertebrate membrane proteins: structure, function, and insights from biophysical approaches. *Pharmacological reviews* **60**, 43–78 (2008).
266. M. A. Lemmon, J. M. Flanagan, H. R. Treutlein, J. Zhang, D. M. Engelman, Sequence specificity in the dimerization of transmembrane alpha-helices. *Biochemistry* **31**, 12719–12725 (1992).
267. M. A. Lemmon, H. R. Treutlein, P. D. Adams, A. T. Brünger, D. M. Engelman, A dimerization motif for transmembrane alpha-helices. *Nature structural biology* **1**, 157–163 (1994).
268. M. L. Plotkowski, S. Kim, M. L. Phillips, A. W. Partridge, C. M. Deber, J. U. Bowie, Transmembrane domain of myelin protein zero can form dimers: possible implications for myelin construction. *Biochemistry* **46**, 12164–12173 (2007).
269. A. Senes, M. Gerstein, D. M. Engelman, Statistical analysis of amino acid patterns in transmembrane helices: the GxxxG motif occurs frequently and in association with beta-branched residues at neighboring positions. *Journal of molecular biology* **296**, 921–936 (2000).
270. A. R. Curran, D. M. Engelman, Sequence motifs, polar interactions and conformational changes in helical membrane proteins. *Current opinion in structural biology* **13**, 412–417 (2003).
271. A. Fink, N. Sal-Man, D. Gerber, Y. Shai, Transmembrane domains interactions within the membrane milieu: principles, advances and challenges. *Biochimica et biophysica acta* **1818**, 974–983 (2012).
272. J. P. Dawson, J. S. Weinger, D. M. Engelman, Motifs of serine and threonine can drive association of transmembrane helices. *Journal of molecular biology* **316**, 799–805 (2002).
273. D. Langosch, J. Heringa, Interaction of transmembrane helices by a knobs-into-holes packing characteristic of soluble coiled coils. *Proteins* **31**, 150–159 (1998).
274. J. P. Dawson, R. A. Melnyk, C. M. Deber, D. M. Engelman, Sequence context strongly modulates association of polar residues in transmembrane helices. *Journal of molecular biology* **331**, 255–262 (2003).
275. V. Anbazhagan, C. Munz, L. Tome, D. Schneider, Fluidizing the membrane by a local anesthetic: phenylethanol affects membrane protein oligomerization. *Journal of molecular biology* **404**, 773–777 (2010).
276. T. Nilsson, C. R. Lundin, G. Nordlund, P. Ädelroth, C. von Ballmoos, P. Brzezinski, Lipid-mediated Protein-protein Interactions Modulate Respiration-driven ATP Synthesis. *Sci Rep* **6**, 24113 (2016).
277. X. Cong, Y. Liu, W. Liu, X. Liang, A. Laganowsky, Allosteric modulation of protein-protein interactions by individual lipid binding events. *Nat Commun* **8**, 2203 (2017).
278. N. Borgese, S. Colombo, E. Pedrazzini, The tale of tail-anchored proteins: coming from the cytosol and looking for a membrane. *J Cell Biol* **161**, 1013–1019 (2003).
279. M. P. A. Henderson, Y. T. Hwang, J. M. Dyer, R. T. Mullen, D. W. Andrews, The C-terminus of cytochrome b5 confers endoplasmic reticulum specificity by preventing spontaneous insertion into membranes. *The Biochemical journal* **401**, 701–709 (2007).

280. H. Kato, K. Mihara, Identification of Tom5 and Tom6 in the preprotein translocase complex of human mitochondrial outer membrane. *Biochemical and biophysical research communications* **369**, 958–963 (2008).
281. Y. A. Chen, R. H. Scheller, SNARE-mediated membrane fusion. *Nature reviews. Molecular cell biology* **2**, 98–106 (2001).
282. M. Germain, J. P. Mathai, G. C. Shore, BH-3-only BIK functions at the endoplasmic reticulum to stimulate cytochrome c release from mitochondria. *The Journal of biological chemistry* **277**, 18053–18060 (2002).
283. F. Wilfling, A. Weber, S. Potthoff, F.-N. Vögtle, C. Meisinger, S. A. Paschen, G. Häcker, BH3-only proteins are tail-anchored in the outer mitochondrial membrane and can initiate the activation of Bax. *Cell Death Differ* **19**, 1328–1336 (2012).
284. V. Andreu-Fernández, M. J. García-Murria, M. Bañó-Polo, J. Martín, L. Monticelli, M. Orzáez, I. Mingarro, The C-terminal Domains of Apoptotic BH3-only Proteins Mediate Their Insertion into Distinct Biological Membranes. *Journal of Biological Chemistry* **291**, 25207–25216 (2016).
285. A. M. Petros, A. Medek, D. G. Nettesheim, D. H. Kim, H. S. Yoon, K. Swift, E. D. Matayoshi, T. Oltersdorf, S. W. Fesik, Solution structure of the antiapoptotic protein bcl-2. *Proceedings of the National Academy of Sciences of the United States of America* **98**, 3012–3017 (2001).
286. Q. Liu, T. Moldoveanu, T. Sprules, E. Matta-Camacho, N. Mansur-Azzam, K. Gehring, Apoptotic regulation by MCL-1 through heterodimerization. *Journal of Biological Chemistry* **285**, 19615–19624 (2010).
287. W. A. Hendrickson, Atomic-level analysis of membrane-protein structure. *Nat Struct Mol Biol* **23**, 464–467 (2016).
288. A. Schinzel, T. Kaufmann, C. Borner, Bcl-2 family members: integrators of survival and death signals in physiology and pathology corrected. *Biochimica et biophysica acta* **1644**, 95–105 (2004).
289. M. Saito, S. J. Korsmeyer, P. H. Schlesinger, BAX-dependent transport of cytochrome c reconstituted in pure liposomes. *Nature cell biology* **2**, 553–555 (2000).
290. R. P. Guedes, E. Rocha, J. Mahiou, H. P. Moll, M. B. Arvelo, J. M. Taube, C. R. Peterson, E. Kaczmarek, C. R. Longo, C. G. Da Silva, et al., The C-terminal domain of A1/Bfl-1 regulates its anti-inflammatory function in human endothelial cells. *Biochimica et biophysica acta* **1833**, 1553–1561 (2013).
291. D. Stehle, M. Grimm, S. Einsele-Scholz, F. Ladwig, J. Johanning, G. Fischer, B. Gillissen, K. Schulze-Osthoff, F. Essmann, Contribution of BH3-domain and Transmembrane-domain to the Activity and Interaction of the Pore-forming Bcl-2 Proteins Bok, Bak, and Bax. *Scientific reports* **8**, 12434 (2018).
292. S. J. Gardai, D. A. Hildeman, S. K. Frankel, B. B. Whitlock, S. C. Frasch, N. Borregaard, P. Marrack, D. L. Bratton, P. M. Henson, Phosphorylation of Bax Ser184 by Akt regulates its activity and apoptosis in neutrophils. *The Journal of biological chemistry* **279**, 21085–21095 (2004).
293. J. Kale, O. Kutuk, G. C. Brito, T. S. Andrews, B. Leber, A. Letai, D. W. Andrews, Phosphorylation switches Bax from promoting to inhibiting apoptosis thereby increasing drug resistance. *EMBO Reports* **19** (2018).
294. X. Pang, J. Zhang, H. Lopez, Y. Wang, W. Li, K. L. O'Neill, J. J. D. Evans, N. M. George, J. Long, Y. Chen, et al., The carboxyl-terminal tail of Noxa protein regulates the stability of Noxa and Mcl-1. *Journal of Biological Chemistry* **289**, 17802–17811 (2014).

295. W. Zhu, A. Cowie, G. W. Wasfy, L. Z. Penn, B. Leber, D. W. Andrews, Bcl-2 mutants with restricted subcellular location reveal spatially distinct pathways for apoptosis in different cell types. *The EMBO journal* **15**, 4130–4141 (1996).
296. K. Setoguchi, H. Otera, K. Mihara, Cytosolic factor- and TOM-independent import of C-tail-anchored mitochondrial outer membrane proteins. *The EMBO journal* **25**, 5635–5647 (2006).
297. B. Egan, T. Beilharz, R. George, S. Isenmann, S. Gratzer, B. Wattenberg, T. Lithgow, Targeting of tail-anchored proteins to yeast mitochondria in vivo. *FEBS letters* **451**, 243–248 (1999).
298. A. D. Linstedt, M. Foguet, M. Renz, H. P. Seelig, B. S. Glick, H. P. Hauri, A C-terminally-anchored Golgi protein is inserted into the endoplasmic reticulum and then transported to the Golgi apparatus. *Proceedings of the National Academy of Sciences of the United States of America* **92**, 5102–5105 (1995).
299. E. Pedrazzini, A. Villa, N. Borgese, A mutant cytochrome b5 with a lengthened membrane anchor escapes from the endoplasmic reticulum and reaches the plasma membrane. *Proceedings of the National Academy of Sciences of the United States of America* **93**, 4207–4212 (1996).
300. N. Borgese, I. Gazzoni, M. Barberi, S. Colombo, E. Pedrazzini, Targeting of a tail-anchored protein to endoplasmic reticulum and mitochondrial outer membrane by independent but competing pathways. *Molecular Biology of the Cell* **12**, 2482–2496 (2001).
301. H. J. Sharpe, T. J. Stevens, S. Munro, A comprehensive comparison of transmembrane domains reveals organelle-specific properties. *Cell* **142**, 158–169 (2010).
302. A. Nechushtan, C. L. Smith, Y. T. Hsu, R. J. Youle, Conformation of the Bax C-terminus regulates subcellular location and cell death. *The EMBO journal* **18**, 2330–2341 (1999).
303. F. Janiak, B. Leber, D. W. Andrews, Assembly of Bcl-2 into microsomal and outer mitochondrial membranes. *The Journal of biological chemistry* **269**, 9842–9849 (1994).
304. P. K. Kim, M. G. Annis, P. J. Dlugosz, B. Leber, D. W. Andrews, During apoptosis bcl-2 changes membrane topology at both the endoplasmic reticulum and mitochondria. *Molecular cell* **14**, 523–529 (2004).
305. C. Kemper, S. J. Habib, G. Engl, P. Heckmeyer, K. S. Dimmer, D. Rapaport, Integration of tail-anchored proteins into the mitochondrial outer membrane does not require any known import components. *Journal of cell science* **121**, 1990–1998 (2008).
306. E. J. Osterlund, N. Hirmiz, D. Nguyen, J. M. Pemberton, Q. Fang, D. W. Andrews, Endoplasmic reticulum protein BIK binds to and inhibits mitochondria-localized antiapoptotic proteins. *The Journal of biological chemistry* **299**, 102863 (2023).
307. W. Nakajima, M. A. Hicks, N. Tanaka, G. W. Krystal, H. Harada, Noxa determines localization and stability of MCL-1 and consequently ABT-737 sensitivity in small cell lung cancer. *Cell Death Dis* **5**, e1052 (2014).
308. K. Lei, R. J. Davis, JNK phosphorylation of Bim-related members of the Bcl2 family induces Bax-dependent apoptosis. *Proceedings of the National Academy of Sciences of the United States of America* **100**, 2432–2437 (2003).
309. C. L. Day, H. Puthalakath, G. Skea, A. Strasser, I. Barsukov, L.-Y. Lian, D. C. S. Huang, M. G. Hinds, Localization of dynein light chains 1 and 2 and their pro-apoptotic ligands. *The Biochemical journal* **377**, 597–605 (2004).

310. P.-F. Cartron, C. Moreau, L. Oliver, E. Mayat, K. Meflah, F. M. Vallette, Involvement of the N-terminus of Bax in its intracellular localization and function. *FEBS letters* **512**, 95–100 (2002).
311. M. Shirane, K. I. Nakayama, Inherent calcineurin inhibitor FKBP38 targets Bcl-2 to mitochondria and inhibits apoptosis. *Nature cell biology* **5**, 28–37 (2003).
312. C.-R. Huang, H.-F. Yang-Yen, The fast-mobility isoform of mouse Mcl-1 is a mitochondrial matrix-localized protein with attenuated anti-apoptotic activity. *FEBS letters* **584**, 3323–3330 (2010).
313. N. Borgese, E. Fasana, Targeting pathways of C-tail-anchored proteins. *Biochimica et biophysica acta* **1808**, 937–946 (2011).
314. G. J. Steel, J. Brownsword, C. J. Stirling, Tail-anchored protein insertion into yeast ER requires a novel posttranslational mechanism which is independent of the SEC machinery. *Biochemistry* **41**, 11914–11920 (2002).
315. M. Yabal, S. Brambillasca, P. Soffientini, E. Pedrazzini, N. Borgese, M. Makarow, Translocation of the C terminus of a tail-anchored protein across the endoplasmic reticulum membrane in yeast mutants defective in signal peptide-driven translocation. *Journal of Biological Chemistry* **278**, 3489–3496 (2003).
316. S. Stefanovic, R. S. Hegde, Identification of a targeting factor for posttranslational membrane protein insertion into the ER. *Cell* **128**, 1147–1159 (2007).
317. V. Favaloro, M. Spasic, B. Schwappach, B. Dobberstein, Distinct targeting pathways for the membrane insertion of tail-anchored (TA) proteins. *Journal of cell science* **121**, 1832–1840 (2008).
318. S. F. Colombo, R. Longhi, N. Borgese, The role of cytosolic proteins in the insertion of tail-anchored proteins into phospholipid bilayers. *Journal of cell science* **122**, 2383–2392 (2009).
319. P. K. Kim, F. Janiak-Spens, W. S. Trimble, B. Leber, D. W. Andrews, Evidence for multiple mechanisms for membrane binding and integration via carboxyl-terminal insertion sequences. *Biochemistry* **36**, 8873–8882 (1997).
320. A. Torrecillas, M. M. Martínez-Senac, A. Ausili, S. Corbalán-García, J. C. Gómez-Fernández, Interaction of the C-terminal domain of Bcl-2 family proteins with model membranes. *Biochimica et biophysica acta* **1768**, 2931–2939 (2007).
321. V. Andreu-Fernández, A. Genoves, T.-H. Lee, M. Stellato, F. Lucantoni, M. Orzáez, I. Mingarro, M.-I. Aguilar, E. Pérez-Payá, Peptides derived from the transmembrane domain of Bcl-2 proteins as potential mitochondrial priming tools. *ACS chemical biology* **9**, 1799–1811 (2014).
322. J. Lauterwasser, F. Todt, R. M. Zerbes, T. N. Nguyen, W. Craigen, M. Lazarou, M. van der Laan, F. Edlich, The porin VDAC2 is the mitochondrial platform for Bax retrotranslocation. *Sci Rep* **6**, 32994 (2016).
323. H. S. Chin, M. X. Li, I. K. L. Tan, R. L. Ninnis, B. Reljic, K. Scicluna, L. F. Dagley, J. J. Sandow, G. L. Kelly, A. L. Samson, et al., VDAC2 enables BAX to mediate apoptosis and limit tumor development. *Nat Commun* **9**, 4976 (2018).
324. M. Fröhlich, B. Dejanovic, H. Kashkar, G. Schwarz, S. Nussberger, S-palmitoylation represents a novel mechanism regulating the mitochondrial targeting of BAX and initiation of apoptosis. *Cell Death Dis* **5**, e1057 (2014).
325. A. Ausili, A. de Godos, A. Torrecillas, S. Corbalán-García, J. C. Gómez-Fernández, The interaction of the Bax C-terminal domain with membranes is influenced by the presence of negatively charged phospholipids. *Biochimica et biophysica acta* **1788**, 1924–1932 (2009).

326. S.-Y. Jeong, B. Gaume, Y.-J. Lee, Y.-T. Hsu, S.-W. Ryu, S.-H. Yoon, R. J. Youle, Bcl-x(L) sequesters its C-terminal membrane anchor in soluble, cytosolic homodimers. *The EMBO journal* **23**, 2146–2155 (2004).
327. M. I. Anasir, S. Caria, M. A. Skinner, M. Kvensakul, Structural basis of apoptosis inhibition by the fowlpox virus protein FPV039. *Journal of Biological Chemistry* **292**, 9010–9021 (2017).
328. K. A. Sarosiek, X. Chi, J. A. Bachman, J. J. Sims, J. Montero, L. Patel, A. Flanagan, D. W. Andrews, P. Sorger, A. Letai, BID preferentially activates BAK while BIM preferentially activates BAX, affecting chemotherapy response. *Molecular cell* **51**, 751–765 (2013).
329. F. Todt, Z. Cakir, F. Reichenbach, R. J. Youle, F. Edlich, The C-terminal helix of Bcl-x(L) mediates Bax retrotranslocation from the mitochondria. *Cell death and differentiation* **20**, 333–342 (2013).
330. Z. Zhang, W. Zhu, S. M. Lapolla, Y. Miao, Y. Shao, M. Falcone, D. Boreham, N. McFarlane, J. Ding, A. E. Johnson, et al., Bax forms an oligomer via separate, yet interdependent, surfaces. *The Journal of biological chemistry* **285**, 17614–17627 (2010).
331. S. Iyer, F. Bell, D. Westphal, K. Anwari, J. Gulbis, B. J. Smith, G. Dewson, R. M. Kluck, Bak apoptotic pores involve a flexible C-terminal region and juxtaposition of the C-terminal transmembrane domains. *Cell Death Differ* **22**, 1665–1675 (2015).
332. Z. Zhang, S. Subramaniam, J. Kale, C. Liao, B. Huang, H. Brahmabhatt, S. G. F. Condon, S. M. Lapolla, F. A. Hays, J. Ding, et al., BH3-in-groove dimerization initiates and helix 9 dimerization expands Bax pore assembly in membranes. *The EMBO journal* **35**, 208–236 (2016).
333. E. Lucendo, M. Sancho, F. Lolicato, M. Javanainen, W. Kulig, D. Leiva, G. Duarte, V. Andreu-Fernández, I. Mingarro, M. Orzáez, Mcl-1 and Bok transmembrane domains: Unexpected players in the modulation of apoptosis. *Proceedings of the National Academy of Sciences of the United States of America* **117**, 27980–27988 (2020).
334. Q. Liu, E. J. Osterlund, X. Chi, J. Pogmore, B. Leber, D. W. Andrews, Bim escapes displacement by BH3-mimetic anti-cancer drugs by double-bolt locking both Bcl-XL and Bcl-2. *eLife* **8** (2019).
335. X. Chi, D. Nguyen, J. M. Pemberton, E. J. Osterlund, Q. Liu, H. Brahmabhatt, Z. Zhang, J. Lin, B. Leber, D. W. Andrews, The carboxyl-terminal sequence of bim enables bax activation and killing of unprimed cells. *eLife* **9** (2020).
336. J. M. Pemberton, D. Nguyen, E. J. Osterlund, W. Schormann, J. P. Pogmore, N. Hirmiz, B. Leber, D. W. Andrews, The carboxyl-terminal sequence of PUMA binds to both anti-apoptotic proteins and membranes. *eLife Sciences Publications, Ltd* (2023).
337. H. Ivanova, A. Ritaine, L. Wagner, T. Luyten, G. Shapovalov, K. Welkenhuyzen, B. Seitaj, G. Monaco, H. de Smedt, N. Prevarskaya, et al., The trans-membrane domain of Bcl-2 $\alpha$ , but not its hydrophobic cleft, is a critical determinant for efficient IP3 receptor inhibition. *Oncotarget* **7**, 55704–55720 (2016).
338. M. Lazarou, D. Stojanovski, A. E. Frazier, A. Kotevski, G. Dewson, W. J. Craigen, R. M. Kluck, D. L. Vaux, M. T. Ryan, Inhibition of Bak activation by VDAC2 is dependent on the Bak transmembrane anchor. *The Journal of biological chemistry* **285**, 36876–36883 (2010).

339. M. J. García-Murria, G. Duart, B. Grau, E. Diaz-Beneitez, D. Rodríguez, I. Mingarro, L. Martínez-Gil, Viral Bcl2s' transmembrane domain interact with host Bcl2 proteins to control cellular apoptosis. *Nat Commun* **11**, 6056 (2020).
340. J. Jumper, R. Evans, A. Pritzel, T. Green, M. Figurnov, O. Ronneberger, K. Tunyasuvunakool, R. Bates, A. Žídek, A. Potapenko, et al., Highly accurate protein structure prediction with AlphaFold. *Nature* **596**, 583–589 (2021).
341. J. Schindelin, I. Arganda-Carreras, E. Frise, V. Kaynig, M. Longair, T. Pietzsch, S. Preibisch, C. Rueden, S. Saalfeld, B. Schmid, et al., Fiji: an open-source platform for biological-image analysis. *Nat Methods* **9**, 676–682 (2012).
342. L. Schrödinger, The PyMOL Molecular Graphics System, Version 2.0 (2023).
343. A. M. Waterhouse, J. B. Procter, D. M. A. Martin, M. Clamp, G. J. Barton, Jalview Version 2--a multiple sequence alignment editor and analysis workbench. *Bioinformatics (Oxford, England)* **25**, 1189–1191 (2009).
344. A. S. Dixon, M. K. Schwinn, M. P. Hall, K. Zimmerman, P. Otto, T. H. Lubben, B. L. Butler, B. F. Binkowski, T. Machleidt, T. A. Kirkland, et al., NanoLuc Complementation Reporter Optimized for Accurate Measurement of Protein Interactions in Cells. *ACS chemical biology* **11**, 400–408 (2016).
345. E. Gasteiger, C. Hoogland, A. Gattiker, S. Duvaud, M. R. Wilkins, R. D. Appel, A. Bairoch, "Protein Identification and Analysis Tools on the ExPASy Server" in *The Proteomics Protocols Handbook* (Humana Press, 2005), pp. 571–607.
346. J. Kyte, R. F. Doolittle, A simple method for displaying the hydropathic character of a protein. *Journal of molecular biology* **157**, 105–132 (1982).
347. T. A. Wassenaar, H. I. Ingólfsson, R. A. Böckmann, D. P. Tieleman, S. J. Marrink, Computational Lipidomics with insane: A Versatile Tool for Generating Custom Membranes for Molecular Simulations. *Journal of chemical theory and computation* **11**, 2144–2155 (2015).
348. K. Pluhackova, T. A. Wassenaar, S. Kirsch, R. A. Böckmann, Spontaneous adsorption of coiled-coil model peptides K and E to a mixed lipid bilayer. *The journal of physical chemistry. B* **119**, 4396–4408 (2015).
349. T. A. Wassenaar, K. Pluhackova, R. A. Böckmann, S. J. Marrink, D. P. Tieleman, Going Backward: A Flexible Geometric Approach to Reverse Transformation from Coarse Grained to Atomistic Models. *Journal of chemical theory and computation* **10**, 676–690 (2014).
350. J. B. Klauda, R. M. Venable, J. A. Freites, J. W. O'Connor, D. J. Tobias, C. Mondragon-Ramirez, I. Vorobyov, A. D. MacKerell, R. W. Pastor, Update of the CHARMM all-atom additive force field for lipids: validation on six lipid types. *The journal of physical chemistry. B* **114**, 7830–7843 (2010).
351. P. Bjelkmar, P. Larsson, M. A. Cuendet, B. Hess, E. Lindahl, Implementation of the CHARMM Force Field in GROMACS: Analysis of Protein Stability Effects from Correction Maps, Virtual Interaction Sites, and Water Models. *Journal of chemical theory and computation* **6**, 459–466 (2010).
352. J. B. Lim, B. Rogaski, J. B. Klauda, Update of the cholesterol force field parameters in CHARMM. *The journal of physical chemistry. B* **116**, 203–210 (2012).
353. J. Huang, S. Rauscher, G. Nawrocki, T. Ran, M. Feig, B. L. de Groot, H. Grubmüller, A. D. MacKerell, CHARMM36m: an improved force field for folded and intrinsically disordered proteins. *Nature methods* **14**, 71–73 (2017).
354. W. L. Jorgensen, J. D. Madura, Temperature and size dependence for Monte Carlo simulations of TIP4P water. *Molecular Physics* **56**, 1381–1392 (1985).

355. M. J. Abraham, T. Murtola, R. Schulz, S. Páll, J. C. Smith, B. Hess, E. Lindahl, GROMACS: High performance molecular simulations through multi-level parallelism from laptops to supercomputers. *SoftwareX* **1-2**, 19–25 (2015).
356. T. Williams, C. Kelley, Gnuplot 4.6: an interactive plotting program.
357. S. Scrima, M. Tiberti, A. Campo, E. Corcelle-Termeau, D. Judith, M. M. Foged, K. K. B. Clemmensen, S. A. Tooze, M. Jäättelä, K. Maeda, et al., Unraveling membrane properties at the organelle-level with LipidDyn. *Computational and Structural Biotechnology Journal* **20**, 3604–3614 (2022).
358. C.-D. Hu, Y. Chinenov, T. K. Kerppola, Visualization of interactions among bZIP and Rel family proteins in living cells using bimolecular fluorescence complementation. *Molecular cell* **9**, 789–798 (2002).
359. A. G. Tebo, A. Gautier, A split fluorescent reporter with rapid and reversible complementation. *Nat Commun* **10**, 2822 (2019).
360. C. Köppl, N. Lingg, A. Fischer, C. Kröß, J. Loibl, W. Buchinger, R. Schneider, A. Jungbauer, G. Striedner, M. Cserjan-Puschmann, Fusion Tag Design Influences Soluble Recombinant Protein Production in Escherichia coli. *International journal of molecular sciences* **23** (2022).
361. C. G. England, E. B. Ehlerding, W. Cai, NanoLuc: A Small Luciferase Is Brightening Up the Field of Bioluminescence. *Bioconjugate chemistry* **27**, 1175–1187 (2016).
362. K. Taskén, B. S. Skålhegg, K. A. Taskén, R. Solberg, H. K. Knutsen, F. O. Levy, M. Sandberg, S. Orstavik, T. Larsen, A. K. Johansen, et al., Structure, function, and regulation of human cAMP-dependent protein kinases. *Advances in second messenger and phosphoprotein research* **31**, 191–204 (1997).
363. A. Landreman, M. Bach, M. Bjerke, Understanding Biology in Real Time. *tpub\_207* (2019).
364. R. Ali, S. Ramadurai, F. Barry, H. P. Nasheuer, Optimizing fluorescent protein expression for quantitative fluorescence microscopy and spectroscopy using herpes simplex thymidine kinase promoter sequences. *FEBS open bio* **8**, 1043–1060 (2018).
365. C. Horie, H. Suzuki, M. Sakaguchi, K. Mihara, Characterization of signal that directs C-tail-anchored proteins to mammalian mitochondrial outer membrane. *Molecular Biology of the Cell* **13**, 1615–1625 (2002).
366. A. Fabritius, D. Ng, A. M. Kist, M. Erdogan, R. Portugues, O. Griesbeck, Imaging-Based Screening Platform Assists Protein Engineering. *Cell chemical biology* **25**, 1554-1561.e8 (2018).
367. N. Nakamura, C. Rabouille, R. Watson, T. Nilsson, N. Hui, P. Slusarewicz, T. E. Kreis, G. Warren, Characterization of a cis-Golgi matrix protein, GM130. *J Cell Biol* **131**, 1715–1726 (1995).
368. J. Han, K. Pluhackova, R. A. Böckmann, Exploring the Formation and the Structure of Synaptobrevin Oligomers in a Model Membrane. *Biophysical journal* **110**, 2004–2015 (2016).
369. L. B. Alexandrov, S. Nik-Zainal, D. C. Wedge, P. J. Campbell, M. R. Stratton, Deciphering signatures of mutational processes operative in human cancer. *Cell reports* **3**, 246–259 (2013).
370. M. Buljan, P. Blattmann, R. Aebersold, M. Boutros, Systematic characterization of pan-cancer mutation clusters. *Molecular systems biology* **14**, e7974 (2018).



371. J. Adams, V. J. Palombella, E. A. Sausville, J. Johnson, A. Destree, D. D. Lazarus, J. Maas, C. S. Pien, S. Prakash, P. J. Elliott, Proteasome inhibitors: a novel class of potent and effective antitumor agents. *Cancer research* **59**, 2615–2622 (1999).
372. E. A. Obeng, L. M. Carlson, D. M. Gutman, W. J. Harrington, K. P. Lee, L. H. Boise, Proteasome inhibitors induce a terminal unfolded protein response in multiple myeloma cells. *Blood* **107**, 4907–4916 (2006).
373. N. P. J. Price, B. Tsvetanova, Biosynthesis of the tunicamycins: a review. *The Journal of antibiotics* **60**, 485–491 (2007).
374. J. Montero, R. Haq, Adapted to Survive: Targeting Cancer Cells with BH3 Mimetics. *Cancer discovery* **12**, 1217–1232 (2022).
375. S. Weller, A. Toennießen, B. Schaefer, T. Beigl, A. Muenchow, K. Böpplé, U. Hofmann, B. F. Gillissen, W. E. Aulitzky, H.-G. Kopp, et al., The BCL-2 inhibitor ABT-199/venetoclax synergizes with proteasome inhibition via transactivation of the MCL-1 antagonist NOXA. *Cell death discovery* **8**, 215 (2022).
376. A. Roca-Portoles, G. Rodriguez-Blanco, D. Sumpton, C. Cloix, M. Mullin, G. M. Mackay, K. O'Neill, L. Lemgruber, X. Luo, S. W. G. Tait, Venetoclax causes metabolic reprogramming independent of BCL-2 inhibition. *Cell Death & Disease* **11**, 616 (2020).
377. C. Correia, P. A. Schneider, H. Dai, A. Dogan, M. J. Maurer, A. K. Church, A. J. Novak, A. L. Feldman, X. Wu, H. Ding, et al., BCL2 mutations are associated with increased risk of transformation and shortened survival in follicular lymphoma. *Blood* **125**, 658–667 (2015).
378. M. A. Hernandez-Luna, L. Rocha-Zavaleta, M. I. Vega, S. Huerta-Yepez, Hypoxia inducible factor-1 $\alpha$  induces chemoresistance phenotype in non-Hodgkin lymphoma cell line via up-regulation of Bcl-xL. *Leukemia & lymphoma* **54**, 1048–1055 (2013).
379. D. Yecies, N. E. Carlson, J. Deng, A. Letai, Acquired resistance to ABT-737 in lymphoma cells that up-regulate MCL-1 and BFL-1. *Blood* **115**, 3304–3313 (2010).
380. A. J. Crowther, V. Gama, A. Bevilacqua, S. X. Chang, H. Yuan, M. Deshmukh, T. R. Gershon, Tonic activation of Bax primes neural progenitors for rapid apoptosis through a mechanism preserved in medulloblastoma. *The Journal of neuroscience : the official journal of the Society for Neuroscience* **33**, 18098–18108 (2013).
381. K. A. Sarosiek, C. Fraser, N. Muthalagu, P. D. Bhola, W. Chang, S. K. McBrayer, A. Cantlon, S. Fisch, G. Golomb-Mello, J. A. Ryan, et al., Developmental Regulation of Mitochondrial Apoptosis by c-Myc Governs Age- and Tissue-Specific Sensitivity to Cancer Therapeutics. *Cancer cell* **31**, 142–156 (2017).
382. M. He, M. S. Chaurushiya, J. D. Webster, S. Kummerfeld, R. Reja, S. Chaudhuri, Y.-J. Chen, Z. Modrusan, B. Haley, D. L. Dugger, et al., Intrinsic apoptosis shapes the tumor spectrum linked to inactivation of the deubiquitinase BAP1. *Science (New York, N.Y.)* **364**, 283–285 (2019).
383. H. Flores-Romero, L. Hohorst, M. John, M.-C. Albert, L. E. King, L. Beckmann, T. Szabo, V. Hertlein, X. Luo, A. Villunger, et al., BCL-2-family protein tBID can act as a BAX-like effector of apoptosis. *The EMBO journal* **41**, e108690 (2022).
384. H. Zhao, T. C. Doyle, R. J. Wong, Y. Gao, D. K. Stevenson, D. Piwnicka-Worms, C. H. Contag, Characterization of coelenterazine analogs for measurements of Renilla luciferase activity in live cells and living animals. *Molecular imaging* **3**, 43–54 (2004).

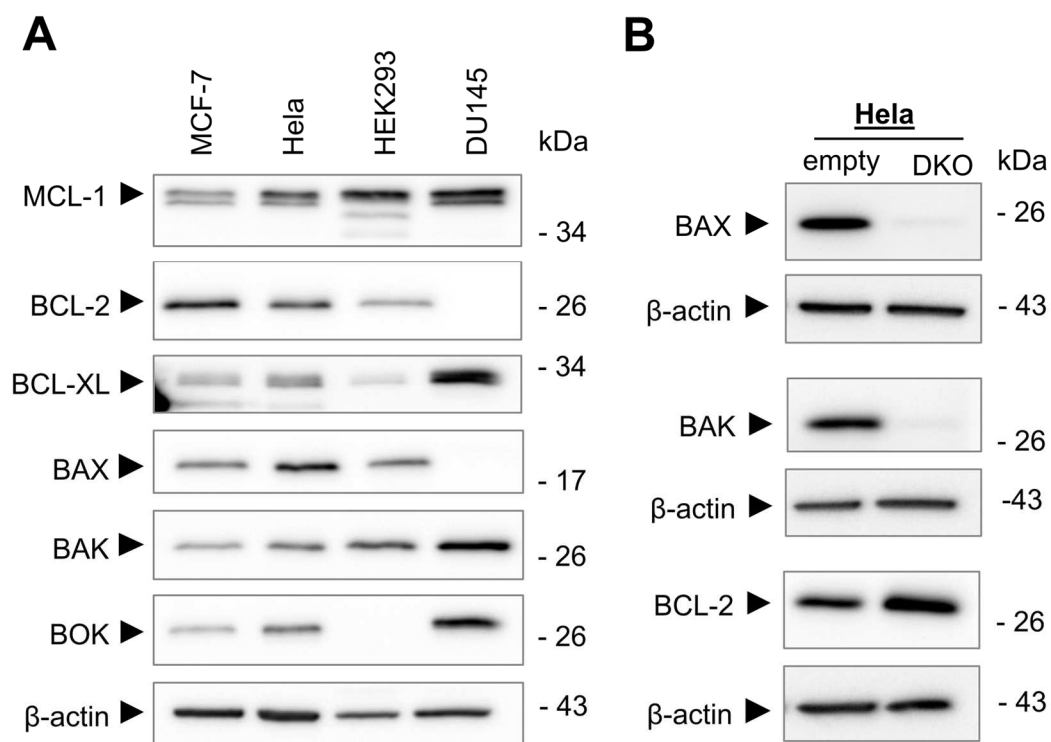
385. N. A. Perry-Hauser, W. B. Asher, M. Hauge Pedersen, J. A. Javitch, "Chapter 3 - Assays for detecting arrestin interaction with GPCRs" in *Methods in Cell Biology : Calcium in Living Cells*, M. Whitaker, Ed. (Academic Press, 2010), pp. 43–65.
386. Z. Liu, O. Chen, J. B. J. Wall, M. Zheng, Y. Zhou, L. Wang, H. R. Vaseghi, L. Qian, J. Liu, Systematic comparison of 2A peptides for cloning multi-genes in a polycistronic vector. *Sci Rep* **7**, 2193 (2017).
387. J. J. Gam, B. DiAndreth, R. D. Jones, J. Huh, R. Weiss, A 'poly-transfection' method for rapid, one-pot characterization and optimization of genetic systems. *Nucleic acids research* **47**, e106 (2019).
388. Y. Miao, Q. Du, H.-G. Zhang, Y. Yuan, Y. Zuo, H. Zheng, Cycloheximide (CHX) Chase Assay to Examine Protein Half-life. *Bio-protocol* **13**, e4690 (2023).
389. S. Rajan, M. Choi, K. Baek, H. S. Yoon, Bcl-XL induced conformational changes in Bcl-XL revealed by crystal structure and comparative analysis. *Proteins* **83**, 1262–1272 (2015).
390. P. Argos, An investigation of oligopeptides linking domains in protein tertiary structures and possible candidates for general gene fusion. *Journal of molecular biology* **211**, 943–958 (1990).
391. R. A. George, J. Heringa, An analysis of protein domain linkers: their classification and role in protein folding. *Protein engineering* **15**, 871–879 (2002).
392. E. J. Osterlund, N. Hirmiz, C. Tardif, D. W. Andrews, Rapid Imaging of BCL-2 Family Interactions in Live Cells Using FLIM-FRET. *Methods in molecular biology (Clifton, N.J.)* **1877**, 305–335 (2019).
393. M. G. Calvagno, C. Celia, D. Paolino, D. Cosco, M. Iannone, F. Castelli, P. Doldo, M. Frest, Effects of lipid composition and preparation conditions on physical-chemical properties, technological parameters and in vitro biological activity of gemcitabine-loaded liposomes. *Current drug delivery* **4**, 89–101 (2007).
394. E. B. van Munster, G. J. Kremers, M. J. W. Adjobo-Hermans, T. W. J. Gadella, Fluorescence resonance energy transfer (FRET) measurement by gradual acceptor photobleaching. *Journal of microscopy* **218**, 253–262 (2005).
395. F. Todt, Z. Cakir, F. Reichenbach, F. Emschermann, J. Lauterwasser, A. Kaiser, G. Ichim, S. W. G. Tait, S. Frank, H. F. Langer, et al., Differential retrotranslocation of mitochondrial Bax and Bak. *The EMBO journal* **34**, 67–80 (2015).
396. A. Y. Denisov, M. S. R. Madiraju, G. Chen, A. Khadir, P. Beauparlant, G. Attardo, G. C. Shore, K. Gehring, Solution structure of human BCL-w: modulation of ligand binding by the C-terminal helix. *Journal of Biological Chemistry* **278**, 21124–21128 (2003).
397. C. O. Eno, E. F. Eckenrode, K. E. Olberding, G. Zhao, C. White, C. Li, Distinct roles of mitochondria- and ER-localized Bcl-xL in apoptosis resistance and Ca<sup>2+</sup> homeostasis. *Molecular Biology of the Cell* **23**, 2605–2618 (2012).
398. L. M. Szczesniak, C. G. Bonzerato, R. J. H. Wojcikiewicz, Identification of the Bok Interactome Using Proximity Labeling. *Front. Cell Dev. Biol.* **9**, 689951 (2021).
399. M. R. Wieckowski, C. Giorgi, M. Lebiedzinska, J. Duszynski, P. Pinton, Isolation of mitochondria-associated membranes and mitochondria from animal tissues and cells. *Nat Protoc* **4**, 1582–1590 (2009).
400. R. Eskes, B. Antonsson, A. Osen-Sand, S. Montessuit, C. Richter, R. Sadoul, G. Mazzei, A. Nichols, J. C. Martinou, Bax-induced cytochrome C release from mitochondria is independent of the permeability transition pore but highly dependent on Mg<sup>2+</sup> ions. *J Cell Biol* **143**, 217–224 (1998).

401. B. M. Polster, G. Basañez, M. Young, M. Suzuki, G. Fiskum, Inhibition of Bax-induced cytochrome c release from neural cell and brain mitochondria by dibucaine and propranolol. *J. Neurosci.* **23**, 2735–2743 (2003).
402. B. Bolognesi, B. Lehner, Reaching the limit. *eLife* **7** (2018).
403. G. Prelich, Gene overexpression: uses, mechanisms, and interpretation. *Genetics* **190**, 841–854 (2012).
404. A. Schinzel, T. Kaufmann, M. Schuler, J. Martinalbo, D. Grubb, C. Borner, Conformational control of Bax localization and apoptotic activity by Pro168. *The Journal of Cell Biology* **164**, 1021–1032 (2004).
405. L. Oliver, M. Priault, K. Tremblais, M. LeCabellec, K. Meflah, S. Manon, F. M. Vallette, The substitution of the C-terminus of bax by that of bcl-xL does not affect its subcellular localization but abrogates its pro-apoptotic properties. *FEBS letters* **487**, 161–165 (2000).
406. L. E. Sperl, F. Rührnöβl, A. Schiller, M. Haslbeck, F. Hagn, High-resolution analysis of the conformational transition of pro-apoptotic Bak at the lipid membrane. *The EMBO journal* **40**, e107159 (2021).
407. P. E. Ferrer, P. Frederick, J. M. Gulbis, G. Dewson, R. M. Kluck, Translocation of a Bak C-terminus mutant from cytosol to mitochondria to mediate cytochrome C release: implications for Bak and Bax apoptotic function. *PLOS ONE* **7**, e31510 (2012).
408. G. Dewson, T. Kratina, H. W. Sim, H. Puthalakath, J. M. Adams, P. M. Colman, R. M. Kluck, To trigger apoptosis, Bak exposes its BH3 domain and homodimerizes via BH3:groove interactions. *Molecular cell* **30**, 369–380 (2008).
409. L. Simonyan, T. T. Renault, M. J. C. Da Novais, M. J. Sousa, M. Côte-Real, N. Camougrand, C. Gonzalez, S. Manon, Regulation of Bax/mitochondria interaction by AKT. *FEBS letters* **590**, 13–21 (2016).
410. V. Fresquet, M. Rieger, C. Carolis, M. J. García-Barchino, J. A. Martinez-Climent, Acquired mutations in BCL2 family proteins conferring resistance to the BH3 mimetic ABT-199 in lymphoma. *Blood* **123**, 4111–4119 (2014).
411. A. Shamas-Din, S. Bindner, X. Chi, B. Leber, D. W. Andrews, C. Fradin, Distinct lipid effects on tBid and Bim activation of membrane permeabilization by pro-apoptotic Bax. *The Biochemical journal* **467**, 495–505 (2015).
412. K. Kanekura, X. Ma, J. T. Murphy, L. J. Zhu, A. Diwan, F. Urano, IRE1 prevents endoplasmic reticulum membrane permeabilization and cell death under pathological conditions. *Science signaling* **8**, ra62 (2015).
413. N. Inohara, D. Ekhterae, I. Garcia, R. Carrio, J. Merino, A. Merry, S. Chen, G. Núñez, Mtd, a novel Bcl-2 family member activates apoptosis in the absence of heterodimerization with Bcl-2 and Bcl-XL. *Journal of Biological Chemistry* **273**, 8705–8710 (1998).
414. M.-S. Hwang, C. T. Schwall, E. Pazarentzos, C. Datler, N. N. Alder, S. Grimm, Mitochondrial Ca(2+) influx targets cardiolipin to disintegrate respiratory chain complex II for cell death induction. *Cell Death Differ* **21**, 1733–1745 (2014).
415. T. M. Bauer, E. Murphy, Role of Mitochondrial Calcium and the Permeability Transition Pore in Regulating Cell Death. *Circulation research* **126**, 280–293 (2020).
416. L. Scorrano, S. A. Oakes, J. T. Opferman, E. H. Cheng, M. D. Sorcinelli, T. Pozzan, S. J. Korsmeyer, BAX and BAK regulation of endoplasmic reticulum Ca2+: a control point for apoptosis. *Science (New York, N.Y.)* **300**, 135–139 (2003).

417. N. Rosa, H. Ivanova, L. E. Wagner, J. Kale, R. La Rovere, K. Welkenhuyzen, N. Louros, S. Karamanou, V. Shabardina, I. Lemmens, et al., Bcl-xL acts as an inhibitor of IP3R channels, thereby antagonizing Ca<sup>2+</sup>-driven apoptosis. *Cell Death Differ* **29**, 788–805 (2022).
418. R. Srivastava, Z. Cao, C. Nedeva, S. Naim, D. Bachmann, T. Rabachini, L. Gangoda, S. Shahi, J. Glab, J. Menassa, et al., BCL-2 family protein BOK is a positive regulator of uridine metabolism in mammals. *Proceedings of the National Academy of Sciences of the United States of America* **116**, 15469–15474 (2019).
419. J. A. Irving, J. C. Whisstock, A. M. Lesk, Protein structural alignments and functional genomics. *Proteins* **42**, 378–382 (2001).
420. M. Lutter, M. Fang, X. Luo, M. Nishijima, X. Xie, X. Wang, Cardiolipin provides specificity for targeting of tBid to mitochondria. *Nature cell biology* **2**, 754–761 (2000).
421. S. Lucken-Ardjomande, S. Montessuit, J.-C. Martinou, Contributions to Bax insertion and oligomerization of lipids of the mitochondrial outer membrane. *Cell death and differentiation* **15**, 929–937 (2008).
422. S. Unterreitmeier, A. Fuchs, T. Schäffler, R. G. Heym, D. Frishman, D. Langosch, Phenylalanine promotes interaction of transmembrane domains via GxxxG motifs. *Journal of molecular biology* **374**, 705–718 (2007).
423. M.-J. Kwon, J. Park, S. Jang, C.-Y. Eom, E.-S. Oh, The Conserved Phenylalanine in the Transmembrane Domain Enhances Heteromeric Interactions of Syndecans. *The Journal of biological chemistry* **291**, 872–881 (2016).
424. S. T. Nawrocki, J. S. Carew, K. Dunner, L. H. Boise, P. J. Chiao, P. Huang, J. L. Abbruzzese, D. J. McConkey, Bortezomib inhibits PKR-like endoplasmic reticulum (ER) kinase and induces apoptosis via ER stress in human pancreatic cancer cells. *Cancer research* **65**, 11510–11519 (2005).
425. K. Haze, H. Yoshida, H. Yanagi, T. Yura, K. Mori, Mammalian transcription factor ATF6 is synthesized as a transmembrane protein and activated by proteolysis in response to endoplasmic reticulum stress. *Molecular Biology of the Cell* **10**, 3787–3799 (1999).
426. M. Baou, S. L. Kohlhaas, M. Butterworth, M. Vogler, D. Dinsdale, R. Walewska, A. Majid, E. Eldering, M. J. S. Dyer, G. M. Cohen, Role of NOXA and its ubiquitination in proteasome inhibitor-induced apoptosis in chronic lymphocytic leukemia cells. *Haematologica* **95**, 1510–1518 (2010).
427. Y. Wang, L. Zhang, Z. He, J. Deng, Z. Zhang, L. Liu, W. Ye, S. Liu, Tunicamycin induces ER stress and inhibits tumorigenesis of head and neck cancer cells by inhibiting N-glycosylation. *American Journal of Translational Research* **12**, 541–550 (2020).
428. L. Raedler, Velcade (Bortezomib) Receives 2 New FDA Indications: For Retreatment of Patients with Multiple Myeloma and for First-Line Treatment of Patients with Mantle-Cell Lymphoma. *American Health & Drug Benefits* **8**, 135–140 (2015).
429. C. Kakiuchi, S. Ishigaki, C. M. Osowski, S. G. Fonseca, T. Kato, F. Urano, Valproate, a mood stabilizer, induces WFS1 expression and modulates its interaction with ER stress protein GRP94. *PLOS ONE* **4**, e4134 (2009).
430. X.-Y. Zhang, S.-M. Yang, H.-P. Zhang, Y. Yang, S.-B. Sun, J.-P. Chang, X.-C. Tao, T.-Y. Yang, C. Liu, Y.-M. Yang, Endoplasmic reticulum stress mediates the arsenic trioxide-induced apoptosis in human hepatocellular carcinoma cells. *The international journal of biochemistry & cell biology* **68**, 158–165 (2015).

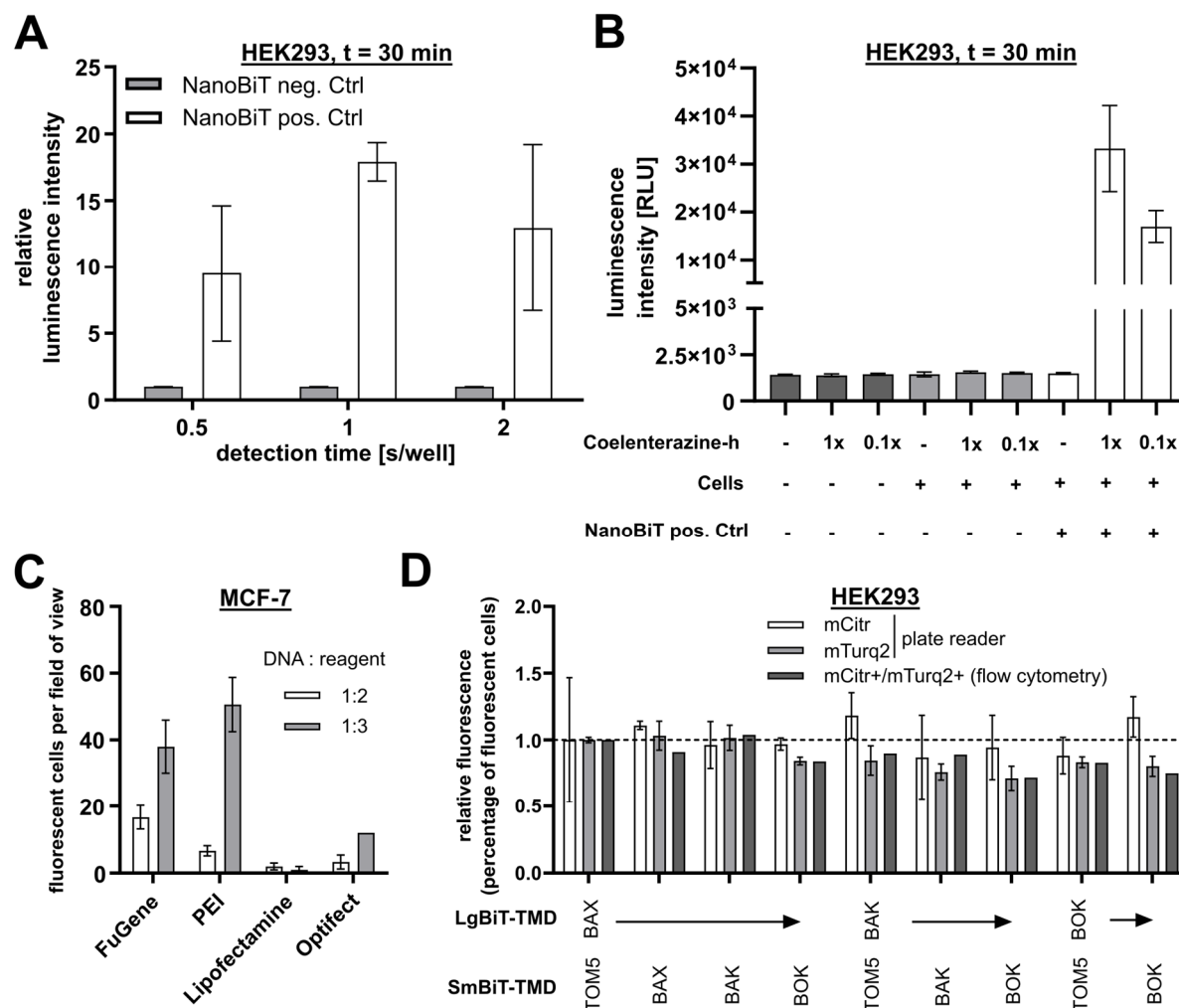
431. Y. Yang, Y. Wu, X. Meng, Z. Wang, M. Younis, Y. Liu, P. Wang, X. Huang, SARS-CoV-2 membrane protein causes the mitochondrial apoptosis and pulmonary edema via targeting BOK. *Cell Death Differ* **29**, 1395–1408 (2022).
432. A.-L. Meinhardt, E. Munkhbaatar, U. Höckendorf, M. Dietzen, M. Dechant, M. Anton, A. Jacob, K. Steiger, W. Weichert, L. Brcic, et al., The BCL-2 family member BOK promotes KRAS-driven lung cancer progression in a p53-dependent manner. *Oncogene* **41**, 1376–1382 (2022).
433. E. Moravcikova, E. Krepela, V. S. Donnenberg, A. D. Donnenberg, K. Benkova, T. Rabachini, Y. Fernandez-Marrero, D. Bachmann, T. Kaufmann, BOK displays cell death-independent tumor suppressor activity in non-small-cell lung carcinoma. *International journal of cancer* **141**, 2050–2061 (2017).
434. E. D. Deeks, Venetoclax: First Global Approval. *Drugs* **76**, 979–987 (2016).
435. D. M. Moujalled, F. C. Brown, C. C. Chua, M. A. Dengler, G. Pomilio, N. S. Anstee, V. Litalien, E. Thompson, T. Morley, S. MacRaild, et al., Acquired mutations in BAX confer resistance to BH3-mimetic therapy in acute myeloid leukemia. *Blood* **141**, 634–644 (2023).
436. P. Blombery, M. A. Anderson, J.-N. Gong, R. Thijssen, R. W. Birkinshaw, E. R. Thompson, C. E. Teh, T. Nguyen, Z. Xu, C. Flensburg, et al., Acquisition of the Recurrent Gly101Val Mutation in BCL2 Confers Resistance to Venetoclax in Patients with Progressive Chronic Lymphocytic Leukemia. *Cancer discovery* **9**, 342–353 (2019).
437. C. Chakraborty, Y. Xu, Y. Yao, E. Morelli, A. Aktas-Samur, M. K. Samur, M. Fulciniti, N. C. Munshi, K. Anderson, Activation of the ERK Pathway Drives Acquired Resistance to Venetoclax in MM Cell Models. *Blood* **136**, 21–22 (2020).
438. H. Yin, A. D. Flynn, Drugging Membrane Protein Interactions. *Annual review of biomedical engineering* **18**, 51–76 (2016).
439. X.-C. Bai, G. McMullan, S. H. W. Scheres, How cryo-EM is revolutionizing structural biology. *Trends in Biochemical Sciences* **40**, 49–57 (2015).
440. Y. Wang, P. Barth, Evolutionary-guided de novo structure prediction of self-associated transmembrane helical proteins with near-atomic accuracy. *Nat Commun* **6**, 7196 (2015).
441. H. Yin, J. S. Slusky, B. W. Berger, R. S. Walters, G. Vilaire, R. I. Litvinov, J. D. Lear, G. A. Caputo, J. S. Bennett, W. F. DeGrado, Computational design of peptides that target transmembrane helices. *Science (New York, N.Y.)* **315**, 1817–1822 (2007).
442. F. Liu, Z. Zhang, A. Levit, J. Levring, K. K. Touhara, B. K. Shoichet, J. Chen, Structural identification of a hotspot on CFTR for potentiation. *Science (New York, N.Y.)* **364**, 1184–1188 (2019).
443. Z. Liu, Y. Ding, N. Ye, C. Wild, H. Chen, J. Zhou, Direct Activation of Bax Protein for Cancer Therapy. *Medicinal research reviews* **36**, 313–341 (2016).
444. J. M. McDonnell, A. J. Beavil, G. A. Mackay, B. A. Jameson, R. Korngold, H. J. Gould, B. J. Sutton, Structure based design and characterization of peptides that inhibit IgE binding to its high-affinity receptor. *Nature structural biology* **3**, 419–426 (1996).

## 7 Appendix



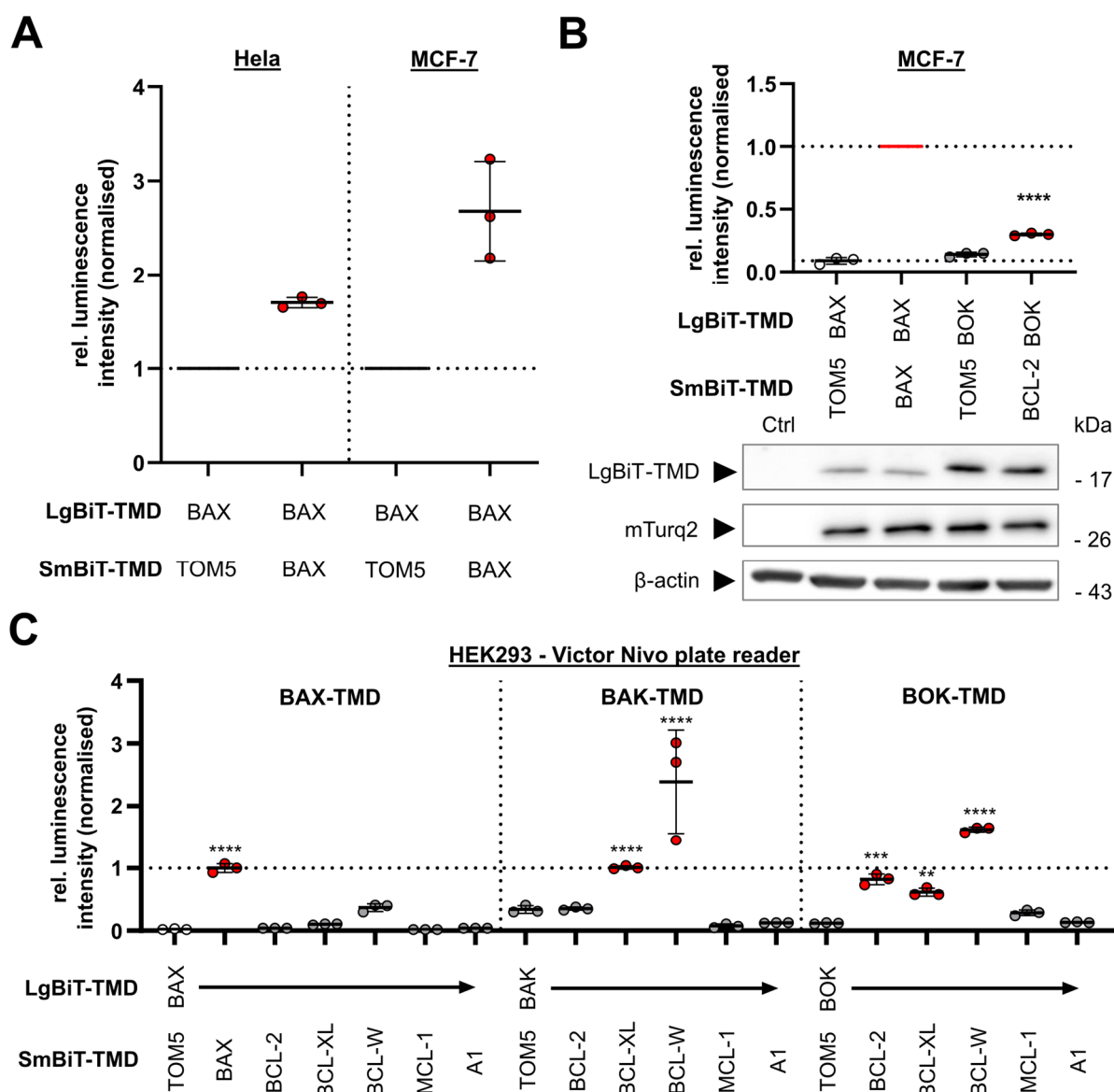
### Supplementary Figure S1: Expression pattern of various Bcl-2 family proteins in cell lines used.

**A** - Whole cell lysates of cell lines used in the present study were analysed by Western Blot. Expression of Bcl-2 family proteins was assessed using antibodies against MCL-1, BCL-2, BCL-XL, BAX, BAK and BOK.  $\beta$ -actin was used as loading control. One representative Blot. **B** - HeLa BAX/BAK double knockout (DKO) validation. Whole cell lines of HeLa empty vector cells and DKO cells were analysed by Western Blot using antibodies against BAX, BAK and BCL-2. One representative Blot.



### Supplementary Figure S2: Parameter optimisation in the NanoBiT assay.

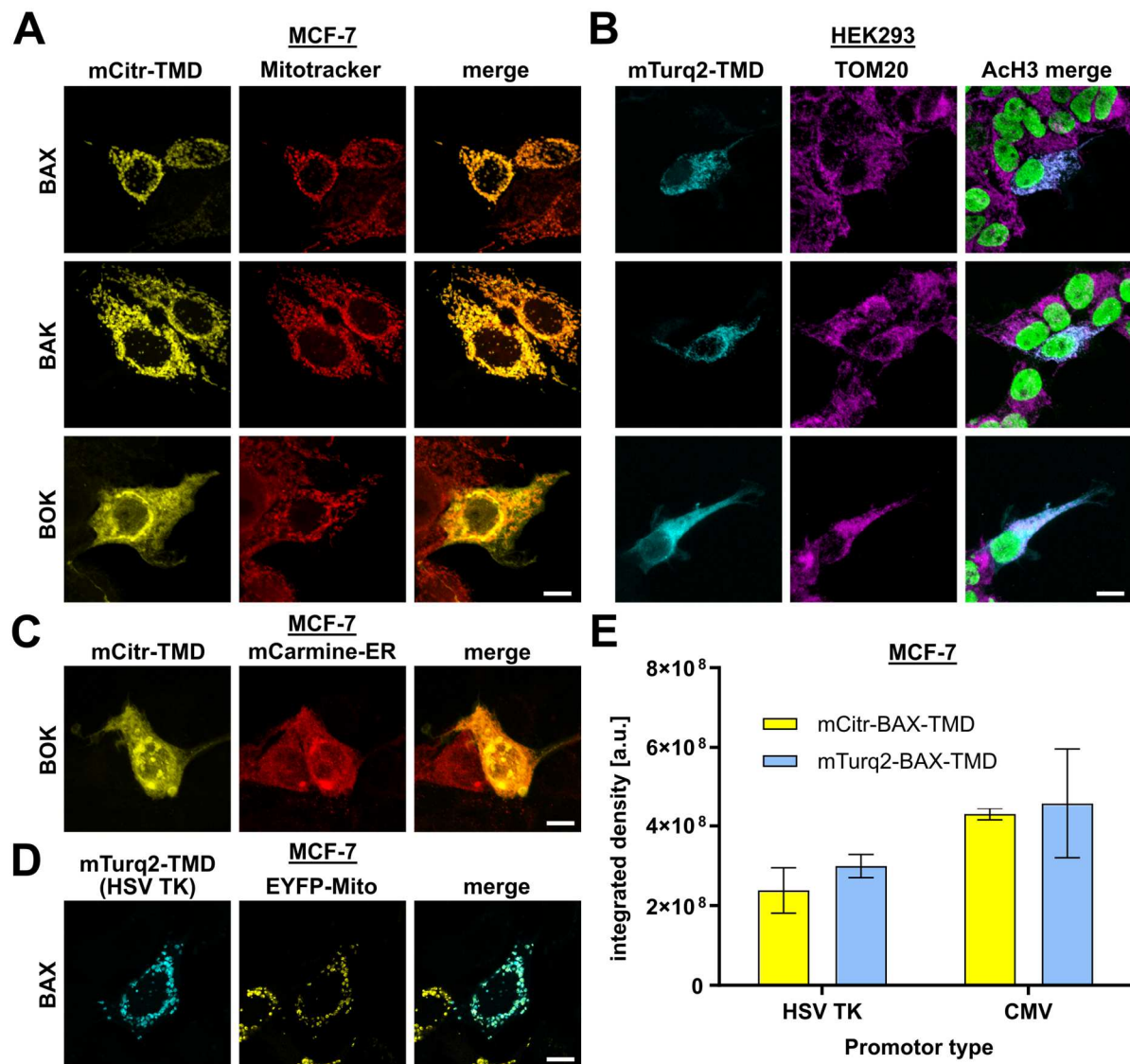
**A** – HEK293 cells were co-transfected to express Promega NanoBiT positive (LgBiT-PRKAR2A/SmBiT-PRKACA) or negative control (SmBiT-Halo tag). After 24 h, cells were harvested for NanoBiT split luciferase assay. For comparison of detection time per well luminescence was assessed 30 min after Vivazine substrate addition for indicated amounts of seconds per well. Mean  $\pm$  sd of technical triplicates from one independent experiment is shown relative to NanoBiT negative control samples. **B** – HEK293 cells transfected to express NanoBiT positive control or left untransfected were harvested after 24 h and subjected to NanoBiT split luciferase assay with or without addition of coelenterazine-h in indicated concentrations (1x – 5  $\mu$ M, 0.1x – 0.5  $\mu$ M). Also, wells without any cells (medium only) were included as background control. Luminescence detect 30 min after substrate addition is shown as mean  $\pm$  sd of technical triplicates from one independent experiment. **C** – Count of fluorescent MCF-7 cells 24 h post transfection with a GFP-encoding control plasmid using different transfection reagents according to the manufacturer's protocol with indicated DNA-to-reagent ratios. Fluorescent cells were counted using a Leica fluorescence microscope (20x Obj.) at randomly chosen fields of view. **D** – HEK293 cells were co-transfected with indicated LgBiT-TMD and SmBiT-TMD-encoding plasmids and harvested 24 h post transfection. Samples were subjected to NanoBiT assay and flow cytometry to assess mCitrine and mTurquoise2 fluorescence. Shown is the relative fluorescence intensity detected using a multimode plate reader (NanoBiT assay) and relative percentage of mCitrine/mTurquoise2 double positive cells detected using flow cytometry. Values were normalised to the negative control sample (BAX-TMD + TOM5-TMD) which's mean was set to one. One representative experiment, mean ( $\pm$  sd of technical triplicate for plate reader data).



**Supplementary Figure S3: Analysis of TMD Interactions in the NanoBiT assay.**

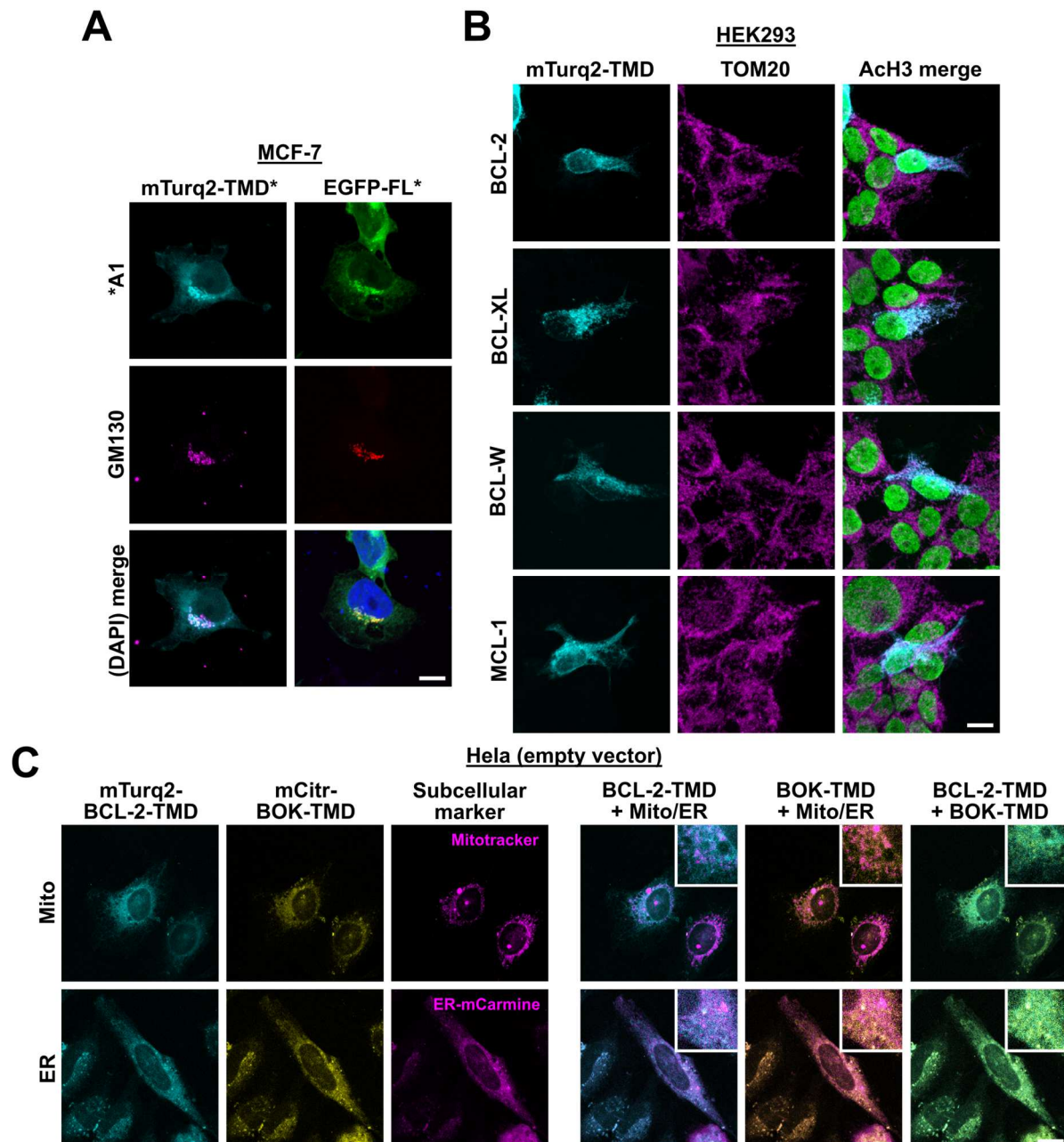
**A** – HeLa or MCF-7 cells were co-transfected with indicated NanoBiT-TMD-encoding plasmids and subjected to NanoBiT assay 24 h post transfection. Fluorescence-normalised luminescence is shown relative to negative control (BAX-/TOM5-TMD). Single dots represent technical triplicates from one independent experiment (HeLa) or means from three independent experiments (MCF-7). Mean  $\pm$  sd is indicated as a horizontal line. **B** - NanoBiT interaction data from MCF-7 cells co-transfected with indicated combinations of LgBiT-TMD-encoding and SmBiT-TMD-encoding plasmids. Cells were harvested 24 h post transfection and subjected to both NanoBiT assay (top) and Western Blot (bottom). For NanoBiT assay, fluorescence-normalised luminescence is shown relative to positive control (BAX-/BAX-TMD). Mean  $\pm$  sd from three independent experiments. Asterisks indicate statistically significant differences compared to negative control. Construct expression was verified via Western Blot (bottom) using antibodies against LgBiT, mTurquoise2 (mTurq2) and  $\beta$ -actin as a loading control. Representative Blot from two independent experiments. **C** - NanoBiT interaction data from HEK293 cells co-transfected with indicated combinations of LgBiT-TMD-encoding and SmBiT-TMD-encoding plasmids as assessed using the Victor Nivo multimode plate reader. Cells were harvested 24 post transfection and subjected to NanoBiT assay. Device settings and detection procedure were kept as described in 2.2.8 for the EnSpire multimode plate reader. Fluorescence-normalised luminescence intensity is shown relative to positive control (BAX-/BAX-TMD, mean set to one). Single dots represent technical triplicates from one independent experiment. Mean  $\pm$  sd is indicated with a horizontal line. Asterisks indicate statistically significant differences compared to negative control.





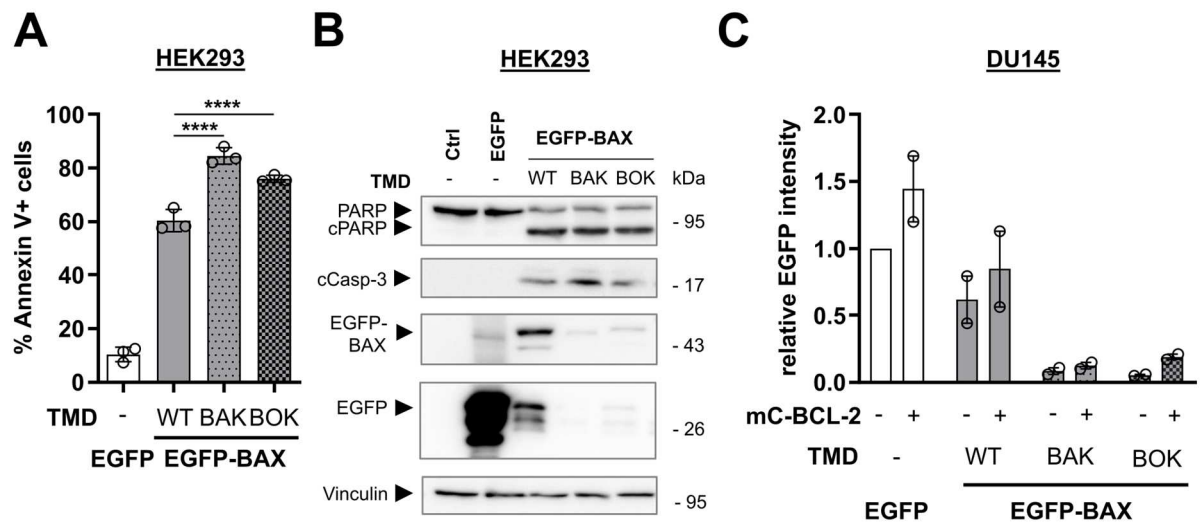
### Supplementary Figure S4: Subcellular localisation of effector protein TMDs.

**A** – cLSM images of MCF-7 cells transfected to express mCitrine-TMD fusions of BAX, BAK and BOK. Cells were stained with Mitotracker red and fixed 24 h post transfection. Representative images out of three independent experiments are shown as maximum projections of z-stacks. **B** – cLSM images of HEK293 cells transfected to expressed mTurq2-TMD fusions of BAX, BAK and BOK. 24 h after transfection, cells were fixed and IF stained for TOM20 and Acteyl-Histone H3 (Ach3) to stain mitochondria and nuclei respectively. Representative images out of three independent experiments are shown as maximum projections of z-stacks. **C** – Representative cLSM image of MCF-7 cells processed as in A but transfected to express mCit-BOK-TMD and ER-mCarmine. **D** – Representative cLSM image of MCF-7 cells processed as in A but transfected with a mTurq2-BAX-TMD-encoding plasmid controlled by a HSV TK promotor (pBiT backbone). **E** – Fluorescence intensity quantification of MCF-7 cells transfected with plasmids encoding for either CMV promotor- or HSV TK promotor-controlled expression of mCitrine/mTurquoise2-BAX-TMD. Cells were fixed 24 post transfection and cLSM images of single cell middle sections were obtained using identical settings. Integrated density within the cell was determined using Fiji. Mean  $\pm$  sd of  $n \geq 3$  cells from one independent experiment. Scale bars = 10  $\mu$ m.



**Supplementary Figure S5: Subcellular localisation of anti-apoptotic Bcl-2 TMDs.**

**A** – Golgi colocalisation of A1(-TMD). cLSM images of MCF-7 cells transfected to express either mTurq2-A1-TMD (left column) or EGFP-A1 (FL = full-length, right column). Cells were fixed 24 h post transfection and IF stained for cis-Golgi marker GM130. For cells expressing EGFP-A1, a DAPI-containing mounting medium was used to stain nuclei. Representative images out of one independent experiment are shown as maximum projections of z-stacks. **B** – cLSM images of HEK293 cells transfected to expressed mTurq2-TMD fusions of indicated anti-apoptotic Bcl-2 proteins. 24 h after transfection, cells were fixed and IF stained for TOM20 and Acteyl-Histone H3 (Ach3) to stain mitochondria and nuclei respectively. Representative images from three independent experiments are shown as maximum projections of z-stacks. **C** - cLSM images of HeLa (empty vector) cells transfected to express mTurq2-BOK-TMD and mCitrine-BCL-2-TMD. Cells were stained with Mitotracker red 24 h after transfection and then fixed (top row) or co-transfected with ER marker ER-mCarmine (bottom row) and fixed 24 post transfection. Representative images from one independent experiment are shown as maximum projections of z-stacks. Zoomed-in insets are in 3x magnification. Scale bar = 10  $\mu$ m.

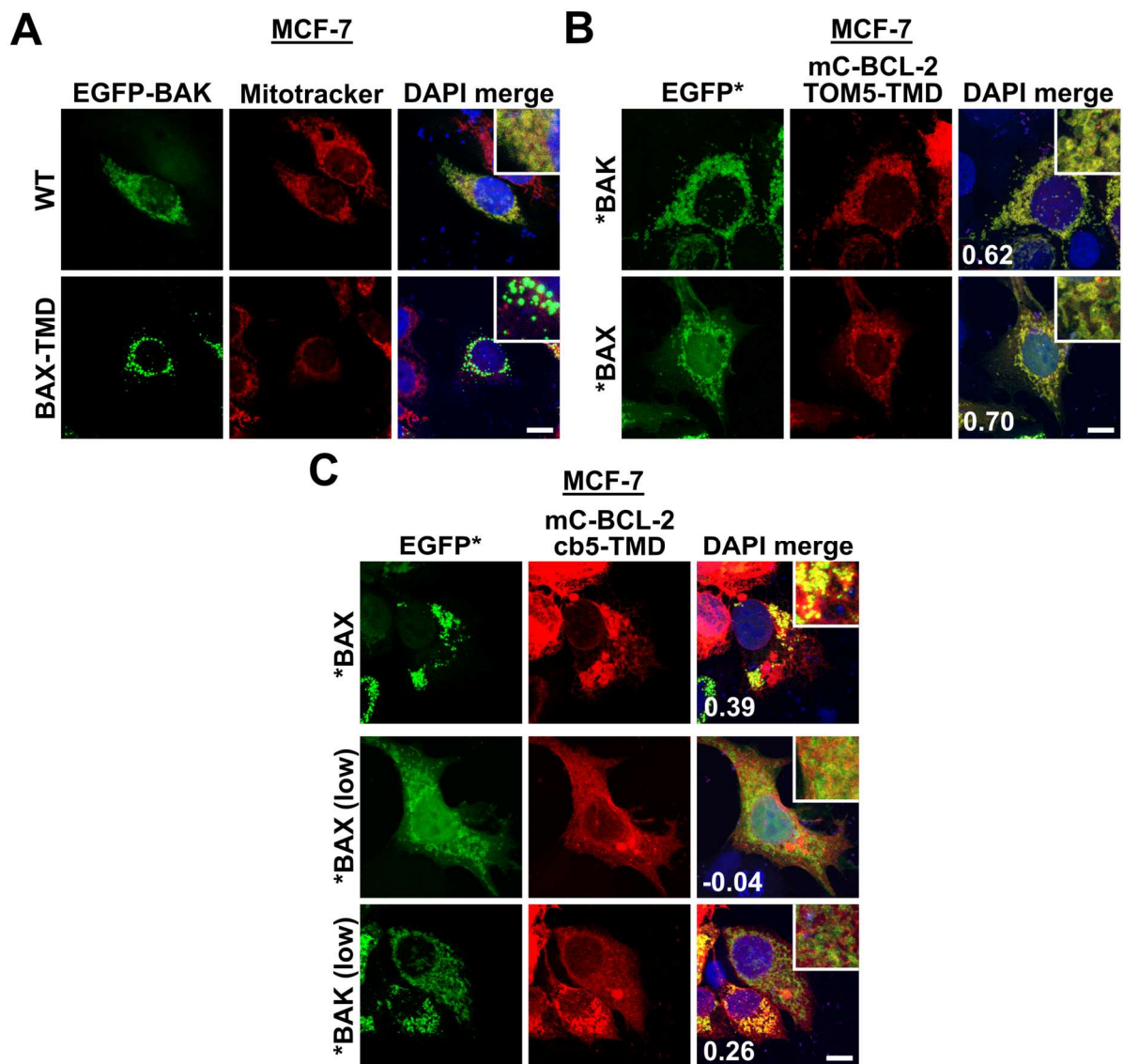


**Supplementary Figure S6: TMD exchange in BAX to BAK- or BOK-TMD impacts BAX pro-apoptotic activity.**

**A** – Flow cytometric analysis of HEK293 cells transfected to express EGFP-fused BAX TMD chimeras, wild-type (WT) or EGFP as a control. Cells were harvested 18 h post transfection and stained with Annexin V-APC to detect dead cells (Annexin V+). Mean  $\pm$  sd from three independent experiments.

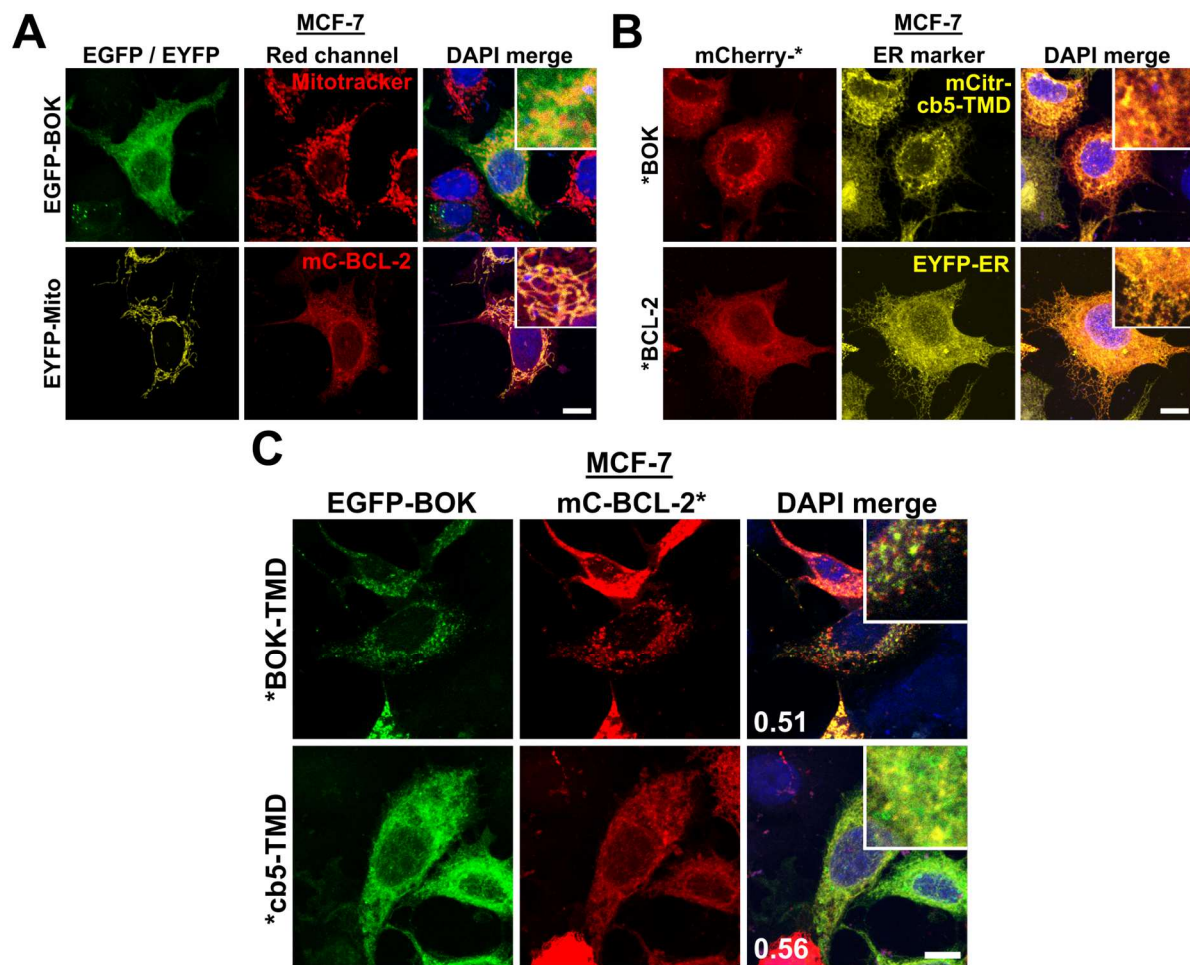
**B** – Western Blot analysis of HEK293 cells transfected as in A or with an empty vector (Ctrl) and harvested 18 h post transfection. Whole cell lysates were analysed using antibodies against (cleaved) PARP, cleaved Caspase-3 (cCasp-3), EGFP and Vinculin as a loading control. Blot from one independent experiment.

**C** – Densitometric analysis of EGFP expression level in whole cell lysates of DU145 cells co-transfected to express EGFP-fused BAX TMD chimeras or EGFP in combination with mCherry-BCL-2 or an empty vector control. EGFP band intensity as analysed with Fiji software is shown relative to EGFP empty vector control. Mean  $\pm$  range from two independent experiments



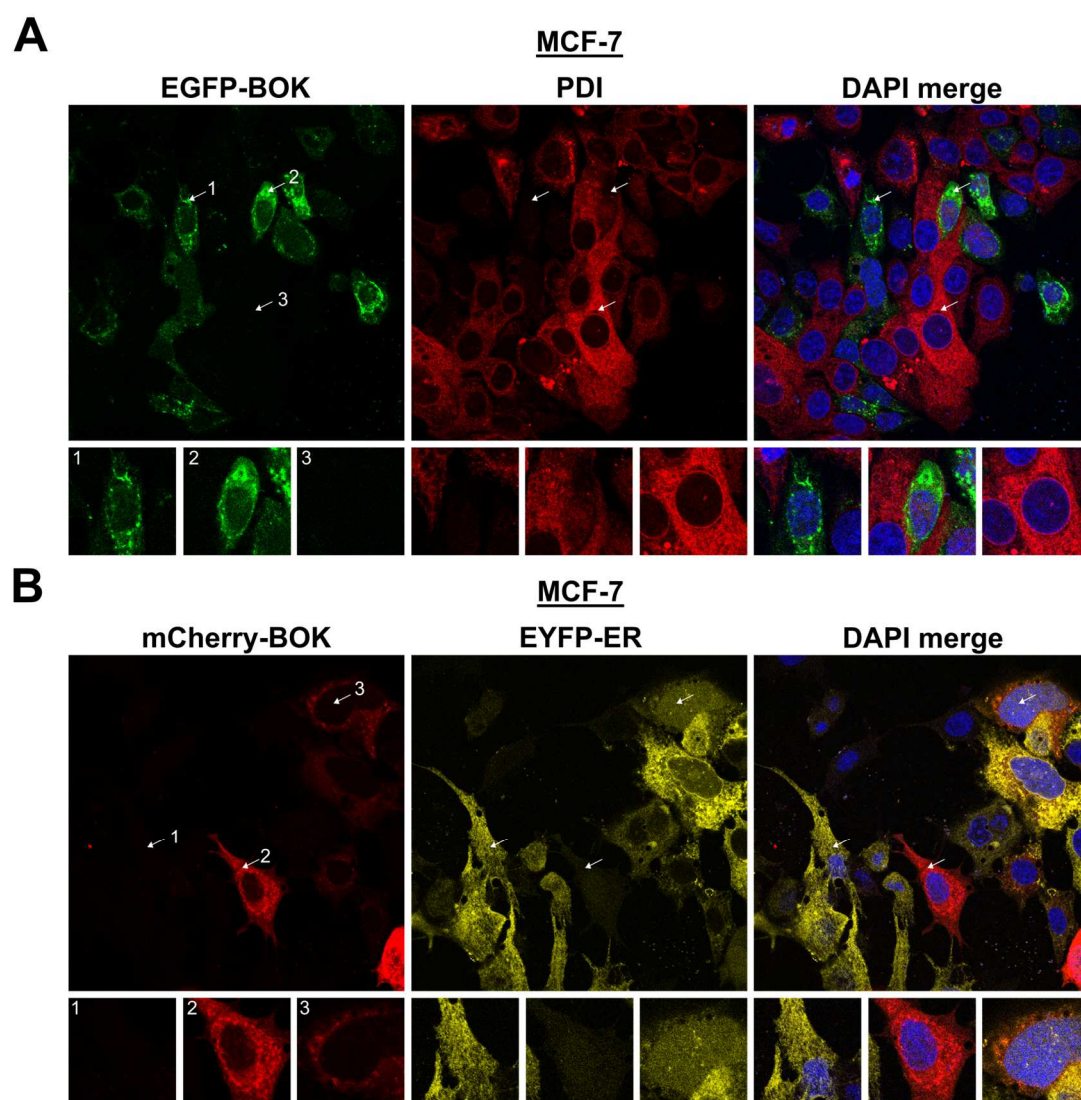
**Supplementary Figure S7: Active BAX and BAK colocalise with BCL-2 in a TMD-independent manner.**

**A** – cLSM images of MCF-7 cells transfected to express EGFP-BAK wild-type (WT) or EGFP-BAK-BAX-TMD. Cells were stained with Mitotracker red prior to fixation 24 h post transfection and mounted using DAPI-containing mounting medium. Representative images are maximum projections of z-stacks from two independent experiments. Scale bar = 10  $\mu$ m. **B** - cLSM images of MCF-7 cells transfected to express EGFP-BAX/-BAK with mCherry-BCL-2<sup>TOM5-TMD</sup> (mC-BCL-2<sup>TOM5-TMD</sup>). Cells were fixed 24 h post transfection and mounted using DAPI-containing mounting medium. Representative images are maximum projections of z-stacks from two independent experiments. Numbers indicate Pearson's r-values for merged channels obtained using Fiji software. Scale bar = 10  $\mu$ m. **C** - cLSM images of MCF-7 cells transfected to express EGFP-BAX/-BAK with mCherry-BCL-2<sup>cb5-TMD</sup> (mC-BCL-2<sup>cb5-TMD</sup>). Cells were fixed 24 h post transfection and mounted using DAPI-containing mounting medium. Representative images are maximum projections of z-stacks from two independent experiments. Two lower panels show cells with a moderate expression of EGFP-BAX/-BAK. Numbers indicate Pearson's r-values for merged channels obtained using Fiji software. Scale bar = 10  $\mu$ m.



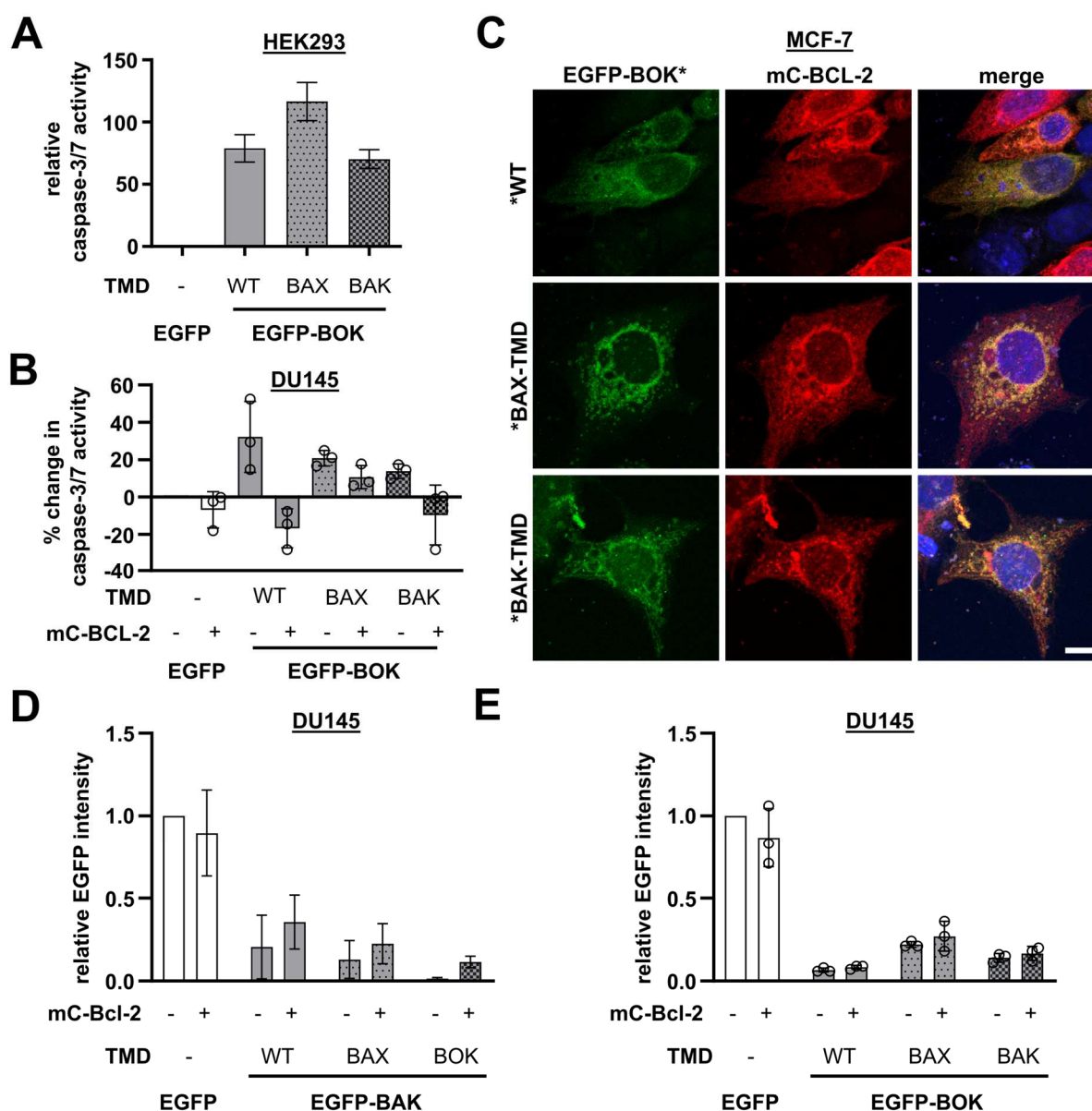
### Supplementary Figure S8: BOK and BCL-2 colocalisation is dependent on TMD sequence.

**A** – cLSM images of MCF-7 cells transfected to express EGFP-BOK and stained with Mitotracker Red prior fixation (upper panels) or MCF-7 cells expressing EYFP-Mito marker which were transfected to express mCherry-BCL-2 (mC-BCL-2, lower panels). Cells were fixed 24 h post transfection and mounted using DAPI-containing mounting medium. Representative images are maximum projections of z-stacks from two independent experiments. Scale bar = 10  $\mu$ m. **B** - cLSM images of MCF-7 cells either transfected to express mCherry-BOK and mCitrcb5-TMD (upper panels) or expressing EYFP-ER and were transfected to express mC-BCL-2 (lower panels). Cells were fixed 24 h post transfection and mounted using DAPI-containing mounting medium. Representative images are maximum projections of z-stacks from two independent experiments. Scale bar = 10  $\mu$ m. **C** - cLSM images of MCF-7 cells transfected to express mC-BCL-2<sup>BOK-TMD</sup> (upper panels) or mC-BCL-2<sup>cb5-TMD</sup> (lower panels) with EGFP-BOK. Cells were fixed 24 h post transfection and mounted using DAPI-containing mounting medium. Representative images are maximum projections of z-stacks from two independent experiments. Numbers indicate Pearson's r-values for merged channels were obtained using Fiji software. Scale bar = 10  $\mu$ m.



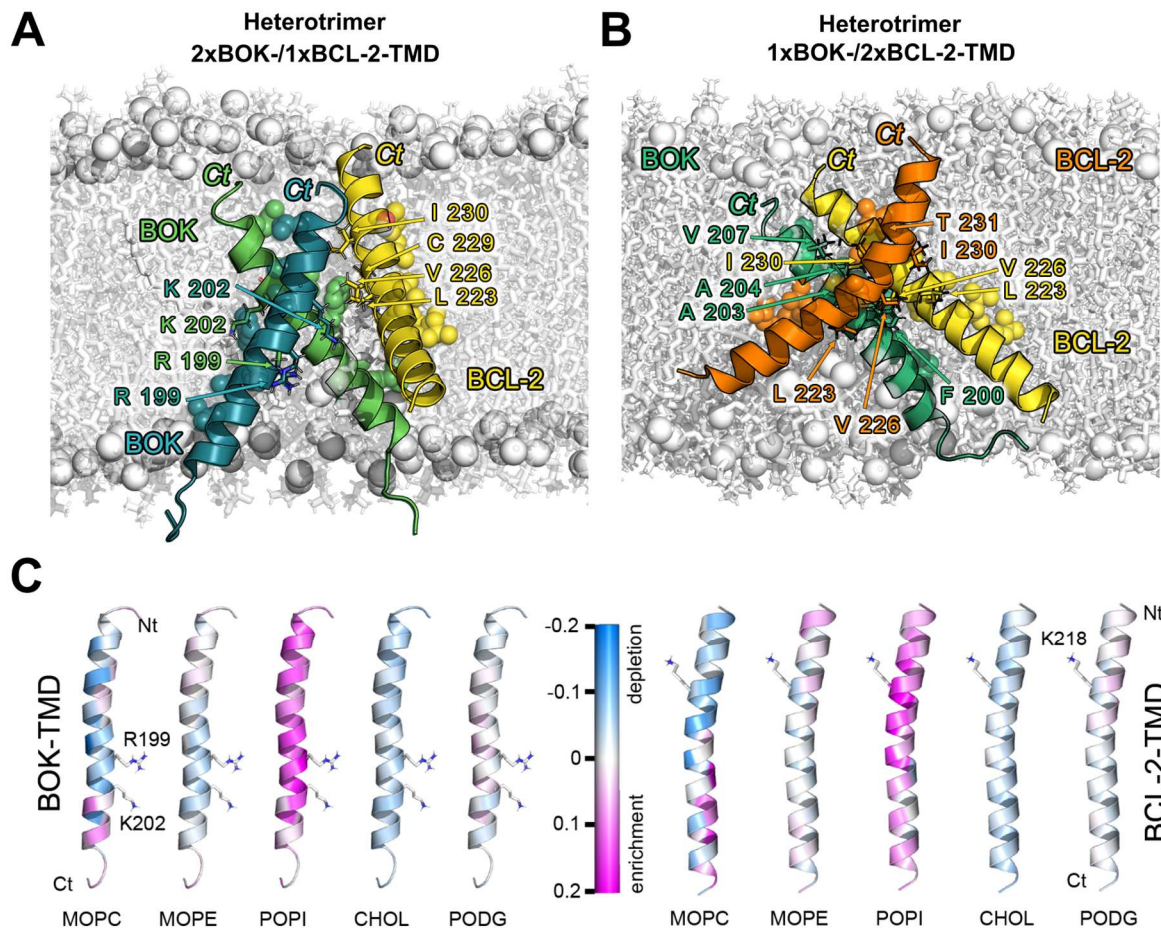
**Supplementary Figure S9: BOK overexpression disturbs ER architecture.**

**A** – MCF-7 cells were transfected to express EGFP-BOK, fixed and IF stained with antibodies against PDI followed by cLSM. DAPI-containing mounting medium was used. White arrows and numbers indicate location of zoomed-in images below at 3x magnification. Representative images from one independent experiment. **B** – cLSM images as in A of MCF-7 cells expressing EYFP-ER and transfected to express mCherry-BOK. Scale bars = 10  $\mu$ m.



**Supplementary Figure S10: BOK-induced cell death and its inhibition by BCL-2 is affected by TMD sequence.**

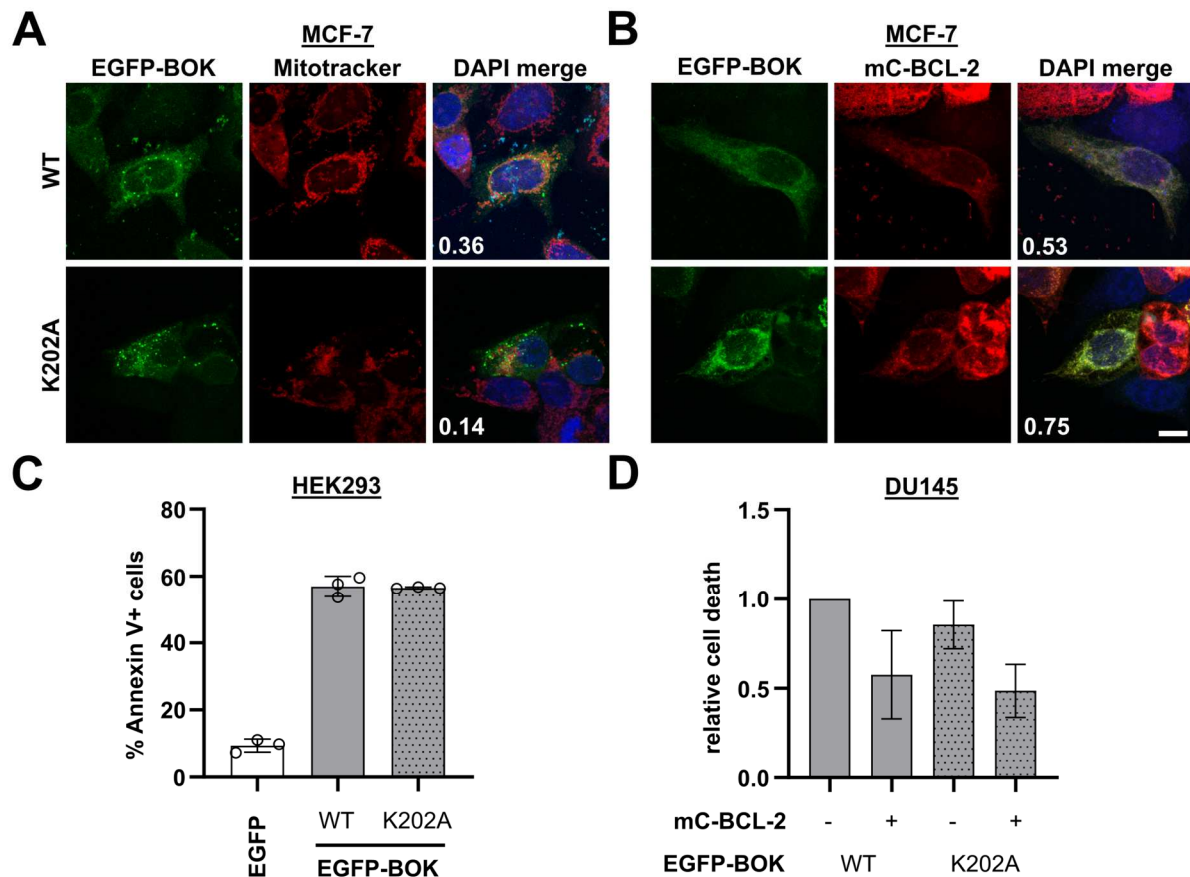
**A** – Caspase-3/7 activity was assessed in HEK293 cells transfected to express EGFP-fused BOK TMD chimeras or EGFP and harvested 18 h post transfection using the Caspase-Glo 3/7 assay. Shown is luminescence reflecting caspase activity as mean  $\pm$  sd from three independent experiments relative to EGFP control. **B** - Caspase-3/7 activity was assessed as in A for DU145 cells transfected to express EGFP-fused BOK TMD chimeras or EGFP in combination with mCherry-BCL-2 (mC-BCL-2) or an empty vector control. Shown is the percent change in caspase-3/7 activity relative to EGFP control as mean  $\pm$  sd from three independent experiments. **C** – cLSM images of MCF-7 cells transfected to express EGFP-fused BOK-TMD chimeras or wild-type (WT) EGFP-BOK in combination with mC-BCL-2. Cells were fixed 18 h post transfection and mounted using a DAPI-containing mounting medium. Representative images from two independent experiments. Scale bar = 10  $\mu$ m. **D, E** - Densitometric analysis of EGFP expression level in whole cell lysates of DU145 cells co-transfected to express EGFP-fused BAK TMD chimeras (D) or BOK TMD chimeras (E) or EGFP in combination with mCherry-BCL-2 or an empty vector control. EGFP band intensity as analysed with Fiji software is shown relative to EGFP empty vector control. Mean  $\pm$  range from two independent experiments (D) or mean  $\pm$  sd from three independent experiments (E).



**Supplementary Figure S11: Molecular dynamics simulations confirm BOK-TMD and BCL-2-TMD interaction.**

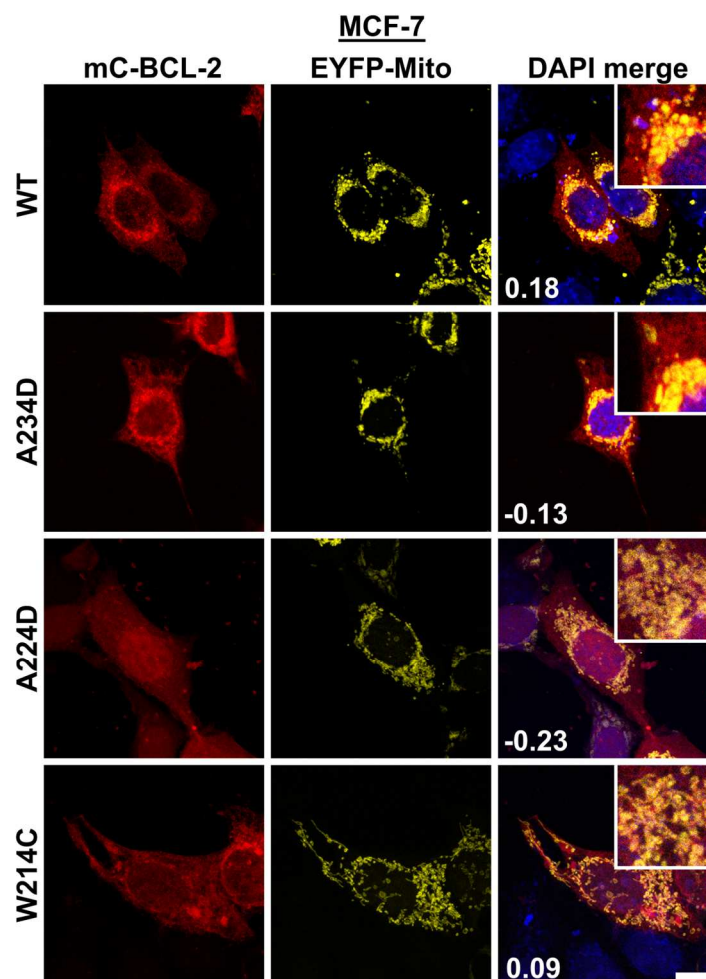
**A, B** – Snapshot of representative heterotrimeric structures out of 2xBOK-/1xBCL-2-TMD (A) or 1xBOK-/2xBCL-2-TMD (B) resulting from 1  $\mu$ s all-atom simulation with two BOK-TMD and two BCL-2-TMD peptides. Most prominent AA interaction sites are labelled and shown as sticks. **C** – Lipid enrichment/depletion shown for BOK-TMD or BCL-2-TMD from 2xBOK-/2xBCL-2-TMD heterotetramers. Colour gradient indicates enrichment or depletion compared to expected interaction frequency of shown lipids with respective residues. Residues R199, K202 (in BOK) and K218 (in BCL-2) responsible for membrane indentation are highlighted as sticks. Experiments were performed and analysed by Thomas Fellmeth and Kristyna Pluhackova.





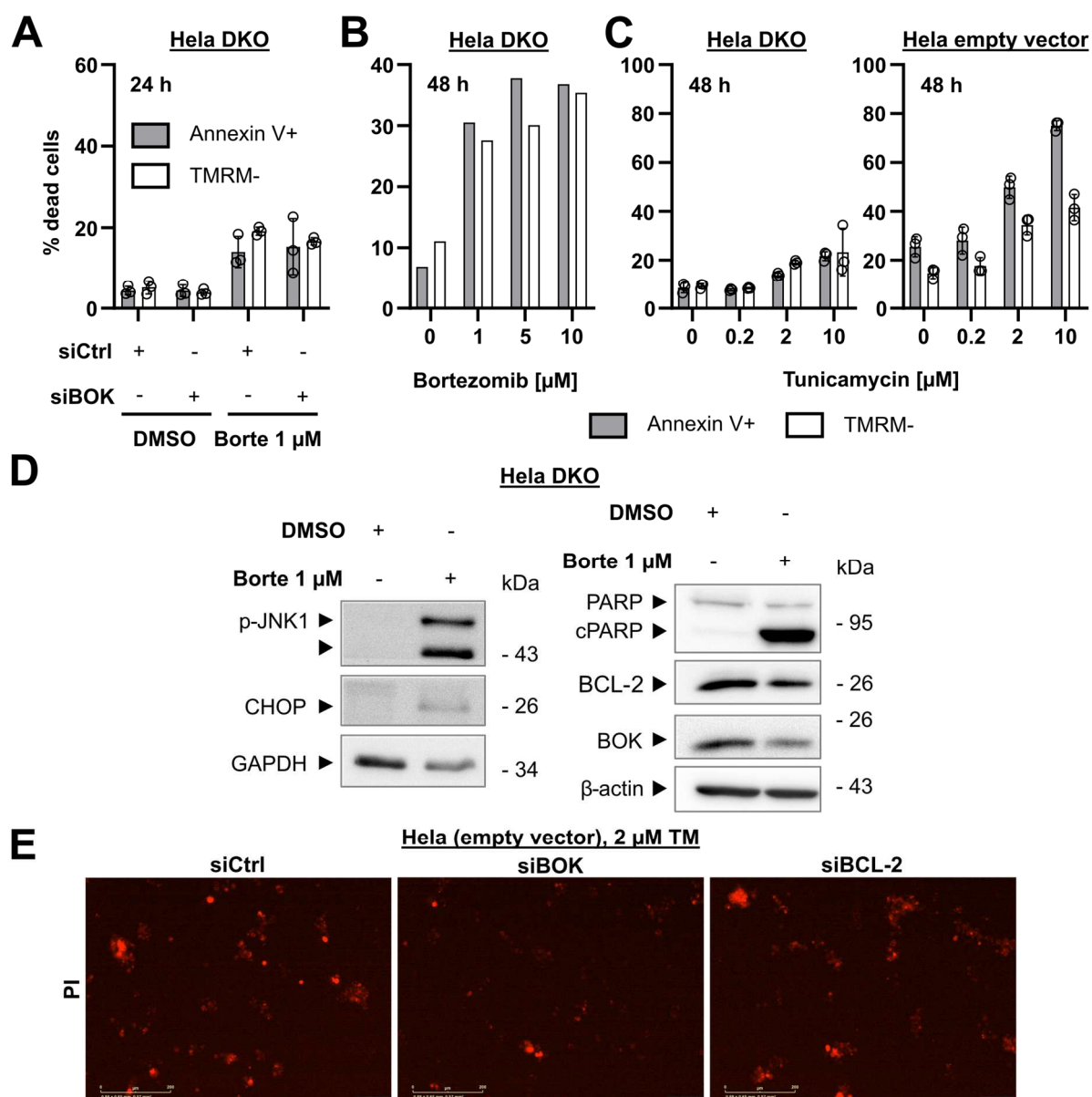
**Supplementary Figure S12: K202 in the BOK TMD is dispensable for localisation and BOK overexpression-induced apoptosis.**

**A, B** - cLSM images of MCF-7 transfected to express EGFP-BOK wild-type (WT) or K202A. Cells were either stained with Mitotracker red prior fixation or co-transfected to express mCherry-BCL-2 (mC-BCL-2). Cells were fixed 24 h post transfection and DAPI-containing mounting medium was used to stain nuclei. Representative images from two independent experiments are maximum projections of z-stacks. Numbers are Pearson's r-values for merged channels obtained using Fiji software. Scale bar = 10  $\mu$ m. **C** - Flow cytometric analysis of HEK293 cells transfected to express EGFP-BOK WT, K202A or EGFP as a control. Cells were harvested 18 h post transfection and stained with Annexin V-APC to detect dead cells (Annexin V+). Mean  $\pm$  sd from three independent experiments. **D** - Flow cytometric analysis of DU145 cells transfected to express EGFP-BOK WT or K202A in combination with mC-BCL-2 or an empty vector control. After 18 h, cells were harvested and stained with Annexin V-APC to detect dead cells. Proportion of dead cells is shown relative to EGFP-BOK-expressing cells as mean + range from two independent experiments.



**Supplementary Figure S13: BCL-2 TMD mutation influences subcellular localisation.**

cLSM images of MCF-7 cells expressing EYFP-Mito and transfected to express mCherry-BCL-2 (mC-BCL-2) wild-type (WT) or mutants. Cells were fixed for imaging 24 h post transfection. DAPI-containing mounting medium was used to stain nuclei. Representative images from three independent experiments are maximum projections of z-stacks. Numbers are Pearson's r-values for merged channels obtained using Fiji software. Zoomed-in insets are in 3x magnification. Scale bar = 10  $\mu$ m. Experiments were performed by Alexander Paul.



**Supplementary Figure S14: BOK-mediated ER-stress is abrogated by BCL-2.**

**A** – Flow cytometric analysis of Hela BAX<sup>-/-</sup>/BAK<sup>-/-</sup> (DKO) cells transfected with siRNA targeting BOK (siBOK) or control siRNA (siCtrl). After 24 h, cells were incubated with 1  $\mu$ M Bortezomib (Borte) or DMSO for another 24 h. Then, cells were stained with TMRM and Annexin V-APC to detect dead cells. Percentage of dead cells (Annexin V+/TMRM-) is shown as mean  $\pm$  sd from three independent experiments. **B, C** – Flow cytometric analysis of Hela DKO or Hela empty vector cells incubated with indicated concentrations of Bortezomib (B) or Tunicamycin (C) for 48 h. Then, cells were stained with TMRM and Annexin V-APC to detect dead cells. Percentage of dead cells (Annexin V+/TMRM-) is shown (B) from one independent experiments or shown as mean  $\pm$  sd from three independent experiments (C). **D** – Western Blot analysis of whole cell lysates from Hela DKO cells incubated with Bortezomib (Borte) or DMSO for 48 h. Antibodies were used against phospho-JNK1 and CHOP as ER-stress markers, (cleaved) PARP to detect cell death and BCL-2 and BOK to validate expression levels.  $\beta$ -actin was used as loading control. One out of two independent experiments is shown. **E** – Fluorescence microscopy images (Incucyte) of Hela (empty vector) cells transfected with control siRNA (siCtrl) or siRNA targeting BOK (siBOK) or BCL-2 (siBCL-2). After 24 h, cells were incubated with 2  $\mu$ M Tunicamycin (TM) and 0.67  $\mu$ g/ml PI to stain dead cells and time-lapse imaging was performed using Incucyte. Shown are representative images of triplicates after 40 h incubation (one independent experiment). Scale bars = 200  $\mu$ m.

## Acknowledgements

First of all, I like to express my gratitude to Markus Morrison who provided me guidance and support throughout all the time since I was a green bachelor student in his lab many years ago and did not hesitate to be my doctor father and the first examiner of this thesis. Thank you, Markus, for always having an open door and your trust in my work and abilities.

Secondly, many thanks go to Frank Essmann for the warm welcome in his group, the refreshing talks and all his help and support through the difficult and less difficult phases. Without him this project would have never existed and developed as it has over these past years.

Next, I want to thank my students and partners in crime in this project: Lynn Barber and Alexander Paul. Thank you for your outstanding work and motivation. It was a pleasure to supervise you and I am sure you will be excellent supervisors yourself.

Also, I am grateful for the strong collaborations in this project outside the group – especially for the help of Kristyna Pluhackova and Thomas Fellmeth who made exceptional contributions to this project with their simulations and for all the time and effort you, Kristyna, spent in the paper we put together.

Moreover, I am more than grateful for my PhD colleagues who shared my “believe” of becoming a doctor someday and with whom I could share joy and sorrow anytime: Sandra, Benni and Kathrin. Thank you for your friendship and camaraderie that lasted even to Panama and back.

Also, a lot of thanks to all other previous group members for the fun times in and outside the lab: Kerstin, Meng, Annika, Damaris, Franzi, Astrid and Lenke. Likewise, thanks go to the members of the Morrison group who kept me in good memory and always made me feel welcome. Thank you, Dani, for never stopping to believe in me and for being a mentor and friend all this time. Thank you, Gavin, for all the encouragement, smiles and not least for proofreading my work.

Thanks also go to the by far best and most intriguing finding of this journey. You were there for me, raised me up and smoothed my forehead – no matter how deep the worry lines were.

In addition, I am thankful for all members of the Dr. Margarete Fischer-Bosch Institute for Clinical Pharmacology (IKP) and Robert Bosch Center for Tumor Diseases (RBCT) who contributed to this valuable experience and brightened my day. I met many awesome people along this way and look forward to seeing you all again someday.

Last, but never least, my deepest gratitude goes to my loved ones. It is your love that makes me the person I am, that makes me go the distance and gives me the strength to reach the peak. Thank you, my dear friends! I know I had not as much time for you as you deserve in these last years, but I enjoy every minute we spend together. It is simply great to know that you are always there - no matter how close or far away you live. And thank you, my dear family! You always stand behind me and give me the certitude that even if my world would break down tomorrow, you'll have my back and carry me through. All of you, I bow before you and I am glad that you are with me – here at the end of all things.

## Declaration of authorship

I hereby certify that the dissertation entitled

**Brought to light: The Bcl-2 transmembrane domain interactome elucidated by a bimolecular split luciferase assay and its impact on apoptosis signalling**

is entirely my own work except where otherwise indicated. Passages and ideas from other sources have been clearly indicated.

---

Ich versichere, dass ich die vorliegende Arbeit mit dem Titel

**Brought to light: The Bcl-2 transmembrane domain interactome elucidated by a bimolecular split luciferase assay and its impact on apoptosis signalling**

selbständig verfasst und keine anderen als die angegebenen Quellen und Hilfsmittel benutzt habe; aus fremden Quellen entnommene Passagen und Gedanken sind als solche kenntlich gemacht.

Signature/Unterschrift:

## Publications and conference contributions

### Publications

S. Weller, A. Toenneßen, B. Schaefer, **T. Beigl**, A. Muenchow, K. Böpple, U. Hofmann, B. F. Gillissen, W. E. Aulitzky, H.-G. Kopp, F. Essmann, The BCL-2 inhibitor ABT-199/venetoclax synergizes with proteasome inhibition via transactivation of the MCL-1 antagonist NOXA. *Cell death discovery* 8, 215 (2022).

**T. B. Beigl**, A. Paul, T. P. Fellmeth, D. Nguyen, L. Barber, S. Weller, B. Schaefer, B. F. Gillissen, W. E. Aulitzky, H.-G. Kopp, M. Rehm, D. W. Andrews, K. Pluhackova, F. Essmann, BCL-2 and BOK regulate apoptosis by interaction of their C-terminal transmembrane domains. *Embo reports* 10.1038/s44319-024-00206-6 (2024).

### Conference contributions – Poster

**T. B. Beigl**, A. Paul, S. Weller, B. Schäfer, W. E. Aulitzky, H.-G. Kopp, T. Fellmeth, K. Pluhackova, M. Rehm, F. Essmann, Abstract 2524: Critical interactions and tumor-specific mutations of Bcl-2 transmembrane domains revealed by a novel split luciferase assay. *Cancer Research* 83, 2524 (2023).

**T. B. Beigl**, S. Weller, B. Schäfer, W. E. Aulitzky, H.-G. Kopp, M. Rehm, F. Essmann, Abstract 3704: The C-terminal transmembrane domain of BAX is essential for BAX auto-inhibition. *Cancer Research* 82, 3704 (2022).

**T. B. Beigl**, S. Weller, B. Schäfer, K. Böpple, L.-S. Rieder, H.-G. Kopp, M. Rehm, W. E. Aulitzky, F. Essmann, Abstract 1947: Brought to light: the homotypic interaction pattern of Bcl-2 effector transmembrane domains in a bimolecular luciferase complementation assay. *Cancer Research* 81, 1947 (2021).

## Curriculum vitae

### Doctorate

- 2019 – 2022                    **Dr. Margarete Fischer-Bosch Institute for Clinical Pharmacology (IKP)** in Stuttgart, under supervision of PD Dr. Frank Essmann
- 2022 - 2024                    **Robert Bosch Center for Tumor Diseases (RBCT)** in Stuttgart, in the group “Apoptosis regulation and targeted therapy” under supervision of PD Dr. Frank Essmann

### Education

- 2017 – 2019                    **University of Stuttgart, Master of Science Technical Biology**  
Master thesis at the department of Biomedicine, University of Bergen, Norway  
“Actin N-terminal acetylation impacts Golgi structural integrity”
- 2013 – 2017                    **University of Stuttgart, Bachelor of Science Technical Biology**  
Bachelor thesis at the institute of cell biology and immunology, University of Stuttgart  
“Spatially-dependent expression of TRAILR1 and TRAILR2 in multicellular tumour spheroids”
- 2005 – 2013                    Max-Born-Gymnasium, Backnang  
Abitur (High school certificate) 2013



